P-14-04

SR-PSU Hydrogeological modelling

TD11 – Temperate climate conditions

Johan Öhman, Geosigma AB

Sven Follin, Golder

Magnus Odén, Svensk Kärnbränslehantering AB

December 2014

Svensk Kärnbränslehantering AB
Swedish Nuclear Fuel
and Waste Management Co

Box 250, SE-101 24 Stockholm
Phone +46 8 459 84 00

ISSN 1651-4416
SKB P-14-04
ID 1395217

SR-PSU Hydrogeological modelling

TD11 – Temperate climate conditions

Johan Öhman, Geosigma AB

Sven Follin, Golder

Magnus Odén, Svensk Kärnbränslehantering AB

December 2014

Keywords: SFR, PSU, Hydrogeology, Bedrock, Modelling, Temperate, Forsmark, Safety assessment, Performance measures, Sensitivity analysis, Parameterisation

Abstract

As a part of the license application for an extension of the existing repository for short-lived low and intermediate radioactive waste (SFR), the Swedish Nuclear Fuel and Waste Management Company (SKB) has undertaken a project to assess the radiological safety for the SFR repository after closure (SR-PSU). The SR-PSU project employs the groundwater flow model, developed in SDM-PSU, to perform hydrogeological modelling tasks that are defined in terms of so-called Task Descriptions (TDs). This report summarises the methodology, setup, and results of the groundwater flow modelling task TD11.

The objective of TD11 is to assess the combined effects of: 1) bedrock heterogeneity, 2) parameterisation uncertainty, and 3) transient flow regime in terms of performance measures. This is assessed by means of a sensitivity analysis, which consists of 17 so-called Bedrock cases (parameterisation variants) that are studied under six selected stages of shoreline retreat. These bedrock cases were chosen to capture the uncertainty/variability in the bedrock parameterisation. Hence, they can be assumed to cover the range of flow through the disposal rooms.

The sensitivity analysis has a threefold outcome: 1) a demonstration of the dynamic hydrogeological setting of SFR, 2) performance measures are delivered to users within SR-PSU, and 3) new tools are introduced to the DarcyTools modelling environment.

The key performance measures from the groundwater flow modelling are:

- Disposal-room cross flow, Q (m^3/s).
- Particle exit location at the bedrock/regolith interface.
- Flow-related transport resistance along bedrock flow paths, F_r (y/m).
- Advective travel times along bedrock flow paths, $t_{w,r}$ (y).

The particle-tracking results for each bedrock case and time slice have been exported to different users within SR-PSU.

Due to the ongoing land uplift, the flow regime will change, as the seabed above SFR successively emerges above sea level, and conform to terrestrial conditions. During early stages of shoreline retreat, up to c. 3500 AD, the performance measures are clearly subject to the changing flow regime, whereas the influence of local topographical gradients successively takes over during later stages, leading to stationary appearances in performance measures by 5000 to 9000 AD. The deeper location of the planned SFR extension (SFR 3) renders systematically longer path lengths, longer advective travel times, and higher flow-related transport resistance, as compared to SFR 1.

The local parameterisation of deformation zones that intersect disposal rooms (primarily ZFMNNW1209 and ZFMWNW0835) has been identified as a key uncertainty for the evaluation of cross flows through the disposal rooms. Out of the 17 studied Bedrock cases, three are selected as representative for covering the range in observed cross flow through disposal rooms. The results of these three Bedrock cases are presented in additional detail, and the flow solutions have been exported to near-field modelling teams.

Sammanfattning

Som en del av ansökan för utbyggnad av Slutförvaret för kortlivat radioaktivt avfall (SFR) har Svensk Kärnbränslehantering (SKB) genomfört ett projekt för att bedöma den radiologiska säkerheten för förvaret efter förslutning (SR-PSU). I SR-PSU tillämpas den grundvattenmodell som utvecklats i SDM-PSU för att genomföra olika hydrogeologiska modelleringsuppgifter, vilka finns definierade i särskilda uppgiftsbeskrivningar (*Eng:* Task Descriptions; TDs). Denna rapport sammanfattar ansats, genomförande och resultat för uppgiftsbeskrivningen TD11.

Syftet med TD11 är att bedöma de kombinerade effekterna av: 1) berggrundens heterogenitet, 2) parameterosäkerhet och 3) den transienta flödesregimen. Detta bedöms med hjälp av en känslighets-analys, som består av 17 varianter av parameteruppsättning för berggrunden (*Eng:* Bedrock cases), samtliga studeras för sex utvalda stadier av strandlinjeförskjutning.

Känslighetsanalysen medför tre huvudsakliga resultat: 1) förståelsen för den dynamiska hydrogeologiska omgivningen kring SFR demonstreras, 2) mått på bergets retentionsegenskaper (*Eng:* performance measures) levereras till användare inom SR-PSU och 3) nya modelleringsprinciper har tillförts DarcyToolsmiljön.

De huvudsakliga måtten på bergets retentionsegenskaper från simuleringarna är:

- Flöde genom förvarsutrymmen, Q (m^3/s).
- Partikelbanors passage vid övergången jord/berg.
- Flödesrelaterat transportmotstånd längs flödesbanor i berg, F_r (y/m).
- Advektiv gångtid längs flödesbanor i berg, $t_{w,r}$ (y).

Resultaten från partikelspårningen har levererats, för varje parameteruppsättning och stadie av strandlinjeförskjutning, till övriga modellörer inom SR-PSU.

I tidiga stadier av strandlinjeförskjutning, t.o.m. 3500AD, påverkas bergets retentionsegenskaper påtagligt av den transienta flödesregimen, men därefter övergår flödesregimen gradvis mot stationära förhållanden som domineras av lokala topografiska gradienter, 5000 till 9000AD. Den djupare belägenheten av den planerade utbyggnaden (SFR 3) ger upphov till systematsikt längre flödesbanor, längre advektiva gångtider och högre flödesrelaterat transportmotstånd, i jämförelse mot det existerande förvaret (SFR 1).

Den lokala parameteriseringen av deformationszoner som skär förvarsutrymmen (huvudsakligen ZFMNNW1209 och ZFMWNW0835) har konstateras utgöra en betydelsefull osäkerhet för beräknade flöden genom förvarsutrymmen. Av de 17 parameteruppsättningarna har tre valts ut som representativa för att täcka in intervallet av beräknade flöden genom förvarsutrymmen. Resultaten för de tre utvalda parameteruppsättningarna beskrivs extra utförligt och deras flödeslösningar har levererats till närfälts-modelleringen.

Contents

1 Introduction

1.1 Background of the SR-PSU project

The final repository for low and intermediate level short-lived radioactive waste (SFR) was constructed in its first stage and taken into operation in 1987. The SFR facility requires a future extension due to: 1) the pending decommissioning of the closed reactors (Barsebäck, Studsvik, and Ågesta), 2) the increased amounts of operational waste caused by the extended operating time of the remaining nuclear power plants, and 3) the future decommission of the remaining nuclear power plants. The existing facility is denoted SFR 1, while the planned extension is denoted SFR 3.

As a part of the license application for SFR 3, the Swedish Nuclear Fuel and Waste Management Company (SKB) initiated the SFR extension project (PSU). In SR-PSU the radiological safety for the entire SFR-repository after closure is addressed. A site descriptive model, SDM-PSU (SKB 2013) was developed to describe the hydrogeological setting at SFR. More or less the same flow model is applied in SR-PSU, as a numerical tool to assess the performance of a backfilled repository. Two different climate conditions are studied in SR-PSU (temperate and periglacial conditions; Odén et al. 2014).

All groundwater-flow modelling tasks within SR-PSU are strictly defined by means of so-called Task Descriptions (TDs). This report describes the model results of tasks defined in TD11, including input-data handling, numerical setup of model cases, simulation procedures, as well as, handling of output. TD11 assesses the impact of bedrock heterogeneity and parameterisation uncertainty on repository performance, under various stages of shoreline retreat, by means of a sensitivity analysis. Only the temperate climate conditions are studied in TD11.

1.2 Objectives

The main objective in TD11 is to analyse the impact of uncertainty/heterogeneity in bedrock parameterisation in terms of performance measures. This is evaluated by means of a sensitivity analysis for selected bedrock cases (Table 2-1). Earlier analyses have demonstrated that the performance measures of SFR are primarily controlled by the ambient bedrock parameterisation (i.e. local structures and local fracture network). Therefore, the sensitivity analysis only addresses parameterisation variants inside the SFR Regional domain (Figure 3-1); outside, the properties are kept fixed.

The impact of the bedrock uncertainty/heterogeneity is evaluated in terms of two types of performance measures (described in more detail in Section 1.3):

1) Flow through disposal rooms, existing SFR 1 and the planned extension SFR 3.
2) Bedrock retention properties (quantified by means of particle tracking).

There are two reasons for this analysis. Firstly, the results demonstrate the understanding of the present day hydrogeological characteristics of the site, as well as, predict how these conditions will change during future stages of shoreline retreat. Secondly, results are delivered to the other modelling teams in SR-PSU (near-field modelling, biosphere modelling, and radionuclide transport modelling).

As the outcome of the TD11 sensitivity analysis, three bedrock cases are selected that are representative for covering the observed range of uncertainty/heterogeneity in bedrock parameterisation. These three bedrock cases are selected based on flow through the 11 disposal rooms in SFR 1 and SFR 3 (Section 6.2.3):

1) One “low-flow” bedrock case: bedrock parameterisation variant with low disposal-room flows.
2) A base case: a basic model setup, representing “average bedrock characteristics” with median disposal-room flows.
3) One “high-flow” bedrock case: bedrock parameterisation variant with high disposal-room flows.

Finally, for code-comparison purposes, bedrock discharge/recharge in biosphere objects is to be determined for the Base case (Section 6.3).

1.3 Considered performance measures

The key performance measures (output) from the groundwater flow modelling are:

- Disposal-room cross flow, Q (m^3/s).
- Particle exit location at the bedrock/regolith interface.
- Flow-related transport resistance along bedrock flow paths, F_r (y/m).
- Advective travel times along bedrock flow paths, $t_{w,r}$ (y).

A performance measure of supporting character is:

- Path length of bedrock flow paths, L_r (m).

As stated in Section 1.2, these performance measures are analysed to demonstrate the understanding of the hydrogeological characteristics of the site (Chapter 6), but also exported to downstream users within the SR-PSU project (e.g. radionuclide transport calculations, hydrogeochemistry, and biosphere analyses), for each bedrock case and time slice. The different performance measures are briefly described below.

The cross flow through disposal rooms, *Q*, is directly assessed from flow-field analysis (Section 5.4.1), whereas the other performance measures require a preceding particle-tracking step (Section 5.4.2). The performance measures F_r (y/m), $t_{w,r}$ (y), and L_r (m) are integrated bedrock properties that are determined along particle trajectories, as defined from a bedrock-entry point to a bedrock-exit point. Particle tracking is initiated by releasing particles randomly within disposal-room volumes. The starting point of a particle trajectory is defined as its tunnel-wall passage (i.e. bedrock entry), whereas the termination point is defined as its bedrock/regolith interface passage (i.e. bedrock exit). The underlying equations for determining these cumulative performance measures along particle trajectories are described in more detail in Section 5.4.2.

Disposal-room cross flow (Q)

Cross flow refers to the total flow, *Q* (m^3/s), over a predefined cross-sectional area in the computational grid. This area is the interface between a subunit of interest and the surrounding, arbitrary grid cells. Cross flow through disposal rooms occurs over an enclosed surface, and therefore inward-directed and outward-directed flow components must be summed separately, as explained in more detail in Section 5.4.1. Cross flow is an important output (performance measure) in the groundwater flow modelling as it affects the strength of the source term in radionuclide transport modelling.

Particle exit location

Exit locations are determined by means of forward particle tracking, and defined as the point where the particle passes the bedrock/regolith surface (expressed in RT90 coordinates).

Flow-related transport resistance (F_r)

The flow-related transport resistance in rock, F_r (y/m), is an entity, integrated along flow paths, that quantifies the flow-related (hydrodynamic) aspects of the possible retention of solutes transported in a fractured medium. It is an important output (performance measure) in groundwater flow modelling. In SR-PSU, information about the flow-related transport resistance governs the calculation of nuclide migration, hydrogeochemical calculations of salt diffusion into and out from the matrix, as well as oxygen ingress. In its most intuitive form, although not necessarily most generalised, the flow-related transport resistance is proportional to the ratio of flow-wetted fracture surface area (FWS) and flow rate (Joyce et al. 2010). An alternative definition is the ratio of FWS per unit volume of flowing water multiplied by the advective travel time.

Advective travel time ($t_{w,r}$)

The cumulative advective residence time for a particle along a trajectory in the rock, $t_{w,r}$ (y).

1.4 Nomenclature

This report contains several terms and acronyms that are rarely used outside SKB work and makes several references to site-specific deformation zones. To facilitate the readability of the report these are listed in Table 1-1.

Table 1-1. Acronyms and structures referred to in the report.

Acronym	Stands for	Explanation
DEM	Digital Elevation Model	Topographic model for the Forsmark area, covering both land and seafloor with a spatial resolution of 20 m in the horizontal plane.
DFN	Discrete Fracture Network	In DFN modelling, fractures, and fracture flow, are typically resolved as a network of planar geologic features.
ECPM	Equivalent Continuous Porous Medium	A hydrogeological modelling concept, where the hydraulic properties of a conductive fracture network are approximated by those of a porous medium. ECPM does not resolve explicit fracture flow, and hence is useful in large-scale simulations and on site-scale if fractures are resolved with fine enough discretization.
GEHYCO	GEnerate HYdraulic COnductivity	The module in DarcyTools used to translate a hydraulic DFN into an ECPM (Svensson et al. 2010).
HCD	Hydraulic Conductor Domain	Hydraulic representation of identified deterministic deformation zones.
HRD	Hydraulic Rock mass Domain	Hydraulic representation of the stochastic fractures between deformation zones.
HSD	Hydraulic Soil Domain	Hydraulic representation of the regolith (Quaternary deposits mainly).
L1BC	Layout for SFR 3	Currently studied layout geometry for the planned SFR extension (SFR 3).
PDZ	Possible Deformation Zone	A borehole section that has geologically been interpreted to have “deformation-zone like characteristics” (i.e. a possible deformation zone intercept). In the geological modelling, deterministic structures (ZFMxxx) are modelled in 3D by linking PDZs to surface lineaments. Remaining PDZs, which cannot be linked to lineaments, are referred to as “Unresolved PDZs”.
SDM	Site-Descriptive Model	A multi-disciplinary description of the site, including both qualitative and quantitative information, that is based on both direct observations and modelling studies.
SFR	SlutFörvaret för kortlivat Radioaktivt avfall	The existing final repository for short-lived radioactive waste. The existing repository is denoted SFR 1, while the planned extension is denoted SFR 3.
SKB	Svensk Kärnbränslehantering AB	The Swedish Nuclear Fuel and Waste Management Company.
ZFM	Deformation zone in the Forsmark area	Deterministically modelled deformation zone in the geological model. Modelled by linking borehole intercepts with “deformation-zone like characteristics” to surface lineaments (see acronym PDZ).

Key deformation zones (Deterministic structures of the Geological model SFR v 1.0)		**Alternatively known as: (Structures in early SFR models)**
ZFMWNW0001	Core of the bounding Southern deformation zone belt (Curtis et al. 2011).	Singö deformation zone
ZFMNW0805A/B	Deformation zones that constitute a Northern boundary belt (Curtis et al. 2011).	Zone 8
ZFMNNW1034	Deformation zone of high transmissivity that cuts across the wedge defined by the intersection of the Northern and Southern boundary belts (Curtis et al. 2011).	Not included in previous SFR models
ZFM871	Gently dipping deformation zone below the existing repository facility (SFR 1).	Zone H2
ZFMENE3115	A deformation zone that terminates ZFM871 to the southeast.	Not modelled in previous SFR models
ZFMNE0870	Low-transmissive deformation zone parallel to the access tunnels.	Zone 9
ZFMNNE0869	High-transmissive deformation zone intersecting access tunnels.	Zone 3
ZFMNNW1209	A deformation zone that intersects the SFR 1 rock vaults.	Zone 6
ZFMWNW1035	A deformation zone that occurs at the northern rim of the Southern boundary belt (Curtis et al. 2011).	Zone 1

1.5 Settings

SFR is located in northern Uppland within the municipality of Östhammar, about 120 km north of Stockholm (Figure 1-1). The site is located about 2 km north of the site selected for the final repository for spent nuclear fuel (SDM-Site Forsmark).

The current ground surface in the Forsmark region forms a part of the sub-Cambrian peneplain in southeastern Sweden. This peneplain represents a relatively flat topographic surface with a gentle dip towards the east that formed more than 540 million years ago. The Forsmark region is characterised by small-scale topography at low elevation (Figure 1-2). The whole area is located below the highest coastline associated with the last glaciation, and large parts of the area emerged from the Baltic Sea only during the last 2,000 years. Both the flat topography and the still ongoing land uplift of about 6 mm per year strongly influence the current landscape. Sea bottoms are continuously transformed into new terrestrial areas or freshwater lakes, and lakes and wetlands are successively covered by peat. Most of the Forsmark-SFR site is currently covered by sea water (Figure 1-3), but the seabed will continue to rise and the seabed above SFR will be at the shoreline within about 1,000 years.

The existing repository facility, SFR 1, consists of four rock vaults and one vertically extending silo. The silo extends from c. –70 m to –140 m (elevation system RHB 70) and the four rock vaults of SFR 1 are located within the elevation range from c. –70 m to –90 m. The planned extension, SFR 3, consists of six rock vaults, which will extend from c. –120 m to –140 m.

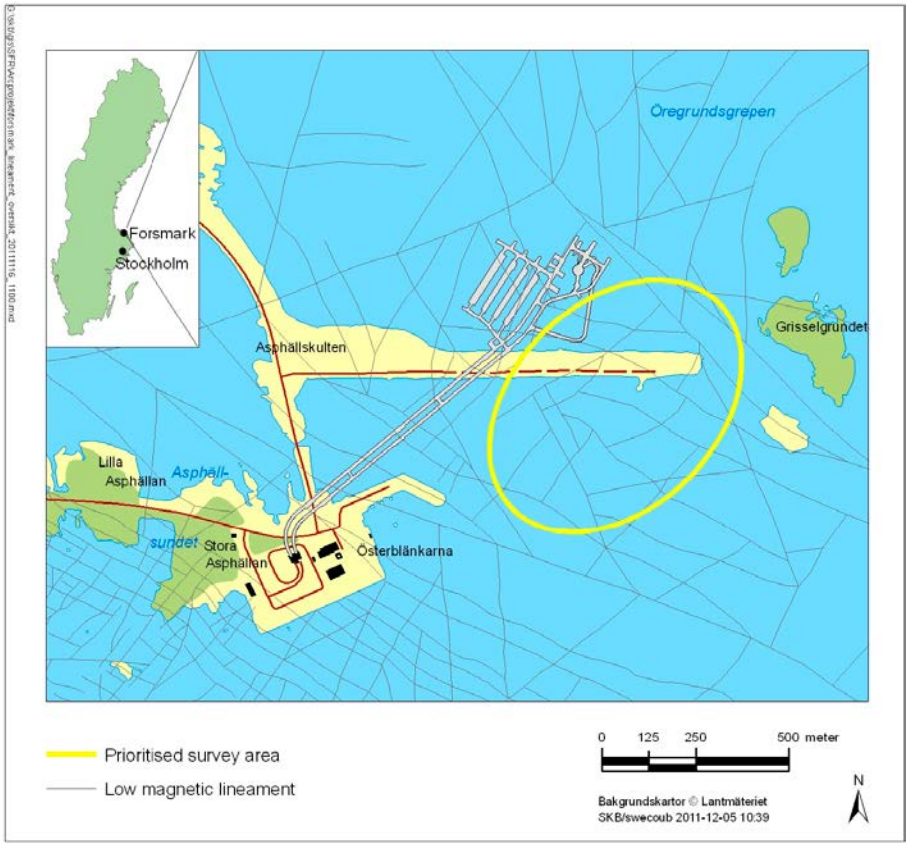

Figure 1-1. *Map of the Forsmark-SFR site showing the location of the existing SFR facility (SFR 1) and the suggested area for the SFR extension (SFR 3). In this report, the man-made wave breaker running above the facility is referred to as the 'SFR Pier'.*

Figure 1-2. *Photograph showing the flat topography and the low-gradient shoreline with recently isolated bays due to land uplift.*

Figure 1-3. *Figure showing the existing SFR facility (SFR 1) and the suggested area (yellow) for the SFR extension (SFR 3) in the foreground and the Forsmark nuclear power plant buildings in the background. The distance from SFR 1 to the shoreline is about 2 km. The man-made wave breaker running above SFR 1 is referred to as the 'SFR Pier', cf. Figure 1-1.*

2 Approach

This chapter presents an outline for the approach taken to meet the objectives of TD11 (Section 1.2). The outline is divided into conceptual model components (Section 2.2) and the more detailed modelling sequence (or, numerical implementation; Section 2.3). The modelling sequence consists of the following key steps: 1) handling of input geometry (Chapter 3), 2) model parameterisation (Chapter 4), and 3) simulation sequence (Chapter 5).

The flow-simulation code used, DarcyTools, is the corner stone in this modelling task, and therefore its inbuilt feasibilities/limitations/user control sets the framework for how the numerical approach can be designed. As the flow-simulation code has a significant influence on the numerical approach, this chapter starts with a brief presentation of DarcyTools (Section 2.1).

2.1 Modelling tool

All flow simulations in this study employ the computer code DarcyTools, which has been specifically developed for the analysis of a repository for spent nuclear fuel (Svensson et al. 2010).

DarcyTools is based on the Continuum Porous-Medium (CPM) approach (Svensson et al. 2010), in which the hydraulic properties of a flowing fracture network are approximated by those of a porous medium. DarcyTools allows transferring fracture-network characteristics, as observed in borehole data, onto its computational grid by means of geometrical upscaling over grid cells. These upscaled properties are referred to as Equivalent Continuous Porous Medium (ECPM) properties. As the ECPM approach is based on an underlying stochastic DFN model, the resulting ECPM properties are also stochastic. The uncertainty related to hydraulic heterogeneity can therefore be handled by addressing multiple DFN realisations.

The appeal of the ECPM approach is its computational parsimony and an upscaled conductivity field that bears the hydraulic traits of an underlying fracture network, for example anisotropic correlation structures. Unfortunately, *geometrical* up-scaling does not always ensure *hydraulic* consistency between the complex heterogeneity of the underlying flowing fracture network and the approximated ECPM. It must therefore be emphasised that the term “equivalent” requires a fine resolution of the computational grid in order to be valid.

Another key feature in DarcyTools is its unstructured Cartesian grid system, which allows great flexibility in local grid refinement to represent detailed geometry of objects (e.g. tunnel layout). All grid geometry is handled via so-called DarcyTools objects (i.e. code-specific file format), which have been constructed from original CAD data geometry (see Chapter 3).

2.1.1 Identified error related to parameter <nbgrad>

All simulations in this study are performed with code versions DarcyTools v.3.4.18 and Migal v. 4.01. During the course of this work an error was identified in this version. Owing to the unstructured grid arrangement, DarcyTools employs a pressure-correction algorithm (controlled by the parameter <nbgrad>), which is intended to hamper artificial gradients between cells of different size. Unfortunately, this algorithm was found to be numerically instable for particular configurations of conductivity/cell-size contrasts.

In TD11, significant attention has been paid to circumvent this error from affecting the performance measures (described in detail in separate PM, SKBdoc 1396127). A particular configuration of grid discretisation and tunnel-conductivity parameterisation in rock cavern 2BMA (Section 3.2) is found to cause large, local artefacts in tunnel-wall flow, and in turn resulting in a one-order-of-magnitude error in its evaluation of disposal-room cross flow, Q. To minimise the effects of these artefacts, the algorithm was changed so as *not* to calculate Q from *tunnel cells*, but instead from the *bedrock cells* surrounding 2BMA (which are unaffected by the numerical error). This workaround reduces the error in 2BMA to c. 4% (SKBdoc 1396127). The error is not observed for other rock caverns.

The occurrence of this type of numerical artefact is rare. However, the phenomenon has been found sporadically in the bedrock, occurring where two components coincide: 1) extreme conductivity contrasts, which may arise in ECPM translation of the underlying stochastic fracture network, and 2) local grid refinement. These artefacts take the form of *local flow cells*, which are not judged to affect the large-scale flow solution, but may force particles into loops, and in turn, overestimate their cumulative performance measures, such as path length, travel time, $t_{w,r}$, and flow-related transport resistance in rock, F_r (Section 1.3). Overall, the impact of particle looping is found to be small; the fraction of particles where the overestimation in transport properties exceeds one order of magnitude is only 0.001%. The particle-tracking algorithm was modified to prevent accumulation inside loops, which effectively eliminates the impact on transport properties (SKBdoc 1396127). All final output from TD11 is obtained by means of the modified particle-tracking algorithm, which is denoted "deplete_loops" (Table A-13) to emphasise this workaround.

The inbuilt pressure-correction algorithm, related to the parameter <nbgrad>, is corrected in all subsequent versions of DarcyTools.

2.2 Conceptual model components

The groundwater flow model developed within SDM-PSU and SR-PSU consists of three conceptual hydrogeological units (see SKB 2013):

- HSD (Hydraulic Soil Domain), representing the regolith, i.e. any loose material covering the bedrock, e.g. Quaternary deposits, filling material, and peat.
- HCD (Hydraulic Conductor Domain), representing deformation zones.
- HRD (Hydraulic Rock mass Domain), representing the less fractured bedrock in between the deformation zones.

The parameterisation of these three hydraulic-domain types implies uncertainty and heterogeneity, which is addressed by means of a sensitivity analysis (Section 1.2). This model task is delimited to the bedrock parameterisation. The regolith-layer thicknesses are modelled as time variant, as the result of modelled dynamic landscape processes (Section 3.3). The HSD parameterisation is described in Section 4.4.

2.2.1 Bedrock parameterisation cases

The bedrock between deformation zones, HRD, is described by means of a stochastic Discrete-Fracture Network (DFN) model, as well as, a stochastic conditional model for Unresolved PDZs (see details in SKB 2013). The heterogeneity in HRD is modelled by means of coupled stochastic realizations of the DFN and the Unresolved-PDZ models (examples presented in Section 4.2.1).

The HCD parameterisation involves two components of variability: 1) heterogeneity and 2) conceptual uncertainties (Section 4.2.2). The spatial heterogeneity is addressed by comparing homogeneous parameterisation versus heterogeneous realisations (Table 2-1). One of the conclusions from SKB (2013) was that the possible existence of a transmissivity depth trend could neither be supported by data, nor could it be rejected. The conceptual uncertainty in this matter is addressed by comparing HCD parameterisation variants that: 1) are based on an underlying depth-trend assumption, versus 2) variants that are not (Table 2-1). Another conceptual uncertainty regards the confidence in local borehole conditioning of HCD parameterisation (i.e. the confidence of local data near disposal rooms, versus the large-scale interpretation of a zone). This uncertainty is addressed by comparing bore-hole conditioned HCD parameterisation, versus non-conditioned parameterisation (Table 2-1). Finally, a separate case is setup to address the uncertainty regarding transversal hydraulic properties of the Singö deformation zone.

2.2.2 Dynamic hydrogeological setting

The hydrogeological setting at SFR is a dynamic system, driven by the ongoing shoreline retreat, which will alter the flow regime during the time span addressed in SR-PSU (e.g. Figure 2-1).

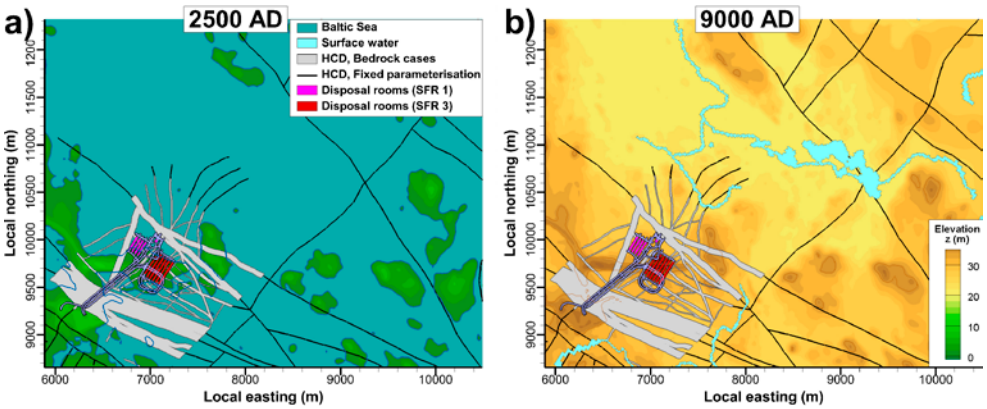

Figure 2-1. *Shoreline retreat between time slices 2500 AD and 9000AD.*

An important aspect is therefore to study the evolution of groundwater flow, from the surface (recharge areas) to the repository, and from the repository to the surface (discharge areas), and its impact on performance measures (Section 1.3). The altering flow regime is addressed by comparing results of steady-state flow solutions for selected shoreline positions. For the Global warming climate case (see SKB 2014a) the identified shoreline positions correspond to the following time slices, see Table 2-1; 2000, 2500, 3000, 3500, 5000, and 9000 AD.

2.2.3 Model components in the sensitivity analysis

The different model aspects of bedrock parameterisation (Section 2.2.1) and transient flow regime (Section 2.2.2) comprise a large number of possible combinations for the sensitivity analysis. Firstly, the number of combinations is reduced by selecting a few HCD variants, HRD realisations, and time slices (Table 2-1), which have been judged as representative in a foregoing analysis, i.e. focusing on the realisations of HRD and HCD that have been found to span the range of observed variability in disposal-room cross flow (SKBdoc 1395200 and Table 5-1 in SKBdoc 1395214). Out of the remaining possible bedrock-parameterisation combinations, 17 are selected for propagation to the TD11 sensitivity analysis (Table 2-2). Each such parameterisation combination is referred to as a "Bedrock case", which consists of one HCD variant paired with one HRD realisation. These 17 Bedrock cases were selected to cover the range in future flow through the disposal rooms.

The combined components of uncertainty/heterogeneity in the bedrock parameterisation is analysed in terms of a sensitivity analysis, where model performance is evaluated for a selection of 17 bedrock parameterisation cases under 6 stages of shoreline retreat (Table 2-1).

Table 2-1. Varied model components in the sensitivity analysis.

Variable	Bedrock case[1)] HCD parameterisation variant	HRD realisation	Time slice
Refers to:	Deterministic structures • Deformation zones • Sheet joints[2)] • SBA structures[2)]	Stochastic features • DFN • Unresolved PDZ	Shoreline retreat Landscape dynamics (RLDM)
Cases	• Base case • Heterogeneity (R01 and R07) • Borehole conditioning (Yes/No) • Depth trend (Yes/No) • Transmissivity across Southern boundary belt (one case)	Stochastic realisations: • R03 • R18 • R85	Selected time slices: • 2000 AD • 2500 AD • 3000 AD • 3500 AD • 5000 AD • 9000 AD

[1)] A bedrock case consists of a HCD-parameterisation variant and a HRD realisation (Table 2-2).

[2)] Parameterisation kept fixed in all bedrock cases.

Table 2-2. Bedrock cases in the sensitivity analysis.

No.	Label	HCD Conditioning	Depth trend	Variability	HRD
1	BASE_CASE1_DFN_R85	Yes	Yes	Homogeneous	R85
2	BASE_CASE1_DFN_R18				R18
3	BASE_CASE2_DFN_R85			Anisotropic SBB	R85
4	nc_DEP_HOM_DFN_R03	No		Homogeneous	R03
5	nc_DEP_HOM_DFN_R85				R85
6	nc_NoD_HOM_DFN_R85		No		
7	CD_DEP_R01_DFN_R85	Yes	Yes	Heterogeneous, R01	R85
8	nc_DEP_R01_DFN_R85	No			
9	nc_DEP_R01_DFN_R18				R18
10	CD_DEP_R07_DFN_R85	Yes		Heterogeneous, R07	R85
11	nc_DEP_R07_DFN_R85	No			
12	nc_DEP_R07_DFN_R18				R18
13	nc_NoD_R01_DFN_R03		No	Heterogeneous, R01	R03
14	nc_NoD_R01_DFN_R85				R85
15	nc_NoD_R01_DFN_R18				R18
16	nc_NoD_R07_DFN_R03			Heterogeneous, R07	R03
17	nc_NoD_R07_DFN_R85				R85

2.3 Modelling sequence and traceability in data management.

As explained above, the task of TD11 is to analyse the differences between 17 bedrock cases, for 6 stages of shoreline retreat (i.e. a total of 102 model setups). Even a single model setup, i.e. a given bedrock-case/time-slice combination, is complex, involving multiple input files that must be processed in several steps (see flow chart in Figure A-1; Appendix A1). Therefore, at least three reasons are identified for applying automatized data-file management in the modelling sequence:

- **Minimisation of data-handling related errors**: automatizing ensures that: 1) all model setups are handled consistently (i.e. all model setups are treated the *same* way), and 2) application of input files is consistent with the specified bedrock-case/time-slice case (i.e. follows specifications in Table 2-1 and Table 2-2).
- **Traceability:** automatizing provides traceable data management via the source codes, and also maintains a strict traceability between sequences by means of case-specific filenames for intermediate input and output (i.e. all I/O filenames are tagged by relevant specification to bedrock-case and/or time-slice combination). Under no circumstances can output can be propagated unless all required input data are available.
- **Time efficiency**: automatizing allows: 1) parallel processing in different working directories and 2) continuous processing over weeks, day and night.

Consequently, the data file management in execution is automatized as far as possible (all details provided in Appendix A). The modelling sequence is divided into four main routines, which are handled by separate file-managing that preserve full traceability between input and output (see flow chart in Figure A-1; Appendix A1). These four routines are:

a) **Data and grid preparation:** managed by a range of customized tools (Appendix A2).

b) **ECPM upscaling:** explained in Section 5.2 (details in Appendix A3).

c) **Final model setup and flow simulation** Section 5.3 (details in Appendix A3).

d) **Post processing** Section 5.4.1 and Section 5.4.2 (details in Appendix A4).

3 Geometric data

3.1 Model domains

3.1.1 Flow domain

The flow domain defines the outer perimeter of the model volume (i.e. the vertical sides of the model; Figure 3-1). The vertical sides of the model have no-flow boundary conditions in flow simulations, and therefore the flow domain is defined based on topographical water divides and sub-catchments. Areas that are currently below sea are chosen with respect to: 1) modelled future topographical divides in RLDM (Brydsten and Strömgren 2013), 2) the deep Seafloor trench (the so-called Gräsörännan), and 3) general expectations of the regional future hydraulic gradient. The flow domain extends vertically from +100 m to –1,100 m elevation.

The flow domain has been revised during the course of SR-PSU. The flow domain employed in TD11 has been updated to conform to the latest available data on topographical water divides, which is explained in the earlier Task Description, TD10 (SKBdoc 1395215). Compared to the flow domain defined for SDM-PSU, the domain is expanded somewhat to the north. A consequence of this is that the bedrock parameterisation outside the SFR Regional domain (as represented by a DFN realisation) requires updated coverage (Section 4.3). The domain is delivered as an enclosed 3D CAD volume [ny_dct_120918.stl], which is converted into a DarcyTools object [Updated_WD_model_domain.dat] by means of the DarcyTools module OGN. The object is rotated into the local DarcyTools coordinate system [R_Updated_WD_model_domain.dat] by means of the Fortran code [Rotate_DT_objects.f90]. Pivot point in local coordinate system: [6400. 9200.], rotation angle: 32.58816946°.

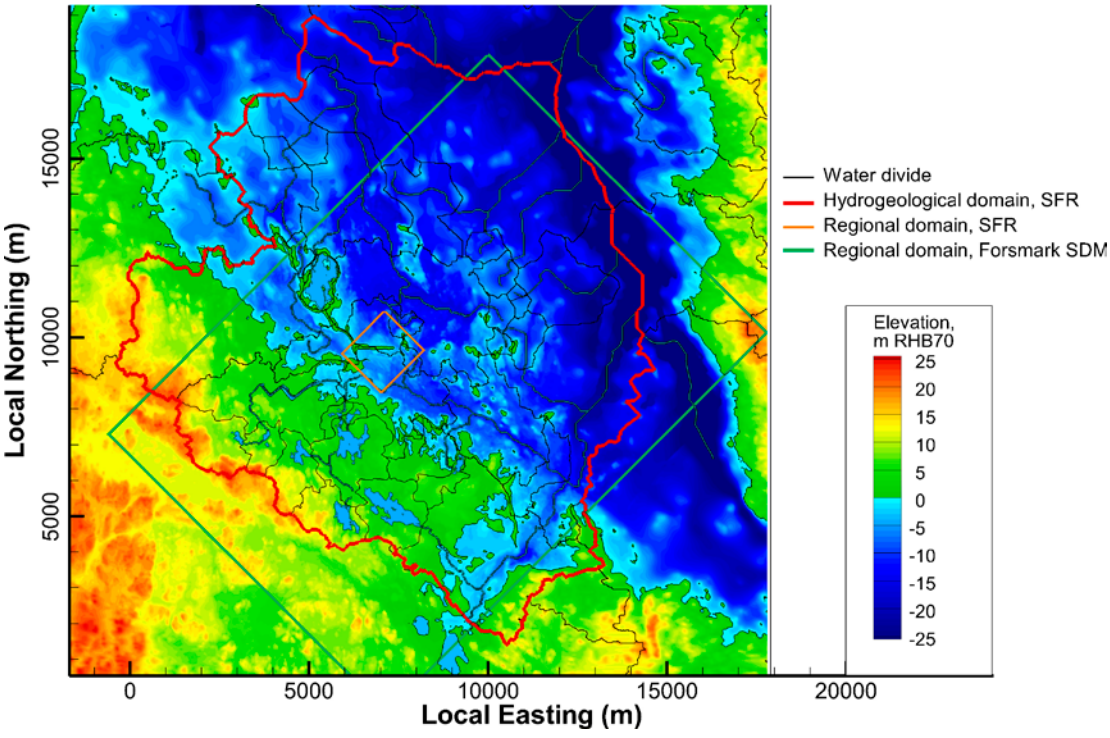

Figure 3-1. *The flow domain (red line) is the outer boundary in the model. The SFR Regional domain (orange line) is the boundary for bedrock parameterization variants studied in sensitivity analysis.*

3.1.2 SFR Regional domain

The geoscientific execution programme (SKB 2008) defined two different model scales for site-descriptive modelling: a local scale and a regional scale. The local-scale model volume covers the near-field of SFR 1 and SFR 3, but is not being used in TD11. The regional-scale model volume, on the other hand, has a key role in the sensitivity analysis, as the bedrock parameterisation variants (Table 2-2) are geometrically confined to the volume *inside* the SFR Regional domain. The bedrock properties outside this domain are kept fixed. Consequently, the SFR Regional domain is a central geometric boundary for merging two types of bedrock parameterization: 1) developed within the SR-PSU/SDM-PSU project inside the SFR Regional domain, addressed by bedrock cases, with 2) developed in the SDM-Site/SR-Site Forsmark outside this domain. The SFR Regional domain also controls grid generation and defines the boundaries for DFN generation. A discussion concerning the application of the DFN-model for model volumes is given in Appendix D. The regional model volume extends from +100 m to –1,100 m elevation. The coordinates defining the horizontal extent of the model volumes are provided in Table 3-1.

Based on the defined coordinates (Table 3-1), a DarcyTools object [SFR_modellområde_v01.dat] was constructed manually (2009-02-16). The object is rotated into the local DarcyTools coordinate system [R_SFR_modellområde_v01.dat] by means of the Fortran code [Rotate_DT_objects.f90]. Pivot point in local coordinate system: [6400. 9200.], rotation angle: 32.58816946°.

Table 3-1. Coordinates defining SFR Regional domain.

Easting (m, RT90)	Northing (m, RT90)
1631920.0000	6701550.0000
1633111.7827	6702741.1671
1634207.5150	6701644.8685
1633015.7324	6700453.7014

3.2 Tunnel geometry

Tunnel and tunnel plug geometry is defined in CAD (complete file list provided in Table B-1). The CAD data set contains: 1) the existing facility (SFR 1), 2) the planned extension (SFR 3), and 3) tunnel plug geometry for both facilities. The geometry of SFR 3 corresponds to layout alternative L1BC in TD10 (SKBdoc 1395215), but has been updated in three aspects:

1) revised geometric definitions of plugs (i.e. some plug geometries have been updated, since TD10).
2) Fix bugs that were discovered in the TD10 delivery (i.e. using geometric data to classify grid-cell functionality: backfill/plug/bedrock/particle-release locations, etc in the DarcyTools model requires that the source CAD objects are defined as watertight solids).
3) The geometric definitions of the disposal room 2BMA has been modified slightly (unexpected effects discussed below).

These geometric tunnel data have two functions in grid generation: 1) to control local grid refinement, and 2) to define grid cells in different tunnel sections, by means of so-called "DarcyTools cell markers". In effect, the tunnel data can be said to have 4 central functions in the flow modelling:

1) Local grid refinement: tunnel cells have a maximum side length of 2 m.

2) Parameterisation: so-called "DarcyTools cell markers" are used to identify the different types of backfill material in tunnel cells, which is used to set hydraulic properties (see Section 4.1; Table 4-1).

3) Particle-release points: defined as the entire volume of disposal rooms (yellow volumes in Figure 3-3; note that Silo barriers are not included). Particle-release points are also identified via DarcyTools cell markers.

4) Tunnel flow: defined as net flow over tunnel walls. Likewise, DarcyTools cell markers are used to identify tunnel walls of disposal rooms.

Combining tunnel data deliveries (TD10 and TD11)

For time efficiency, TD11 uses the same grid discretisation as in TD10. This allows initiating the time-consuming ECPM conversion prior to the final delivery of tunnel data. To ensure that the grid discretisation is identical to TD10, the following approach was taken:

1) The TD10 tunnel geometry data were used for grid refinement (the merged geometries [R_Entire_SFR1_(silo_mod).dat] and [R_SFR-1_Silo_Outer_bnd.dat]), while
2) The TD11 tunnel data (Table B-1) were used to define tunnel-cell properties and particle release locations.

The geometry of 2BMA was changed since the TD10 CAD delivery, which has implications on calculation of tunnel flow (see separate PM SKBdoc 1396127). In the TD11 definitions, 2BMA is 1.2 m wider and has also been moved 2.65 m away from 5BLA (i.e. compared to TD10 definitions; see Figure 3-2). This change in geometry for 2BMA may seem insignificant, as the side length of tunnel cells is still 2 m; however, the 2BMA tunnel cells are in direct contact with coarser bedrock cells (side length = 4 m; Figure 3-2c). DarcyTools employs a pressure-correction algorithm (controlled by the DarcyTools parameter <nbgrad>), which is implemented to hamper artificial gradients between cells of different size. Unfortunately, this algorithm was found to be numerically instable for the particular configuration of conductivity/cell-size contrasts in 2BMA (SKBdoc 1396127). This complicates the calculation of tunnel flow for 2BMA. As the solution, tunnel-flow calculation for 2BMA is *not* based on tunnel cells, but instead on surrounding *bedrock cells*. Results indicate that the error in flow calculations due to the coarse meshing outside 2BMA is reduced from a factor of 10 to only 4% if based on *bedrock cells* (SKBdoc 1396127).

Special care is taken to the definition of the Silo and its barriers (same as in TD10). Grid refinement and an *initial* cell classification are based on TD10 geometry data. The conductivity parameterisation and particle-release locations are then edited, see footnote (11) in Figure A-1, to encompass a more realistic model representation of the silo (Figure 4-2, Figure 4-3, and Table 4-1).

Data processing for DarcyTools implementation

The implementation of tunnel geometry (Figure 3-3) into the DarcyTools computational grid requires processing of delivered data (Table B-1 in Appendix B):

1) all geometric tunnel data (original CAD format *.stl) are converted into the so-called DarcyTools-object format (changing file extension to *.dat). The file conversion is a standard procedure, and managed by the DarcyTools module OGN.
2) all geometric objects (*.dat) are translated and rotated into the local model coordinate system (adding the prefix “R_”*.dat). Filename traceability from original CAD files to the applied DarcyTools-object files is provided by means of Table B-1 (Appendix B).

Manual fixes

The planned layout of SFR 3 has a vertical ventilation shaft (Figure 4-1b). By the time of the TD11 simulations, no decision had been taken concerning the potential needs to plug this shaft, and consequently no such plug geometry data were available. In TD11 it was decided to assume the ventilation shaft to be bentonite-plugged from –88 to –120 m elevation (Figure 4-1b). This is implemented via the manually constructed DarcyTools object [R_Bentonite_in_L1BC_shaft_brown_pts.dat].

One part of the SFR 3 ramp is not watertight (L1BC_2DT_del3_white.stl). Gaps in the CAD object imply ambiguity in classification of cells by cell markers (e.g. in this case, a cluster of adjacent bedrock cells become erroneously classed as part of the SFR 3 ramp in the grid generation). This leakage was mended manually (Appendix B; Table B-2).

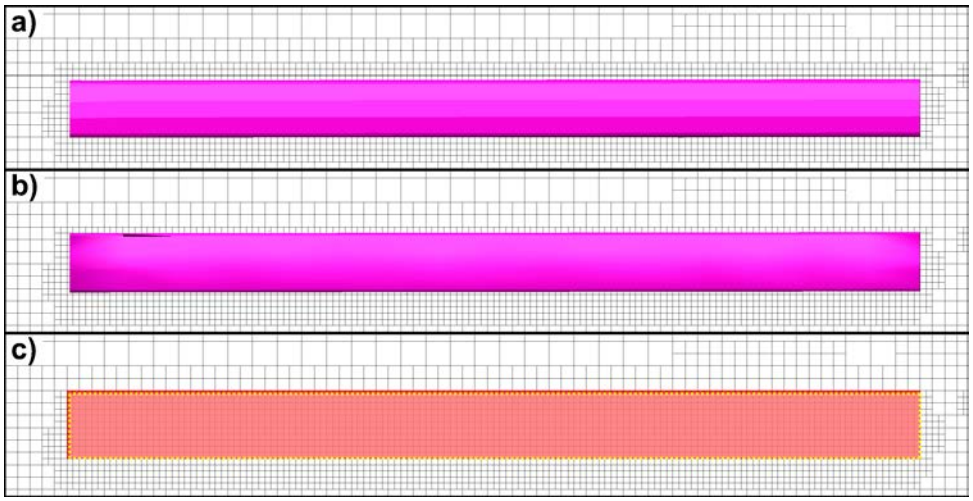

Figure 3-2. *Discretisation and cell marking of 2BMA; a) the TD10 definition of 2BMA used for grid discretisation; b) the TD11 definition of 2BMA used for cell marking, and c) cells marked as 2BMA (red) compared to actual CAD geometry (yellow dashed lines). Compared to TD10, 2BMA is 1.2 m wider and has been moved 2.65 m away from 5BLA in TD11 definitions.*

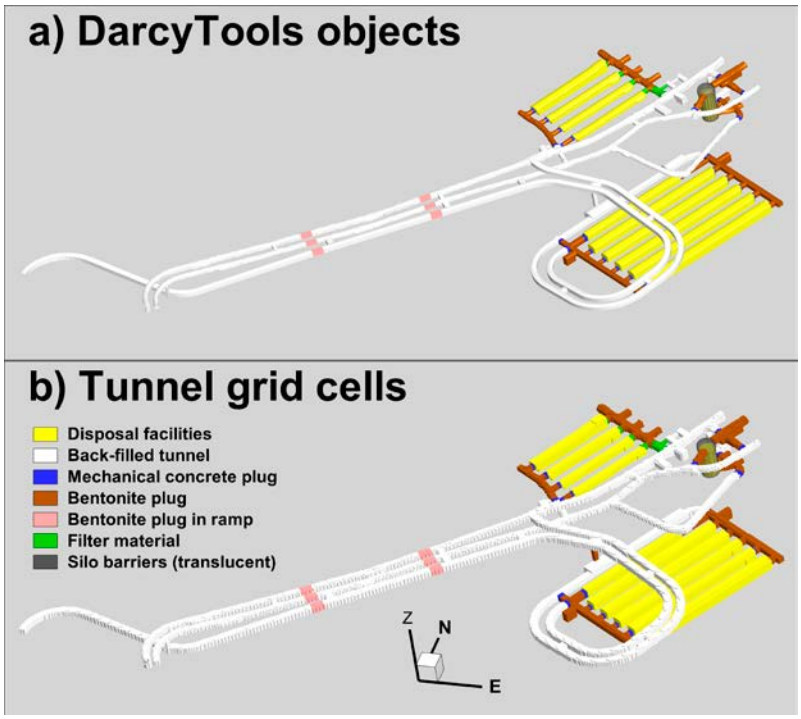

Figure 3-3. *DarcyTools objects used in discretisation of tunnel geometry.*

3.3 RLDM data

3.3.1 Topography (DEM) and Regolith layers

The model top boundary is controlled by topography data and regolith layering (less strictly referred to as "soil layering"). The regolith consists of three components: 1) Quaternary deposits, 2) filling material, and 3) peat (Table A-1). Two types of regolith data are at hand: 1) the *static* regolith model, developed within SDM Site/SR Site Forsmark, which covers the present conditions, and 2) *dynamic* predictions from the Regolith-Lake Development Model (RLDM; Brydsten and Strömgren 2013), which covers future development of regolith layering.

It should be noted that, the RLDM data are not conditioned to the current data on regolith thickness, and that therefore the static regolith model is a tempting alternative for simulating the time slice 2000AD. However, due to conceptual model differences (Figure 3-4a), the dynamic landscape model, RLDM, must be consistently used *for all time slices*. This is necessary to ensure consistency in comparisons of results between the 2000 AD and other time slices (i.e. not model artefacts arising from conceptual differences).

The modelled RLDM data are defined in terms of upper-surface elevations (Table A-1) and are delivered for all 6 selected time slices (Table 2-1). Owing to a "fixed-bedrock" model convention used (Section 3.3.5), the bedrock surface is modelled as *static* (i.e. envisaged as constant elevation over time). The bedrock surface can therefore be defined based on the original definition in the static regolith model.

The RLDM data have several different applications in modelling. The data are processed differently depending on application (see Section 3.3.2):

1) **Grid generation**: In the flow model, HSD is defined by grid cells between the bedrock surface (constant) and topography (varies over time, as modelled in RLDM). Grid generation requires pre-processing of geometric data into so-called "DarcyTools objects" (constructed from *.xyz files).
2) **HSD parameterisation**: raster data (*.asc files, after fixed-bedrock conversion) are used directly in the model parameterisation (Section 5.3.1).
3) **Maximum head at ground surface:** a so-called "basin-filled DEM" is used to define a criterion for maximum head in ground-surface cells, for a given time slice, in the so-called "Recharge-phase" simulations (see Section 5.3.2).
4) **Prescribe river-bed head:** river cells are prescribed fixed head in flow simulations, which are interpolated from a constructed input data file [River_head.in]. This file is based on river trajectories, lake thresholds, sea level, and basin-filled DEMs.
5) **Visualisation**: visual confirmation of topography and surface hydrology objects, as well as, production of figures based on *.asc files converted into TecPlot *.plt format.

Model areas outside RLDM coverage (grey-shaded parts of the Flow domain; Figure 3-4) are complemented by topography data from the static regolith model [DEM_xyz_batymetri_20120131.txt].

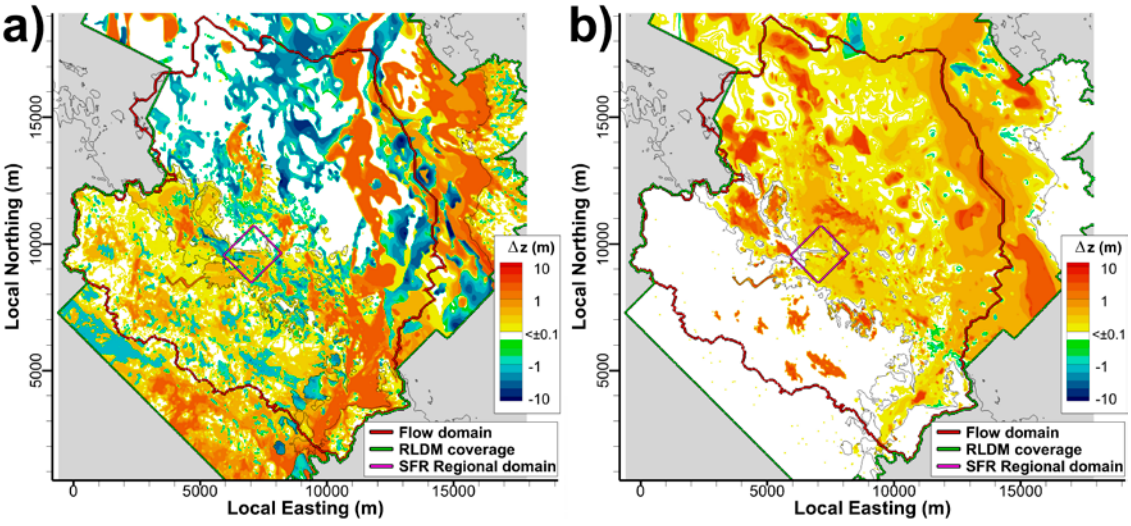

Figure 3-4. *Overview of regolith layers modelled in RLDM; a) topography discrepancy between RLDM (2000AD) and the static HSD model, and b) modelled change in topography between time slices 2000 AD and 9000AD. Area outside RLDM coverage shaded in grey.*

3.3.2 Processing RLDM data

This section describes the necessary processing of RLDM data to use as input to the DarcyTools modelling. A more detailed description, along with reference to file-management traceability is provided in Appendix A (summarised in Table A-2).

Conversion to fixed-bedrock format

One of the main objectives of TD11 is to study effects of shoreline retreat resulting from the on-going shoreline retreat. The DarcyTools simulations employ the bedrock surface as a fix reference system for elevation (i.e. at land uplift per 1970, m RHB 70). In this fixed-bedrock reference system, shoreline retreat is modelled by means of relative sea level displacement (SKB 2014c; Section 3.3.5).

However, all delivered regolith data (Table A-1) account for the land uplift (i.e. the bedrock surface elevation is not constant over time). The first step in processing RLDM data is therefore to encompass the delivered RLDM elevation data to the fixed-bedrock reference system, in which the bedrock elevation is constant over time. The elevation data are back-calculated by means of land-lift data (SKB 2014c; documentation for traceability in Table A-2).

Basin-filling the topography data to control surface head

Surface runoff is not modelled explicitly in DarcyTools. Consequently, simulations will render local excess ground-surface head at any location where the net precipitation exceeds recharge (i.e. head locally exceeding topography). This model artefact can be circumvented by controlling that the simulated head in the uppermost cell layer of the model does not exceed ground surface; the principles of this modelling approach is explained in detail in Sections 5.3.2 and 6.1. As such, the uppermost RLDM layer, also referred to as "DEM", has a central role in defining the local upper bound for simulated head at ground surface. Note that areas modelled as submerged in RLDM (lakes, rivers, or below sea level) are treated separately (Sections 3.3.3, 3.3.4, and 3.3.5).

The RLDM landscape dynamics modelling resolves only surface water above a certain cut off. Consequently, the resulting DEM contains local depressions that fall below the threshold for deterministic modelling. In reality, such depressions may be peat-filled or hold surface water, e.g. minor lakes, wetlands, or pools. Irrespectively of which, it can be argued that the simulated head in minor depressions should not be bounded by the elevation of the actual basin floor, but instead by the topographical threshold of the basin (i.e. the maximum water level, if entirely water filled). In other words, a necessary preparatory step for implementation as a head criterion in simulations is to process the topography data such that all local basins are eliminated and replaced by their basin-threshold levels. This procedure is referred to as "basin-filling", which is performed in two steps: 1) automatized basin-filling (e.g. Figure 3-5), complemented by manual editing in areas of more complex geometry (e.g. Figure 3-6). The procedure as well as the file-management traceability is explained in Appendix A.

The basin filled DEM is used as a criterion for maximum local groundwater level (i.e. the maximum head in a local depression is determined by the *geometric* threshold of the surrounding DEM elevations). Although the basin-fill is a substantial improvement for constraining surface head in flow simulations, it does *not guarantee* absence of local depressions, due to inexact matching between RLDM and the DarcyTools grid. The inexact matching is due to: 1) discretisation differences (e.g. the DarcyTools grid has variable refinement) and 2) coordinate-system differences (e.g. the DarcyTools grid has a rotated coordinate system).

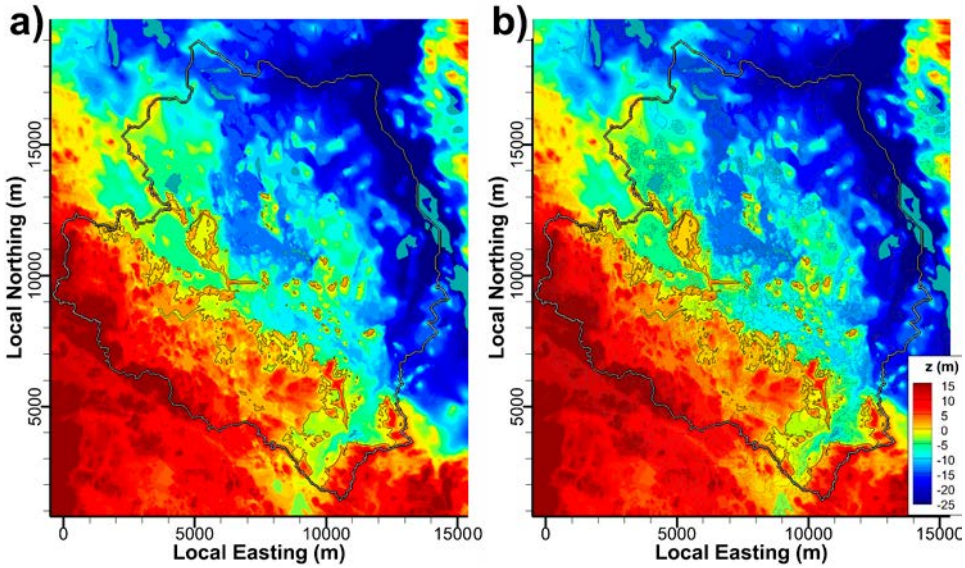

Figure 3-5. *Example of automatized basin filling above sea level; a) original DEM 9000 AD and b) filled DEM, where all topographical basins above sea level 9000 AD have been filled up to the basin threshold. Lakes shown as blue areas.*

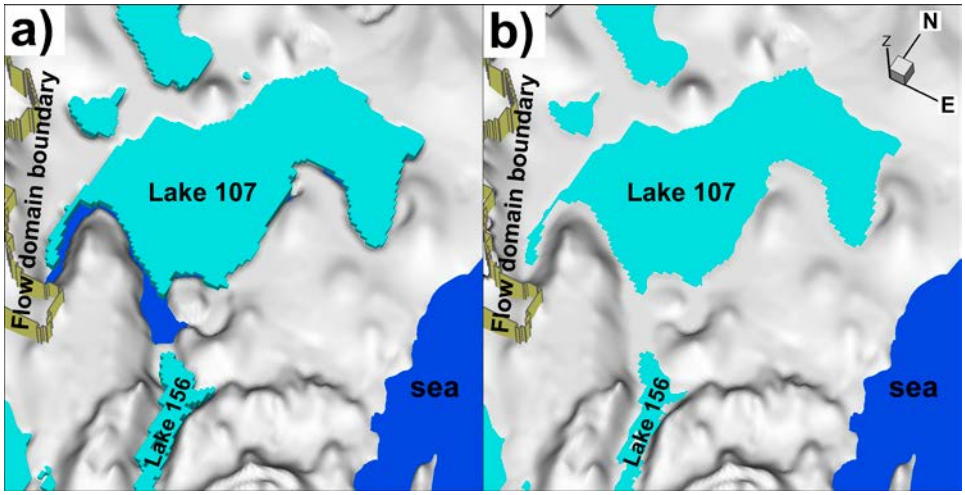

Figure 3-6. *Example of manually filled topographical basins that are partly below sea level (dark blue surface); a) identified depressions near Lake 107, and b) final filled topography.*

Constructing DarcyTools objects to implement HSD in grid generation

In the standard DarcyTools procedure, the model top boundary is defined by removal of grid cells above topography. TD11 addresses several stages of shoreline retreat (time slices), during which the topography alters due to landscape dynamics. The altering topography is honoured by using time-specific computational grids, where the model top boundary is defined by the DEM (basin-filled and in the fixed-bedrock system). For time efficiency, a *cell inactivation* method is used, where:

1) Cells are *permanently* deleted, if located above the maximum DEM elevation, determined over the time period 2000 to 9000AD.
2) Cells are *inactivated* in the time-specific grid, if only located above the DEM under a particular time slice.

The benefit of this method is that the discretisation of all time-specific grids is identical, which allows re-using the same upscaled ECPM properties for all time slices (i.e. ECPM upscaling is a time-consuming step that is only valid for a specific grid discretisation). The top boundary is defined as the uppermost layer of active cells in the grid (i.e. immediately below a permanently deleted cell or a temporarily inactivated cell). The regolith is defined as above computational cells above the bedrock surface.

3.3.3 Lakes

Lakes are used as prescribed head-boundary conditions in the flow model. More precisely, "Lake cells" are defined and refined in the computational grid by means of so-called "DarcyTools objects". Lake cells are identified via a unique DarcyTools cell marker, which is associated to a prescribed-head value in the subsequent flow simulations (Table A-3). The prescribed-head values (Table A-3) are taken from the modelled lake thresholds in RLDM. The number of lakes, as well as the spatial extent of individual lakes, varies over time. The 6 time slices studied involve a total of 107 time-specific lake objects (including geometric variants over time). Lake data are also used as fix points in defining prescribed head along riverbeds (Section 3.3.4). The geometry of RLDM lakes and rivers has been delivered in GIS vector format for all 6 time slices. As the implementation of geometry in the DarcyTools grid generation is limited to the so-called "DarcyTools object" file format, the data must first undergo a file conversion process, which is described in Appendix A.

3.3.4 Rivers

Rivers (streams and brooks rather) are also treated as prescribed head-boundary conditions in the flow model. Similar to the representation of lakes (Section 3.3.3), "river cells" are implemented in the computational grid by means of so-called "DarcyTools objects" (Table A-4). However, unlike the lakes, the riverbed head varies along the trajectory of modelled rivers, which requires a somewhat different modelling procedure (i.e. the specification of head is not as straightforward). Prior to simulations, the river head along predefined trajectories is interpolated based on geometrical conditioning. As explained in Appendix A, this conditioning involves three corner stones: 1) lake thresholds, 2) ground-surface elevation, and 3) the gradient must always slope downstream. In the flow simulations, any cell associated to a river can then be prescribed a head value that is consistent with topography data (Table A-4).

3.3.5 Relative sea level displacement in fixed-bedrock reference

One of the main objectives of TD11 is to study effects of shoreline retreat resulting from the on-going land uplift. For practical reasons, the DarcyTools simulations employ the bedrock surface as a fix reference for elevation (i.e. land uplift per 1970 AD, expressed in m, RHB 70). In this fixed-bedrock reference system, shoreline retreat is modelled by means of relative sea level displacement (Table 3-2). The relative shore level data are taken from the Global warming climate case (SKB 2014c).

Table 3-2. Relative sea level at selected time slices.

Year AD	Relative sea level*), m
2000	–0.17
2500	–3.08
3000	–5.92
3500	–8.69
5000	–16.60
7000	–26.16
9000	–34.62

*) Land uplift is expressed as a relative sea level displacement to the bedrock surface, since 1970 AD (reproduced from SKB 2014c).

4 Model parameterisation

4.1 Tunnel parameterisation

The parameterisation of tunnel plugs and Silo barriers is taken from the *intact* plug case of SKB 2014b (see Table 4-1). General tunnel sections, ramps, and disposal rooms (except the Silo), which are *not* defined as plugs, are parameterised as backfill with a conductivity of 10^{-5} m/s (Figure 4-1). The parameterisation is made via DarcyTools makers (referred to as Mk in Table 4-1), which define different tunnel sections. Special attention is given to the Silo, to encompass a realistic representation of the details in the parameterisation and particle-release locations (Figure 4-3).

The evaluated performance measures reflect only the bedrock outside tunnel walls (Section 5.4.2), and hence the hydraulic properties of tunnel backfill do not, *per se*, affect the particle tracking results (i.e. the backfill has only indirect effects, via its influence on the flow field).

Table 4-1. Tunnel backfill parameterisation (Figure 4-1 and Figure 4-3).

	Mk	Tunnel	Conductivity (m/s)	Description in Swedish (SKB 2014b)
SFR 1	11 12 13 14	1BTF 2BTF 1BLA 1BMA	10^{-5}	Rock vaults, assumed to be backfilled by macadam[1]. (Non-filled, open section of 1BLA not resolved).
	15/21[2]	Silo interior	5×10^{-9}	Outer concrete cylinder, inner vertical shafts with intervening concrete walls, waste packages and concrete grouting.
	16	1DT, 1BT	10^{-5}	Ramp backfilled with macadam[1].
	21[3]	Silo exterior	10^{-5}	Compacted fill of friction material, e.g. crushed rock or macadam and, at the very top, with cement-stabilized sand.
			10^{-9}	Compacted fill of bentonite/sand mixture (10/90 percentage by weight) at the bottom and top of the silo.
			Single-layer walls: $K(z) = 2.1\times10^{-10} + 1.6\times10^{-12}*\mathbf{z}$	Pure bentonite in silo walls, with hydraulic conductivity expressed as function of elevation, z (m RHB70), due to variable degree of self-compaction. In the lower part $K(z) \approx 9\times10^{-12}$ m/s and the upper part $K(z) \approx 9\times10^{-11}$ m/s (SKB 2014b).
SFR 3	22 23 24 25 26 27	2BLA 3BLA 4BLA 5BLA 2BMA 1BRT	10^{-5}	Rock vaults, assumed to be backfilled by macadam[1]. (Non-filled, open section of BLA caverns not resolved).
	28	1RTT	10^{-5}	Ramp backfilled with macadam[1].
Intact plugs	30[4]	Blue	10^{-6}	Mechanical concrete plug (i.e. for mechanical support).
	31	Brown	10^{-10}	Hydraulic tight section with bentonite.
	32[4]	Green	10^{-6}	Earth-dam plug, consisting of transition material (e.g. 30/70 bentonite crushed rock).
	33	Pink	5×10^{-10}	Plugs in access tunnels, made up of 10 metre long tight hydraulic sections of bentonite surrounded by concrete plugs for mechanical support .

[1] The hydraulic conductivity in macadam is high, initially higher than 10^{-2} m/s. For numerical stability in modelling, the lower value 10^{-5} m/s is assumed in a project decision.

[2] The silo is divided into two DarcyTools cell markers: particles are released from the inner concrete cylinder (Mk = 15), which is enclosed by barriers from which no particles are released (Mk = 21). The value is based on Holmén and Stigsson (2001).

[3] Conductivity parameterisation of the silo exterior not based on cell marking, but differentiated by geometric bounds based on a combined interpretation of CAD data and SKB 2014b (see Figure 4-3).

[4] The conductivity value is assumed in a project decision.

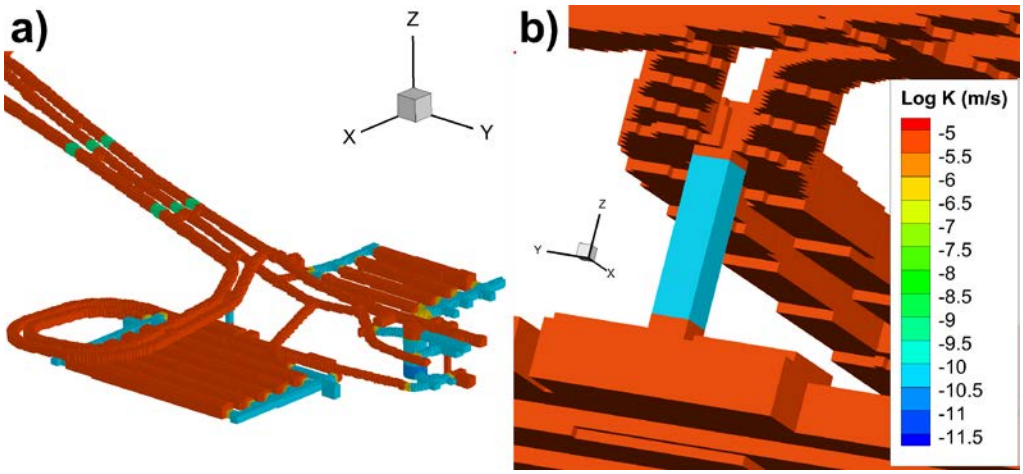

Figure 4-1. *Conductivity parameterisation of tunnel backfill; a) SFR 1 and SFR 3, b) bentonite-filling in ventilation shaft assigned from –88 to –120 m elevation.*

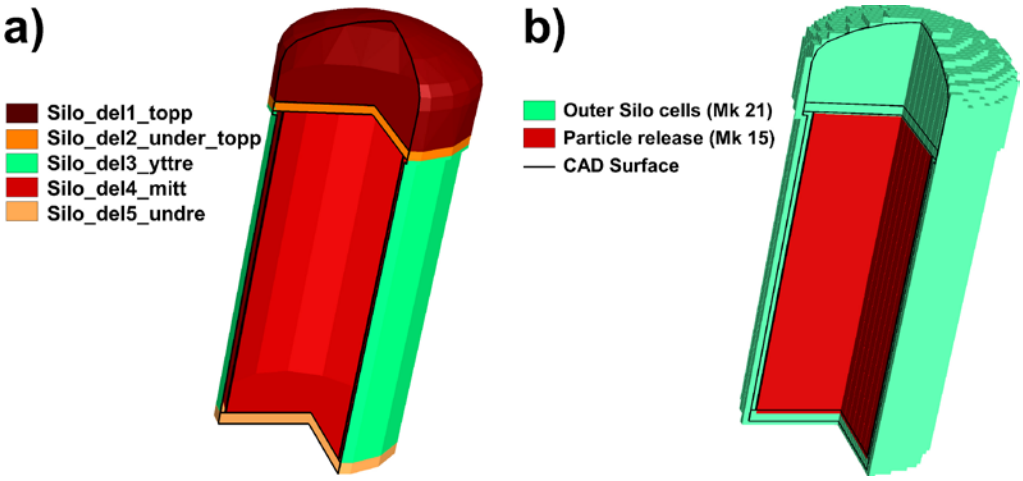

Figure 4-2. *Cell marking of the discretised Silo; a) Silo sub-volumes defined by CAD data (Table B-1), differentiated by colour, and b) defined particle-release location (CAD definitions in black lines).*

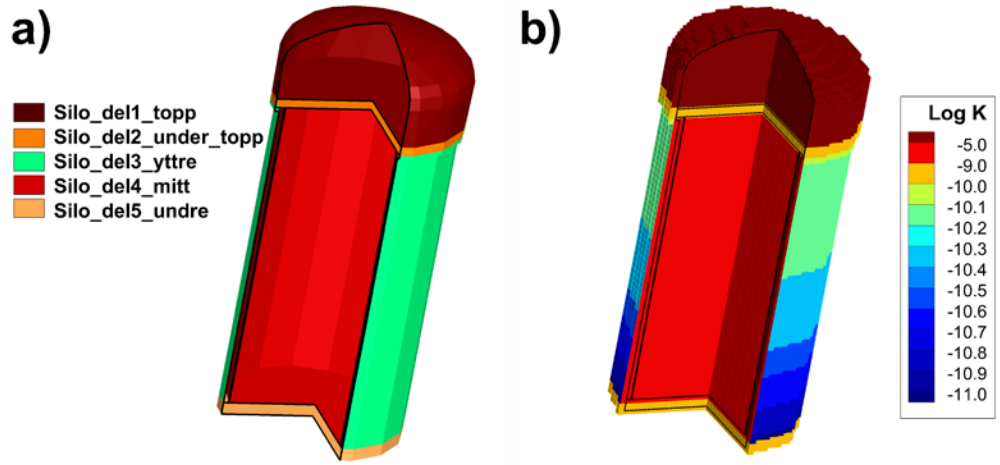

Figure 4-3. *Parameterisation of the Silo; a) Silo sub-volumes defined by CAD data (Table B-1), differentiated by colours, and b) assigned conductivity (CAD definitions in black lines).*

4.2 Bedrock cases inside SFR Regional domain

The performance of the groundwater flow model is subject to *heterogeneity* and *conceptual uncertainty* in the bedrock parameterization. In the groundwater flow model, the bedrock is conceptually divided into two hydraulic domains: HRD and HCD. Heterogeneity is addressed by means of stochastic realisations, while conceptual uncertainties in HCD-parameterisation are addressed by means of variants. The combined effect of uncertainty/heterogeneity in bedrock parameterisation is studied by means of a sensitivity analysis of 17 bedrock cases (Table 2-2). Here, a "bedrock case" refers to a combination of parameterization variants of the two hydraulic domains (Figure A-1). "HRD variants" are combined stochastic realisations of discrete fracture networks (DFN) and Unresolved PDZs (as defined in Öhman et al. 2013; Section 4.2.1). "HCD variants" refer to parameterization variants of deterministic structures, i.e. structures for which the geometry is kept fixed, but where the conceptual parameterization uncertainties and within heterogeneity is addressed by means of parameterisation variants (Section 4.2.2).

SBA structures

As no SBA structures are in direct contact with disposal rooms in SFR 1 or SFR 3, variants of SBA structures are not addressed in the sensitivity analysis. Similarly to earlier TDs, all simulations include a fixed SBA variant, in which all 8 structures are included (SBA1 to SBA8). Used file is: [R_Parameterized_SFR_SBA1_to_SBA8], based on parameterisation in Appendix B and H in Öhman et al. (2012).

4.2.1 HRD variants (coupled DFN and Unresolved PDZ realisations)

The HRD represents the rock mass domain outside deterministic deformation zones and consists of stochastic realisations of connected discrete fracture networks (DFN) and Unresolved PDZs (conceptually modelled as connected to deformation zones of the Southern and Northern boundary belts; Öhman et al. 2012). The connectivity of the DFN/Unresolved PDZs is coupled in the stochastic realisations (i.e. the connected fracture network of RXX, is coupled to the stochastic realisation RXX of Unresolved PDZs). An explanation regarding cut offs applied to delimit the size range of modelled fractures with respect to model domain is provided in Appendix D.

Three stochastic HRD realisations are selected to represent the HRD heterogeneity (Table 4-2; Figure 4-4). As part of TD05 (SKBdoc 1395200), realisations R18 and R85 were identified as "optimistic" and "pessimistic", respectively, for inflow to disposal rooms of SFR 1. R85 was selected as pessimistic, as it had the largest number of fractures intersecting more than one disposal room in SFR 1. Vice-versa, R18 had no fractures that intersect more than one disposal room. Similarly, an additional realisation, R03, was selected in TD11 to represent a "pessimistic" case for SFR 3. The statistics of the three selected realisations are compared to a larger ensemble of DFN realisations in Figure 4-5 and Figure 4-6.

Table 4-2. HRD realisations (Discrete fracture network + Unresolved PDZs).

Variant	Files	Description
R03	R_SFR_DFN_connected_R03_L1BC_knwn R_Unresolved_PDZ_R03_knwn	Pessimistic for SFR 3 (4BLA, 5BLA and 2BMA), but also for 1BMA
R18	R_SFR_DFN_connected_R18_L1BC_knwn R_Unresolved_PDZ_R18_knwn	Optimistic realisation for SFR 1, used earlier (no large fractures connecting disposal rooms in SFR 1)
R85	R_SFR_DFN_connected_R85_L1BC_knwn R_Unresolved_PDZ_R85_knwn	Pessimistic realisation for SFR 1, used earlier (large fractures connecting disposal rooms in SFR 1)

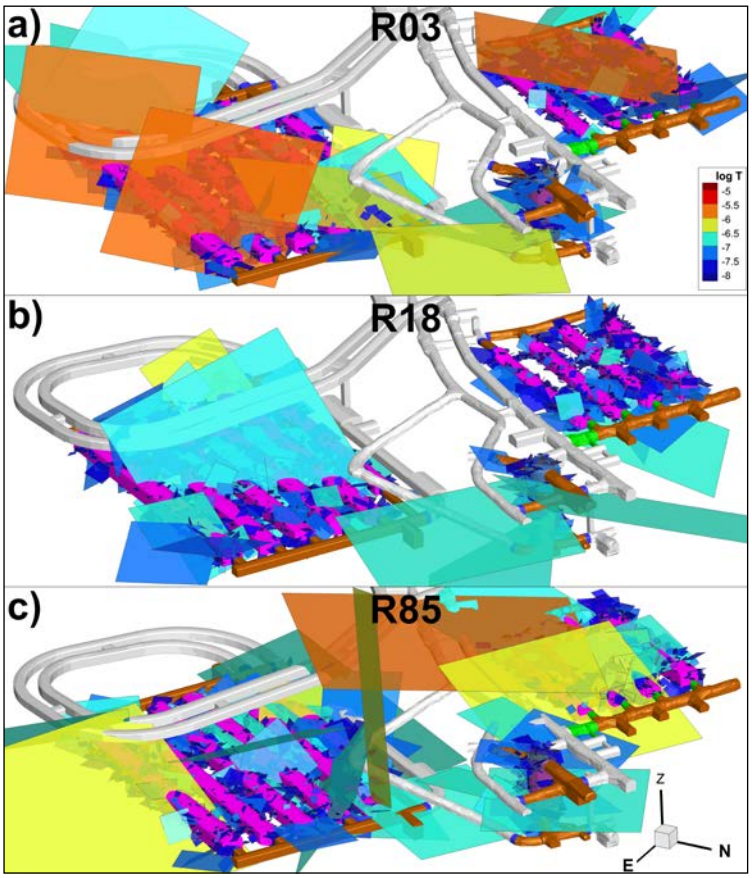

Figure 4-4. *Transmissivity of stochastic fractures intersecting the disposal rooms of SFR 1 and SFR 3; a) realisation R03, b) realisation R18, and c) realisation R85.*

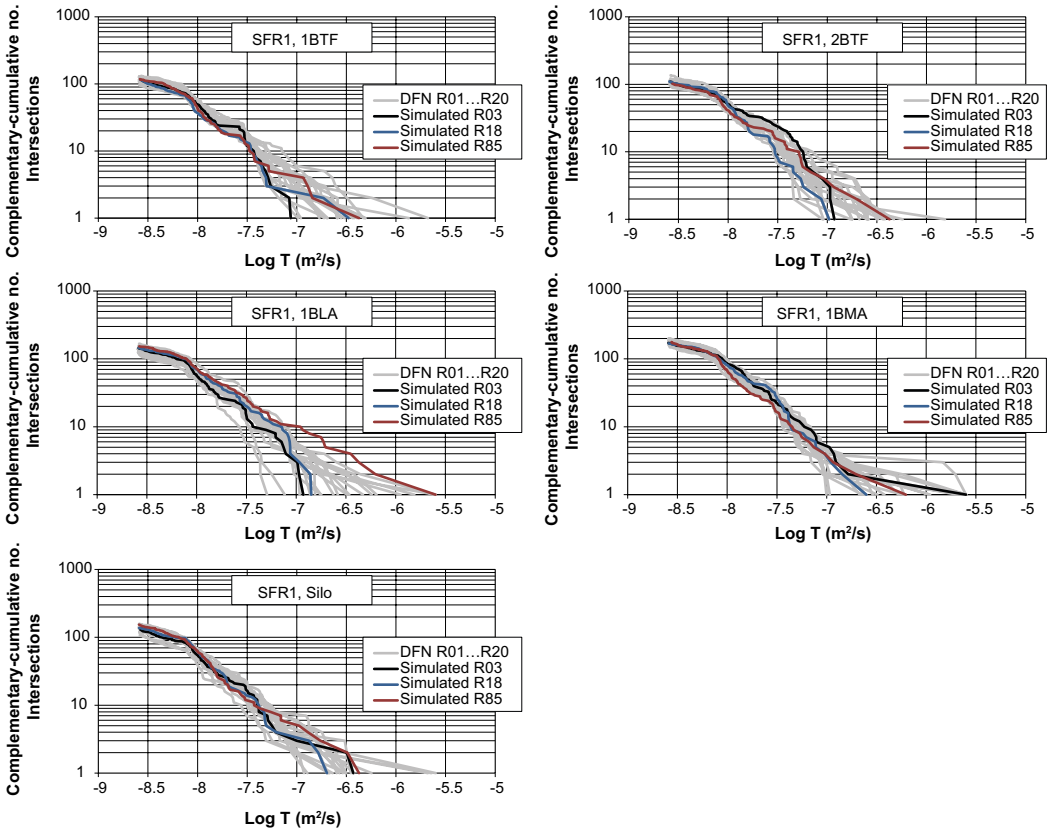

Figure 4-5. *Complementary-cumulative transmissivity distribution of fractures intersecting SFR 1.*

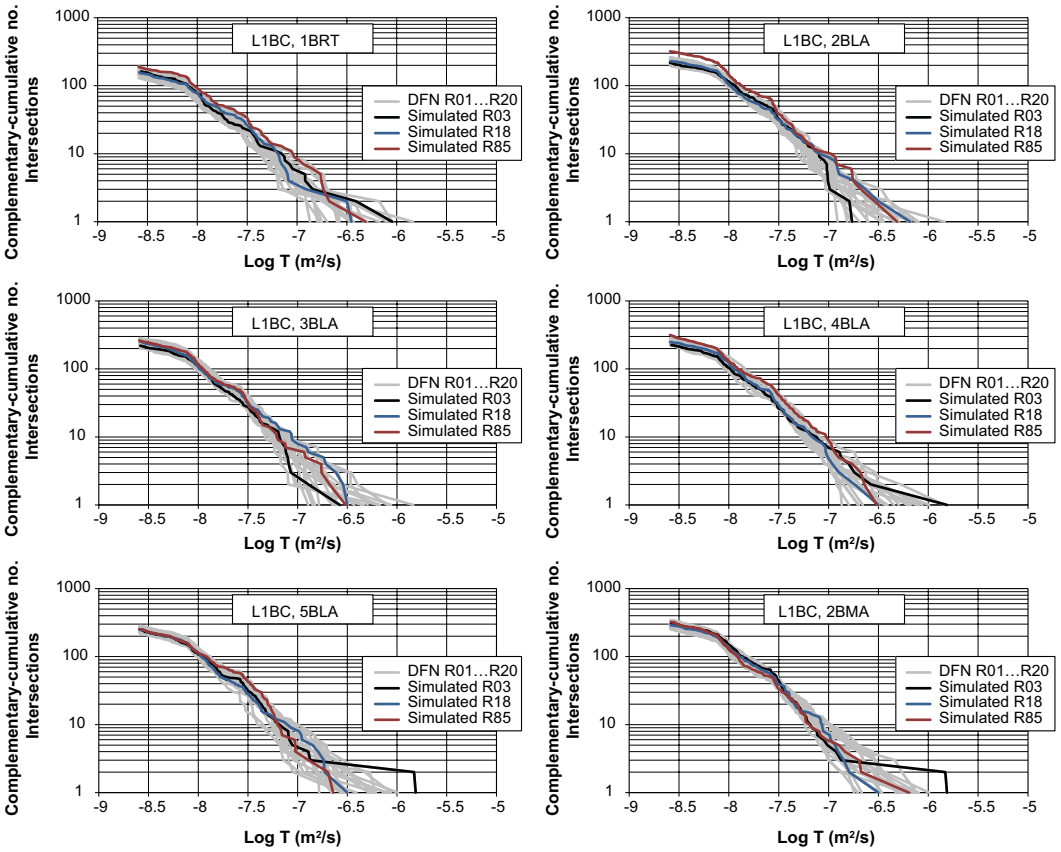

Figure 4-6. *Complementary-cumulative transmissivity distribution for fractures intersecting SFR 3 (L1BC).*

4.2.2 HCD parameterisation concepts

The confidence in deterministic HCD geometry is relatively high, in comparison to uncertainties in hydraulic parameterisation. Different parameterisations are therefore tested, while their geometry is kept fixed. Due to intersections with disposal rooms, the most critical uncertainties are expected to be: 1) ZFMNNW1209 for the SFR 1 and 2) ZFMWNW0835 and ZFMENE3115 for SFR 3. The SBA structures are not in direct contact to disposal rooms, and hence, they are not varied in model alternatives.

The uncertainty in HCD transmissivity parameterisation is demonstrated by elaborating four different concepts:

1) **Transmissivity variability**: HCDs are modelled as either homogeneous (Base Case and HOM in Table 4-4) or heterogeneous (HCD realisations R01 and R07, selected as "median" and "pessimistic", respectively, based on preceding simulations in TD08, SKBdoc 1395214).

2) **Borehole conditioning**: Local borehole data in the elevation interval of the planned SFR extension indicate low transmissivity of ZFMWNW0835 and ZFMENE3115. The confidence in borehole conditioning is unclear (i.e. how far can data be extrapolated deterministically without being overly optimistic?). Conditioned model alternatives are regarded to be optimistic.

3) **Depth trend**: The SFR data set is insufficient for delineating the character of HCD transmissivity with depth (Öhman et al. 2012). Two alternatives are compared: 1) assuming the established HCD depth trend in SDM-Site Forsmark, where transmissivity is reduced by an order of magnitude over the interval $k = 232.5$ m (transmissivity parameterisation presented in SKB (2013, Appendix 6), versus, 2) no depth trend (transmissivity parameterisation presented in Table 4-3). Assuming the depth trend may lead to a higher transmissivity parameterisation of ZFMWNW0835 and ZFMENE3115, which have been identified as key deformation zones for the performance measures of SFR 3.

4) **Anisotropic Southern boundary belt**: In SDM-Site Forsmark, Singö deformation zone was hypothesised as anisotropic (less transmissive across the structure). This notion is tested in one of the 17 bedrock cases (referred to as BASE_CASE2), where the transversal transmissivity contribution from four zones of the Southern Belt is *eliminated*. The preparation of BASE_CASE2 input files are presented in Appendix A.

Table 4-3. Transmissivity parameterisation for HCD variant without depth trend.

Zone	Log $T_{constant}$	σ_{LogT}	Log $T_{eff}(0)$	$\sigma_{LogTeff(0)}$	Basis for determining $T_{constant}$
ZFM871[1)]	–5.7	0.93	–5.2	80	Taken as T_{eff}(z = –120 m)
ZFMA1[2)]	–7.2	0.55	–4.8	0.55	Taken from PFM 2.3; $T_{eff}(z_{max}$ = –550 m in SFR Reg dom)
ZFMB10[2)]	–5.7	0.55	–4.8	0.55	Taken from ZFMA1 (PFM); $T_{eff}(z_{max}$ = –200 m in SFR Reg dom)
ZFMENE3115[4)]	–7.4	0.58	–6.5	0.91	Average transmissivity of all intercepts
ZFMENE3135	–7.4	0.55	–6.7	0.55	Average of all NNE to ENE HCDs (new data)
ZFMENE3151	–7.4	0.55	–6.7	0.55	Average of all NNE to ENE HCDs (new data)
ZFMENE8031	–7.4	0.55	–6.7	0.55	Average of all NNE to ENE HCDs (new data)
ZFMENE8034	–7.4	0.55	–6.7	0.55	Average of all NNE to ENE HCDs (new data)
ZFMNE0870	–6.7	0.51	–6.3	0.46	Average transmissivity of all intercepts
ZFMNE3112	–7.4	0.6	–6.6	0.62	Average transmissivity of all intercepts
ZFMNE3118	–6.9	0.1	–6.6	0.29	Average transmissivity of all intercepts and non-transmissive Tunnel intercept
ZFMNE3134	–7.4	0.55	–6.7	0.55	Average of all NNE to ENE HCDs (new data)
ZFMNE3137	–8.0	0.48	–7.3	0.3	Average transmissivity of all intercepts
ZFMNNE0725[3)]	–4.5	0.55	–4.0	0.55	Taken from PFM 2.3; T_{eff}(z = –120 m)
ZFMNNE0869	–4.9	0.26	–4.6	0.28	Average transmissivity of all intercepts
ZFMNNE2308[3)]	–6.6	0.55	–6.1	0.55	Taken from PFM 2.3; T_{eff}(z = –120 m)
ZFMNNE3130	–7.4	0.55	–6.7	0.55	Average of all NNE to ENE HCDs (new data)
ZFMNNE3264	–7.4	0.55	–6.7	0.55	Average of all NNE to ENE HCDs (new data)
ZFMNNE3265	–7.4	0.55	–6.7	0.55	Average of all NNE to ENE HCDs (new data)
ZFMNNE3266	–7.4	0.55	–6.7	0.55	Average of all NNE to ENE HCDs (new data)
ZFMNNW0999[3)]	–8.3	0.55	–7.8	0.55	Taken as T_{eff}(z = –120 m) from NNW group average in PFM 2.3
ZFMNNW1034	–5.0	0.17	–4.4	0.27	Average transmissivity of all intercepts
ZFMNNW1209	–6.1	0.55	–5.9	0.55	Average transmissivity of all intercepts
ZFMNNW3113[3)]	–8.3	0.55	–7.8	0.55	Taken as T_{eff}(z = –120 m) from NNW group average in PFM 2.3
ZFMNS3154	–5.0	0.55	–4.4	0.55	Assumed similar to ZFMNNW1034
ZFMNW0002[3)]	–5.1	0.55	–4.6	0.55	Taken from PFM 2.3; T_{eff}(z = –120 m)
ZFMNW0805a	–5.1	0.51	–4.7	0.55	Average transmissivity of all intercepts
ZFMNW0805b	–5.9	0.53	–5.5	0.48	Average transmissivity of all intercepts
ZFMWNW0001[1)]	–4.4	0.62	–3.9	0.56	Taken as T_{eff}(z = –120 m)
ZFMWNW0813	–6.6	0.55	–5.9	0.55	KFM11A and non-transmissive Tunnel intercept
ZFMWNW0835[4)]	–6.3	0.4	–5.2	0.71	Average transmissivity of 2 intercepts in KFR27
ZFMWNW0836[3)]	–7.6	0.55	–7.1	0.55	Taken from PFM 2.3; T_{eff}(z = –120 m)
ZFMWNW1035[1)]	–5.5	1.3	–5.0	0.64	Taken as T_{eff}(z = –120 m)
ZFMWNW1056[3)]	–7.6	0.55	–7.1	0.55	Taken from PFM 2.3; T_{eff}(z = –120 m)
ZFMWNW3259	–6.2	0.55	–5.3	0.55	KFM11A and non-transmissive Tunnel intercept
ZFMWNW3262	–5.0	0.55	–4.6	0.55	Average transmissivity of all intercepts
ZFMWNW3267	–7.7	0.55	–6.7	0.55	Average transmissivity of all intercepts
ZFMWNW3268	–6.4	0.55	–5.8	0.55	Average of WNW to NW set (NEW data)
ZFMWNW8042	–6.6	0.55	–6.0	0.55	Single intercept transmissivity
ZFMWNW8043	–7.1	0.55	–6.5	0.55	Average of WNW to NW set (NEW data)

[1)] Zones calibrated to flow simulations (Öhman et al. 2013), are adjusted to $T_{constant} = T_{eff}(–120\ m) = 10^{(\log Teff(0) – 120/232.5)}$.

[2)] Two horizontal zones lacking borehole support from the SFR Site investigation are assigned the value at maximum elevation in the depth-dependent SDM-Site Forsmark model, i.e. $T_{constant} = T_{eff}(z_{max}) = 10^{(\log Teff(0) + zmax/232.5)}$. The reason is to reduce artificially high $T_{eff}(0)$ arising from an assumed depth trend.

[3)] Zones lacking borehole support from the SFR Site investigation are assigned the value at –120 m elevation in the depth-dependent SDM-Site Forsmark model, i.e. $T_{constant} = T_{eff}(–120\ m) = 10^{(\log Teff(0) – 120/232.5)}$.

[4)] Two effects are noted for the two key zones (yellow marking) for the planned SFR extension: their transmissivity is reduced by c. an order of magnitude, and their standard deviation in log T is almost halved.

The current HCD parameterisation is based on an assumed depth trend in transmissivity (or expectation value in heterogeneous cases); the method has been explained in Öhman et al. (2013). Addressing the effects of *absence* from depth trend in HCD transmissivity, requires a revision of hydraulic borehole-intercept data. The resulting HCD parameterisation, based on *an assumed absence of depth-dependency*, is referred to as $T_{constant}$ (Table 4-3). Two principles are used to calculate the revised constant HCD transmissivity (or constant expectation value), $T_{constant}$:

1) In straightforward cases, $T_{constant}$ is calculated as the geometric mean transmissivity of available borehole intercepts for each zone, and data are pooled for HCDs with scarce or unavailable intercepts (i.e. same principles as for $T_{eff}(0)$ values in Öhman et al. (2013), but intercept transmissivity data are used directly *without* adjusting to T_0, at z = 0 m).
2) In less straightforward cases (indicated by footnotes in Table 4-3), $T_{constant}$, is based on the existing model (i.e. the depth-dependent parameterisation), but adjusted to a specific elevation. For SR-Site, the relevant elevation for transferring "depth-dependent" transmissivity to "constant" transmissivity is –120 m. In other words, $T_{constant} = T_{eff}(z = -120\ m) = 10^{(\log Teff(0) - 120/232.5)}$. This principle was used: a) where zone parameterisation is taken from SDM-Site Forsmark and b) where zone parameterisation is not entirely based on borehole data (ZFM871, ZFMWNW0001, and ZFMWNW1035). The –120 m elevation does not provide very realistic values for two deep sub-horizontal zones (ZFMA1 and ZFMB10); instead their maximum elevation is used to calculate $T_{constant}$.

4.2.3 Implementation of selected HCD variants

The four concepts can be combined to form a number of HCD variants; ten of these parameterisation variants (Table 4-4) are selected for the sensitivity analysis in TD11 (see Table 2-2). The ten selected HCD variants are prepared in an input-file format that is accepted by DarcyTools; the details on this processing and name conventions for traceability is presented in Appendix A (Table A-5).

ZFMNNW1209 is of particular significance for the existing SFR 1, as it intersects all four rock caverns (Figure 4-7). Two zones, ZFMWNW0835 and ZFMENE3115, have been identified as particularly significant for the planned extension SFR 3. As a demonstration, a few HCD parameterisation variants are shown in context of field data (Figure 4-7, Figure 4-8 and Figure 4-9). Heterogeneity is parameterised by superimposing a lognormal-distributed random component. This random component follows $N(0,\sigma_{HCD})$, where σ_{HCD} is the standard deviation of logarithmic transmissivity of an individual HCD, or a group of HCDs (tabulated in Table 4-3, for cases without depth trend, and in SKB (2013, Appendix 6) for the depth dependent cases). Extreme values, outside 95% variability, are rejected and re-sampled. Note that for a given realisation, RXX, the distribution of the random component is identical, regardless of magnitude in σ_{HCD}, conditioning, or imposed depth trend.

Table 4-4. Notation of HCD variants used in Table 2-2.

HCD variant[1)]	Conditioning	Depth trend[2)]	Transmissivity variability[3)]
BASE_CASE1	Yes	Yes	Homogeneous
BASE_CASE2	Yes	Yes	Homogeneous, Anisotropic SBB
nc_DEP_HOM	No	Yes	Homogeneous
nc_NoD_HOM	No	No	Homogeneous
CD_DEP_R01	Yes	Yes	Heterogeneous, R01
nc_DEP_R01	No	Yes	Heterogeneous, R01
CD_DEP_R07	Yes	Yes	Heterogeneous, R07
nc_DEP_R07	No	Yes	Heterogeneous, R07
nc_NoD_R01	No	No	Heterogeneous, R01
nc_NoD_R07	No	No	Heterogeneous, R07

[1)] The "known-fracture" format filenames are "**Param_SFR_HCD_<HCD variant>**".

[2)] For depth-trend cases, transmissivity is parameterised based on SKB (2013, Appendix 6). Cases without depth trend are parameterised according to Table 4-3 (this appendix).

[3)] Transmissivity variability is modelled as a superimposed random component assumed to follow the log-normal distribution, i.e. Log T + N(0, σ_{HCD}), where σ_{HCD} is taken from SKB (2013, Appendix 6) or Table 4-3 for the cases with depth trend and without depth trend, respectively. In homogeneous cases, $\sigma_{HCD} = 0$.

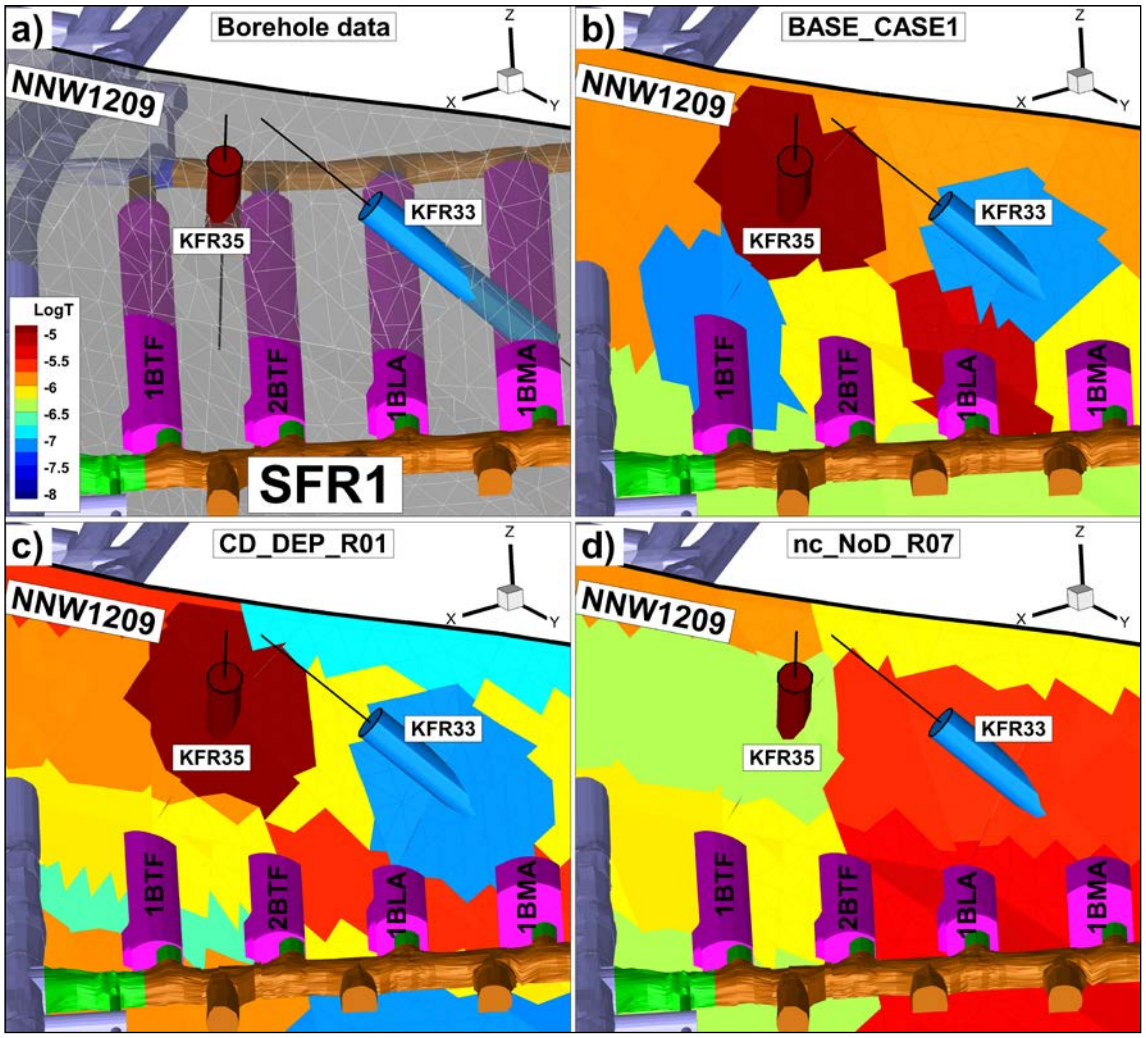

Figure 4-7. *Three parameterisation variants of ZFMNNW1209, which is the two key zone for the existing SFR 1; a) triangulated HCD geometry and borehole-intercept data (cylinders), b) Base case with depth trend and local conditioning at borehole and tunnel intercepts, c) borehole-conditioned heterogeneous realisation R01 with depth trend, and d) non-conditioned realisation R07 without depth trend.*

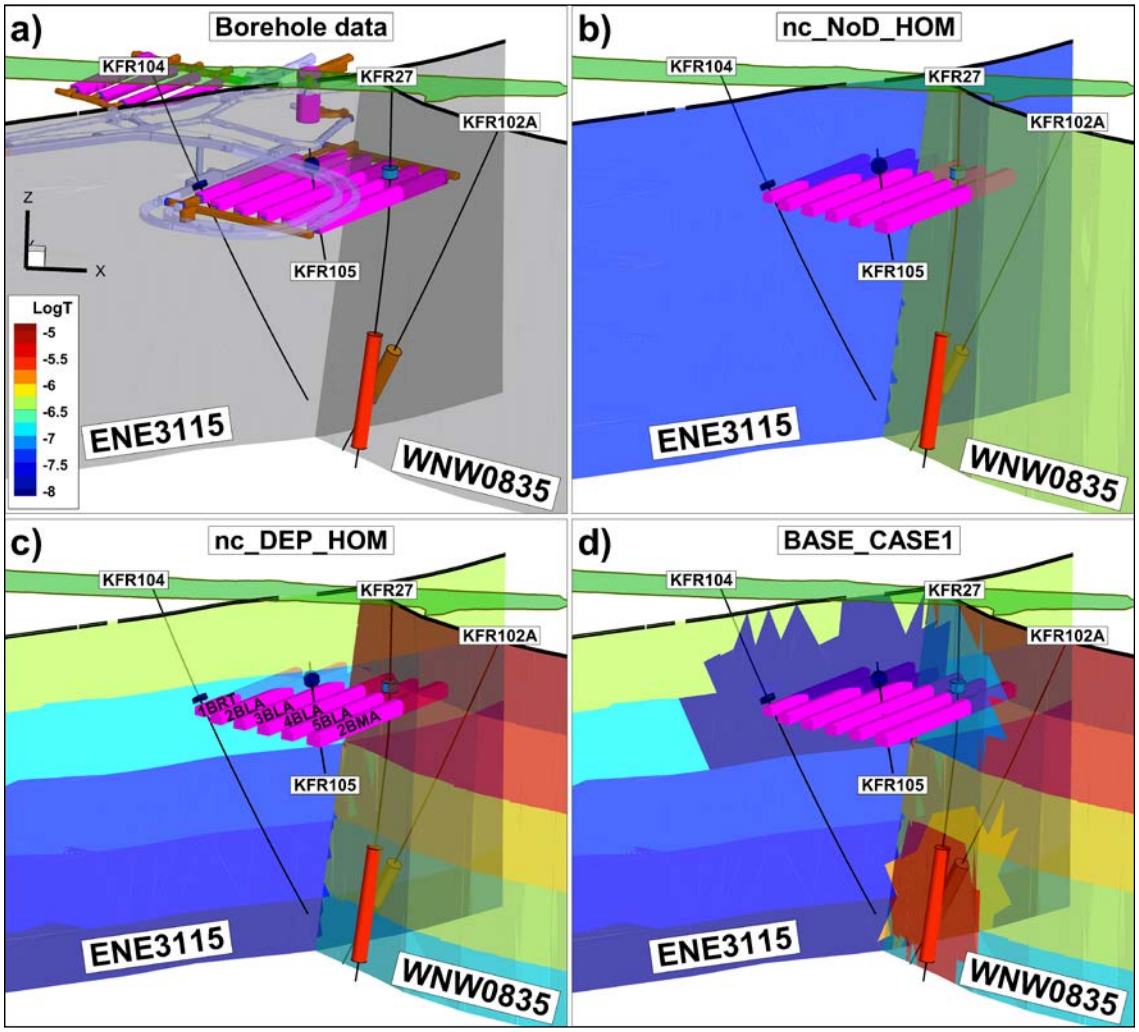

Figure 4-8. *Homogeneous HCD variants of the two key zones for the planned extension; a) borehole-intercept data (cylinders), b) homogeneous transmissivity without depth trend, c) homogeneous with depth trend, and d) borehole-conditioned Base case with depth trend.*

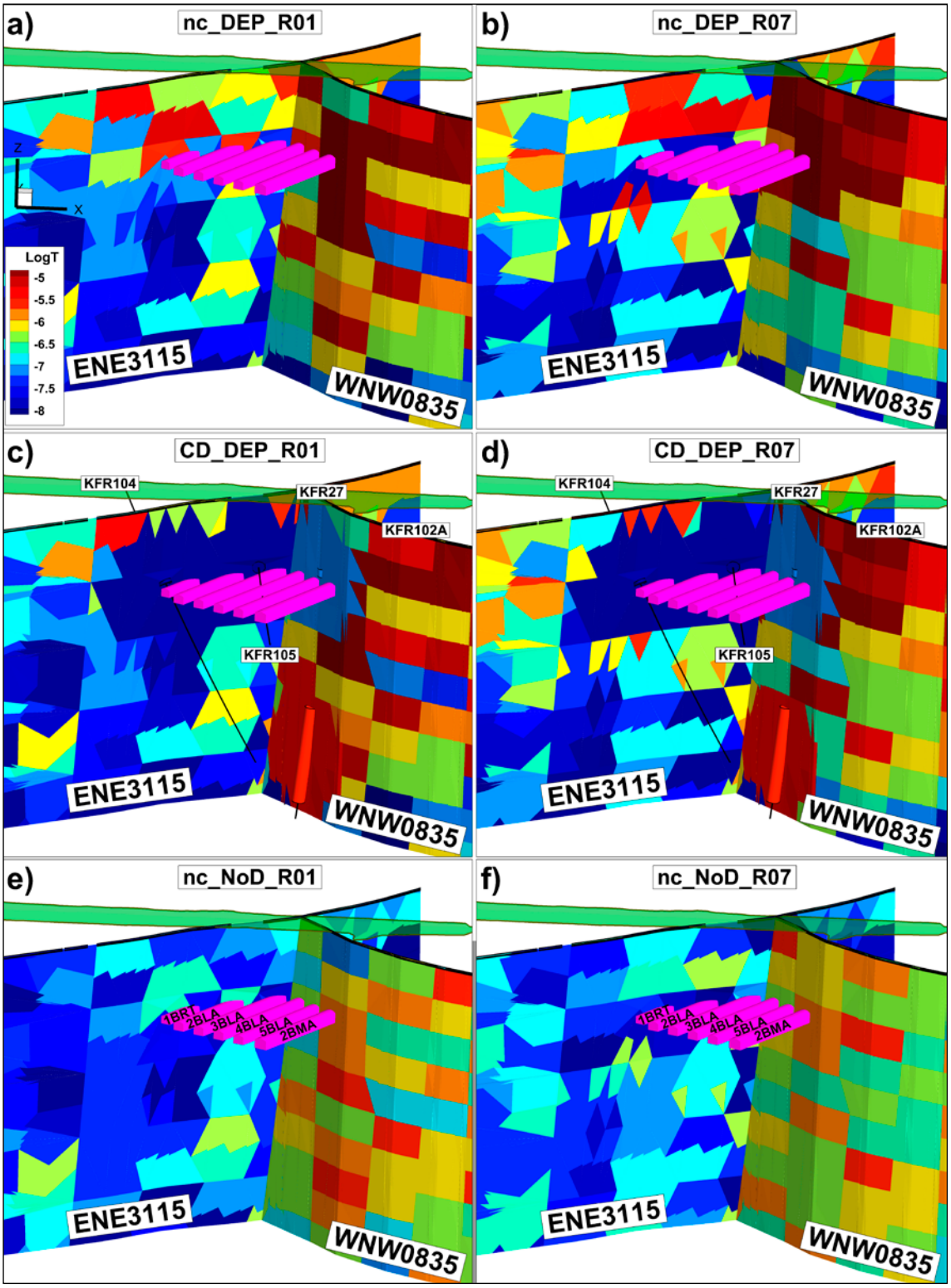

Figure 4-9. *Heterogeneous HCD variants of the two key zones for the planned extension; the depth-dependent variants are: a) and b) non-conditioned realisations R01 and R07, c) and d) conditioned realisations R01 and R07, and e) and f) the corresponding non-conditioned variants without depth dependence.*

4.3 Bedrock outside SFR Regional domain

Earlier analyses have demonstrated that the performance measures of SFR are primarily controlled by the bedrock parameterisation in the near-field (i.e. local structures and local fracture network). The sensitivity analysis of the bedrock parameterisation is therefore confined to the SFR Regional domain (Figure 3-1). The bedrock description outside the SFR Regional domain is taken from SR-Site/SDM-Site Forsmark and kept constant in all model setups, as explained in Appendix A (Table A-6). Combining input data from two models requires special care to avoid overlapping artefacts at the domain interface, along which the two models are being merged, which is explained in detail in Öhman et al. (2013).

In essence, the parameterisation outside the SFR Regional domain is identical to what was used in TD10. However, a consequence of the updated model flow domain (Figure 3-1) is that the coverage of the DFN realisation must be expanded to fully cover the new flow domain (this was done during TD10). The data-file processing undertaken to conform the DFN coverage to the updated flow domain is described in Appendix A.

It should be noted that the DFN realisation outside SFR Regional domain lack full DFN coverage above z = 0 m elevation, which causes an artificially low hydraulic conductivity in bedrock above c. z = –10 m elevation and has implications to bedrock recharge in the elevated parts of the Forsmark inland. To compensate this, a minimum bedrock conductivity of 3×10^{-8} m/s is assigned above z = –10 m elevation (see Table 4-5). All fracture files representing the bedrock outside the SFR Regional domain are specified in Appendix A (Table A-6).

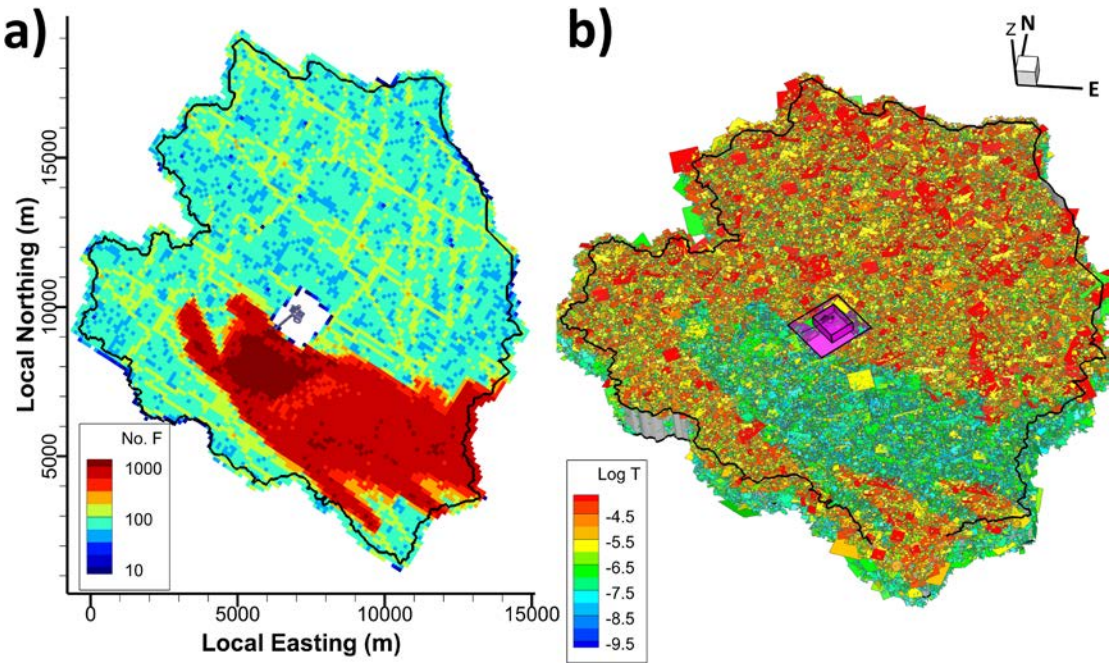

Figure 4-10. *HRD outside SFR Regional domain defined by a single fracture-network realisation [UPDATED_SERCO_DFN_WITH_HOLE]; a) fracture-count map and b) 3D view of fracture planes.*

4.4 HSD parameterisation

HSD conductivity of RLDM regolith layers is based SR-Site/SDM-Site Forsmark, where porosity is assumed equal to specific yield (Table 4-5). However, particle-tracking performance measures address only bedrock properties and therefore porosity and flow-wetted surface area in HSD are nullified during particle tracking to eliminate the risk of contribution to accumulated transit time or F-quotient.

As an overview for the SFR near-field, the modelled HSD is visualised in the area where particle-tracking exit points occur (Figure 4-11). The following should be noted in this visualisation:

1) The SFR Regional model domain (orange lines) and land above sea level, 2000 AD are included for spatial reference of the areal extent visualised (c.f. Figure 3-1).
2) Lakes and rivers are not included in the figure (c.f. Figure 3-1).
3) The visualisation employs the "fixed-bedrock" elevation reference, where the bedrock elevation is envisaged as static over time (Section 3.3.5).
4) The filling material of the constructed SFR pier is not visualised (model implementation of fill material is given more attention in Figure 4-12 to Figure 4-14).
5) The "filled peat layer" (Figure 4-11e and f) includes two components: 1) peat, as modelled in RLDM, and 2) additional basin-filling of local depressions (performed exclusively in DarcyTools modelling to circumvent model artefacts in modelled groundwater table; Section 3.3.2).

Till is modelled as static (i.e. constant thickness and elevation over time) with wide-spread areal coverage and thicknesses typically ranging from a few meters to 10 m (Figure 4-11b). The till layer is covered by three low-conductive layers (Glacial clay and Lacustrine/Marine accumulated postglacial deposits; Table 4-5). The modelled total thickness of these three layers in RLDM has a patchy appearance, depending on exposure to wave erosion (Figure 4-11c and d). The change over time is small for these low-conductive layers; the most notable effects are found north of the SFR pier (Figure 4-11d). Basin-filled areas are potential wetlands (i.e. local depressions where the groundwater level is locally allowed to exceed ground surface); these areas are assigned the same properties as peat (Table 4-5).

Table 4-5. HSD hydraulic conductivity of regolith layers. From Bosson et al. (2010, Table 2-3).

Regolith layer	K_h (m/s)	K_v (m/s)	Porosity[4] (–)	Layer definition (Table A-1)
Peat[1]	3.00E–7	3.00E–7	0.2	From <lpgd> to <Filled_pdem[1]>
Lacustrine accumulation of postglacial deposits	1.50E–8	1.50E–8	0.05	From <mpgd> to <lpgd>
Marine accumulation of post glacial deposits	1.50E–8	1.50E–8	0.03	From <gkl> to <mpgd>
Glacial clay	1.50E–8	1.50E–8	0.03	From <fill> to <gkl>
Filling[2]	1.50E–4	1.50E–4	0.2	From <glfl> to <fill>. Special handling of the SFR pier[2].
Glaciofluvial material	1.50E–4	1.50E–4	0.2	From <till> to <glfl>
Till	7.50E–6	7.50E–7	0.05	From <bedr> to <till>
Upper bedrock[3]	≥3.0E–8	≥3.0E–8	≥1.0E–5	Thin soil coverage (soil depth < 4.0 m) and elevated bedrock (z>–10 m)

[1] Note that the upper surface of peat refers to the basin-filled DEM (Section 3.3.2), which implies that local basins are assumed to be peat-filled, or at least filled with a relatively high-conductive material.

[2] Special attention is given to the SFR pier. To avoid artefacts in the determination of the surface head in the Pier, the "conductivity of fill" is expanded 2 grid cells, horizontally (2*8 m). Below an elevation of z = – 3 m, a layer of till is assumed to underlie the filled areas around the SFR pier [prpgen_TD11_Model_parameterisation.f].

[3] A minimum bedrock conductivity of 3×10–8 m/s is assigned in two cases: 1) at thin soil coverage (soil depth < 4 m), and above an elevation of –10 m (this is to compensate that DFN coverage above z = 0 m, is unavailable outside the SFR Regional domain, Section 4.3).

[4] HSD porosity set equal to 0.0 in particle tracking to avoid unintentional contribution to performance measures of the bedrock.

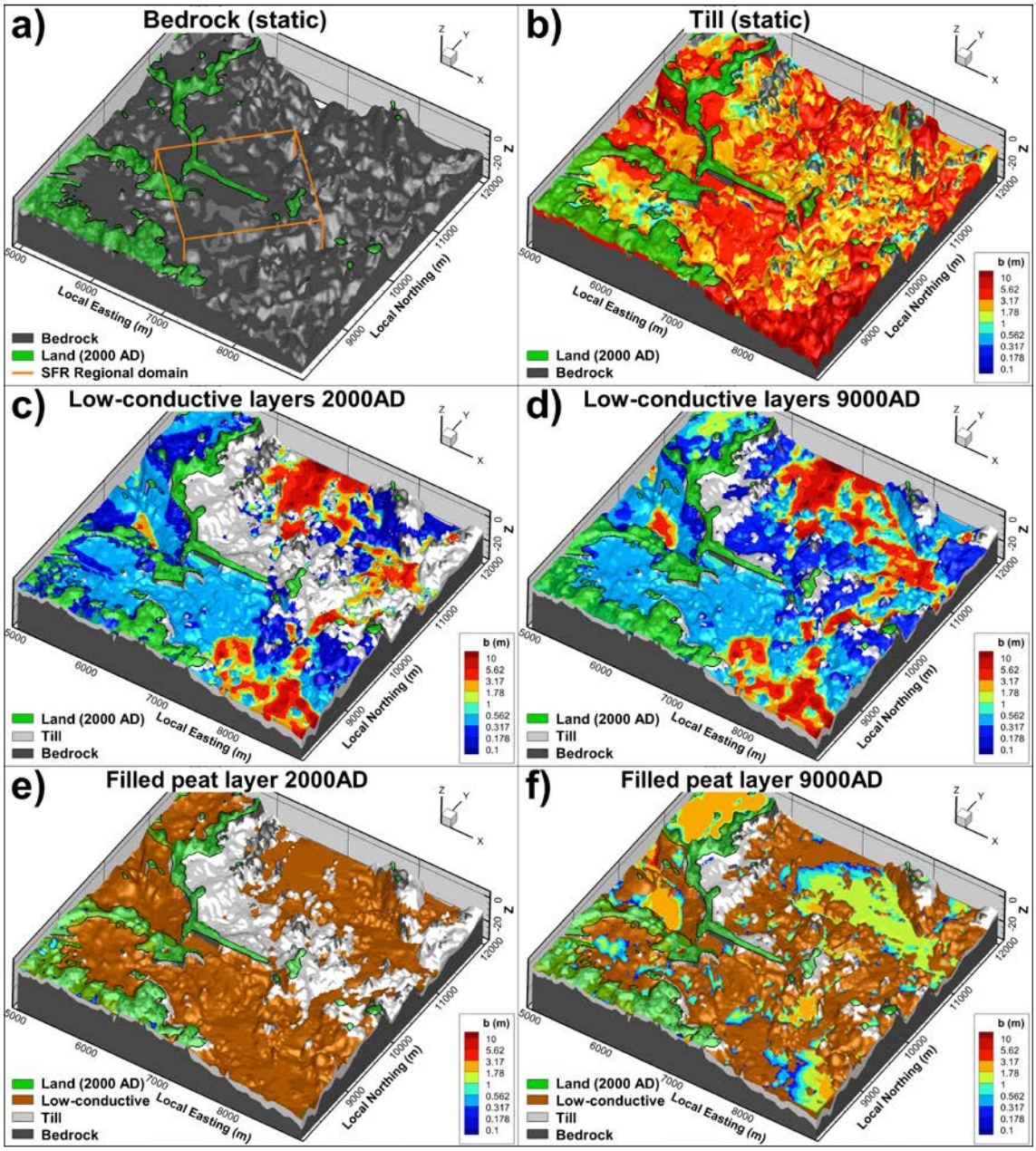

Figure 4-11. *Regolith layers in the SFR near-field, as modelled in RLDM; a) static bedrock surface (dark grey), SFR Regional domain (orange), and land above current sea level (green), b) static till layer thickness (contoured), c) and d) total thickness of low-conductive layers (K = 1.5×10^{-8} m/s; Table 4-5) of two time slices, and e) and f) modelled peat thickness (i.e. including filling of local basins).*

The SFR Pier; parameterisation and groundwater table

It was demonstrated in Td10 that the model representation of the constructed pier at SFR may, owing to its location above SFR, affect the local flow field, at least during later stages of shoreline retreat. Uncertainties in model representation may be significant for the Safety Assessment performance measures. Therefore the SFR pier is given special attention.

As of today, the pier is not expected to hold a groundwater table significantly above sea level. The pier itself is constructed from coarse, high-permeable materials (sand, gravel, and blocks, parameterised as K = 1.5×10^{-4} m/s; Table 4-5). Groundwater levels in stand pipes confirm that its current groundwater table is very close to sea level. However, it should be emphasised that these data reflect the coarse filling material, extending above sea 2000 AD, and provide little inference for the

groundwater level during later stages of shoreline retreat, as the material properties below current sea level are not known in detail. Three modelling aspects are considered, which motivate extra precaution to modelling groundwater table in the pier:

1) The modelled regolith-layer sequence in RLDM, with post-glacial deposits above filling material, implies a risk of erroneously implementing post-glacial deposits along the lateral sides of the pier (red oval 1 in Figure 4-12), resulting in an unrealistic groundwater table (as demonstrated in TD10). This model artefact is related to the resolution in the RLDM data (dx = dy = 20 m) and the rotated DarcyTools grid. The risk of artificial deposits along the sides of the pier is circumvented by extending the pier filling horizontally, by two grid cells (i.e. 2×8 m), see [prpgen_TD11_ Model_parameterisation.f].
2) The material properties of the pier below the current sea level are not modelled in detail in RLDM, but assumed to extend to the bedrock surface (red oval 2 in Figure 4-12). Data indicates presence of quaternary deposits below the coarse construction material (Table 4-6; Figure 4-13), which may constrain the hydraulic contact between the Pier and underlying deformation zones. Even though the coarse filling material evidently does not hold a groundwater table today, a potential underlying natural ridge, of less permeable deposits, may act as a future local water divide. Based on available borehole data (Table 4-6; Figure 4-13), it is assumed that the pier (including all filling material in the surroundings of the pier) is constructed on top of natural deposits. Below an elevation of –3 m, the pier and its surroundings (Figure 4-14) is modelled as a *till layer* (i.e. $K_H = 7.5\times10^{-6}$ m/s, $K_V = 7.5\times10^{-7}$ m/s, which is considerably less permeable than fill material $K_V = 1.5\times10^{-4}$ m/s).
3) The coarse construction material may alter over time (e.g. pore-filling processes, due to sedimentation or soil formation).

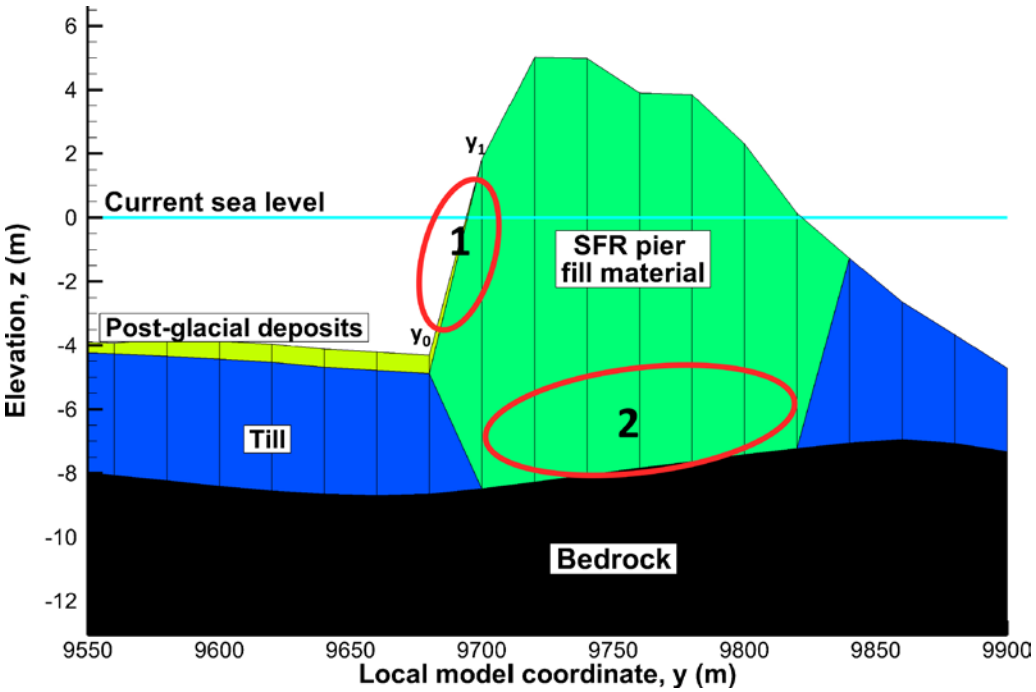

Figure 4-12. *Cross section of modelled sediment layers in RLDM 2000 AD (local model coordinate x = 6600 m). Note vertical exaggeration. Two concerns regarding DarcyTools implementation: 1) linear interpolation below RLDM resolution (e.g. between points y_0 and y_1) and 2) existence of sediments below the SFR pier.*

Table 4-6. Available borehole data on Pier material (see Figure 4-13).

Borehole	Elevation From (m)	To (m)	Regolith type[1)]
SFR0001	2.19	–3	Fill
	–3	–4.3[2)]	Assumed glacifluvial sand
SFR0002	2.53	–2.7	Fill
	–2.7	–3.8[2)]	Assumed glacifluvial sand
SFR0003	3.54	–3.6	Fill
	–3.6	–4.2[2)]	Assumed glacifluvial sand
HFR101	2.30	–3.57	Unspecified, above bedrock
HFR102	2.02	–1.96	Fill
	–1.96	–4.01	Interpreted till/clay
KFR101	2.26	–3.92	Fill
	–3.92	–7.78	Interpreted till/clay
KFR102B	2.26	–3.89	Fill
	–3.89	–7.58	Interpreted till/clay
KFR103	2.27	–7.22	Unspecified, above bedrock
KFR104	2.64	–1.46	Fill
	–1.46	–3.42	Interpreted till/gravel

[1)] Data source for SFM0001- SFM0001 is SKBdoc 1396258. Data for PSU boreholes (HFR and KFR) taken from drilling notes (Table 4-7).

[2)] Not confirmed bedrock surface. Possibly block.

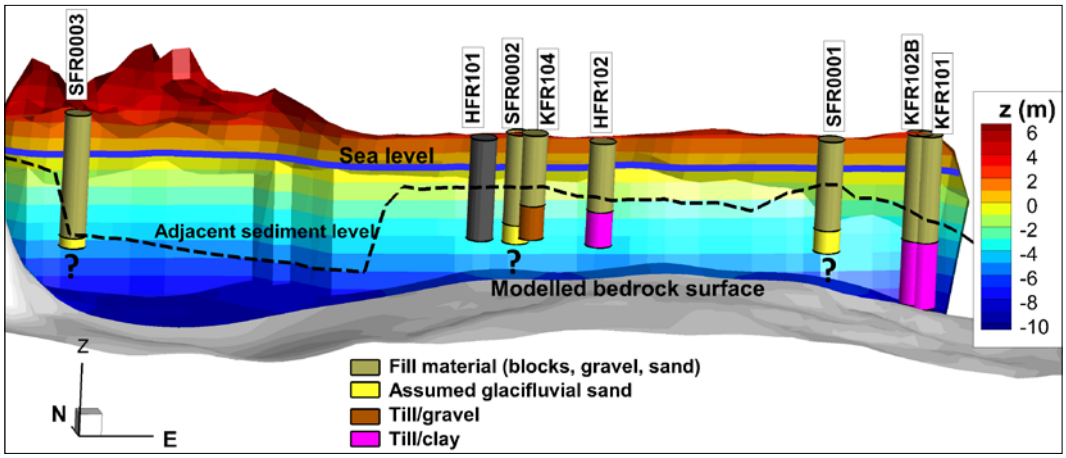

Figure 4-13. *Model geometry of the SFR pier (contoured by elevation) compared to borehole data (cylinders coloured by interpreted regolith type). The lower end of cylinders indicates measured bedrock elevation (non-confirmed in SFR0001-3). For reference, the adjacent sediment level outside the Pier and current sea level are indicated by lines. Vertical exaggeration x20.*

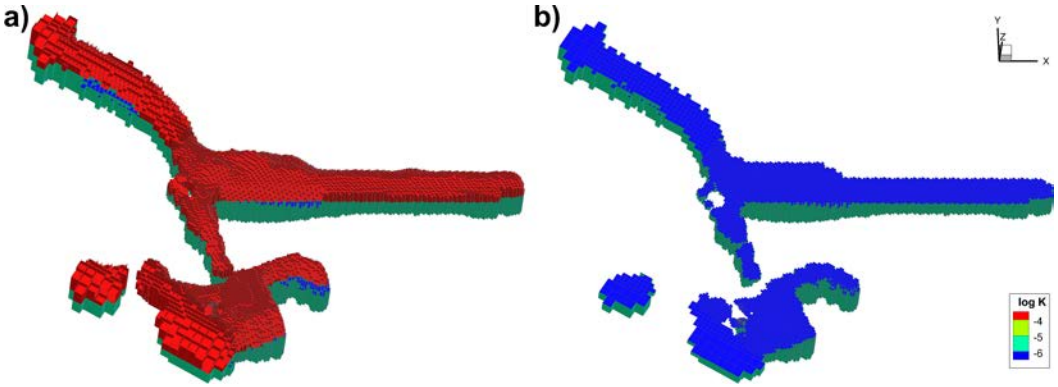

Figure 4-14. Model parameterisation of the SFR pier; a) the pier is assumed to consist of high-conductive construction material (red contour) on top of natural deposits (cyan-blue contours), and b) the underlying deposits are represented by anisotropic till, extending to –3 m elevation. Vertical exaggeration x20.

Table 4-7. Evidence of natural deposits below rockfill in the SFR pier.

Borehole	Notes from drilling
KFR101	Probably rockfill/blast stone from 0.0 to 7.5 m borehole length, followed by till/clay from 7.5 m down to the bedrock surface at 12.2 m borehole length. Bedrock confirmed between 12.2 and 13.5 m borehole length. Borehole reference level defined by cast concrete slab/ground surface.
KFR102B	Probably rockfill/blast stone from 0.0 to 7.5 m borehole length, followed by till/clay from 7.5 m down to the bedrock surface at 12.04 m borehole length. Bedrock confirmed between 12.04 and 13.6 m borehole length. Borehole reference level defined by cast concrete slab/ground surface.
KFR103	Bedrock surface 11.60 m below cast concrete slab/ground surface.
KFR104	Probably rockfill/blast stone from 0.0 to 5 m borehole length, followed by till/gravel from 5 m down to the bedrock surface at 7.40 m borehole length. Bedrock confirmed between 7.40 and 8.5 m borehole length. Borehole reference level defined by cast concrete slab/ground surface.
HFR101	Bedrock surface 6.6 m below reference level Top Of Casing (TOC).
HFR102	Probably rockfill/blast stone from 0.0 to 5 m borehole length, followed by till/clay from 5 m down to the bedrock surface at 7.4 m borehole length. Borehole reference level defined by TOC.

5 Simulation sequence

5.1 Grid generation

Computational grids are generated by means of the DarcyTools module GridGen. The grids are unstructured, which allows the flexibility of local refinement (e.g. near ground surface and tunnel geometry). The discretization is carried out via a sequence of commands specified in the standardised Compact Input File on xml-format (Svensson et al. 2010). A discretisation command consists of a geometric reference (i.e. DarcyTools objects in Chapter 3) and either: 1) a specification on local maximum cell side length, and/or 2) classification of grid subdomains by means of a cell marker ID. Cell-marker IDs have a key role in subsequent modelling; for example they are used in property assignment, boundary conditions, and particle release points. All details on grid discretisation are given in Appendix A3 (Table A-7).

Cell-inactivation principle

In the standard DarcyTools approach, the model top boundary is defined by removal of grid cells above topography (i.e. as defined by a DEM). SR-PSU addresses six stages of shoreline retreat (time slices), for which topography alteration is modelled in the dynamic landscape model, RLDM. This time aspect makes the standard "cell-removal approach" very inefficient. The reason is that upscaled ECPM properties (Section 5.2) are valid for a unique grid discretisation, only, which would imply that ECPM conversion must be repeated for each time slice (time consuming and complex file management). Instead, a so-called *cell-inactivation* method is employed, to mimic this topography alteration via cell makers in a *static* grid discretisation. The benefit of the static discretisation is that full compatibility is maintained between grids and ECPM properties. In principle, only time-invariant geometries are used in discretisation, while both time-variant and static geometries are used in classification of cell markers (e.g. Mk 999 = cell inactivation).

5.2 ECPM upscaling

DarcyTools employs a Continuum Porous-Medium (CPM) representation (Svensson et al. 2010), in which the hydraulic properties of a flowing fracture network are approximated by those of a porous medium. DarcyTools allows transferring fracture-network characteristics onto its computational grid by means of geometric upscaling. The upscaled properties are referred to as Equivalent Continuous Porous Medium (ECPM) properties. As the ECPM approach is based on an underlying stochastic DFN model, the resulting ECPM properties are also stochastic. Geometric up-scaling does not always ensure *hydraulic* consistency between the complex heterogeneity of the underlying flowing fracture network and the approximated ECPM. Thus, "Equivalent" implies a fine resolution of the computational grid in order to be valid.

DarcyTools employs a *staggered* grid arrangement with ECPM properties which are derived from geometric fracture-network upscaling over local control volumes (Svensson et al. 2010). This staggered grid involves *scalar* properties, defined at cell centres (e.g. porosity and flow-wetted surface area), and so-called *tensor* properties, stored at cell walls (e.g. conductivity). In other words, scalar and tensor ECPM properties do not represent identical control volumes, but are offset by half a grid cell.

A consequence of the staggered grid arrangement is that each step in the cell-jump particle tracking approach involves *one* cross-cell flow, but *two* grid-cell porosities and fws-values (Section 5.4.2). The ECPM conversion relies on several approximations:

- All fractures[1] inside a cell-wall control volume contribute to advection.
- The advection takes place over their full fracture surface area.
- Porosity of fractures below the fracture-size truncation is negligible for flow.

Transport aperture (ECPM Porosity)

Kinematic porosity is a critical parameter for determining particle transport time. Unfortunately the parameter is difficult to measure in field. In the numerical flow model, kinematic porosity can be calculated in the GEHYCO algorithm (Svensson et al. 2010) by the ECPM conversion of transport apertures of fracture networks. Äspö Task Force 6c results (Dershowitz et al. 2003), has suggested a fracture transport aperture correlated to transmissivity, according to

$$e_t = 0.46\sqrt{T} \qquad (5\text{-}1)$$

which was also used as a starting point for model calibration in SDM-Site Forsmark (Follin 2008). For SR-PSU, it has been decided to upscale porosity (i.e. an ECPM property) from the transport apertures of the underlying fracture network, as defined by Equation (5-1), with a minimum porosity value set to 10^{-5} [–]. Performance measures are only calculated for the bedrock; therefore both porosity and fws are nullified in tunnel backfill and in overlying sediments when particle tracking is performed.

All the details on the management of model files and naming conventions during ECPM conversion are presented in Appendix A3 (Table A-8)

5.3 Flow simulations

DarcyTools is primarily a modelling tool for site-scale groundwater flow in deep rock. As such, surface runoff can typically not be resolved in detail. Consequently, a model artefact of local excess head may occur at ground surface, if net precipitation exceeds local recharge (i.e. local excess head defined as exceeding topography). Two methods are commonly applied to circumvent this model artefact:

1) Prescribed-head boundary condition at the model top boundary (e.g. assume $H = z_{topography}$).
2) Free-groundwater table (inbuilt DarcyTools algorithm).

Both approaches have their merits and drawbacks. The prescribed-head approach is a numerically convenient approach, as it is determined from topography alone. However, it *assumes* that saturated conditions apply without consideration to locally varying hydrogeological conditions, and therefore it is not very realistic in areas that can be expected to be unsaturated (e.g. local topographical peaks and glaciofluvial deposits). This approach is particularly inappropriate in SR-PSU, as the model representation of SFR pier has a significant impact on model performance (Section 4.4). The standardised free-groundwater algorithm, on the other hand, is based on a combination of topographical data and a rudimentary depiction of hydraulic properties in the uppermost 20 m of the soil/bedrock (i.e. not data based). The result is a smooth groundwater table and a realistic representation of unsaturated areas. The drawbacks are: 1) the method allows excess head, 2) the parameterisation is not expected to be generic (calibrated for the current shoreline, and for a specific lake/river data set), and 3) a generalization of the uppermost 20 m is inappropriate for the shallow location of SFR.

Instead, a hybrid approach is suggested, where the two boundary-condition types "flux" and "fixed head" are mixed in a preceding "Recharge phase" to simulate realistic head for the model top boundary (allowing unsaturated areas, but not excess head). The top-boundary head is then applied

[1] More precisely, only fractures within a specified size interval are included; minimum fracture side length ranges from 2 to 16 m, depending on fracture set and depth domain (see Appendix D). Furthermore, only the hydraulically connected subset of the fracture network is modelled, details provided in TD05 (SKBdoc 1395200).

as a fixed-head boundary condition in subsequent steady state simulations, in order to establish a high-convergent flow field. The flow simulations are managed in three steps (i.e. sequence c) in Figure A-1):

1) Final setup of the model parameterisation (Section 5.3.1).
2) Solve a realistic top-boundary condition in a so-called "Recharge phase" (Section 5.3.2).
3) Apply the top-boundary condition in a so-called "Steady-state phase" to obtain a high-convergent flow solution.

The automatized execution of flow simulations and its traceable management of input and output data files are described in Appendix A3.

5.3.1 Finalising model setup

The final model setup (i.e. property assignment in the computational grid) is performed by means of the DarcyTools module PropGen (Svensson et al. 2010), as compiled from the customized source code [prpgen_TD11_Model_parameterisation.f]. PropGen has the following key functions:

1) Finalise the hydraulic-domain parameterisation. Input data on bedrock ECPM conductivity (HRD and HCD in Table A-8) and HSD conductivity (Table 4-5) are merged and converted into permeability (i.e. the operational unit in DarcyTools). Any bedrock conductivity below 10^{-10} m/s are re-set to a minimum value of 3×10^{-11} m/s. Cells marked as 999 are inactivated, by setting cell-wall conductivities $K_{inactive} = 10^{-20}$ m/s (Section 4.4).
2) Identify tunnel and tunnel-plug cells, based on cell markers (Table 4-1), and implement as permeability (i.e. over-writing "bedrock values"),
3) Calculate cell porosity, n, defined as sum of intersectional fracture volume per cell volume, i.e. fracture volume is based on fracture area and transport aperture in Equation (5-1). A minimum porosity of 10^{-5} [–] is applied.
4) Output is also exported in TecPlot format for visual verifications (e.g. Figure 4-1 and Figure 4-3).

The principles for numerical implementation of HSD parameterisation and the automatized management of input and output data files are described in Appendix A3 (Table A-9).

Numerical implementation inactive cells

The modelling procedure employs a *cell inactivation method*, to be able to represent topographical changes between different time slices with a single grid. Grid cells above the basin filled DEM for a given time slice are defined by setting the DarcyTools cell marker to 999. Two measures are taken to isolate these cells from taking part in the flow solution: 1) an extremely low conductivity value is assigned to all cell walls, $K_{inactive} = 10^{-20}$ m/s, and 2) an arbitrary fixed-head boundary condition is prescribed to the cells, i.e. H = 0.0 m. In effect, the cells marked 999 are isolated from the flow solution. The benefit is that the cells are not permanently deleted, but can be re-activated for modelling a different time slice. Special care must be taken to inactivated cells in recharge calculations.

5.3.2 Determining top-boundary condition in a recharge phase

The top boundary is defined as the uppermost layer of *active cells* in the grid (i.e. immediately below either permanently deleted or temporarily inactivated cells). The purpose of this initial "recharge phase" is to establish a realistic top-boundary condition for the subsequent steady-state simulation (i.e. head in surface-layer cells). As such, the recharge phase has two primary targets:

1) Constrain unrealistic excess head (i.e. head exceeding ground surface, as defined by the DEM).
2) Allow unsaturation, for example, in local topographical peaks. Two such examples with particular significance for the local flow field in SR-PSU are: 1) the SFR pier and 2) islets east of the pier.

The determination of head in the model top boundary is primarily based on the following four key components:

1) Fixed head in the surface-water areas that are defined in RLDM (Section 3.3; Table 5-1).
2) Spatially variable recharge, locally ranging from 0 to full net precipitation, P-PET = 160 mm/yr.
3) Maximum-head criterion in surface-layer cells, determined by local topography.
4) Local HSD conductivity.

Maximum-head criterion in surface-layer cells

Excess head in ground-surface cells is defined as head exceeding the local topography. It should be noted that the DEMs modelled in RLDM [pdem<time slice>.asc] contain local depressions that are below the scale for defining lakes. These depressions may hold surface water, e.g. minor lakes, wet lands, pools, or be peat-filled. Irrespectively of which, it can be argued that the head criterion should not relate to the elevation in local depressions, but by the geometric *threshold* surrounding depression. Therefore, the "excess head" in top-boundary cells is defined as $H - z_{DEM}$ (m, elevation in fixed-bedrock reference), where z_{DEM} refers to the local basin-filled DEM elevation (Section 3.3.2). The local z_{DEM} for ground-surface cells is determined from [Filled_pdem<**time slice**>_Fixed_bedrock.asc], i.e. after a step of back-rotating and translating cell coordinates into the RT90 coordinate system. This mapping between RLDM and DarcyTools is inexact due to combined effect of: 1) discretisation differences and 2) coordinate-system rotation. Although the basin-fill is a substantial improvement, the inexact matching implies that a complete absence of local depressions cannot be guaranteed in groundwater flow simulations.

Ground-surface head oscillates between iterations, due to: 1) step-wise adjustments in local recharge, and 2) resulting non-stationary flow solution. Therefore, an "excess-head tolerance" was introduced, which declines as a function of iterations (Figure 5-1). After 44 iterations, this tolerance levels out to a constant 0.25 m, which is judged to reflect the combined errors from: 1) RLDM modelling and 2) the inexact mapping between DarcyTools and RLDM. For ground-surface cells exceeding the tolerance, the boundary-condition type is switched from "flux" to "fixed head", where $H = z_{DEM}$ (m, elevation). The resulting ground-surface head after 100 iterations are used to specify fixed head in the subsequent steady-state phase.

Table 5-1. Fixed head in pre-defined surface-water areas.

Surface-water	Identification	Prescribed head, H (m, elevation)
1. Seafloor	Uppermost cell layer below relative sea level (Table 3-2)	$z_{sea\ level}$ (Table 3-2)
2. Lakes	cell markers (Table A-3)	$z_{lake\ threshold}$ (Table A-3)
3. Rivers	cell marker Mk = 102	[River_head.in][1)]

[1)] The input file [River_head.in] contains river-trajectory nodes (x,y) and estimated riverbed head for each time slice (Section 3.3.4). Prescribed head for river cells are interpolated based on the nearest two river-trajectory nodes.

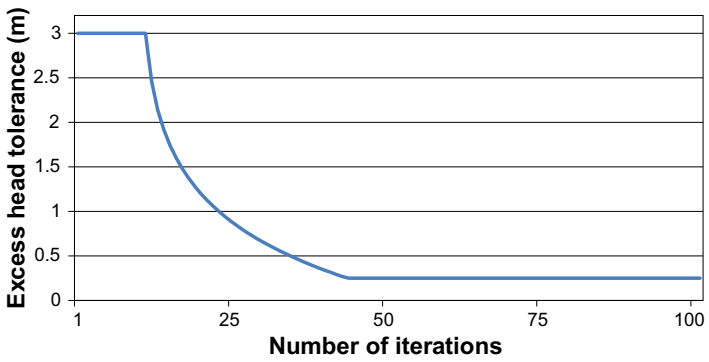

Figure 5-1. *Tolerance in simulated excess head of ground-surface cells in the recharge phase.*

Conceptualisation of local recharge

The flow domain has a generally flat topography (Figure 3-1), particularly in areas that are currently below sea. Therefore, large areas are expected to be saturated with large runoff components (i.e. in addition to the pre-defined open-water types in Table 5-1). Surface runoff is controlled by surface-hydrology components below the resolution scale of the DarcyTools model setup (e.g. small brooks and overland flow); in other words, geometric details with high hydraulic contrasts, that cannot be realistically represented in a model that primarily targets bedrock and future conditions. Consequently, neglecting the runoff component leads to local excess head where net precipitation exceeds local recharge (i.e. local excess head defined as exceeding topography). Excess head is an unrealistic model artefact, which implies exaggerating local gradients and flow, as well as, distorting the particle-tracking exit locations. Two means are therefore taken to deplete artificial excess head in surface-layer cells:

1) Local recharge is envisaged as [net precipitation – runoff]. In cells with excess head, the local recharge is therefore reduced, sequentially by iterations, from a maximum of P-PET = 160 mm/yr to a minimum of 0.0 mm/yr. The reduction is done on a cell-specific basis.
2) Excess head larger than the tolerance (Figure 5-1) changes the boundary condition of the individual cell from "flux type" to "fixed-head type".

The automatized transfer of input and output data files between the two phases during the flow simulations is described in Appendix A3 (Table A-10 and Table A-11 for the recharge and steady-state phases, respectively).

5.4 Post process

The performance measures (Section 1.3) are calculated by means of post-processing of flow solutions. This is conducted by means of the DarcyTools module PropGen, as compiled from customized Fortran codes (see Table A-12 and Table A-13). The post-processing is executed in batches, in which the traceability between input and output data is automatized.

Two types of performance measures (Section 1.3) are analysed:

1) Analysis of the simulated flow field (Section 5.4.1) provides cross-flow, head, and hydraulic gradients in disposal rooms, as well as, bedrock re/discharge in biosphere objects.
2) Bedrock retention properties, L_r, F_r, and $t_{w,r}$, as well as, disposal-room interactions, are determined by means of particle tracking (Section 5.4.2).

5.4.1 Flow-field analysis

The flow-field post processing has two objectives:

1) Calculate cross flow over disposal rooms as a performance measure.
2) Calculate bedrock re/discharge in biosphere objects for inter-code comparison with the Biosphere modelling.

Cross flow refers to the total flow over a predefined cross-sectional area in the computational grid. This area is the interface between a subunit of interest, i, (e.g. a tunnel section or bedrock surface) and surrounding, arbitrary grid cells, j. For example, this ij-interface may refer to a tunnel wall between tunnel cells identified by marking, Mk = i (Table 4-1), and surrounding bedrock/plugs with grid-cell marking Mk = $j \neq i$ (i.e. j may include several cell markers). Four components of the cross flow can be determined over the ij-interface:

1) Total inflow to subunit i, ΣQ_{ij+}
2) Total outflow from subunit i, ΣQ_{ij-}
3) Total outflow from surrounding grid cells j, ΣQ_{ji-}
4) Total inflow to surrounding grid cells j, ΣQ_{ji+}

By symmetry, $\Sigma Q_{ij+} = -\Sigma Q_{ji-}$ and $\Sigma Q_{ij-} = -\Sigma Q_{ji+}$. Furthermore, mass balance in a convergent flow solution holds that, if no sink or source terms are present in subunit i, $\Sigma Q_{ij+} = \Sigma Q_{ji+} = |\Sigma Q_{ij-}| = |\Sigma Q_{ji-}|$. As the exception, due to an inbuilt error in the DarcyTools pressure correction between cells of different sizes (SKBdoc 1396127) the tunnel flow of 2BMA must be based on *bedrock cells*.

In order to reduce local "corner-flow" effects, the cross-flow calculation is performed on so-called "cell-net flow basis". Here, "corner flow" refers to cells with more than one cell-wall flows, of opposite direction, over the *ij* interface (e.g. may occur in tunnel corners and along the curved silo walls). In other words, "corner flows" are envisaged as typical discretisation artefacts that should not be included in the net flow over the subunit *i*. The cell-net flow for a cell with marker Mk = *i* is defined as

$$Q_{ij}^{cell,net} = \sum_{n} Q_{ij}^{wall},\ i \neq j. \tag{5-2}$$

where Q_{ij}^{wall} is the cell-wall flows from the grid cell (Mk = *i*) to *n* ambient grid cells (Mk = j ≠ *i*). The total cross flow over subunit *i* is then calculated as the sum of *positive* cell-net flows, ΣQ_{ij+}, and the sum of *negative* cell-net flows, ΣQ_{ij-}, for all cells with marker Mk = *i*. The cell marking defining disposal rooms and bedrock/HSD interface in the computational grid is presented in Table A-7.

The management of input and output data files during the automatized calculations of disposal-room flow is described in Appendix A4 (Table A-12).

5.4.2 Particle tracking

DarcyTools facilitates two inbuilt particle-tracking methods: 1) stream-line routing and 2) the so-called cell-jump method (Svensson et al. 2010). Unfortunately, the inbuilt particle-tracking methods are not very feasible due to the extensive demands of SR-PSU (involving multiple model setups and large numbers of particles released). Instead, particle tracking is performed as a post process applied to a steady-state flow field (i.e. outside the DarcyTools flow solver).

There are reasons for using a standalone post process:

1) Rapid execution time (processing steady-state solutions reduces particle tracking to a geometric problem, circumventing the computational demanding (and time consuming!) iterative time-stepping within the DarcyTools solver. The post-processor algorithm also allows simultaneous processing in parallel working folders).
2) Flexibility: the code can easily be adapted to meet the various needs within the SR-PSU project (customize definition of performance measures, target specific issues, etc.).
3) File management: Output can be customized to meet the particular demands within the SR-PSU project (e.g. apply file-naming conventions, condense output to reduce file sizes, export in defined delivery structures, user-specified Tecplot output, etc.).

In principle, the used algorithm [P_track_random_TD11_deplete_loops.f] is very similar to the so-called "DarcyTools to MARFA interface" used in SR-Site Forsmark. It is based on the cell-jump method, where particles (i.e. discretisation of water volumes) traverse the computational grid on a cell-to-cell basis, according to inter-nodal flow between cells. The method assumes complete mixing of water in all cells, which implies a stochastic component in the routing of particle trajectories.

Particle-tracking principles and performance measures

A particle trajectory represents the advective flow path of a discretised water volume through the bedrock. The purpose of particle tracking is to quantify cumulative bedrock retention properties along an ensemble of trajectories. The evaluation targets only the retention properties in bedrock, and therefore no properties of tunnel-backfill or HSD are included in the performance measures.

Particles are released uniformly within disposal rooms (identification via cell markers, Table A-13). However, the "release point" is defined as the tunnel-wall passage (i.e. or put in other words, the bedrock entry point). A proportionality exists between density of particle-release points and tunnel-wall flux in terms of a bounding envelope (Figure 5-2). Particle trajectories are terminated at the bedrock surface, where the "exit point" is defined by the cell wall between a bedrock cell and a HSD cell.

The probability, P_{ij}, of navigating from cell i to cell j is assumed to be proportional to the flow in that direction, Q_{ij}, where a *sign-criterion* applies to Q_{ij}, depending on the *direction* of particle tracking:

$$P_{ij} = \frac{Q_{ij}}{\sum Q_{ij}}. \qquad (5\text{-}3)$$

Particle tracking can be performed in two directions: in *forward* tracking, only outward-directed flows are included in Equation (5-3), whereas in *backward* tracking only includes inward-directed flows.

The performance measures L_r, F_r, and $t_{w,r}$ (Section 1.3), are determined as cumulative bedrock properties for particle trajectories (i.e. from bedrock entry to bedrock exit). The underlying equations for accumulating these bedrock properties along a particle trajectory are presented below.

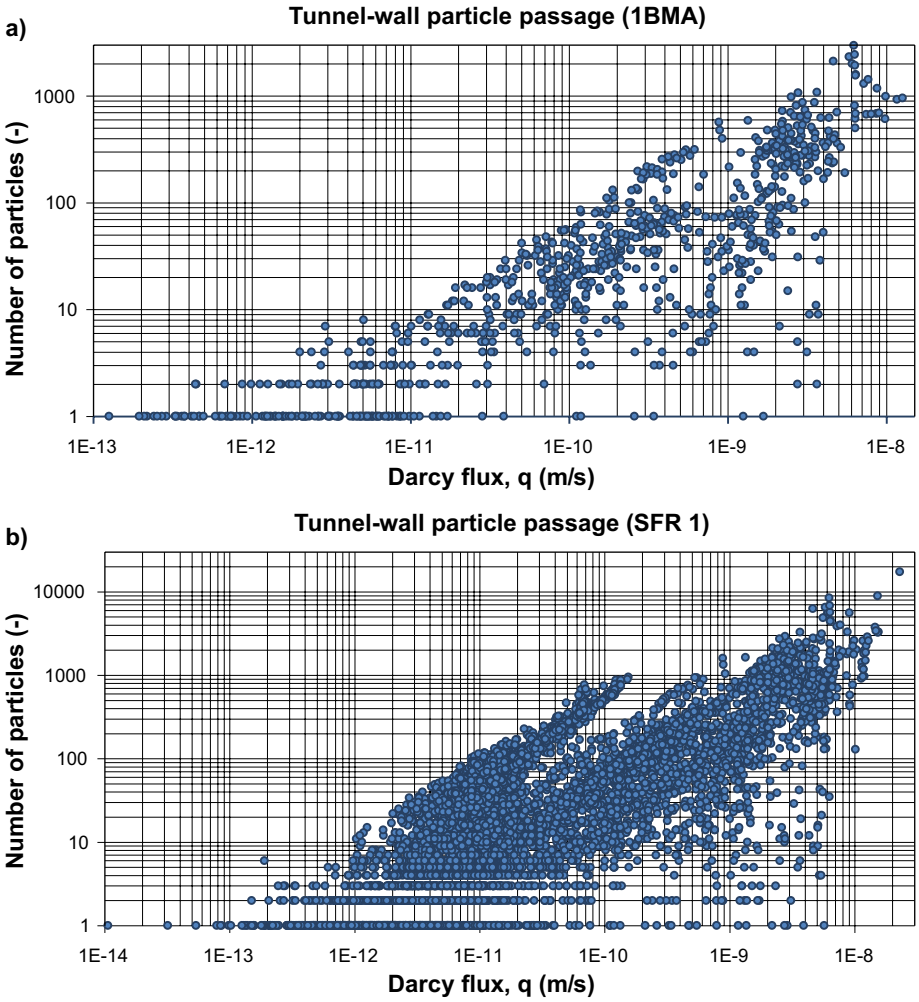

Figure 5-2. *Cross-plot between the number of tunnel-wall crossings versus tunnel-wall flux; a) an envelope, proportional to tunnel-wall flux, seems to control the maximum number of particle crossings, and b) a combination of different envelopes seem to apply when particles are released in more than one disposal room.*

The total path length of particle trajectories, L_r (m), is calculated as the sum of distances between the centre points of passed cell walls. Note that cell-wall centre coordinates are used in the path-length calculation, as opposed to cell-centre coordinates. The purpose of using cell-wall centre coordinates is to allow for diagonal "corner cutting" through cells (i.e. to some extent reducing the overestimation due to rectilinear nature of particle jumps).

Likewise, the advective travel time of a flow path, $t_{w,r}$ (y), is determined as the sum of travel times for each discrete particle step along the trajectory. The discrete travel time, t_{ij}, taken to move from the centre of cell i to the centre of cell j, is assumed to be:

$$t_{ij} = \frac{n_i V_i + n_j V_j}{2Q_{ij}} \tag{5-4}$$

where n is cell porosity and V is cell volume (i.e. the product nV is the cell volumetric water content). The factor 2 in the denominator reflects that only *half* of the cell volumetric water contents, $n_i V_i$ and $n_j V_j$, are involved in the inter-nodal flow Q_{ij}.

Analogously, the cumulative flow-related transport resistance, F_r (y/m), or F-quotient, is also determined as the summed bedrock properties for discrete particle jumps. The transport resistance for each discrete jump, from cell centre i to cell centre j, F_{ij}, is assumed to be:

$$F_{ij} = a_w\, t = \frac{fws_i + fws_j}{2Q_{ij}} \tag{5-5}$$

where a_w is flow-wetted fracture surface area per volume of water and fws is the flow-wetted fracture surface areas in cells i and j, respectively (based on Svensson et al. 2010 and MARFA interface). Calculated performance measures only reflect the bedrock; therefore both porosity and fws are nullified in tunnel backfill and in overlying sediments.

The management of input and output data files during the automatized particle-tracking analysis is described in Appendix A4 (Table A-13).

6 Results

6.1 Demonstration of the top-boundary simulation

This section demonstrates the results of the model approach taken to determine the top-boundary condition in a preceding "Recharge phase" (Section 5.3.2). Owing to the automatized execution approach (Section 5.3), the simulation of all bedrock cases are performed under the same premises (convergence criteria, number of iterations, etc.). As an example, the results of bedrock case BASE_CASE1_DFN_R85 are presented in detail.

Topography and shoreline retreat

The shoreline retreat in the SFR near-field is shown for the six selected time slices (Figure 6-1). Note that all elevations are expressed in the so-called fixed-bedrock reference system, where the sea level is envisaged as declining, relatively to a static bedrock surface (Section 3.3.5). Pre-defined surface water areas in RLDM (lakes and rivers) are shown as blue-grey surfaces. Head is monitored below two topographical peaks (one in the pier and the other in an islet, east of the pier; grey points in Figure 6-1).

Local recharge and fixed head

Local recharge and cells switched to "fixed-head" conditions are shown in Figure 6-2. The spatial pattern in simulated recharge can be described as patchy and of "binary character" (i.e. distinct recharge and discharge subareas). The fixed-head conditions (i.e. ground-surface cells where simulated head has exceeded the tolerance in Figure 5-1) tend to occur: 1) along the coast line, 2) along topographical depressions (i.e. typical discharge areas), and 3) in low-conductive sediments (c.f. Figure 4-11).

Relative ground-surface head

The outcome of the applied "recharge-phase concept" is demonstrated in terms of simulated "relative head" in the top boundary (Figure 6-3).This relative head is expressed as ground-surface head relative to local ground surface, $H - z_{DEM}$ (m, elevation in fixed-bedrock reference), where z_{DEM} refers to the local basin-filled DEM elevation (Section 3.3.2). In other words, this measure demonstrates the difference between the *applied boundary condition* (i.e. simulated outcome) versus the simpler boundary condition assuming $H = z_{DEM}$ (discussed in Section 5.3). *Less strictly speaking*, the absolute value of this relative head can be envisaged as an approximate measure of groundwater depth (i.e. this analogy requires that the vertical hydraulic gradients are negligible). This relative head is high in topographical depressions (i.e. head is equal to or close to basin-filled DEM elevation; Figure 6-1), particularly in presence of low-conductive deposits (Figure 4-11). Vice-versa, relative head is low in local topographical peaks (i.e. can be envisaged as deep groundwater table; Figure 6-1), and particularly so in the high-conductive SFR pier (and surrounding fill material; c.f., Figure 4-14).

Top-boundary head

In general, the ground-surface head has a smoother appearance, as compared to topography (e.g. islets east of the pier; c.f. Figure 6-1 and Figure 6-4). Owing to spatial contrasts in HSD-conductivity (Figure 4-11), the ground-surface head does not necessarily follow topography variations intimately (Figure 6-4). For example, the high-conductive fill material renders an even head pattern in the pier (i.e. low horizontal gradient). Notably, at 2000 AD, the maximum head inside the pier is only one centimetre above sea level, while during later stages of shoreline retreat its head is controlled by the surrounding elevation of low-conductive sediments in all directions. Isolated local peaks in head are noted in a few small islets that emerge out of the sea at c. 3000 AD. These islets are not assigned fixed-head (Figure 6-2), but reflect the recharge-simulation result of low-conductive outcropping bedrock (i.e. depending on the underlying DFN realisation).

Monitored performance

An example of model performance during iterations is presented in (Figure 6-5 and Figure 6-6). The overall convergence of the flow solution by simulation progress (Figure 6-5a, c, and e, and Figure 6-6a, c, and e) is evaluated in terms of the root-mean-square of error in head solution (i.e. standard DarcyTools output). After the initial recharge phase, run in 100 iterations, the subsequent steady-state phase, run in 25 iterations, improves the convergence by c. 4 orders of magnitude, which is considered to provide sufficient accuracy for the later post-processing (Section 5.4). Simulated head is also monitored at two points during simulation progress (Figure 6-5b, d, and f, and Figure 6-6b, d, and f). The lateral positions of these monitoring points are shown as grey points in Figure 6-1 to Figure 6-4, and their elevations are –7 m in the pier, and –4 m in the islet east of the pier. At 2000 AD, the head in the pier stabilises rapidly to c. 1 cm above sea level. At later stages, the head in the pier is still rising at the end of the recharge phase, after which it stabilises rapidly – with only minor changes – in the steady state phase. This suggests that a higher head could have been obtained in the pier if only the recharge phase would have been prolonged by additional iterations. However, this notion must be considered in context of three model uncertainties:

1. Uncertainties regarding material properties in the SFR pier are discussed in Section 4.4. For example, the significance of potential natural deposits below the fill material is expected to outweigh the observed uncertainty regarding the groundwater level in the Pier.
2. The combination of variable cell size in a rotated model-coordinate system causes an ambiguity in the mapping between DarcyTools grid cells and the ground-surface level, as modelled in RLDM. This uncertainty has been judged to correspond to a 0.25 m tolerance in the ground-surface head criterion (Section 5.3.2), which can be taken as an approximate estimate of the level of accuracy in the determined groundwater level.
3. The mixed boundary condition is a novelty in DarcyTools modelling, and as such it has not yet reached its full potential. A limitation in the current implementation is that the change in boundary-condition type, is as of yet, permanent (i.e. one-way switch from flux to prescribed head). A consequence of this is that numerical oscillations tend to successively “trap” ground-surface cells into the prescribed-head condition, which in turn causes an artificial gradual rise in groundwater level with iterations. Hence it is motivated to interrupt the recharge phase before reaching a fully stationary appearance. Based on judgment of simulation results (Figure 6-1 to Figure 6-4) and convergence appearance (Figure 6-5 and Figure 6-6), it was decided to run the recharge phase for 100 iterations.

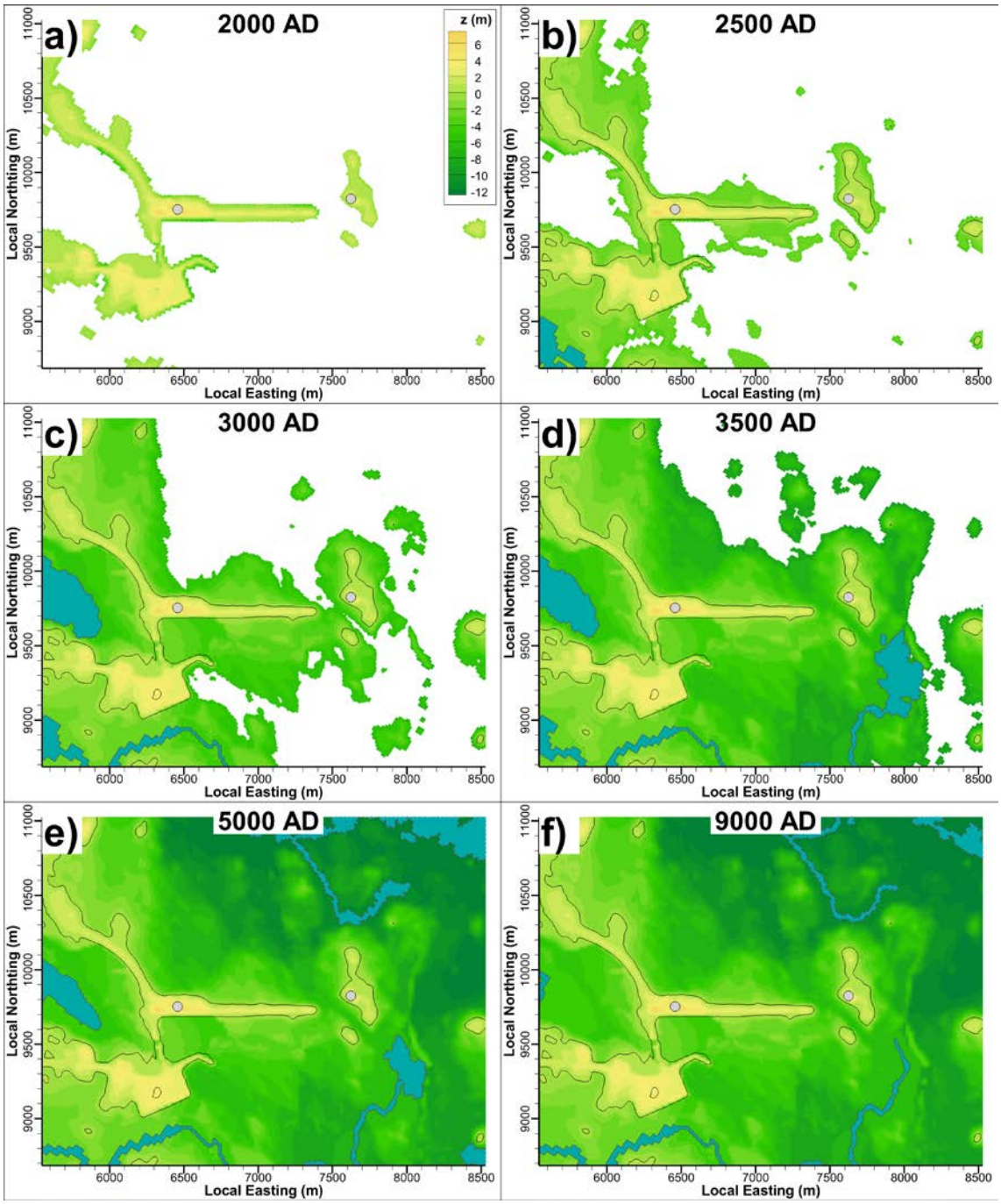

Figure 6-1. *Elevation of ground-surface cells above the retreating sea level, expressed in the so-called fixed-bedrock elevation reference (Section 3.3.5). Pre-defined surface water shown as blue-grey surfaces. Head is monitored below topographical peaks in the pier and in an islet east of the pier (grey points).*

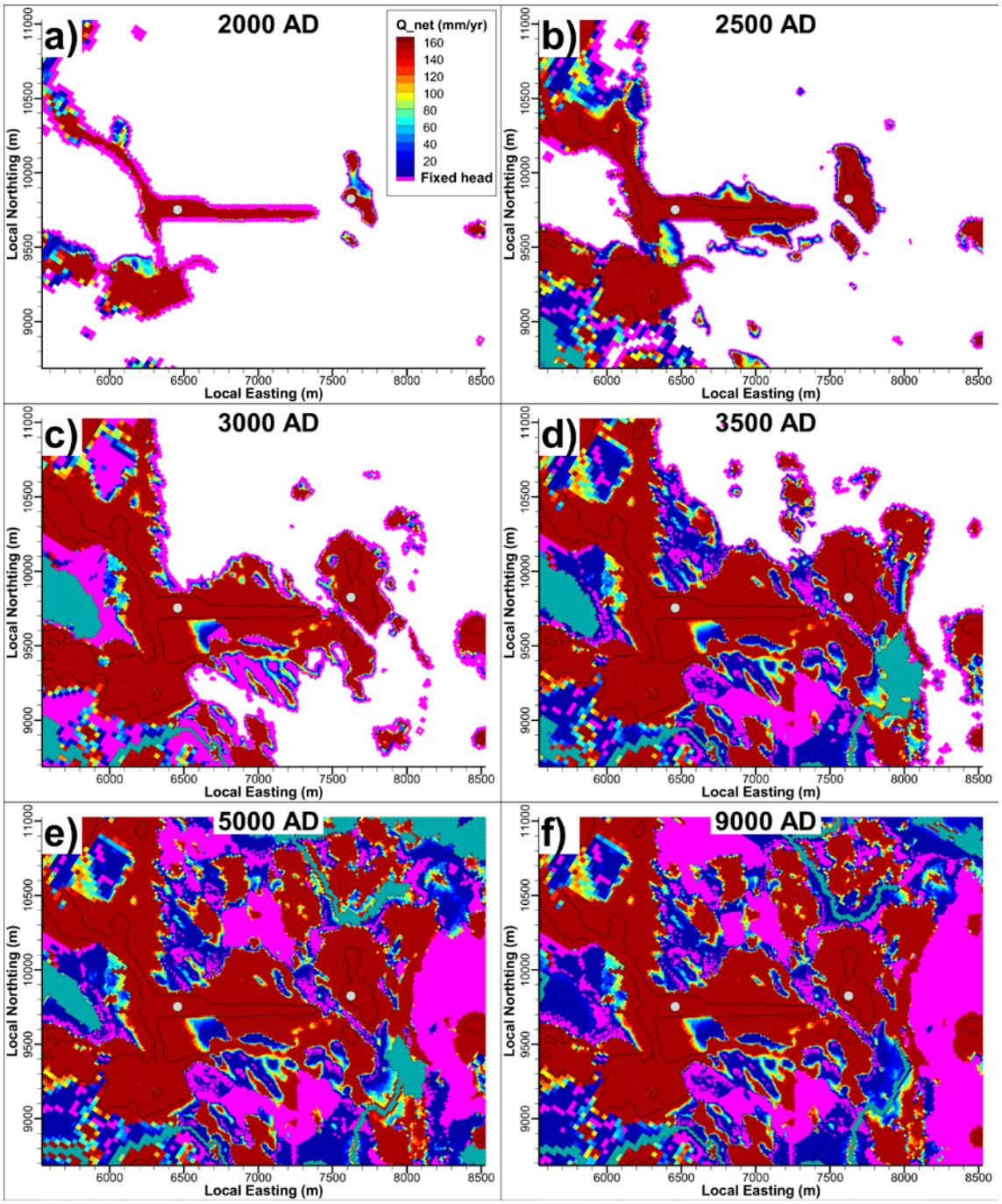

Figure 6-2. *Simulated local recharge for BASE_CASE1_DFN_R85 over studied time slices. Fixed-head cells shown as pink surface. Head monitored below topographical peaks in the pier and in an islet east of the pier (grey points).*

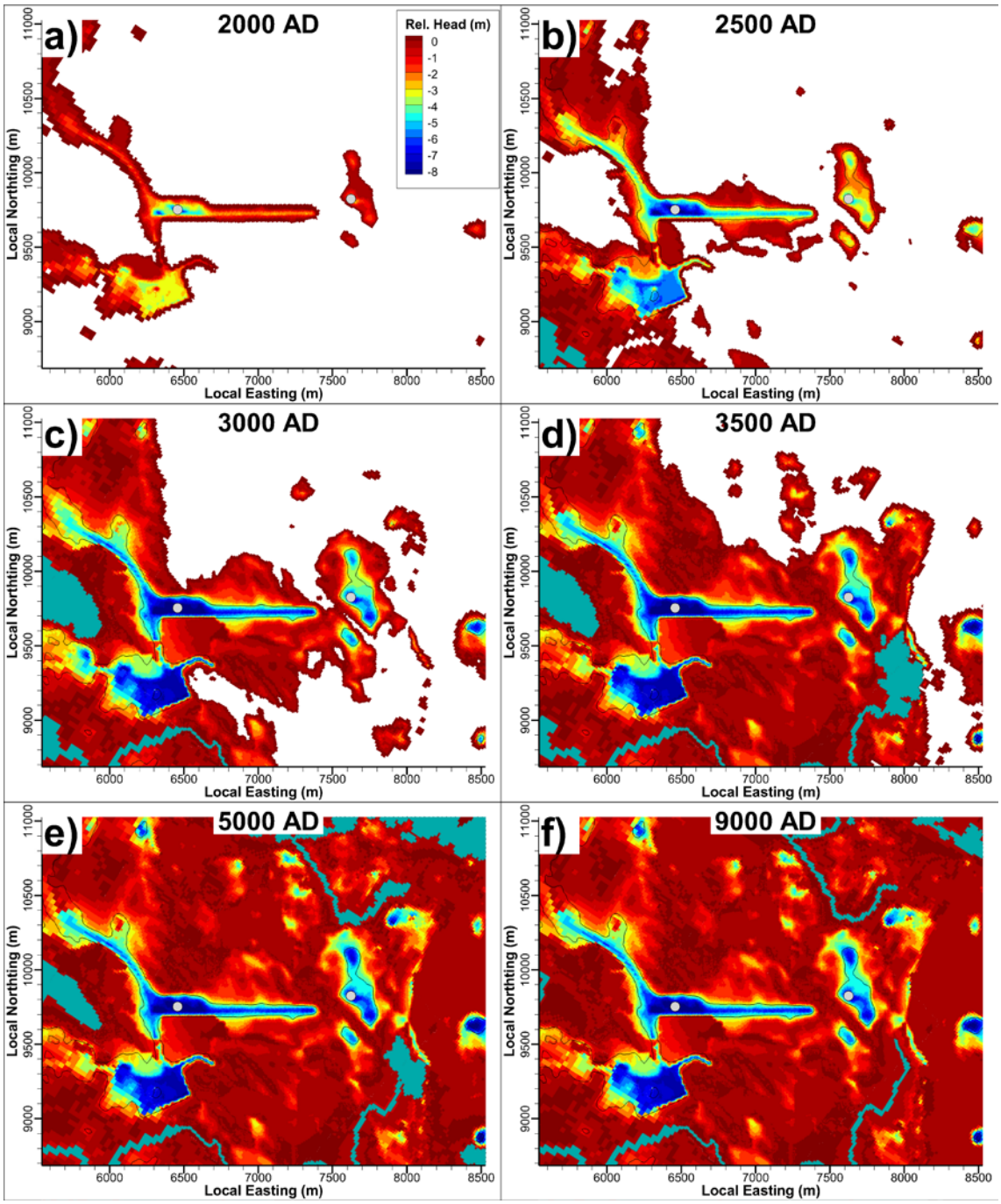

Figure 6-3. *Simulated relative ground-surface head, H – zDEM (m), for BASE_CASE1_DFN_R85 for studied time slices. This relative head is expressed as head in the uppermost active cell layer, relative to local elevation of ground surface. Pre-defined surface water shown as blue-grey surfaces. Head monitored below topographical peaks in the pier and in an islet east of the pier (grey points).*

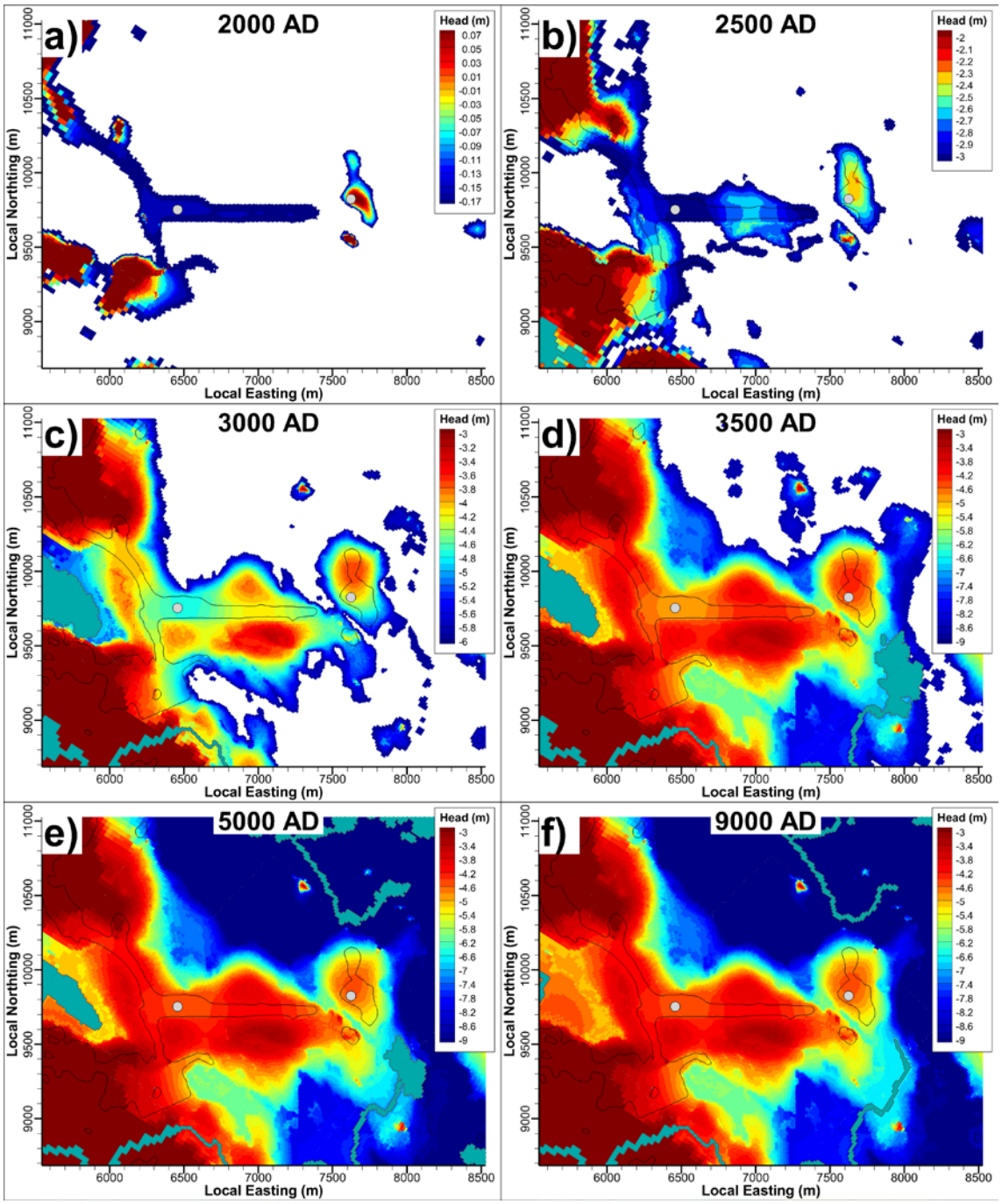

Figure 6-4. *Simulated ground-surface head for BASE_CASE1_DFN_R85 for studied time slices. Head is expressed in the fixed-bedrock reference (Section 3.3.5). Pre-defined surface water shown as blue-grey surfaces. Head monitored below topographical peaks in the pier and in an islet east of the pier (grey points).*

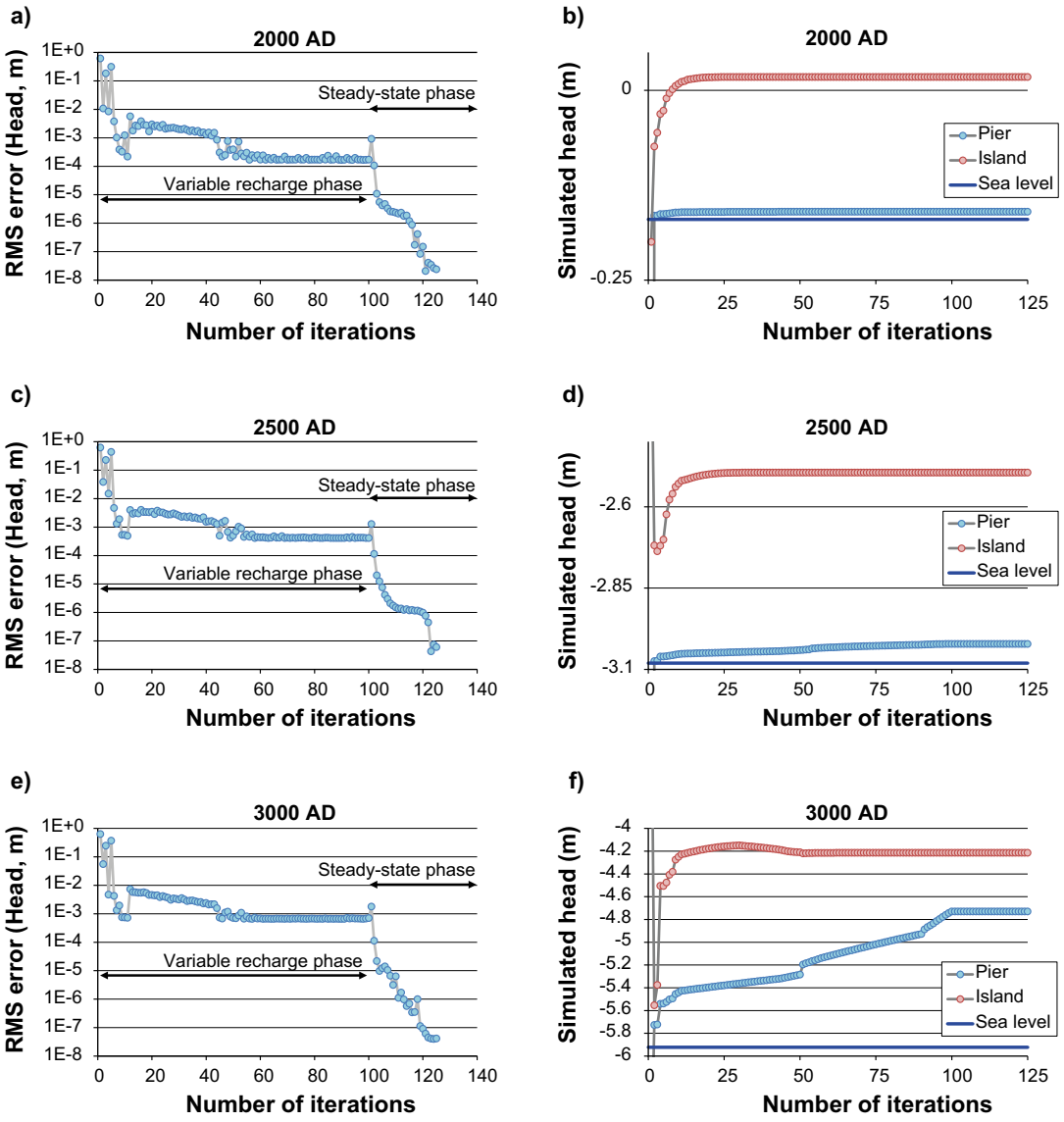

Figure 6-5. *Summarised statistics of the two flow-simulation phases for BASE_CASE_1_DFN_R85; flow-solution convergence and monitored head at two points (location indicated by grey points in Figure 6-1 to Figure 6-4). Extracted data from the history files in Table A-11.*

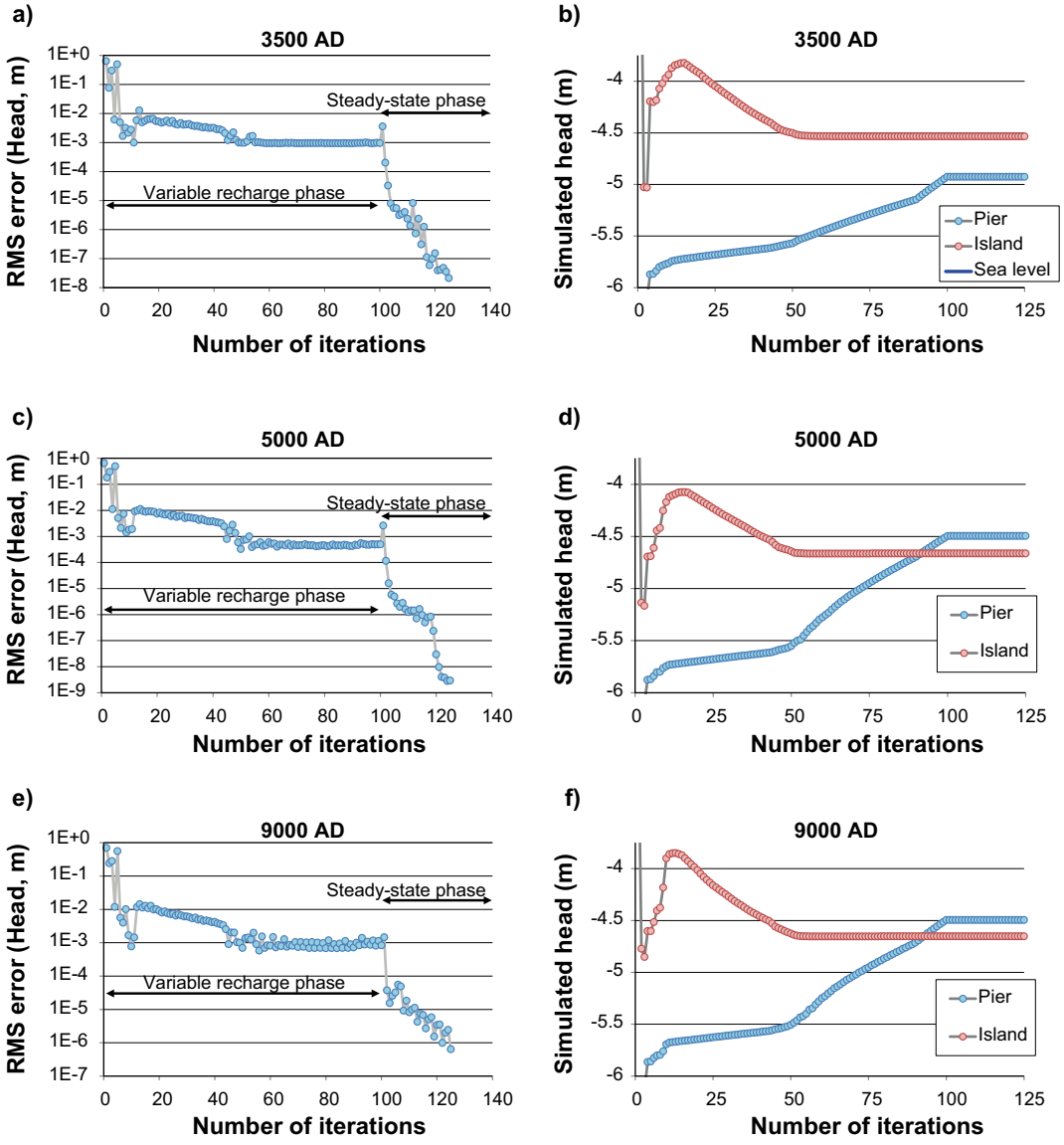

Figure 6-6. *Summarised statistics of the two flow-simulation phases for BASE_CASE_1_DFN_R85; flow-solution convergence and monitored head at two points (location indicated by grey points in Figure 6-1 to Figure 6-4). Extracted data from the history files in Table A-11.*

6.2 Cross flow in disposal rooms

6.2.1 Mass balance in evaluation of disposal-room cross flow

Cross flow over disposal rooms are evaluated for all bedrock cases and all time slices (i.e. 11 disposal rooms × 17 bedrock cases × 6 time slices = 1,122 tunnel flows). A relative mass-balance error in disposal-room cross flow can be determined as: $(\Sigma Q_{ij+} - |\Sigma Q_{ij-}|)/\Sigma Q_{ij+}$, see Equation (5-2). In general, this relative error is very small, with a maximum of 0.25 % (Figure 6-7).

6.2.2 Simulated distribution of disposal-room cross flow for 17 bedrock cases

The range of variation in simulated disposal-room cross flow among the 17 bedrock cases can be illustrated by means of box-whisker plots. The grey-shaded box covers 50% of the bedrock cases, whiskers indicate the bedrock cases with minimum and maximum flow, respectively, and the median bedrock case is shown by a black line (Figure 6-8f). In general the cross flows are in similar magnitudes for most disposal rooms. However, the cross flow through the Silo is considerably lower than it is in other disposal rooms (Silo cross flow resolved in detail in Figure 6-9). The disposal-room cross flow increases during the early of stages shoreline retreat, to reach approximately stationary conditions at the time slice of c. 5000AD (Figure 6-9 and Figure 6-10). From the time slice of c. 3000 AD, 1BLA and 1BMA stand out with higher cross flows; this is probably related to their intersection with deformation zone ZFMNNW1209 (formerly referred to as Zone 6). Among the SFR 3 disposal rooms, 2BMA stands out with higher cross flows, particularly at early time slices. The appearance of simulated flow distributions vary from uniform or normal (e.g. 3BLA) to log-normal (e.g. 5BLA).

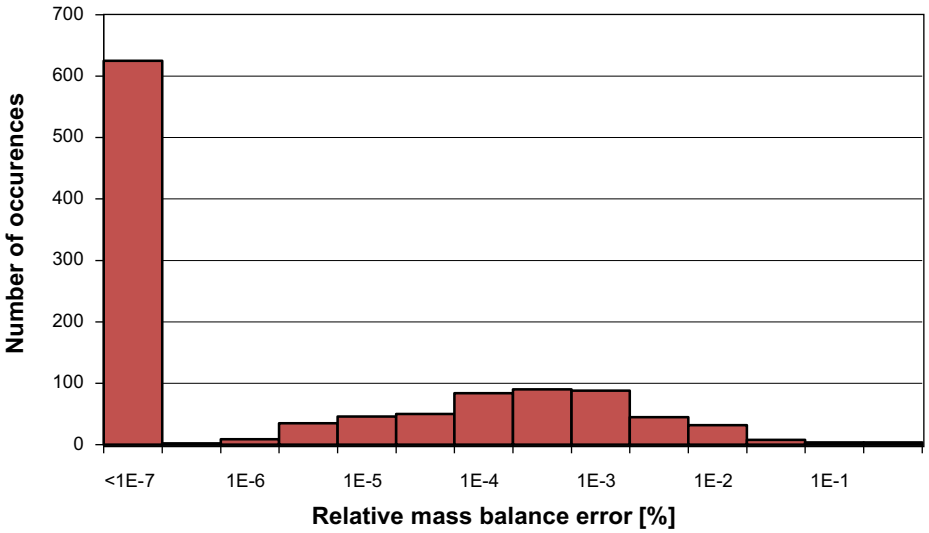

Figure 6-7. *Distribution of mass balance errors for 1,122 evaluated tunnel flows.*

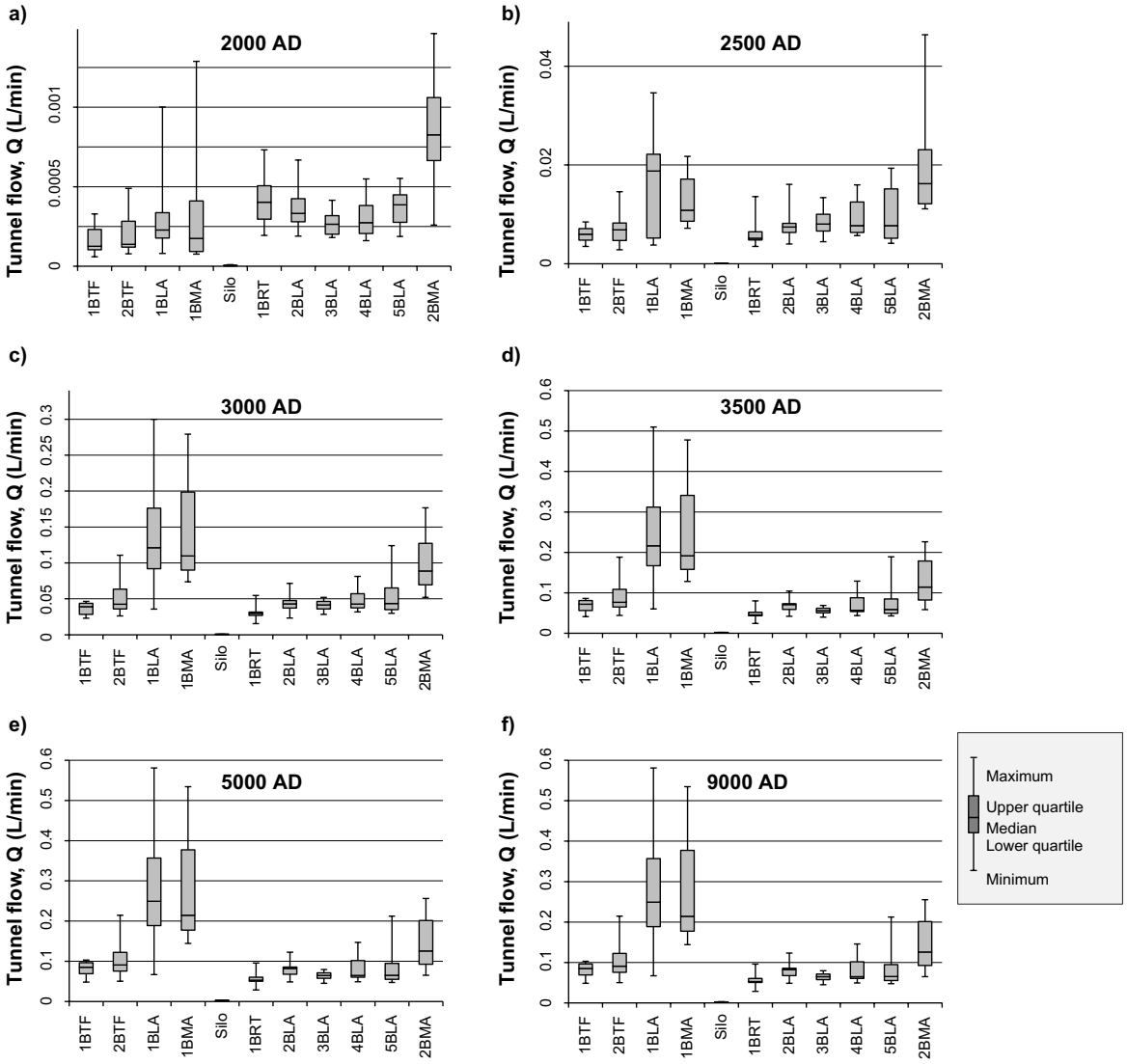

Figure 6-8. *Box-whisker plots of the distribution of simulated disposal-room cross flow in the sensitivity study of 17 bedrock cases (Table 2-2). Distributions of individual disposal rooms are compared, and the progress over time is shown for 6 time slices (Table 2-1). The low cross flow through the Silo is resolved in Figure 6-9.*

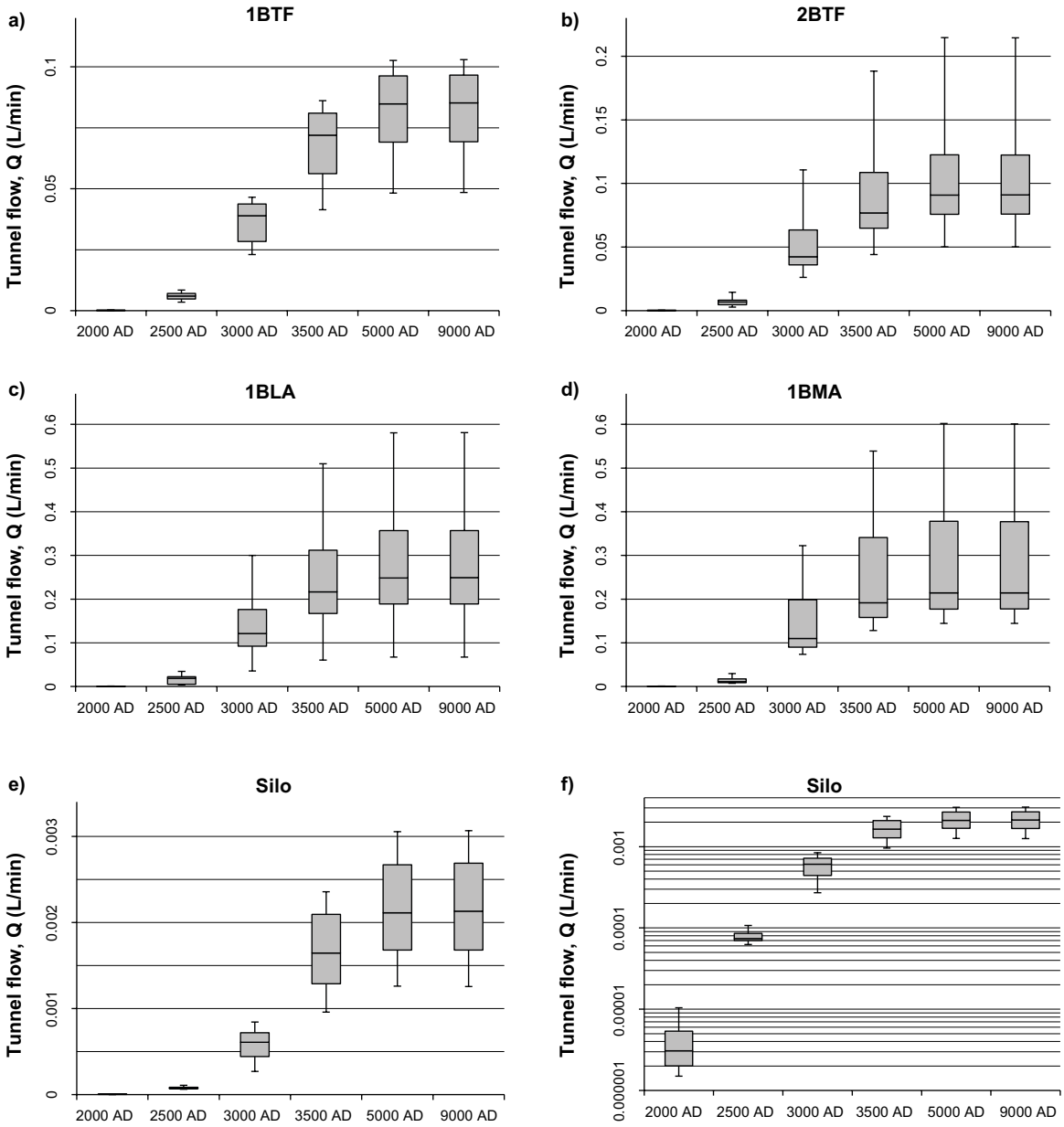

Figure 6-9. *Box-whisker plots of simulated disposal-room cross flow in the sensitivity study of 17 bedrock cases (Table 2-2), and the progress over time is shown for 6 time slices (Table 2-1). Individual disposal rooms of SFR 1 are compared in a) to e). To resolve the low early cross flow through the Silo, both linear e) and logarithmic scales f) are compared.*

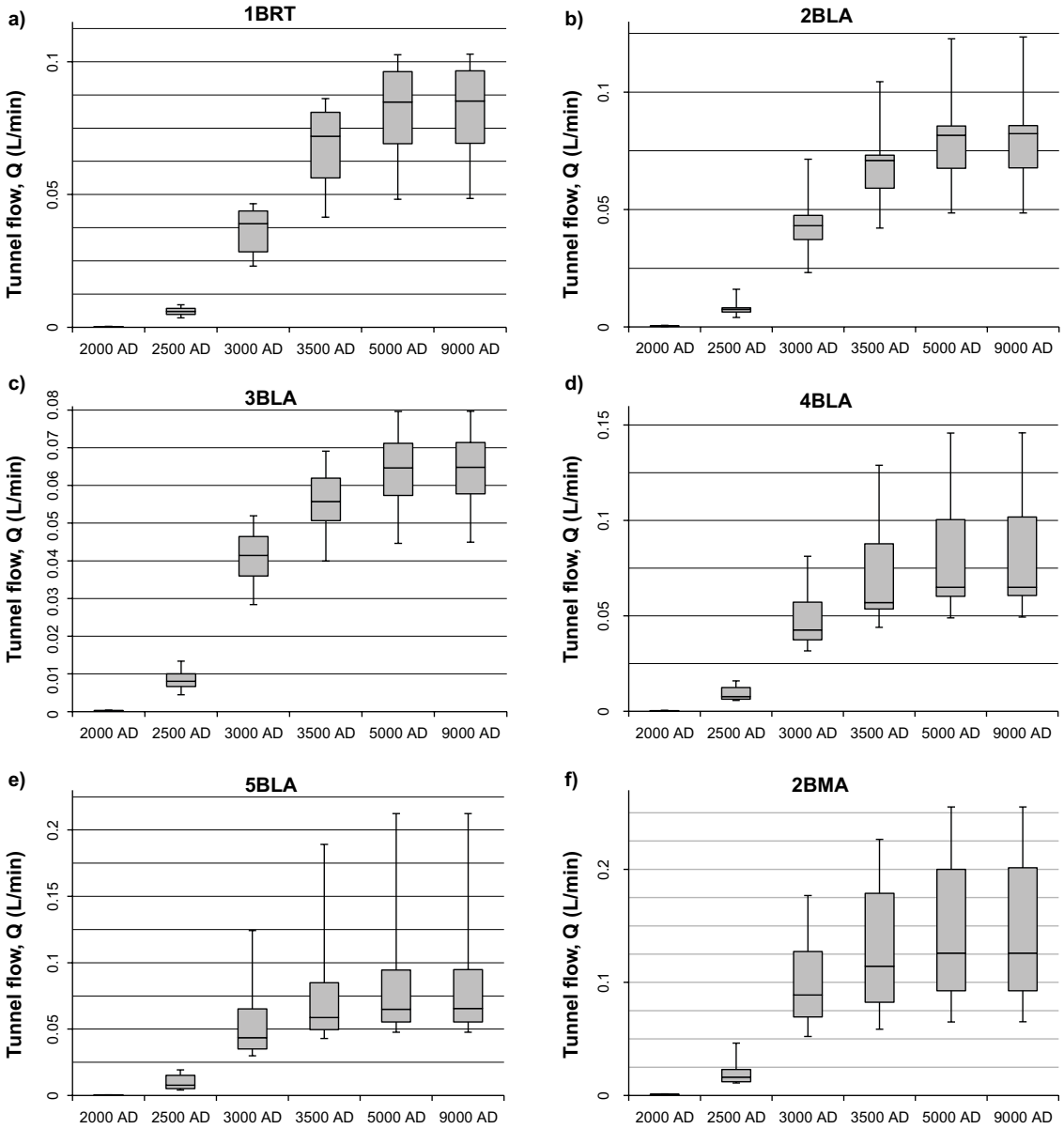

Figure 6-10. *Box-whisker plots of simulated disposal-room cross flow in the sensitivity study of 17 bedrock cases (Table 2-2), and the progress over time is shown for 6 time slices (Table 2-1). Individual disposal rooms of SFR 3 are compared in a) to e).*

6.2.3 Ranking bedrock cases with respect to disposal-room cross flow

One of the objectives in the TD11 sensitivity analysis is to determine three bedrock cases that cover the range of uncertainty/heterogeneity in bedrock parameterisation. The three representative bedrock cases are selected based on flow through the 11 disposal rooms in SFR 1 and SFR 3. However, the ranking of bedrock cases involves the following complexities of variability:

- The number of disposal-room cross flows is large (1,122), which requires a structured approach.
- The ensemble of cross flows is analysed as a multivariate, $Q(i, t, n)$, consisting of three variability components: 1) disposal room, i, 2) time slice, t, and 3) bedrock case, n.
- The range of disposal-room flow spans over several orders of magnitude (Figure 6-8); therefore the range of flows is linearized in terms of *percentiles*, in order to harmonise the relative weights between disposal rooms.

The ranking of bedrock cases requires that the complexity in variability is reduced, and this is done in two steps. Firstly, ensembles of disposal-room flows, Q, are translated into cumulative-distribution percentiles, $Q_{\%}$. This translation is done for each [time slice]/[disposal room]-combination, (i, t), i.e. $Q(i, t, n = 1…17)$, are translated into $Q_{\%}(i, t, n = 1…17)$, see example in Table 6-1. In other words, the highest flow, for a given (i, t)-combination, is assigned the highest percentile, 0.97, while the lowest flow is assigned the lowest percentile, 0.03.

Secondly, the ranking of n bedrock cases requires variability analysis to cover aspects of: 1) changing flow regime with retreating shoreline, t, and 2) differences among the different disposal rooms, i. The complexity in variability is therefore further reduced by analysing flow percentiles in terms of *ensemble-averages*, $\{Q_{\%}\}$, one at the time, where the variable of averaging is denoted by a dash, "-". The time aspect, $\{Q_{\%}\}(-, t, n)$, is analysed in terms of averaging over disposal rooms, $i = 1…N_i$:

$$\{Q_{\%}\}(-,t,n) = \sum_{i=1}^{N_i} \frac{Q_{\%}(i,t,n)}{N_i} \tag{6-1}$$

while disposal-room variability, $\{Q_{\%}\}(i, -, n)$, is analysed in terms of averaging over time slices, $t = 2…N_t$:

$$\{Q_{\%}\}(i,-,n) = \sum_{t=2}^{N_t} \frac{Q_{\%}(i,t,n)}{N_t} \tag{6-2}$$

It is noted that the time slice 2000 AD exhibits a clearly deviating pattern in disposal-room flow (Table 6-2), which is related to the submerged flow regime below sea. Therefore, the time slice 2000 AD is not included in Equation (6-2).

Inspection of ensemble-mean flow percentiles (Table 6-2 and Table 6-3) suggests the following:

- The variability component related to shoreline retreat, t, is small after 2500 AD (Table 6-2). However, the flow regime at 2000 AD exhibits a clearly different appearance.
- The variability component is large between disposal rooms, i (Table 6-3). None of the 17 bedrock cases is a clear outlier, with consistently large flow percentiles for *all* disposal rooms.
- The assumed depth trend in HCDs clearly renders higher average flow percentiles (Table 6-2 and Table 6-3). Bedrock case no. 15 [nc_NoD_R01_DFN_R18] has the lowest average flow percentiles and is therefore selected as the "low-tunnel flow bedrock case".
- Bedrock case no. 1 [BASE_CASE1_DFN_R85] has, on average, typically median flow percentiles (Table 6-3). Moreover, it has the most basic HCD parameterisation, assuming homogeneous transmissivity with depth trend. It is therefore selected as the "median-tunnel flow bedrock case".
- Bedrock cases including the DFN realisation R85 and HCD realisation R07 render higher average flow percentiles (Table 6-2 and Table 6-3). Bedrock case no. 11 [nc_DEP_R07_DFN_R85] has the highest average flow percentiles and is therefore selected as the "high-tunnel flow bedrock case".

Table 6-1. Cross flow percentile (*i*=1BMA, *t*=5000 AD).

n	Bedrock case	Q(1BMA,5000AD,*n*) [L/min]	$Q_{\%}$(1BMA,5000AD,*n*) [–]
1	BASE_CASE1_DFN_R85	0.19	0.32
2	BASE_CASE1_DFN_R18	0.16	0.15
3	BASE_CASE2_DFN_R85	0.19	0.38
4	nc_DEP_HOM_DFN_R03	0.34	0.68
5	nc_DEP_HOM_DFN_R85	0.20	0.44
6	nc_NoD_HOM_DFN_R85	0.16	0.09
7	CD_DEP_R01_DFN_R85	0.23	0.56
8	nc_DEP_R01_DFN_R85	0.21	0.5
9	nc_DEP_R01_DFN_R18	0.18	0.26
10	CD_DEP_R07_DFN_R85	0.44	0.79
11	nc_DEP_R07_DFN_R85	0.49	0.91
12	nc_DEP_R07_DFN_R18	0.44	0.85
13	nc_NoD_R01_DFN_R03	0.30	0.62
14	nc_NoD_R01_DFN_R85	0.17	0.21
15	nc_NoD_R01_DFN_R18	0.14	0.03
16	nc_NoD_R07_DFN_R85	0.36	0.74
17	nc_NoD_R07_DFN_R03	0.54	0.97

Table 6-2. Ensemble average {$Q_{\%}$} (-, *t*, *n*) over disposal room[s1]).

n	Bedrock case	2000AD	2500AD	3000AD	3500AD	5000AD	9000AD
1	BASE_CASE1_DFN_R85	0.38	0.45	0.44	0.49	0.49	0.48
2	BASE_CASE1_DFN_R18	0.22	0.26	0.32	0.28	0.29	0.29
3	BASE_CASE2_DFN_R85	0.13	0.43	0.44	0.45	0.49	0.48
4	nc_DEP_HOM_DFN_R03	0.46	0.55	0.48	0.55	0.54	0.54
5	nc_DEP_HOM_DFN_R85	0.57	0.63	0.61	0.64	0.63	0.62
6	nc_NoD_HOM_DFN_R85	0.84	0.32	0.25	0.31	0.34	0.33
7	CD_DEP_R01_DFN_R85	0.28	0.46	0.53	0.54	0.53	0.54
8	nc_DEP_R01_DFN_R85	0.34	0.71	0.7	0.66	0.64	0.65
9	nc_DEP_R01_DFN_R18	0.16	0.6	0.64	0.56	0.55	0.55
10	CD_DEP_R07_DFN_R85	0.45	0.64	0.68	0.64	0.66	0.66
11	nc_DEP_R07_DFN_R85	0.68	0.81	0.76	0.76	0.76	0.76
12	nc_DEP_R07_DFN_R18	0.47	0.7	0.64	0.59	0.58	0.59
13	nc_NoD_R01_DFN_R03	0.54	0.33	0.37	0.39	0.39	0.39
14	nc_NoD_R01_DFN_R85	0.66	0.39	0.43	0.43	0.39	0.4
15	nc_NoD_R01_DFN_R18	0.57	0.23	0.25	0.24	0.24	0.24
16	nc_NoD_R07_DFN_R85	0.91	0.54	0.53	0.52	0.52	0.53
17	nc_NoD_R07_DFN_R03	0.84	0.44	0.43	0.45	0.45	0.46

[1)] Average percentiles coloured by value. High = red, median = yellow, low = green. Bedrock cases n = 1, 11, and 15 (marked yellow) are selected as representative for covering the range of uncertainty/heterogeneity in bedrock parameterisation, with respect to disposal-room flow.

Table 6-3. Ensemble average {$Q_{\%}$} (i, -, *n*) over time slice[s1]).

n	Bedrock case	1BTF	2BTF	1BLA	1BMA	Silo	1BRT	2BLA	3BLA	4BLA	5BLA	2BMA
1	BASE_CASE1_DFN_R85	0.22	0.61	0.72	0.31	0.77	0.48	0.63	0.69	0.42	0.18	0.15
2	BASE_CASE1_DFN_R18	0.12	0.41	0.45	0.11	0.78	0.03	0.26	0.18	0.34	0.44	0.04
3	BASE_CASE2_DFN_R85	0.28	0.64	0.76	0.32	0.82	0.42	0.56	0.65	0.37	0.15	0.09
4	nc_DEP_HOM_DFN_R03	0.38	0.12	0.12	0.70	0.36	0.74	0.28	0.54	0.95	0.97	0.70
5	nc_DEP_HOM_DFN_R85	0.89	0.49	0.50	0.45	0.31	0.62	0.76	0.84	0.85	0.69	0.50
6	nc_NoD_HOM_DFN_R85	0.55	0.34	0.36	0.15	0.31	0.24	0.37	0.31	0.36	0.21	0.23
7	CD_DEP_R01_DFN_R85	0.92	0.66	0.58	0.52	0.83	0.32	0.50	0.78	0.14	0.17	0.30
8	nc_DEP_R01_DFN_R85	0.77	0.39	0.52	0.51	0.50	0.97	0.97	0.82	0.44	0.64	0.88
9	nc_DEP_R01_DFN_R18	0.71	0.28	0.21	0.26	0.61	0.91	0.91	0.49	0.41	0.81	0.81
10	CD_DEP_R07_DFN_R85	0.90	0.96	0.95	0.81	0.92	0.46	0.79	0.52	0.57	0.03	0.28
11	nc_DEP_R07_DFN_R85	0.52	0.92	0.92	0.91	0.14	0.85	0.82	0.95	0.85	0.62	0.96
12	nc_DEP_R07_DFN_R18	0.68	0.77	0.66	0.81	0.34	0.26	0.22	0.69	0.82	0.71	0.89
13	nc_NoD_R01_DFN_R03	0.09	0.05	0.05	0.63	0.41	0.69	0.09	0.06	0.58	0.85	0.61
14	nc_NoD_R01_DFN_R85	0.58	0.26	0.37	0.25	0.44	0.66	0.62	0.35	0.11	0.35	0.45
15	nc_NoD_R01_DFN_R18	0.45	0.14	0.12	0.04	0.61	0.09	0.19	0.08	0.04	0.50	0.37
16	nc_NoD_R07_DFN_R85	0.38	0.81	0.86	0.74	0.16	0.54	0.50	0.39	0.51	0.36	0.55
17	nc_NoD_R07_DFN_R03	0.05	0.65	0.32	0.97	0.21	0.22	0.03	0.16	0.75	0.83	0.71

[1)] Time slice 2000 AD **not** included. Average percentiles coloured by value. High = red, median = yellow, low = green. Bedrock cases n = 1, 11, and 15 (marked yellow) are selected as representative for covering the range of uncertainty/ heterogeneity in bedrock parameterisation, with respect to disposal-room flow.

6.3 Biosphere objects

Biosphere objects have been defined within the SR-PSU project (e.g. Figure 6-11), based on the simulation results in SKBdoc 1395214. To verify that the biosphere objects have been properly defined, the simulated flow across the bedrock surface is analysed inside these biosphere objects (see Section 6.3.1). A single bedrock case is studied [BASE_CASE1_DFN_R85], with particular emphasis to the time slice 5000 AD. Two aspects are analysed:

1) Recharge/discharge over the bedrock surface.
2) Backward particle tracking from a particular biosphere object (157_2; located immediately north of the SFR pier).

6.3.1 Recharge and discharge over the bedrock surface

Biosphere objects are temporarily defined in the computational grid, by means of input data presented in Table A-12. The flow across the bedrock surface inside each biosphere object is then calculated according to the cell-net principle, Equation (5-2). Locally variable recharge/discharge in biosphere objects is expressed in terms of normalised flux, q_{norm} (-), which is expressed as a factor of modelled net precipitation (160 mm/yr; Figure 6-11). High local fluxes, $|q_{norm}| > 1$, are associated to ground-surface intersections with deformation zones.

Net-bedrock flow is also calculated for biosphere objects (i.e. the *net* of recharge and discharge flow across the bedrock surface, as summed per biosphere-object basis). The calculations are performed for all time slices and all biosphere objects that are fully covered by the DarcyTools flow domain (Table 6-4). These biosphere-net flows are expressed in terms of area-normalised flux, q (mm/yr). The highest net discharge is found in Lake Kylvattenkanalen (biosphere object ID = 120), and the largest net recharge is found in Lake Biotestsjön (biosphere object ID = 179).

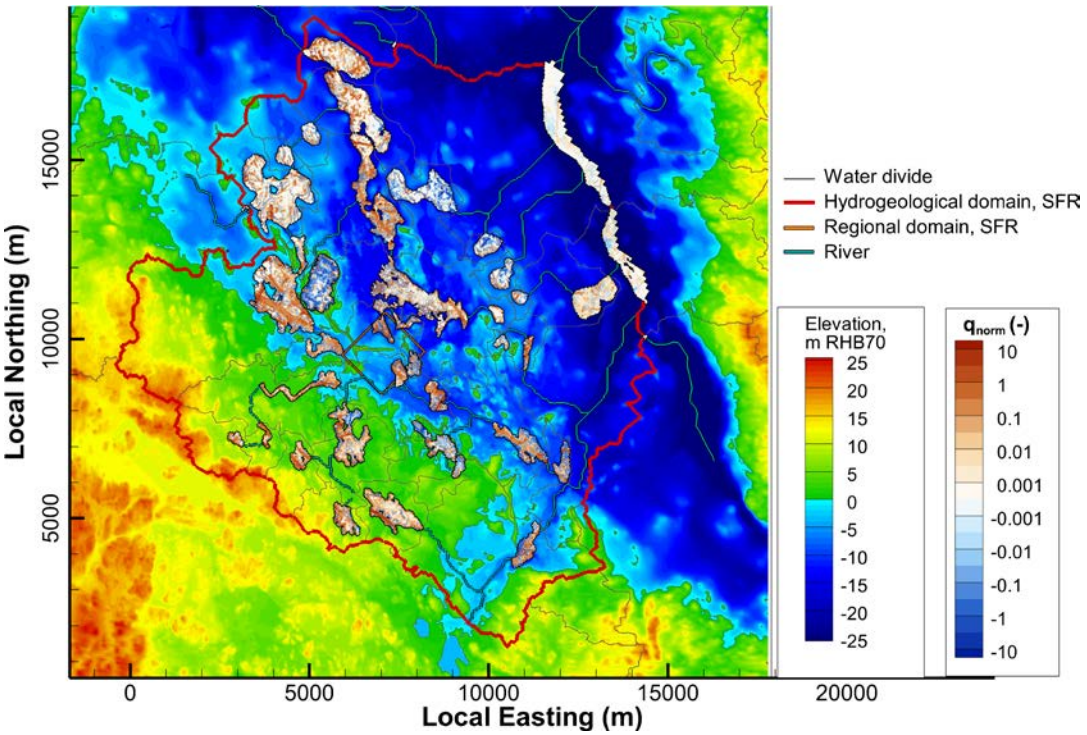

Figure 6-11. *Simulated flux, q, across bedrock surface in biosphere objects, BASE_CASE1_DFN_R85, 5000AD. Local recharge, into the bedrock (blue), and discharge, from the bedrock (red), normalised by modelled recharge (160 mm/yr).*

Table 6-4. Bedrock recharge[1] in biosphere objects, q (mm/yr).

Object ID	2000AD	2500AD	3000AD	3500AD	5000AD	9000AD
107	1.4	6.4	19.9	21.3	19.8	18.9
108	0.1	0.3	1	3.3	39	29.4
110	0.5	6.8	46.4	25.7	21.1	21.7
116	0	0.3	1.8	3.8	27.9	18.9
117	3.4	24.4	57.6	52.8	51.8	47.2
118	1.4	9.8	19.5	16.2	15.8	13
120	53.7	267	251.7	226.4	131.7	125.7
121_1	3.6	21.2	46.5	82.3	118.7	97
121_2	0.7	3.1	17.5	44.6	43.3	44
123	1	4.9	17.7	45	88.6	58.4
124	92.7	29.3	–3.1	–15	–27.9	–18.4
125	22.3	11.2	10	9.9	11.9	3.3
126	0.1	0.6	2	7.9	28	10.9
129	130.1	156.7	161	153.4	50.8	54.4
132	175	167	161.9	172	130.9	131.4
134	20.6	33	13.3	0.1	–3.9	–3.9
136	51.1	44.9	42.8	42.8	48.5	38
142	176.9	169.9	157.3	140.2	64.3	65.4
144	7.6	–0.9	–2.3	–2.6	–4.7	–4.6
146	0.1	0.2	0.7	4.3	25	31.1
148	75.1	73	72.3	70.5	67	63.2
149	69.3	66.9	65.1	67.2	58.3	54.7
150	1.5	8.7	19.1	28.4	27.7	26.1
152	0	0	0.1	1.4	43	32
153	0	0.2	3.2	17.6	0.3	–2.3
154	0	0	0.1	0.8	25.1	20
155	0	0.4	6	5.9	2.5	3.1
156	2.4	14.5	45.8	40.8	33.9	24.5
157_1	0	0.1	0.3	1.2	20.7	16.6
157_2	0	0.5	8.8	51.5	79.6	80.4
158	0.1	0.4	2.2	23.2	19	19.3
159	0	0	1.1	7	52	37.1
160	0.1	0.6	6.4	–2.1	–7.9	–8.4
173	0	0	0.4	3.1	–26.6	–24.4
175	0	0	0.2	2.9	–25.7	–26.3
176	9.2	56.2	58.5	62.7	78.7	86.3
177	0	0	2.1	23.7	–10	–14.1
178	0	0.2	9.3	46.1	6.3	8.3
179	5.5	–22	–49.2	–48.2	–46.8	–38.9
180	0	0	0	0.1	3.6	0.6

[1] Bedrock case [BASE_CASE1_DFN_R85].

6.3.2 Particle tracking from biosphere object 157_2

Biosphere object 157_2 has been identified as an important discharge area for the SR-PSU project (discharge presented in Table 6-4). At later stages of shoreline retreat, high densities of particle-exit locations are obtained in object 157_2 (Section 6.4). There are several reasons for this:

1) **Geology**: Groundwater flow from SFR (i.e. downstream flow paths) is more or less enclosed by three deformation zones: the steeply dipping zones NNE0869 and NW0805A/B (Figure 6-12), and the gently dipping zone ZFM871 located just below the existing SFR facility. The junction between these deformation zones occurs underneath biosphere object 157_2.
2) **Location and topography**: Biosphere object 157_2 is a local topographical depression just north of SFR (Figure 6-12 and Figure 6-13), which according to the topographical gradient is downstream of SFR.
3) **Sediment coverage**: the thickness of low-conductive sediment layers is thin north of the pier (Figure 4-11).

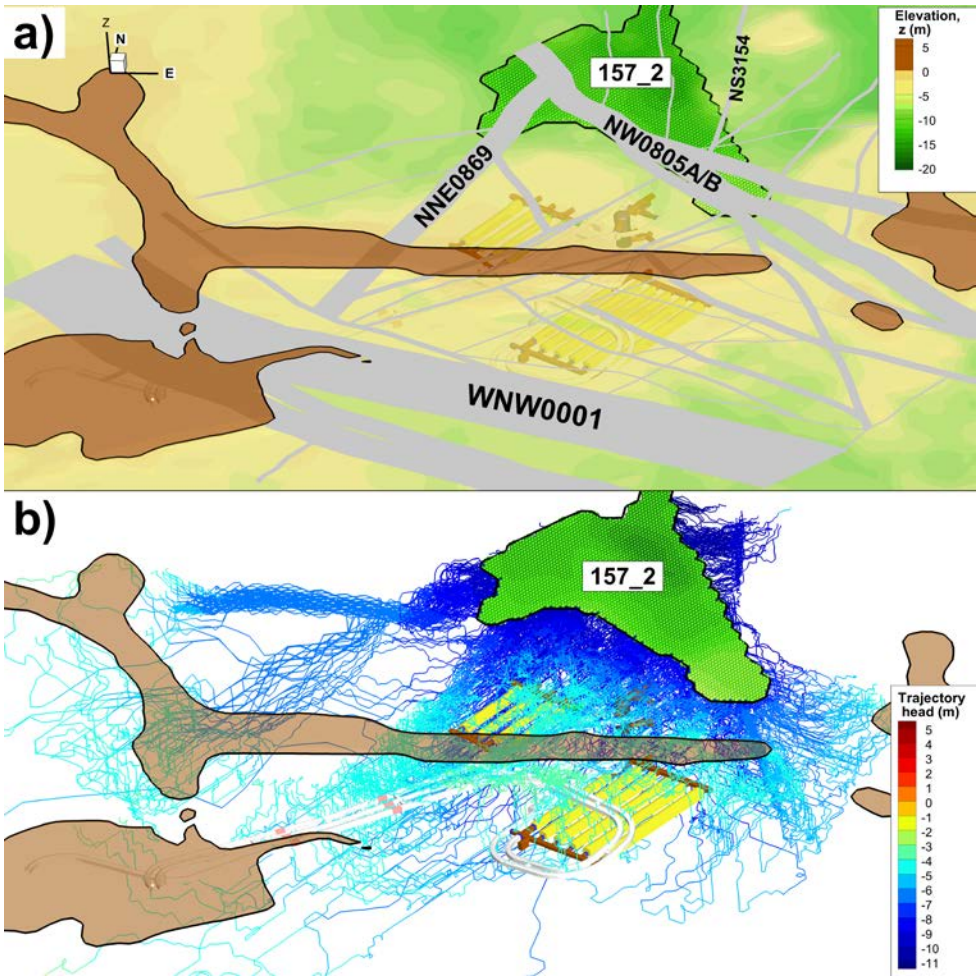

Figure 6-12. *Backward particle-tracking from biosphere object ID 157_2, [BASE_CASE1_DFN_R85], 5000AD; particle-release points contoured by elevation, recharge trajectories contoured by head (m), tunnels shaded by backfill (c.f. Figure 3-3), and ground intercepts with deformation zones grey-shaded.*

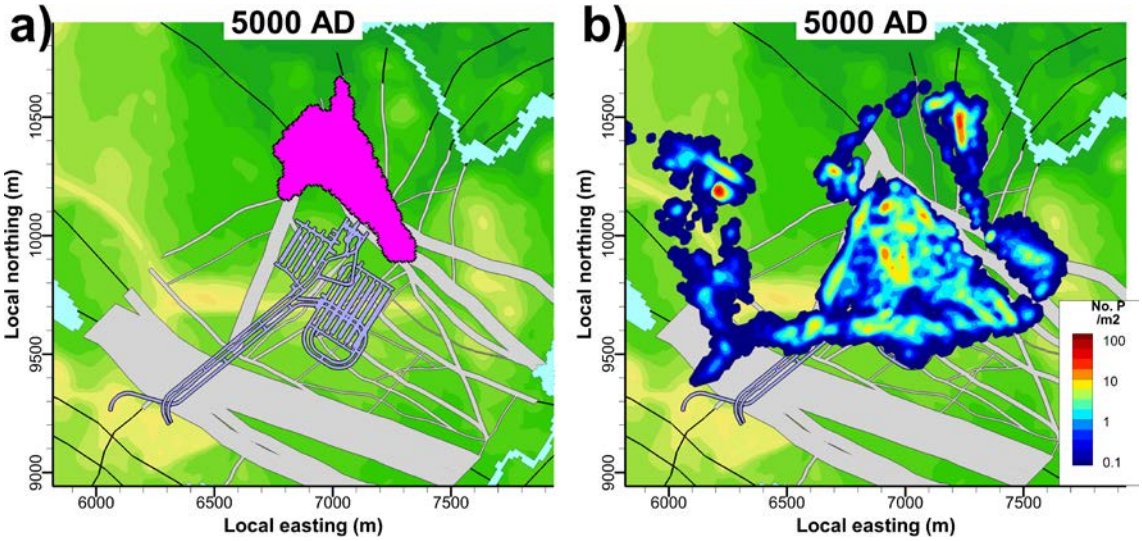

Figure 6-13. *Recharge locations for biosphere object ID 157_2, [BASE_CASE1_DFN_R85], 5000AD; a) particle-release points for backward particle-tracking (pink) and b) areal density of recharge locations. 1,000,000 particles released at bedrock surface. Direct recharge not included (i.e. trajectories must pass at least one bedrock cell). Few recharge locations are found in the Forsmark inland (not shown).*

It is therefore of interest to perform backward-particle tracking, to determine the source of discharging groundwater, i.e. the amount of groundwater passing the SFR facility. 1,000,000 particles are released at the bedrock surface inside biosphere object 157_2. Local flux varies within the biosphere object, including fluxes of opposite directions (Figure 6-11). To eliminate artefacts of "direct local recharge", a criterion was setup where backward trajectories reaching the HSD interface directly are rejected from results (i.e. trajectories must *at least* pass one bedrock cell outside biosphere object 157_2). A number of remote recharge locations are also found in the more elevated parts of the Forsmark inland (not shown; the fraction of remote recharge locations is shown in Figure 6-14). About 4% of the recharge to biosphere object 157_2 passes disposal rooms of SFR 1 or SFR 3 (Table 6-5).

Table 6-5. Fraction of recharge crossing disposal rooms.

Disposal room	Recharge fraction
1BTF	0.29%
2BTF	0.36%
1BLA	1.25%
1BMA	0.66%
Silo	0.02%
2BLA	0.45%
3BLA	0.26%
4BLA	0.15%
5BLA	0.12%
2BMA	0.17%
1BRT	0.34%
Total	**4.06%**

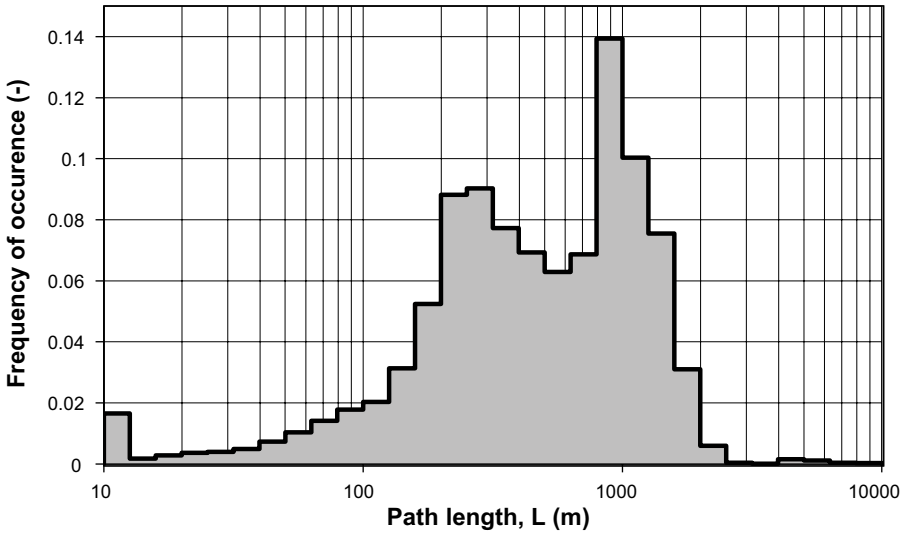

Figure 6-14. *Distribution of path lengths in backward particle-tracking from 157_2, [BASE_CASE1_ DFN_R85], 5000AD. Only path lengths shorter than c. 1,000 m shown in Figure 6-12 and Figure 6-13.*

6.4 Particle tracking

Recharge and discharge locations for flow across disposal rooms are simulated by means of particle tracking. The recharge/discharge refers to flow across the bedrock surface (i.e. the interface between bedrock and overlying HSD). The spatial distribution of these locations is quantified in terms of areal density, number of particles/m^2, based on 1,000,000 particles released uniformly within the disposal rooms of SFR 1 and SFR 3, respectively. Recharge flow paths are determined by means of *backward* particle tracking, with the disposal rooms as the starting point (i.e. only including *upstream* flow components in Equation (5-3)). Analogously, discharge locations (or, "exit locations") are determined by means of *forward* particle tracking, with the disposal rooms as the starting point (i.e. only including *downstream* flow components in Equation (5-3)).

The starting point of trajectories is defined at the tunnel-wall passage, and the termination point of trajectories (i.e. "recharge location" or "discharge location", depending on direction of particle tracking) is defined at the bedrock/HSD interface passage.

6.4.1 Recharge locations

The spatial distribution of recharge locations for SFR 1 and SFR 3 is compared in terms of areal density (No. particles/m^2; Figure 6-15 and Figure 6-16, respectively). The occurrence of recharge locations is associated to topographical peaks, as well as, hydraulic conduits. The change in recharge locations over time is analysed by comparisons between the six selected time slices (shown in the sequence a) to f) in Figure 6-15 and Figure 6-16, respectively).

At the present shoreline (time slice 2000 AD), the simulated recharge occurs near the shore of the Forsmark mainland (i.e. not from the constructed pier above SFR). This is reasonable, as data indicate that the pier does not hold groundwater level significantly above sea level (Section 4.4). The recharge locations of SFR 1 and SFR 3 are more or less identical (c.f., Figure 6-15a and Figure 6-16a).

By the time slice 2500 AD, natural sediments have been lifted above sea level on both sides along the pier (land uplift per 500 years is approximately 3 m; Section 3.3.5). This relatively modest change in cost line causes a distinct turnover in the local flow regime around SFR (c.f., head solution in Figure 6-4b), which shifts the simulated recharge location from the Forsmark coast to the SFR pier (Figure 6-15b and Figure 6-16b). It is noted that the deeper SFR 3 still have some recharge from the Forsmark coast (Figure 6-16b).

From the time slice 3000 AD and onwards, the simulated pattern in recharge locations stabilises to more or less stationary. The dominant recharge to SFR 1 occurs via ZFMNNW1209 (formerly Zone 6; Figure 6-15d; note logarithmic scaling of density), although a minor contribution also comes from the elevated sediments, south of the SFR pier. In comparison, SFR 3 involves deeper and longer flow paths, which displaces the recharge towards the elevated sediments, south of the SFR pier. The deformation zones in this area are interpreted as less transmissive, and hence the recharge locations for SFR 3 are comparatively less correlated to deformation-zone intercepts than those for SFR 1. However, the thin zone ZFMWNW8042 can be identified as a major recharge location for SFR 3 (Figure 6-16d), which has a very similar transmissivity parameterisation to ZFMNNW1209 (Table 4-3).

The corresponding recharge locations for [BASE_CASE**2**_DFN_R85] are analysed to demonstrate the role of the Singö deformation zone (Figure 6-17 and Figure 6-18). Overall, the differences are small. However, inland recharge component for SFR 3 by 2500 AD (Figure 6-16b) exists only if the Southern boundary belt is parameterised as transmissive in the transversal direction (c.f., Figure 6-18b).

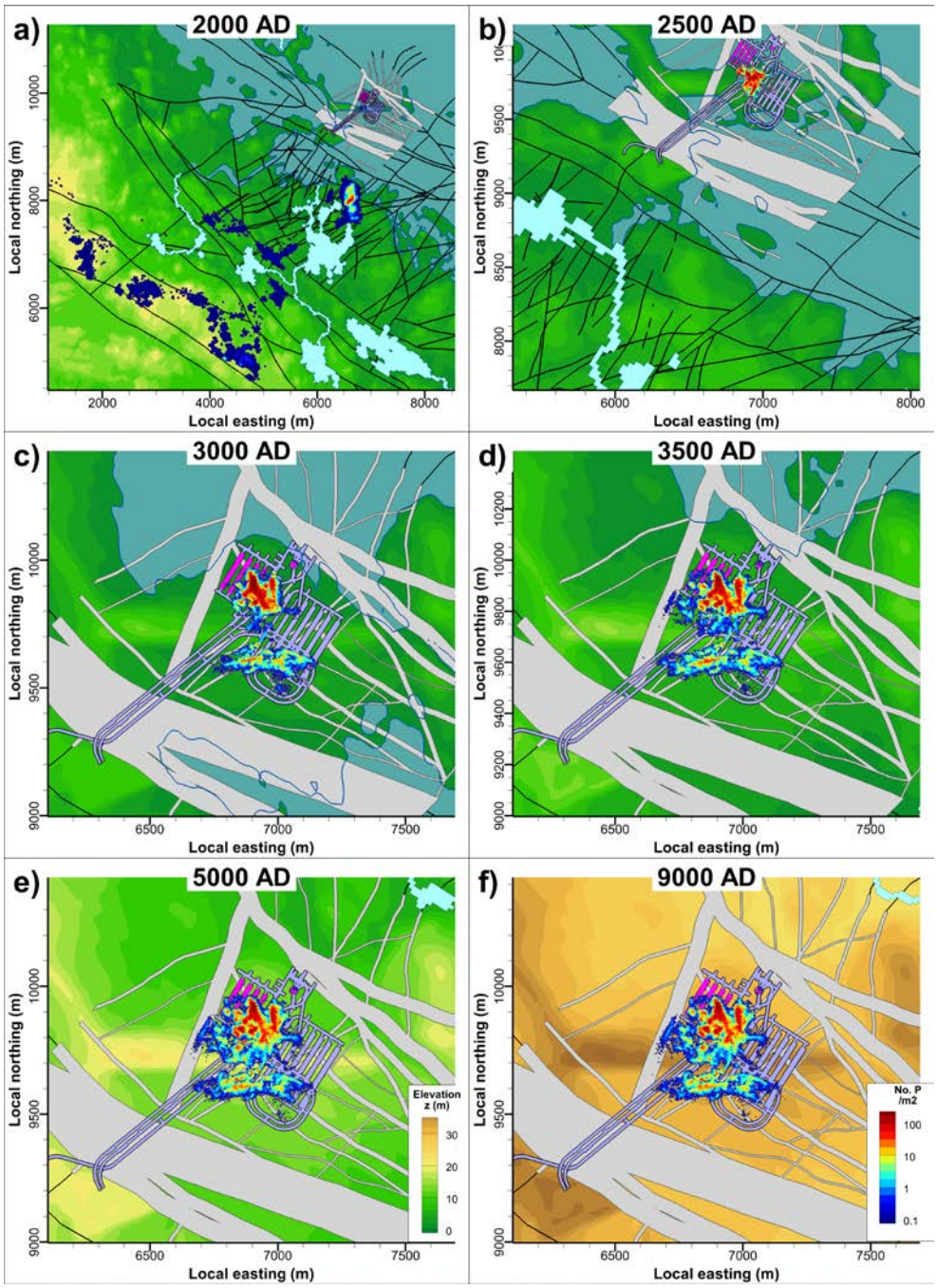

Figure 6-15. *Density of recharge locations for SFR 1 disposal rooms over time [BASE_CASE1_DFN_R85]. ZFMNNW1209 identified as a major recharge location.*

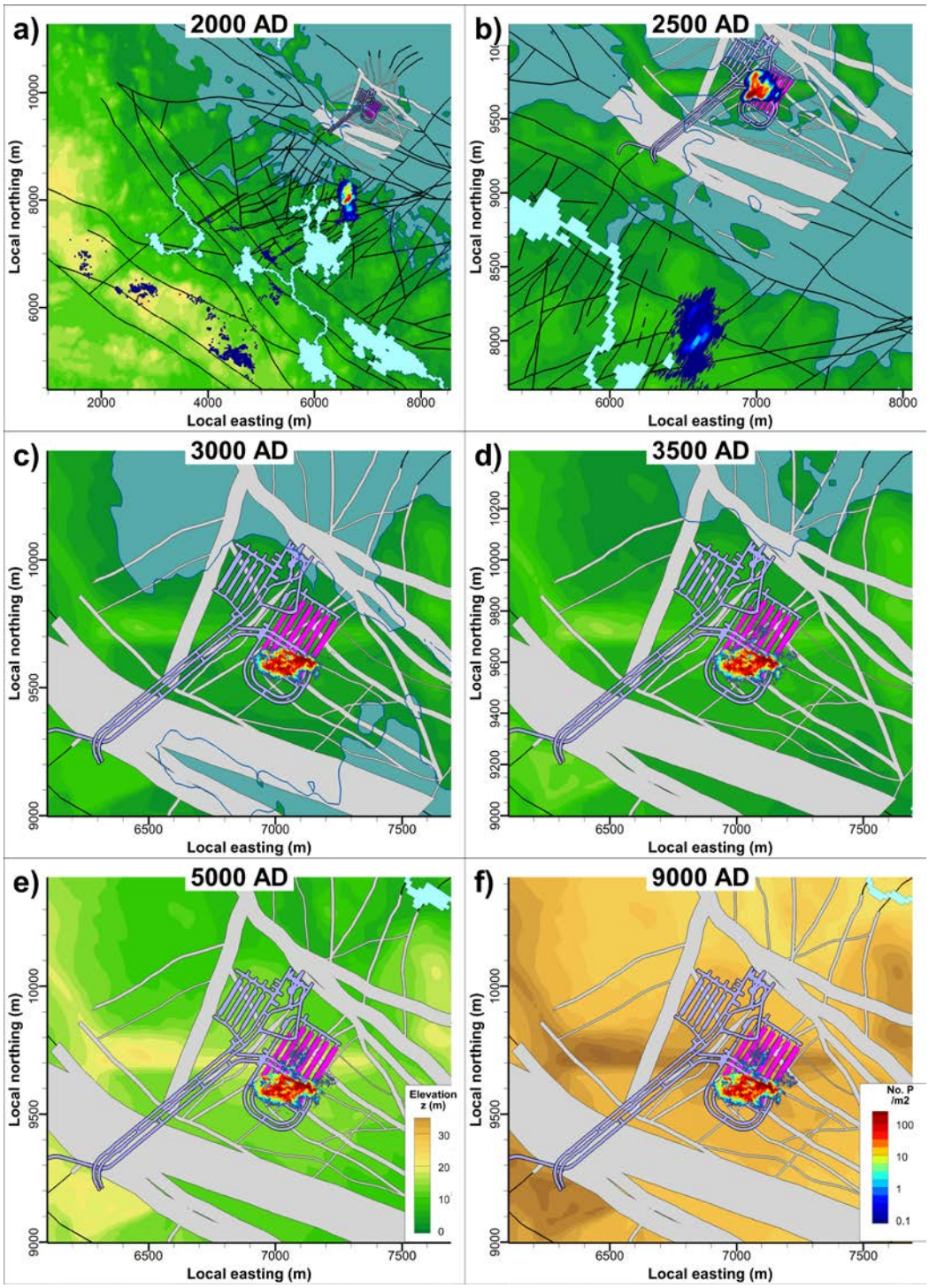

Figure 6-16. *Density of recharge locations for SFR 3 disposal rooms over time [BASE_CASE1_DFN_R85]. ZFMWNW8042 identified as a major recharge location.*

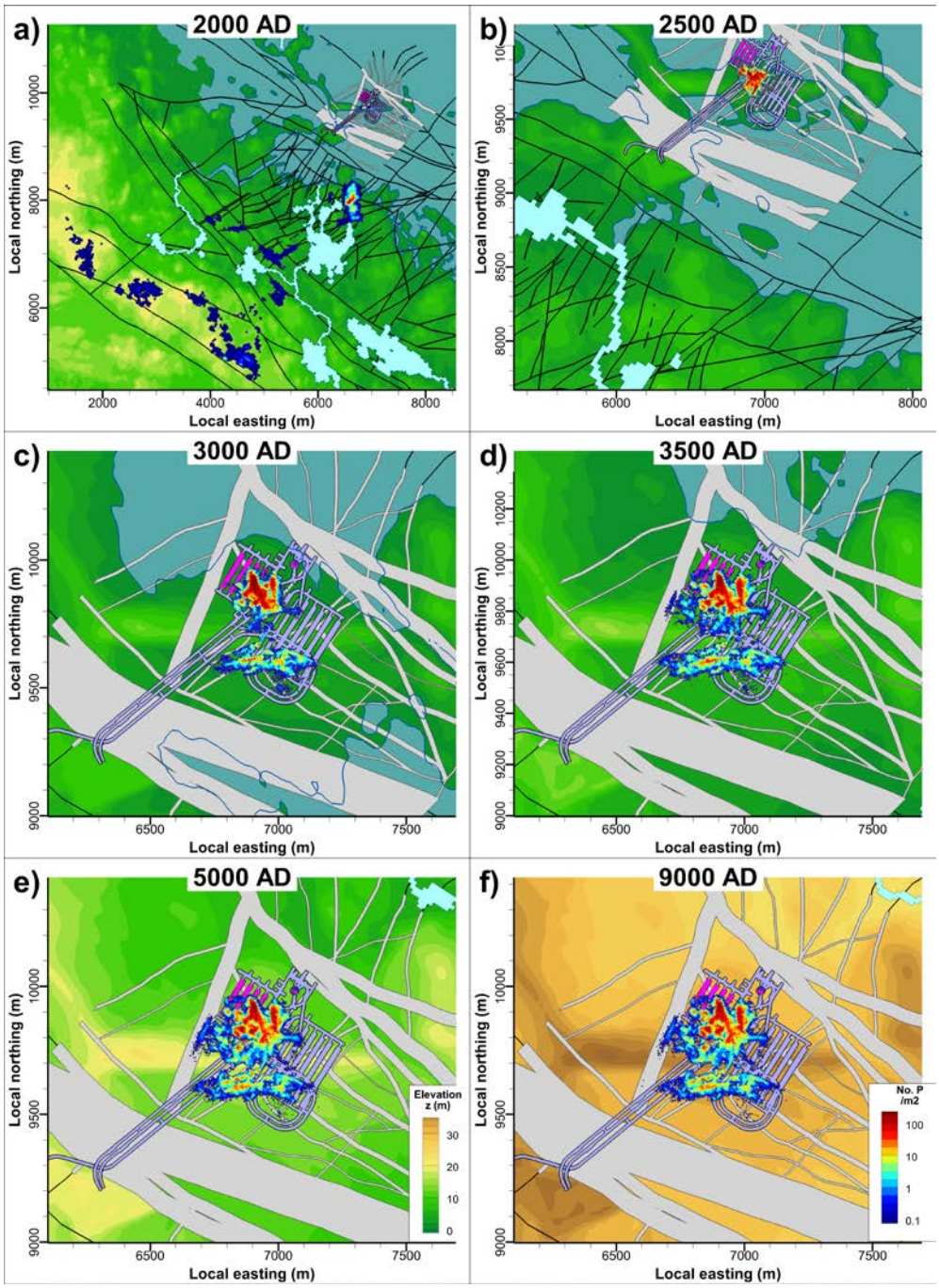

Figure 6-17. *Density of recharge locations for SFR 1 disposal rooms over time [BASE_CASE2_DFN_R85].*

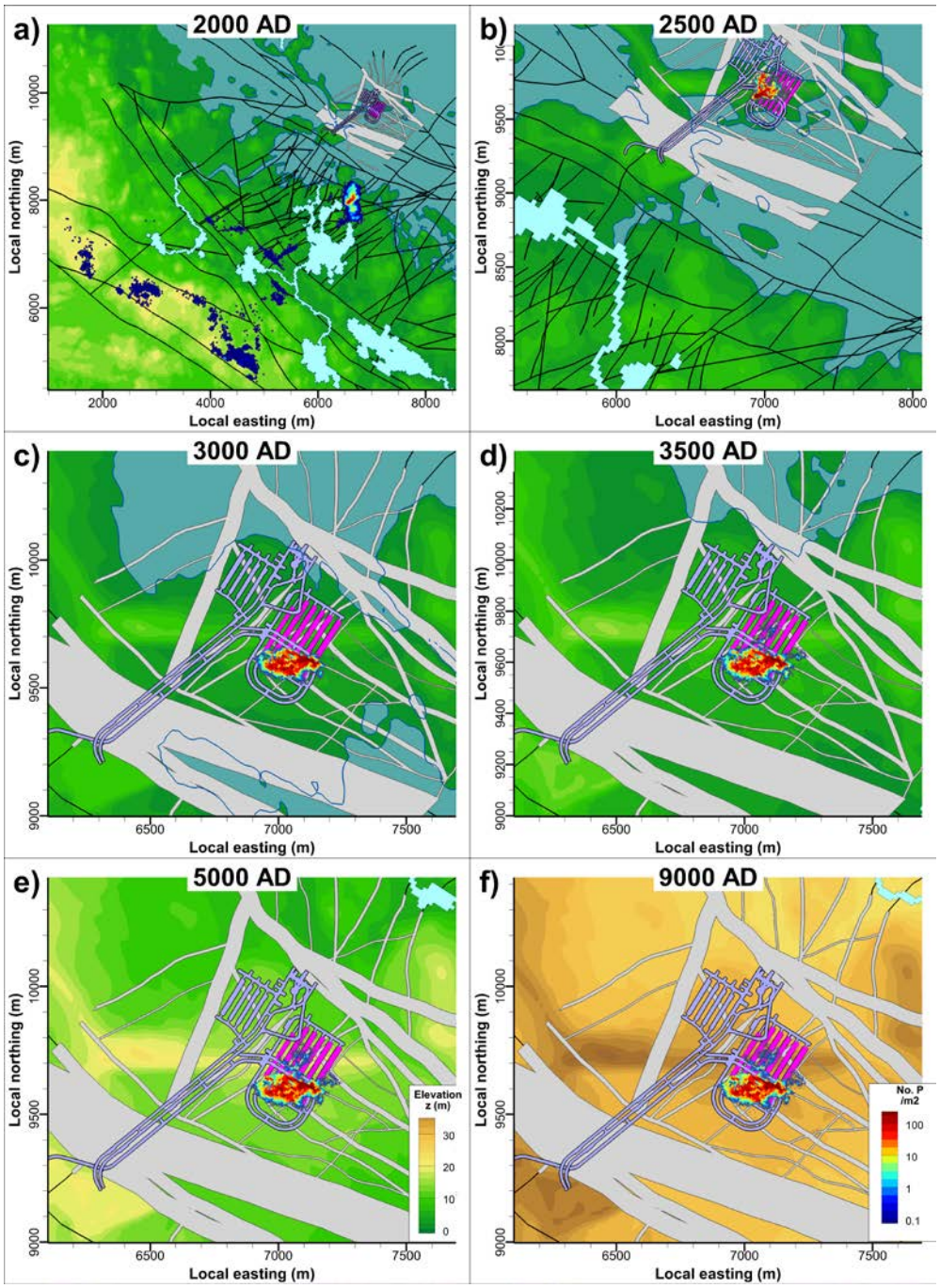

Figure 6-18. *Density of recharge locations for SFR 3 disposal rooms over time [BASE_CASE2_DFN_R85].*

6.4.2 Exit locations

The spatial distributions of discharge locations (or "exit locations") are evaluated analogously to the recharge locations (Section 6.4.1). The patterns in discharge locations of SFR 1 and SFR 3 are compared over time, in terms of the six selected time slices (Figure 6-19 and Figure 6-20). A couple of characteristics can be noted:

Shoreline displacement successively forces the exit locations further away from the release points. Before the time slice 3500 AD, exit locations are essentially below the cost line. The flow regime changes from upward-directed, under early time slices, to increasingly horizontal, during later time slices.

The density of exit locations is strongly correlated to ground intercepts of deformation zones (most likely, also transmissive stochastic DFN fractures). The dominant discharge path for SFR 1 is ZFMNNW1209 (Zone 6) during time slices 2000 to 2500 AD, after which ZFMNNE0869 and ZFMNW0805A/B dominates during time slices 3000 to 3500 AD. The pattern of exit locations from SFR 1 appears stationary between time slices 5000 and 9000 AD and in essence, all particles discharge to biosphere object 157_2 (e.g. Figure 6-19).

During early stages, SFR 3 has exit locations both north and south of the SFR pier. As the horizontal component in the flow regime successively grows, the exit locations are driven north, towards ZFMNW0805A/B and ZFMNS3154. Most particles discharge into biosphere object 157_2, although owing to its deeper location, a lesser amount of particles discharge into biosphere objects 27 and 31 (i.e. related to biosphere object 116, which is also referred to as Charlie's lake).

6.4.3 Performance measure statistics (Q, F_r, $t_{w,r}$, and L_r)

This section presents a brief summary of the performance-measure characteristics obtained for the 11 disposal rooms of SFR 1 and SFR 3. The focus is on the impact of the changing flow regime over time, which is evaluated by comparing the performance measures at six selected time slices. Median values are studied to simplify the presentation, e.g. median tunnel-cross flow, Q (dots in Figure 6-21), and the range of variability among 17 Bedrock cases (error bars in Figure 6-21). As discussed in Section 6.2, all cross flows increase in accordance with the shoreline retreat up to about 5000 AD (Figure 6-21). Thereafter, the driving force imposed by the downstream condition associated with the Baltic Sea becomes less important relative to topographically driven flow.

The same pattern related to the changing flow regime can also be observed in performance measures of particle tracking (Figure 6-22 to Figure 6-24). Here, the measures F_r, $t_{w,r}$, and L_r have been determined by means of forward tracking of 100,000 particles released in each of the 11 disposal rooms of SFR 1 and SFR 3, but only for the three selected Bedrock cases (Section 6.2.3). The output of each particle-tracking simulation is a distribution of performance measures (i.e. $3\times11\times100{,}000$), but in order to simplify the presentation only median values are studied., The largest and lowest median values among these three Bedrock cases are shown as error bars in Figure 6-22 to Figure 6-24, whereas the middle median value is indicated by a dot. Examples of the corresponding underlying distributions are presented in sections 6.4.4 to 6.4.6 (although not resolved at the individual disposal-room level).

The median path length increases over time, up to c. 5000 AD (Figure 6-22), which reflects the discharge successively taking place at more distant downstream locations (Figure 6-19 and Figure 6-20). Owing to its deeper location, SFR 3 has systematically longer path lengths than SFR 1. As the flow-field grows stronger over time, the advective travel time and flow-related transport resistance decrease (Figure 6-23 and Figure 6-24). In other words, in the determination of these performance measures, the significance of increasing flows outweighs the increasing path lengths. Again, SFR 3 has systematically longer advective travel times and higher flow-related transport resistance, which is – at least partly – due to its generally lower flows and deeper location.

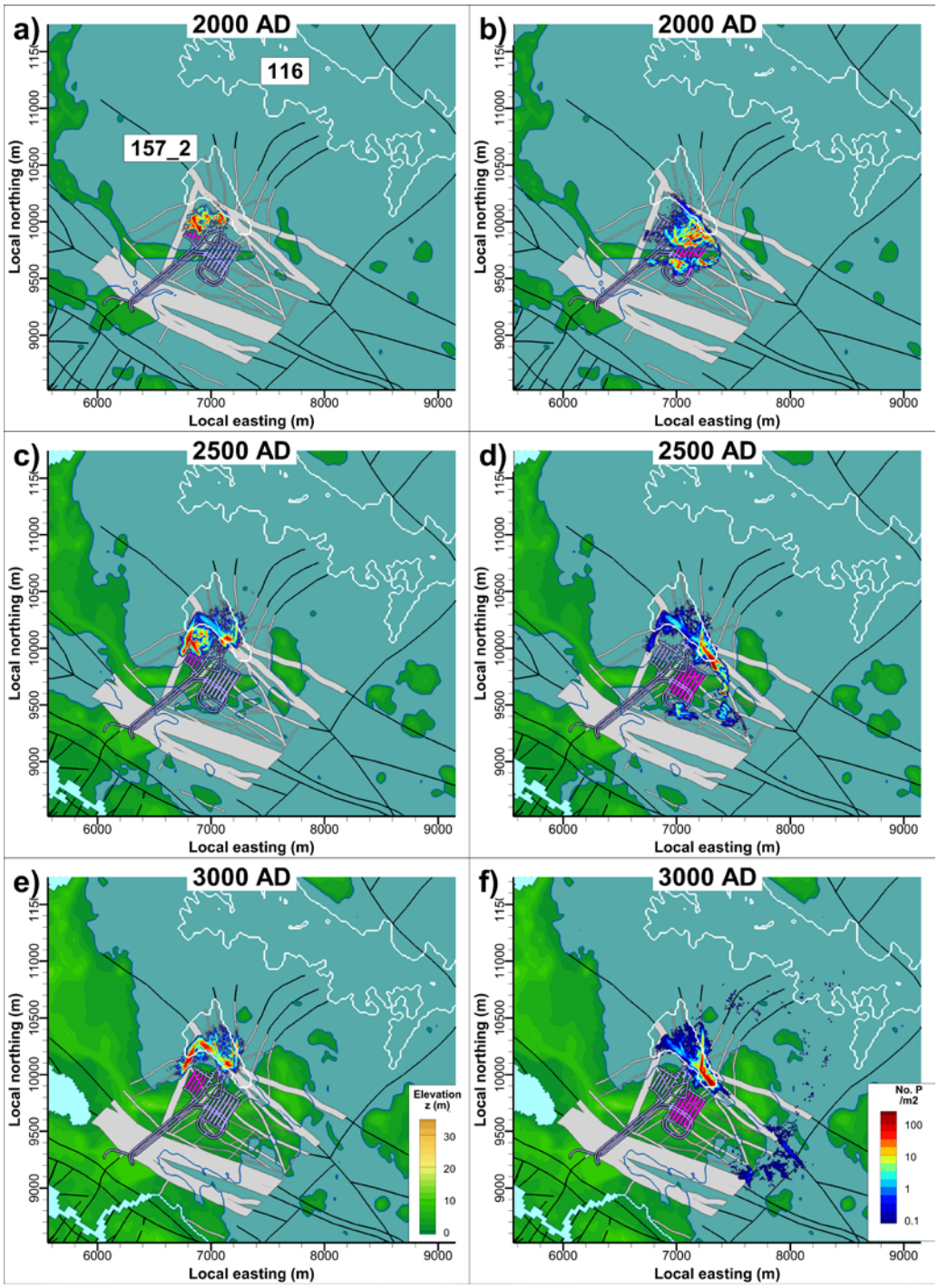

Figure 6-19. *Early exit locations from disposal rooms in SFR 1 (pink shade; left) and SFR 3 (pink shade; right), [BASE_CASE1_DFN_R85], time slices 2000 to 3000 AD. Biosphere object IDs 116 and 157_2 included for reference (white lines).*

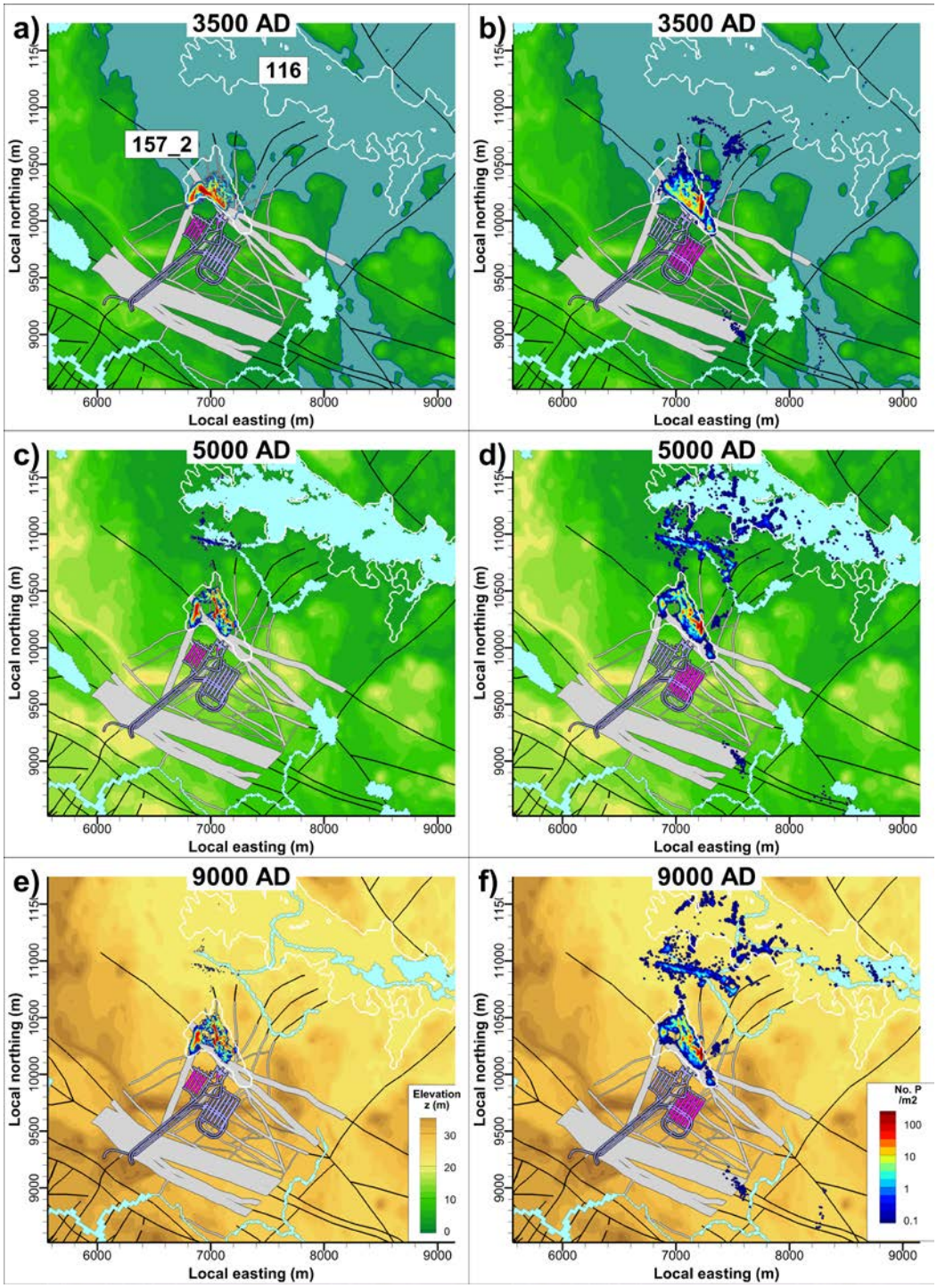

Figure 6-20. *Late exit locations from disposal rooms in SFR 1 (pink shade; left) and SFR 3 (pink shade; right), [BASE_CASE1_DFN_R85], time slices 3500 to 9000 AD. Biosphere object IDs 116 and 157_2 included for reference (white lines).*

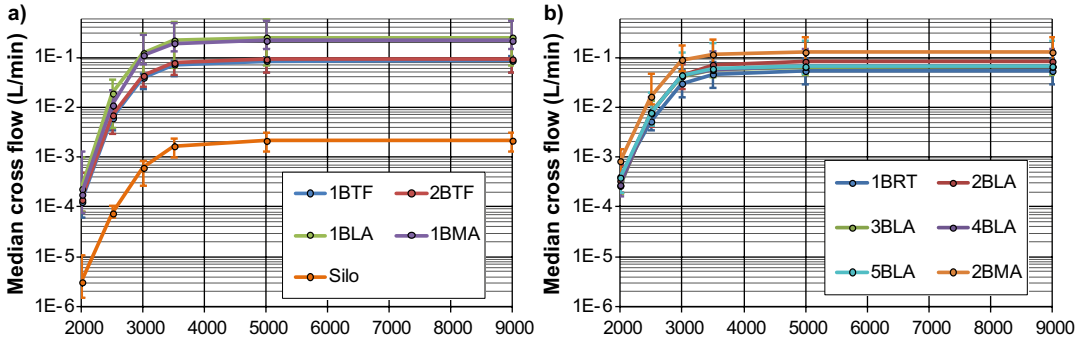

Figure 6-21. *Cross flow (Q) in disposal rooms over time: a) in SFR 1 and b) in SFR 3. Dots indicate median values over all 17 Bedrock cases, while the bars indicate the observed variability among the Bedrock cases (c.f., Figure 6-8 to Figure 6-10 in Section 6.2.2).*

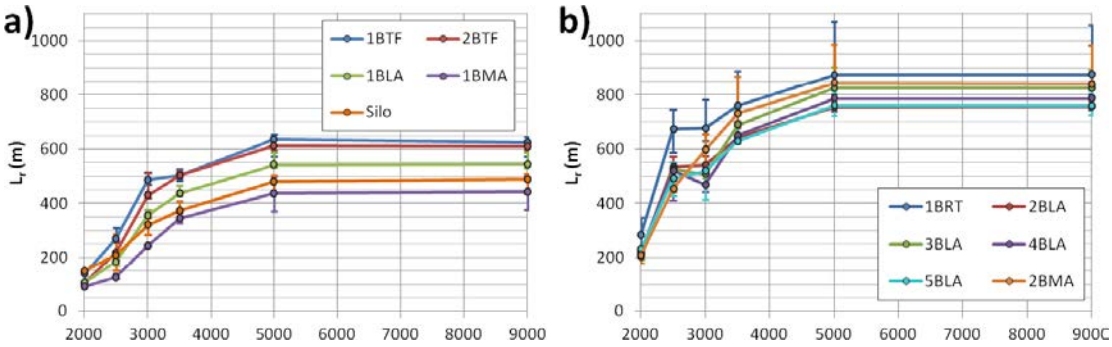

Figure 6-22. *Path length (Lr) from disposal rooms over time; a) in SFR 1 and b) in SFR 3. The results are taken over the three selected Bedrock cases (1, 15, and 11; see Section 6.2.3) as indicated by the range of the bars.*

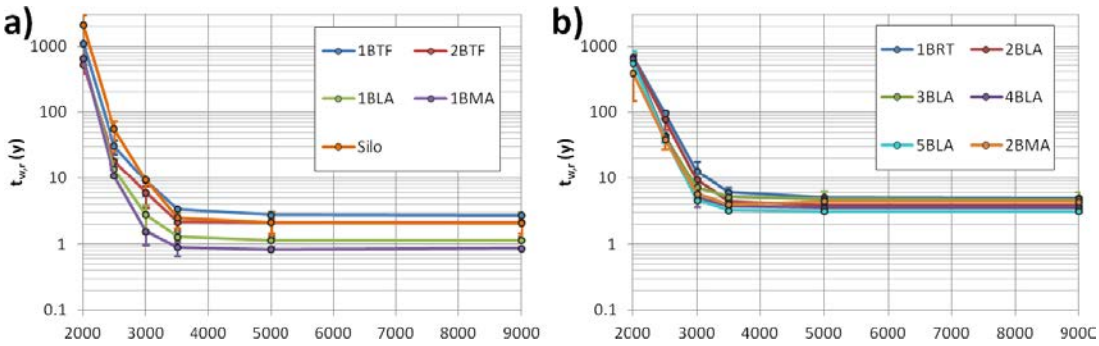

Figure 6-23. *Median advective travel times (tw,r) for trajectories from disposal rooms over time; a) in SFR 1 and b) in SFR 3. The results are taken over three bedrock cases (1, 15, and 11) as indicated by the range of the bars.*

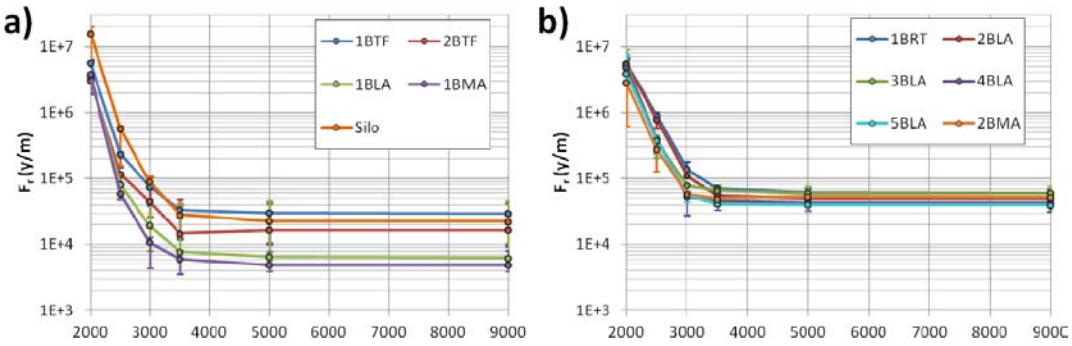

Figure 6-24. *Median flow-related transport resistance (Fr) for trajectories from disposal rooms over time; a) in SFR 1 and b) in SFR 3. The results are taken over three bedrock cases (1, 15, and 11) as indicated by the range of the bars.*

6.4.4 Flow-related transport resistance

The flow-related transport resistance, F_r, for particles starting in SFR 1 and SFR 3, respectively, is studied for the three selected Bedrock cases (Section 6.2.3) and for all six time slices (Figure 6-25 to Figure 6-27). During the submerged conditions at 2000 AD, the flow-related transport resistance is high, c. 10^7 y/m, and the difference between SFR 1 and SFR 3 is small, compared to future time slices. The transport resistance decreases as the flow increases with the ongoing shoreline retreat, but appears to reach stationary values at around 5000 AD. The particle trajectories from SFR 3 tends to have higher transport resistance (Table 6-6), which is probably due to its deeper location and lower flows. The differences between the three bedrock cases are fairly small.

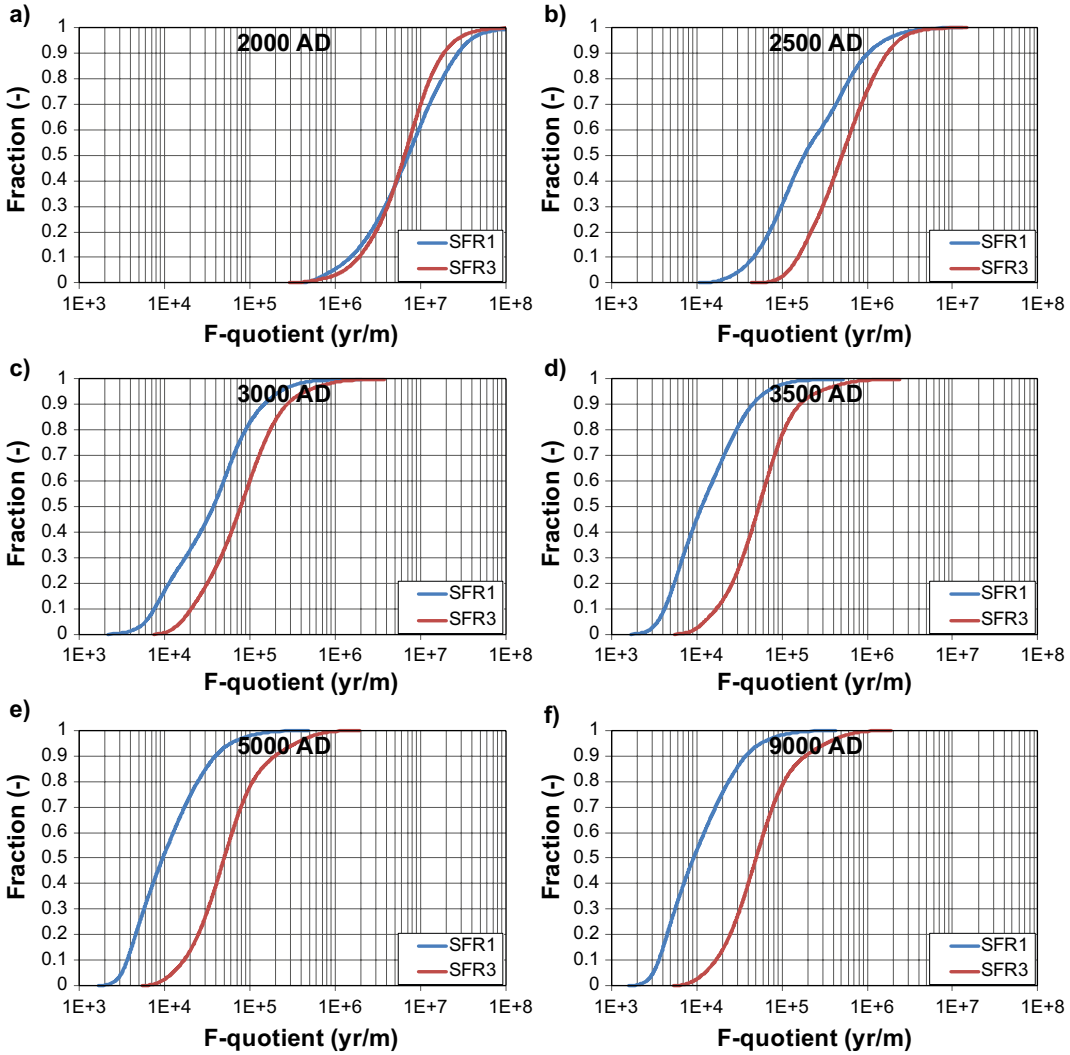

Figure 6-25. *Evolution of the distribution of Fr with time for Bedrock case No.1 [BASE_CASE1_DFN_R85].*

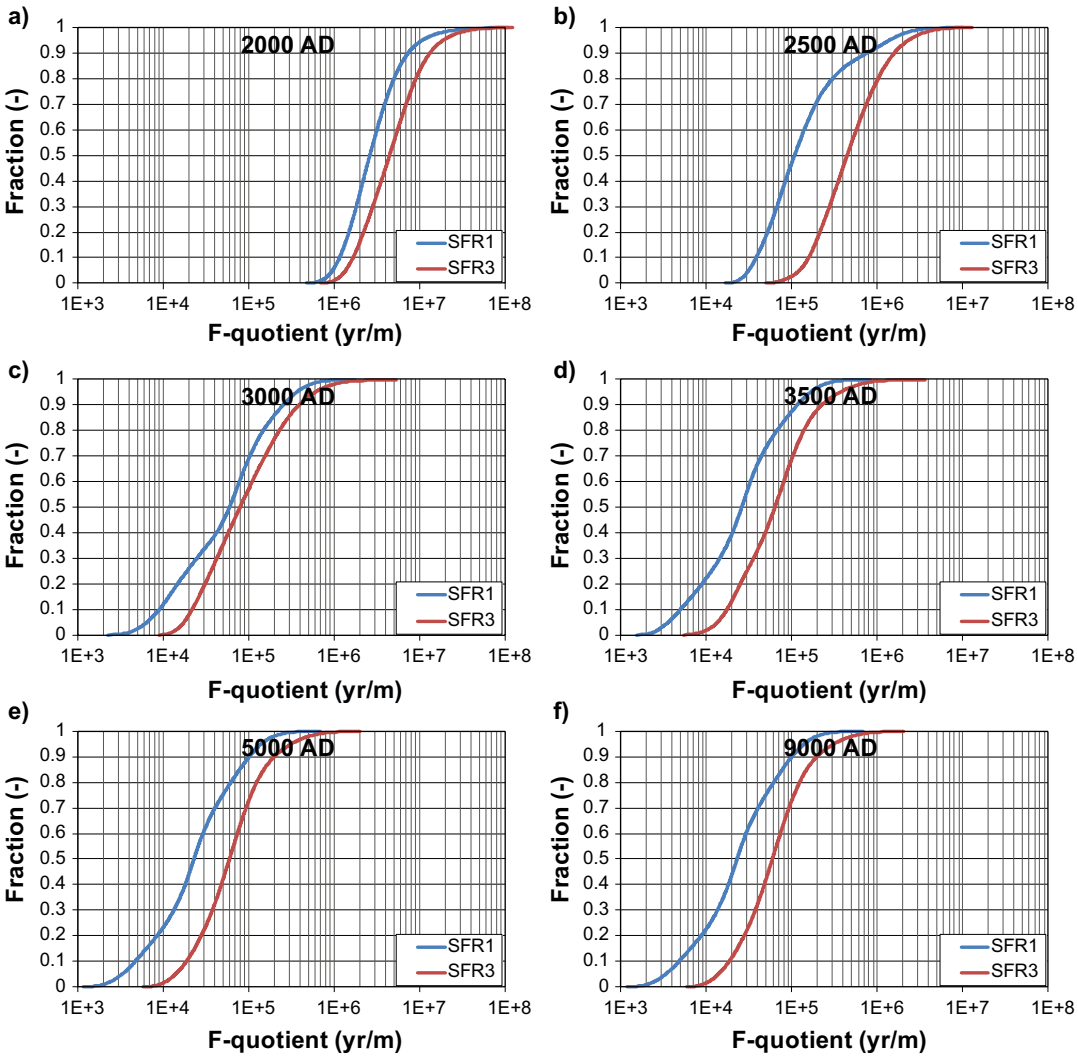

Figure 6-26. *Evolution of the distribution of Fr with time for Bedrock case No.15 [nc_NoD_R01_DFN_R18].*

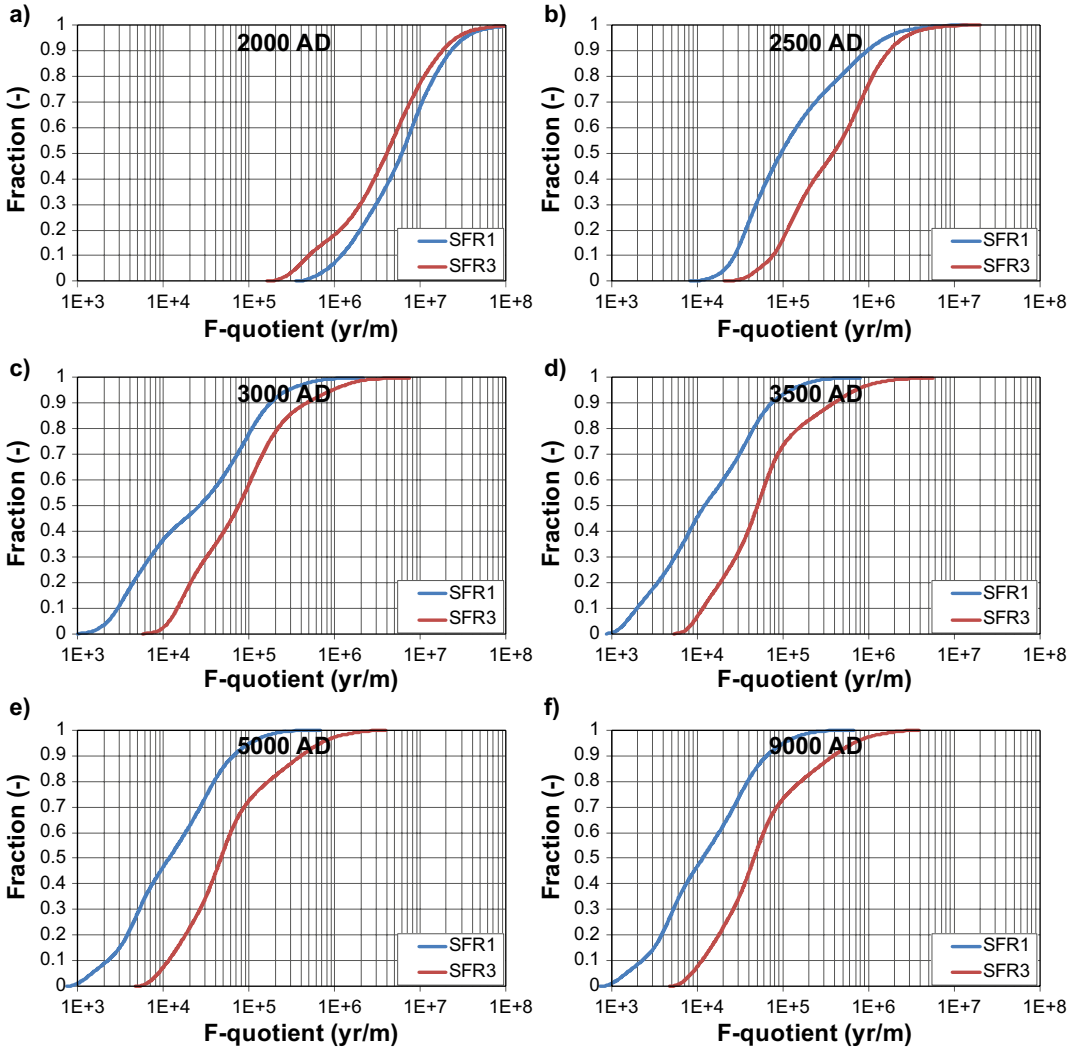

Figure 6-27. Evolution of the distribution of Fr with time for bedrock case No.11 [nc_DEP_R07_DFN_R85].

Table 6-6. Compilation of flow-related transport resistance percentiles (5%, 50%, and 95%), F_r (y/m), at characteristic time slices.

Bedrock case	Source	2000AD			3000AD			5000AD		
		5%	50%	95%	5%	50%	95%	5%	50%	95%
1	SFR 1	9.4E+5	7.1E+6	3.8E+7	6.0E+3	3.7E+4	2.2E+5	3.1E+3	9.5E+3	6.0E+4
	SFR 3	1.3E+6	6.5E+6	2.6E+7	1.6E+4	7.8E+4	4.4E+5	1.2E+4	5.0E+4	3.5E+5
15	SFR 1	9.6E+5	2.6E+6	1.1E+7	6.4E+3	6.0E+4	3.6E+5	3.3E+3	2.3E+4	1.4E+5
	SFR 3	1.4E+6	4.5E+6	1.9E+7	1.8E+4	7.9E+4	6.0E+5	1.4E+4	6.0E+4	3.1E+5
11	SFR 1	8.2E+5	6.0E+6	3.2E+7	2.2E+3	2.6E+4	2.8E+5	1.4E+3	1.2E+4	1.0E+5
	SFR 3	3.5E+5	4.0E+6	2.6E+7	1.2E+4	7.5E+4	9.0E+5	8.6E+3	4.6E+4	6.8E+5

6.4.5 Advective travel time

The advective travel time, $t_{w,r}$, for particles starting in SFR 1 and SFR 3, respectively, is studied for the three selected Bedrock cases (Section 6.2.3) and for all six time slices (Figure 6-28 to Figure 6-30). At 2000 AD, the travel times are long, c. 100 to 1,000 years, and the difference between SFR 1 and SFR 3 is small, compared to future time slices. Notably, SFR 1 has the longest travel times at 2000 AD (see Appendix C for further discussion), whereas the travel times from SFR 3 are consistently longer at later time slices (Table 6-7). The differences between the three bedrock cases are fairly small.

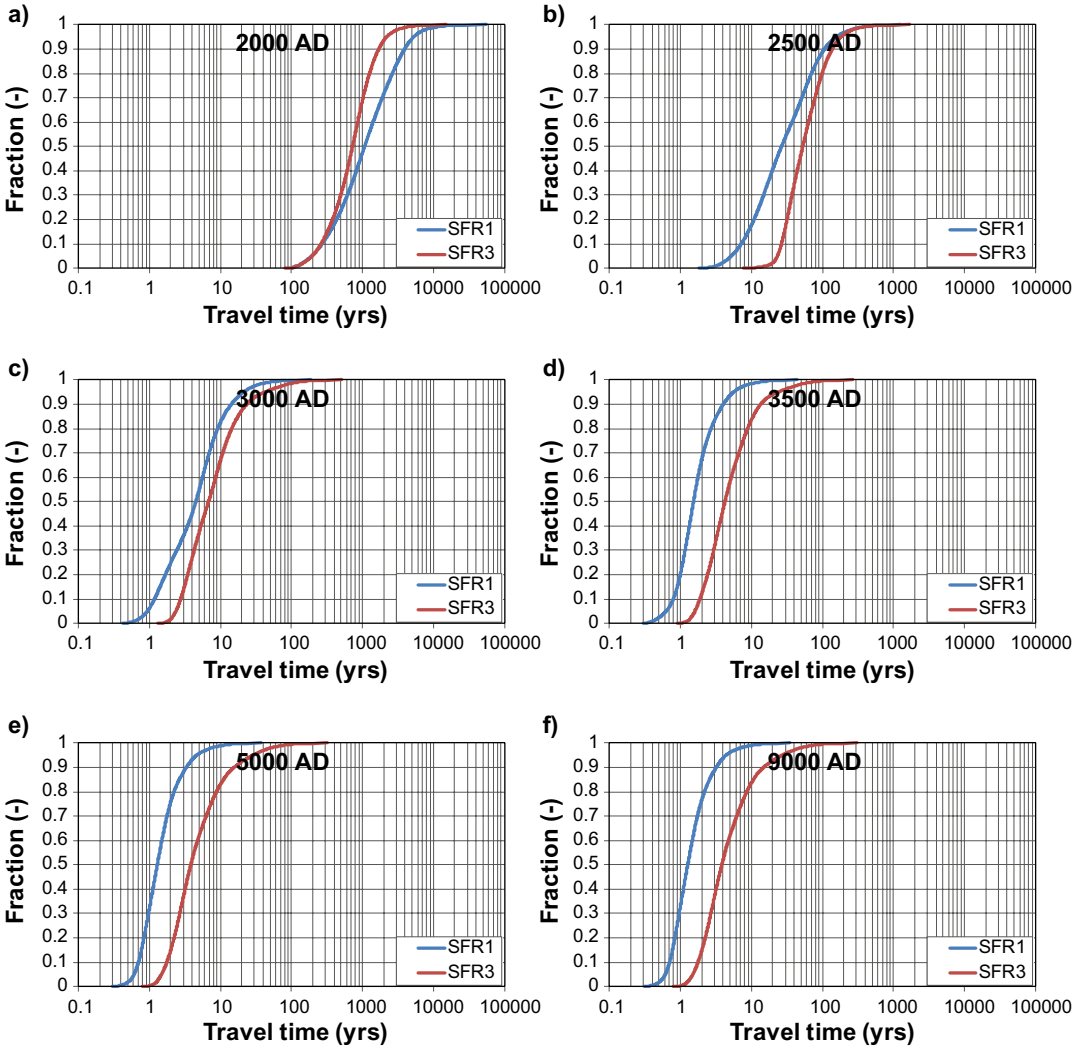

Figure 6-28. *Evolution of the distribution of tw,r for Bedrock case No.1 [BASE_CASE1_DFN_R85].*

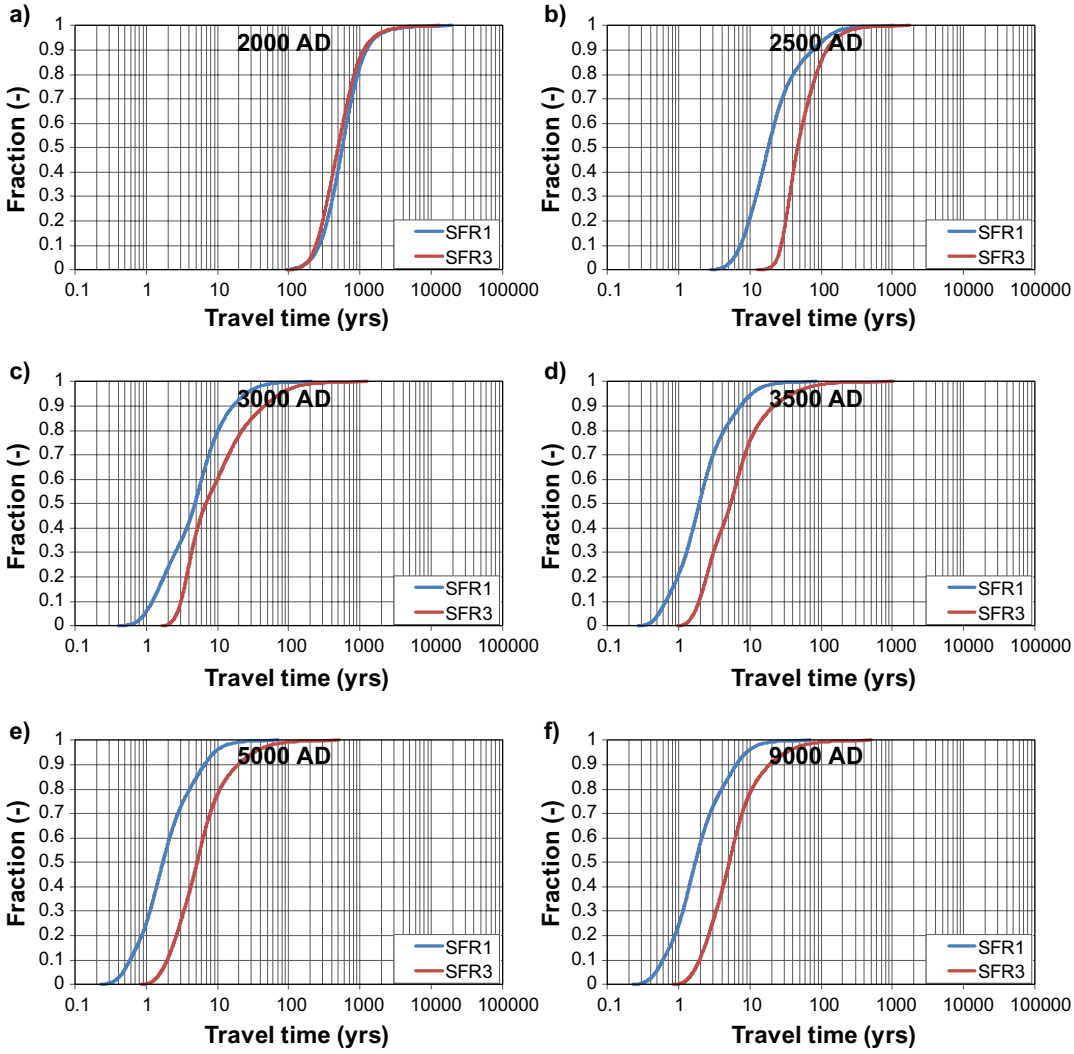

Figure 6-29. *Evolution of the distribution of tw,r for Bedrock case No.15 [nc_NoD_R01_DFN_R18].*

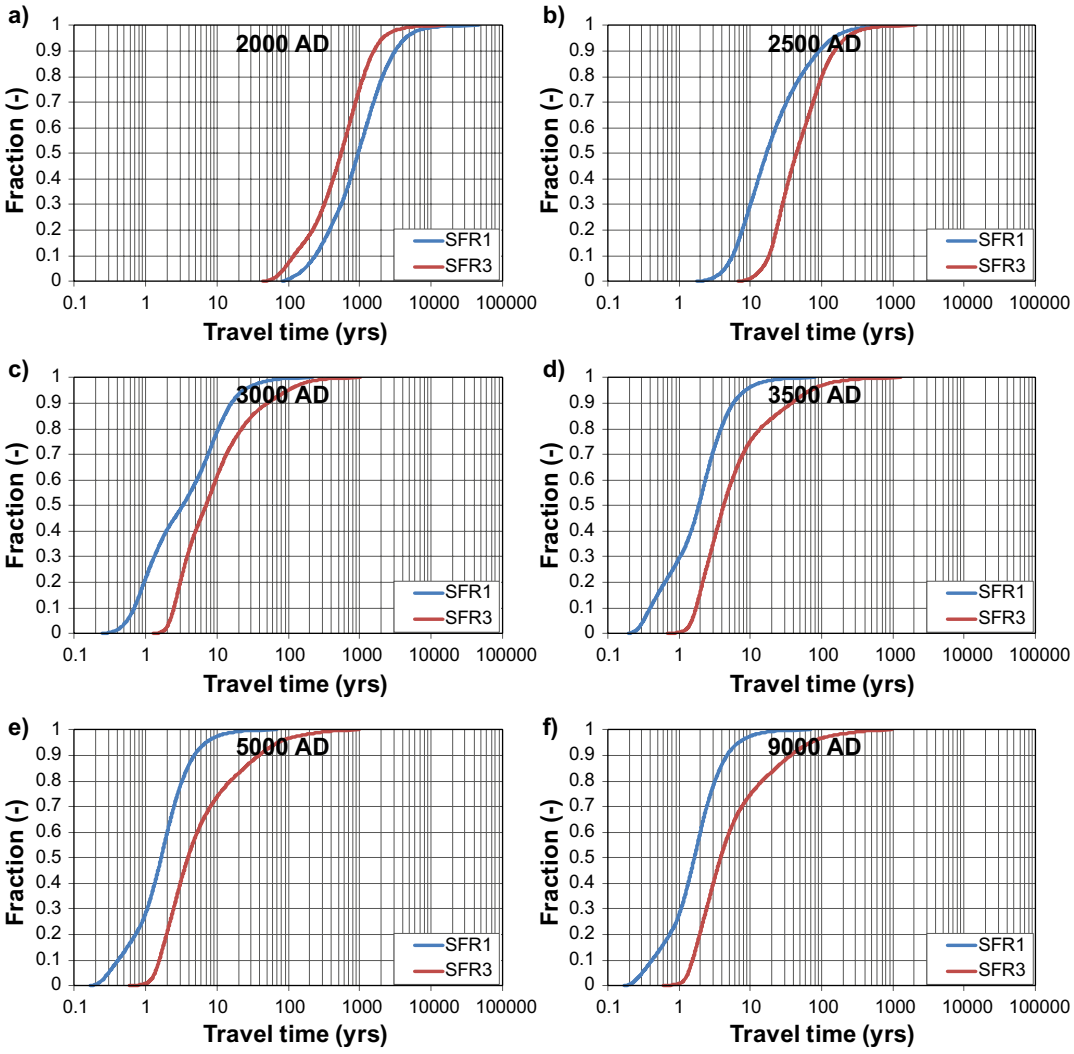

Figure 6-30. *Evolution of the distribution of tw,r for Bedrock case No.11 [nc_DEP_R07_DFN_R85].*

Table 6-7. Compilation of travel-time percentiles (5%, 50%, and 95%) of $t_{w,r}$ (y) at characteristic time slices.

Bedrock case	Source	2000AD			3000AD			5000AD		
		5%	50%	95%	5%	50%	95%	5%	50%	95%
1	SFR 1	192	1,070	5,270	0.9	4.5	21	0.6	1.3	4.6
	SFR 3	194	725	2,200	2.4	6.8	42	1.5	3.8	29
15	SFR 1	213	562	1,620	1	4.8	25	0.5	1.7	9
	SFR 3	202	491	1,530	2.7	6.8	76	1.6	5.1	32
11	SFR 1	168	948	4,360	0.5	3.3	23	0.3	1.6	6.9
	SFR 3	87	547	2,090	2.2	7	98	1.3	3.9	71

6.4.6 Path length

The path length, L_r, for particles starting in SFR 1 and SFR 3, respectively, is studied for the three selected Bedrock cases (Section 6.2.3) and for all six time slices (Figure 6-31 to Figure 6-33). The shortest path lengths are found in the upward-directed flow regime at 2000 AD. Over time, the path lengths increase owing to the changing flow regime (can be seen in e.g. Figure 6-19 and Figure 6-20). The path lengths from are consistently longer from SFR 3 than from SFR 1 (Table 6-8), which is probably due to its deeper location, as well as, the fact that a lesser fraction of particles exit in biosphere object 157_2 (Figure 6-19 and Figure 6-20). The differences between the three bedrock cases are fairly small.

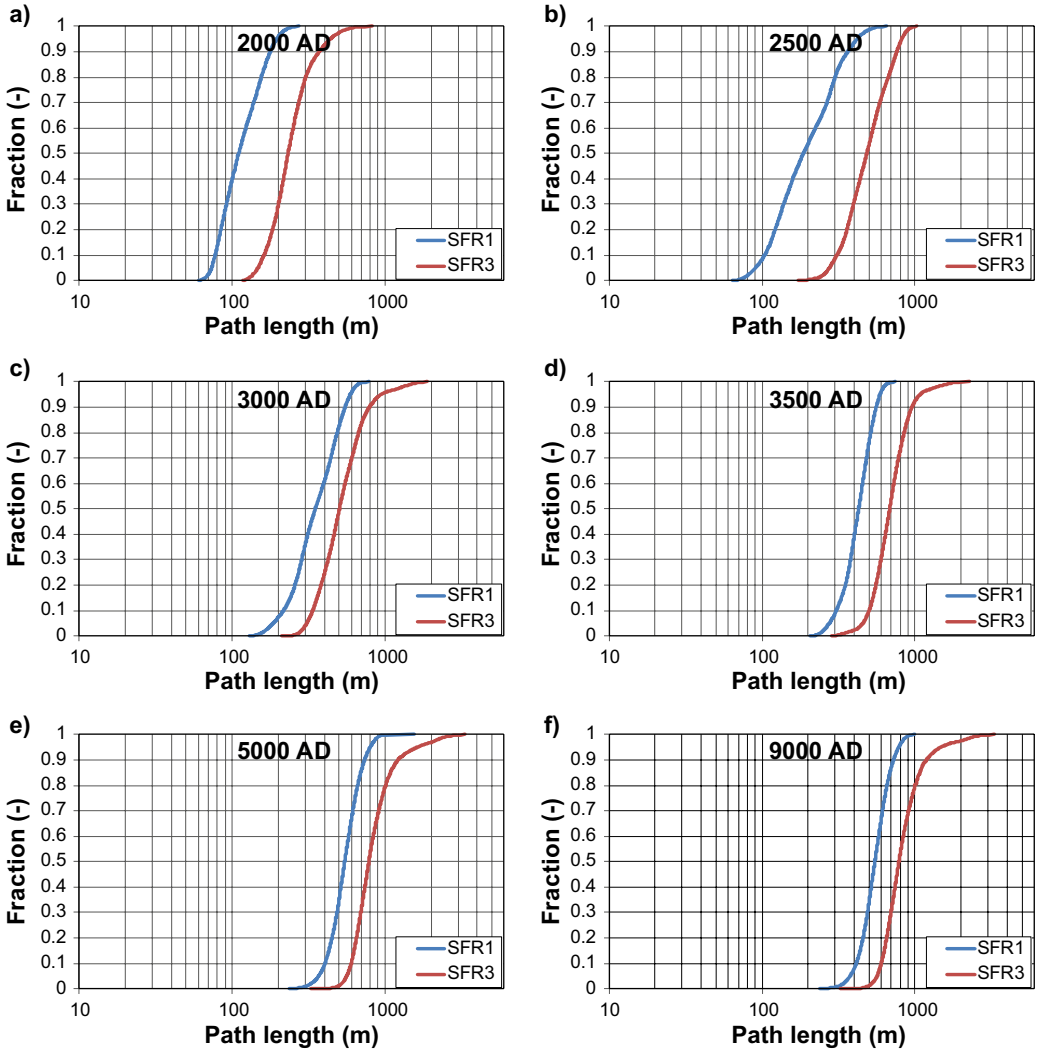

Figure 6-31. *Evolution of the distribution of Lr for Bedrock case No.1 [BASE_CASE1_DFN_R85].*

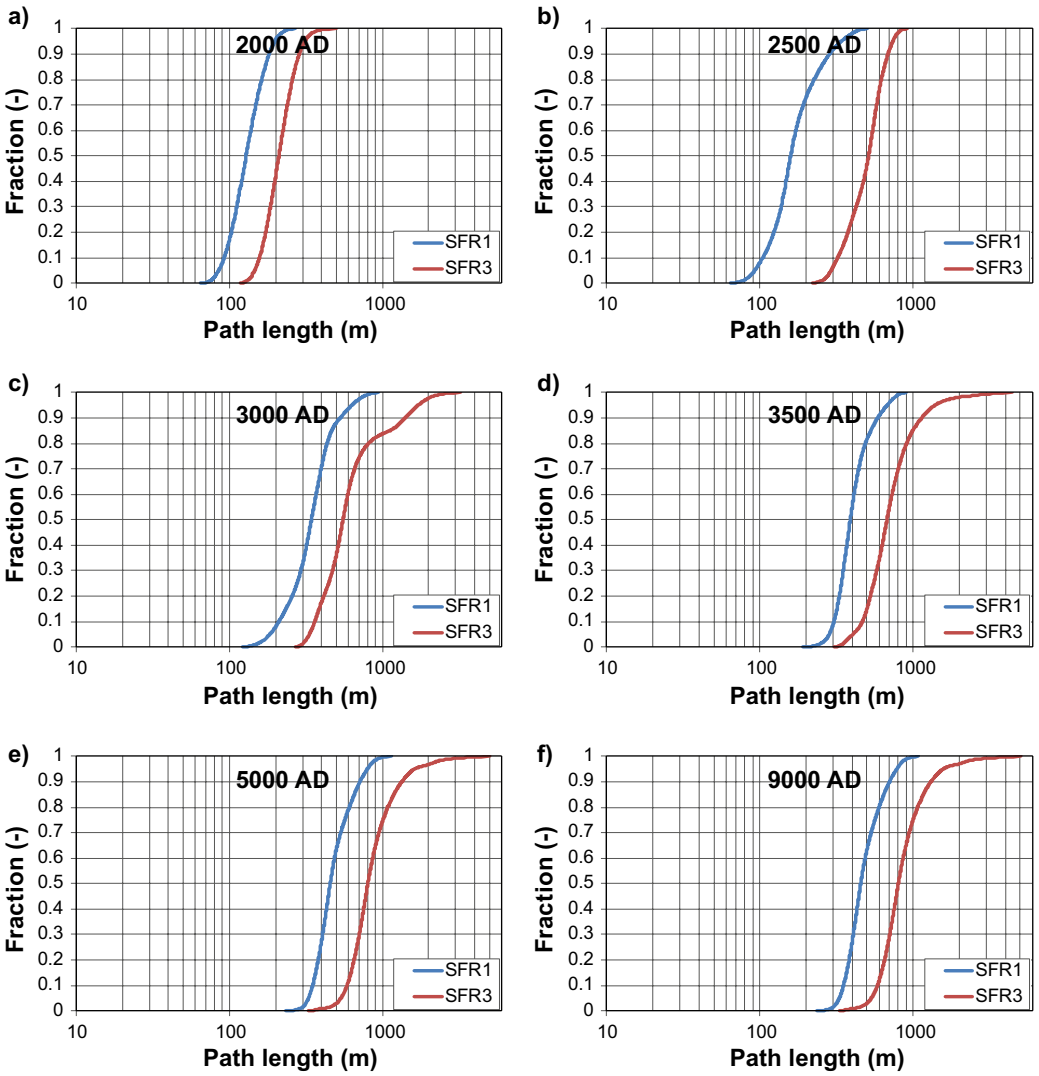

Figure 6-32. *Evolution of the distribution of Lr for Bedrock case No.15 [nc_NoD_R01_DFN_R18].*

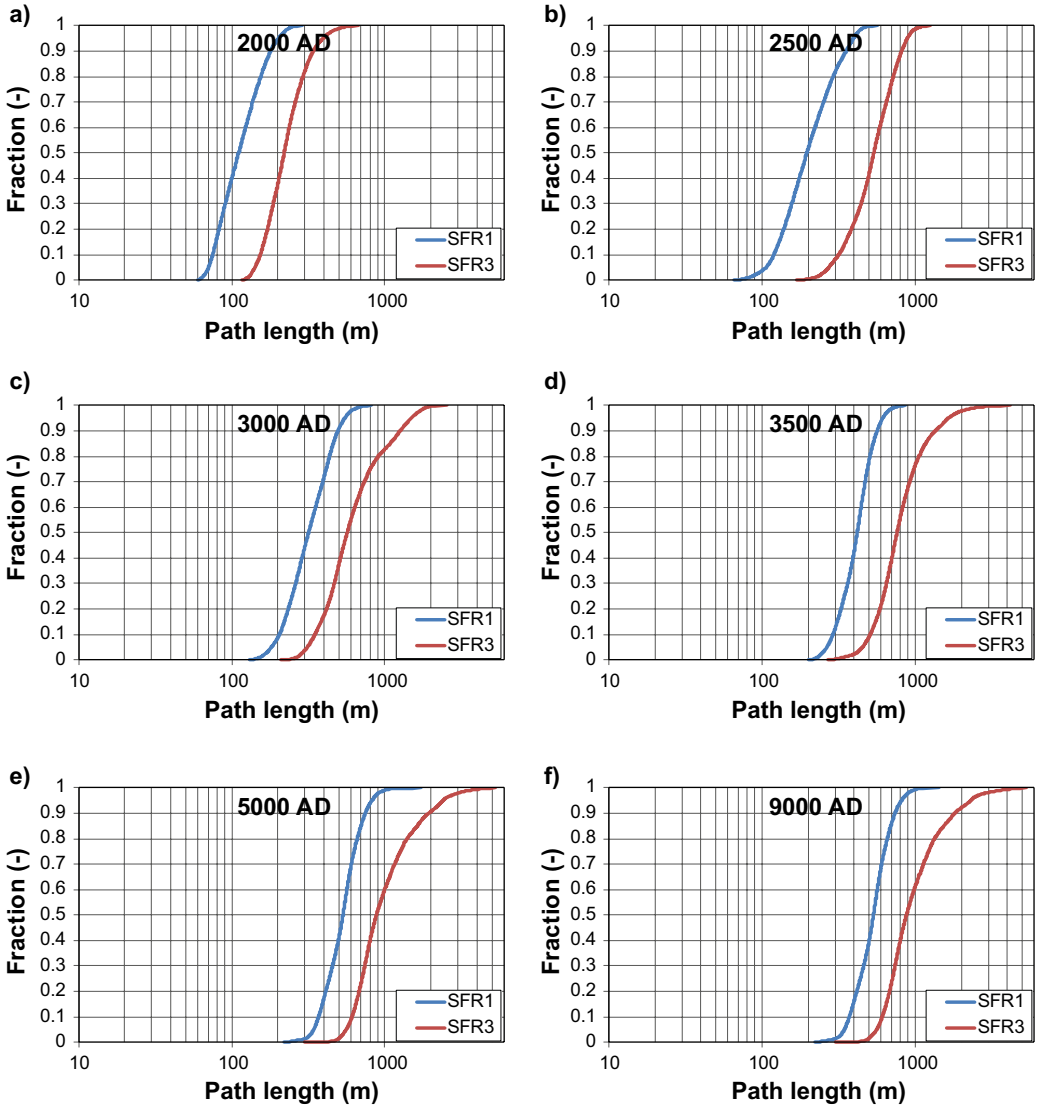

Figure 6-33. Evolution of the distribution of Lr for Bedrock case No.11 [nc_DEP_R07_DFN_R85].

Table 6-8. Compilation of path-length percentiles (5%, 50%, and 95%) of L_r (m) at characteristic time slices.

Bedrock case	Source	2000AD			3000AD			5000AD		
		5%	50%	95%	5%	50%	95%	5%	50%	95%
1	SFR 1	73	110	196	185	349	592	366	544	798
	SFR 3	147	232	437	307	502	939	561	781	1,610
15	SFR 1	85	128	198	184	343	628	328	455	795
	SFR 3	146	210	310	333	551	1,710	534	800	1,610
11	SFR 1	71	111	202	182	317	547	343	532	822
	SFR 3	141	220	393	311	567	1480	558	879	2,390

6.4.7 Interactions

The term "interaction" refers to the fraction of particle trajectories that are released in one disposal room and cross another, downstream disposal room. The interior of disposal rooms are not resolved in detail in the DarcyTools model (i.e. explicit waste packages, local drains, interior barriers, etc.), and therefore an "interaction" modelled in DarcyTools does *not* necessarily imply an actual chemical interaction between different types of disposed waste. It should be emphasised that TD11 assumes intact plugs (Section 4.1) and that interactions for degraded plugs are larger (see TD10).

The full interaction matrix between disposal rooms is complex (i.e. 17 bedrock cases, 6 time slices, 11 release locations, and 11 possible interaction locations). Therefore, the analysis is divided into two parts: 1) interactions from the planned extension, SFR 3, to the existing SFR 1 and 2) internal interactions within SFR 3 (see below). Internal interactions within SFR 1 are not presented.

Trajectories from SFR 3 interacting with SFR 1

The planned extension, SFR 3, is upstream of SFR 1, i.e. none of the particles released in SFR 1 interact with any of the SFR 3 disposal rooms. Weak interactions are found in the opposite direction, with small fractions of particles released in SFR 3 reaching the downstream disposal rooms of SFR 1 (typically on the order 1/10,000 released particles; Table 6-9). The number of interacting disposal rooms is largest during the submerged flow regime 2000 AD, where the hydraulic gradients are low and primarily vertical (i.e. all 11 disposal rooms are more or less involved in SFR 3/SFR 1 interactions). After c. 2500 AD, the primary SFR 3/SFR 1 interactions are *from* 1BRT and 2BLA *to* the SFR 1 Silo (Table 6-9).

In an analysis of variability related to bedrock cases (Table 6-10), the base case [BASE_CASE1_DFN_R85], $n = 1$, stands out with the highest fraction of SFR 3/SFR 1 interactions. Interactions are primarily controlled by two parameterisation components: 1) HCD depth-dependency (bedrock cases *without* depth dependency, $n = 6$, 13 to 17 in Table 2-2, render significantly lower interactions) and 2) DFN realisation (interaction for cases with R03 or R18, $n = 2$, 4, 9, 12, 13, 15, and 17, are high 2500 AD, but are low for other time slices).

Table 6-9. SFR 3/SFR 1 particle interactions, by release location [%][1].

SFR 1 / SFR 3	2000AD 1BTF	2000AD 2BTF	2000AD 1BLA	2000AD 1BMA	2000AD Silo	2500AD Silo	3000AD Silo	3500AD Silo	5000AD Silo	9000AD Silo
1BRT	0.034	0.024	0.006	0.0001	0.005	0.044	0.016	0.020	0.020	0.018
2BLA	0.007	0.005	0.002	0.0001	0.001	0.020	0.012	0.021	0.022	0.022
3BLA	0.007	0.003	0.001				0.0003	0.001	0.001	0.001
4BLA	0.002	0.001	0.0002							
5BLA	0.004	0.003	0.001							
2BMA	0.003	0.003	0.0005							

[1] Fraction of particles released in SFR 3 disposal rooms that cross SFR 1 disposal rooms, expressed in percentage. Average percentage for all 17 bedrock cases, coloured by value; high = red, median = yellow, low = green, none = blank.

Table 6-10. SFR 3/SFR 1 particle interactions, by bedrock case [%][1].

n	2000AD 1BTF	2BTF	1BLA	1BMA	Silo	2500AD Silo	3000AD Silo	3500AD Silo	5000AD Silo	9000AD Silo
1	0.030	0.035	0.014	0.0002	0.002	0.005	0.012	0.016	0.016	0.018
2	0.002				0.0002	0.022	0.003	0.004	0.006	0.005
3	0.015	0.014	0.007	0.0002	0.004	0.004	0.011	0.016	0.017	0.013
4	0.0002					0.019	0.006	0.007	0.005	0.009
5	0.032	0.019	0.005	0.0002		0.007	0.008	0.012	0.014	0.016
6						0.007	0.004	0.009	0.008	0.005
7	0.026	0.017	0.001		0.003	0.007	0.009	0.014	0.017	0.012
8	0.016	0.005	0.001	0.0002		0.004	0.003	0.007	0.007	0.010
9						0.014	0.002	0.001	0.001	0.002
10	0.035	0.019			0.010	0.007	0.011	0.015	0.016	0.014
11	0.006	0.003	0.001			0.006	0.003	0.005	0.003	0.004
12	0.0002					0.032	0.002	0.001	0.003	0.002
13						0.011	0.002	0.004	0.003	0.003
14						0.002	0.002	0.004	0.005	0.003
15						0.014	0.001	0.002	0.002	0.002
16						0.004	0.001	0.001	0.001	0.001
17						0.019	0.002	0.001	0.0002	0.001

[1] Fraction of particles released in SFR 3 disposal rooms that cross SFR 1 disposal rooms, expressed in percentage. Average percentage for all SFR 3 disposal rooms, coloured by value; high = red, median = yellow, low = green, none = blank.

Interactions within SFR 3

This section presents interacting particle trajectories within SFR 3. The internal interactions within SFR 3, are also higher in the early flow regimes (i.e. compare Table 6-11 to interactions with SFR 1 in Table 6-9 and Table 6-10). At the time slices 2000 and 2500 AD, the largest interactions occur in the adjacent rock cavern located further *away* from SFR 1 (e.g. interactions from 2BLA to 3BLA exceed interactions from 2BLA to 1BRT). The pattern of interactions stabilises at later time slices, c. 3500 to 9000 AD, where interactions are typically confined to the nearest adjacent disposal rooms. This stabilisation agrees with earlier observations of tunnel flow (Section 6.2) and with SFR 1 interactions (Table 6-9).

The variability among bedrock cases (n = 1 to 17) is presented in Table 6-12. This variability demonstrates the uncertainty in the quantified magnitude of interactions (i.e. percentage of crossing trajectories, %). DFN realisations R03 and R18 have typically lower interactions. Besides the bedrock-case variability, the systematic pattern in Table 6-12 demonstrates that the flow regime (i.e. stage of shoreline retreat and topography) is a key component in interactions within SFR 3.

Table 6-11. Interactions within SFR 3, by time slice [%][1].

Time slice	From \ To	1BRT	2BLA	3BLA	4BLA	5BLA	2BMA
2000AD	1BRT	–	25.45	0.51	0.02		
	2BLA		–	4.52	0.07	<0.01	
	3BLA		0.5	–	5.48	0.03	<0.01
	4BLA			<0.01	–	1.36	<0.01
	5BLA				1.83	–	0.54
	2BMA					0.03	–
2500AD	1BRT	–	7.59	0.33	0.02	0.02	0.03
	2BLA	0.01	–	12.56	0.66	0.14	0.08
	3BLA			–	12.16	1.09	0.28
	4BLA				–	14.91	4.54
	5BLA				1.43	–	16.91
	2BMA				<0.01	<0.01	–
3000AD	1BRT	–	6.73	0.01			
	2BLA	0.1	–	2.95	0.02		
	3BLA		0.05	–	2.71	<0.01	
	4BLA			0.04	–	0.81	
	5BLA			<0.01	2.33	–	0.42
	2BMA				<0.01	0.47	–
3500AD	1BRT	–	4.05	<0.01			
	2BLA	0.44	–	0.27	<0.01		
	3BLA		1.34	–	0.54		
	4BLA		<0.01	0.96	–	0.02	
	5BLA			<0.01	5.54	–	0.05
	2BMA				0.03	1.33	–
5000AD	1BRT	–	3.82	<0.01			
	2BLA	0.46	–	0.26	<0.01		
	3BLA	<0.01	1.48	–	0.53		
	4BLA		<0.01	1.08	–	0.03	
	5BLA		<0.01	<0.01	5.32	–	0.05
	2BMA			<0.01	0.03	1.26	–
9000AD	1BRT	–	3.85				
	2BLA	0.45	–	0.27	<0.01		
	3BLA		1.42	–	0.55		
	4BLA		<0.01	1.05	–	0.03	
	5BLA			<0.01	5.3	–	0.06
	2BMA				0.03	1.26	–

[1] Fraction of particles released in SFR 3 disposal rooms that cross adjacent rooms in SFR 3, expressed in percentage. Average percentage for all bedrock cases, coloured by value; high = red, <0.01% = white none = blank.

Table 6-12. Interactions within SFR 3, variability between bedrock cases [%][1)].

From	To	Bedrock case, *n*																
		1	2	3	4	5	6	7	8	9	10	11	12	13	14	15	16	17
Time slice 2000AD																		
1BRT	2BLA	38	6	31	16	40	40	41	32	1.8	33	31	12	14	40	8.5	35	12
	3BLA	0.02			<0.01	2.8	0.56	0.11			0.3	2.9	0.42	<0.01	0.2		0.95	0.32
	4BLA					0.15					<0.01	0.12	0.01				<0.01	
2BLA	3BLA	0.03	1.2		0.91	6.4	3.3	0.3		0.02	3.4	17	21	0.32	1.5	4.7	7.9	8.8
	4BLA		<0.01		0.02	0.02					<0.01	0.23	0.85	<0.01		<0.01	0.02	0.07
	5BLA												<0.01					
3BLA	2BLA	0.45		2.8				0.25	5	0.03	<0.01				<0.01			
	4BLA	0.99	8.8	0.17	8.4	8.9	2	0.01	0.42	4.4	6.4	9.4	13	7.5	0.35	6.3	5.6	10
	5BLA		0.02										0.47			<0.01		<0.01
	2BMA												<0.01					
4BLA	3BLA			<0.01				0.07										
	5BLA		5.5		<0.01							0.24	12	0.17		4.6		1.1
	2BMA												<0.01					
5BLA	4BLA	5.4		2.4	0.02	0.66	1.6	7.2	4	<0.01	5.3	<0.01			4.2		0.27	
	2BMA		1.5	0.06					0.07	0.05	1.6	1.5	3.3	<0.01		0.47	0.47	0.11
2BMA	5BLA	0.02		<0.01	0.19	0.15	0.06	<0.01	<0.01			<0.01		0.08	0.02			0.05
Time slice 2500AD																		
1BRT	2BLA	4	3.5	2.4		5	12	4	21	22	3.5	6.1	6.9	0.66	10	11	12	4.5
	3BLA	<0.01				<0.01	0.12	<0.01	1.5	3	<0.01	0.08	0.21		0.07	<0.01	0.45	0.06
	4BLA								0.09	0.24		<0.01	0.04			<0.01	<0.01	0.03
	5BLA								0.34	0.02		<0.01	<0.01				<0.01	
	2BMA								0.55	<0.01		<0.01						
2BLA	1BRT				0.18													
	3BLA	8.8	4	7.1	2.9	13	15	7.6	33	26	9.3	16	15	1.5	15	7	22	11
	4BLA	0.04	0.05	0.03	0.07	0.09	0.09	0.02	3.1	3.3	0.04	1.1	2.2		0.13	0.03	0.61	0.3
	5BLA	0.03				0.04		0.01	1.3	0.3	<0.01	0.46	0.07		0.03		0.04	
	2BMA	0.02				0.03		0.01	0.86	0.07	<0.01	0.29	<0.01		0.02		<0.01	
3BLA	4BLA	9.8	15	9.3	4.3	4.6	7.7	9.4	26	28	9.8	14	23	4.1	8.2	12	11	9.8
	5BLA	0.66	<0.01	0.14		0.48	0.16	0.75	6.5	3	0.21	3.3	1.9		0.75	0.02	0.66	
	2BMA	0.45		0.02		0.26	<0.01	0.74	1.3	0.05	0.19	1.1	0.05		0.52	<0.01	0.14	
4BLA	5BLA	16	0.77	8.8		12	14	21	55	35	9.4	23	16		23	2.9	17	
	2BMA	8.8		0.83		4.5	2.2	12	12	1.5	7.6	8.3	0.4		11	0.03	7.1	
5BLA	4BLA				5.4									9.8				9.1
	2BMA	24	6.8	22	0.01	17	24	28	24	14	30	16	11	<0.01	31	14	28	<0.01

From	To	Bedrock case, *n*																
		1	2	3	4	5	6	7	8	9	10	11	12	13	14	15	16	17
2BMA	4BLA													0.04				<0.01
	5BLA													0.06				0.06
Time slice 3000AD																		
1BRT	2BLA	6.3	0.11	6.6		7.9	11	7.2	18	13	7.3	8	1.4		12	3.9	11	
	3BLA						<0.01		0.1	<0.01		0.02			<0.01		0.06	
2BLA	1BRT		<0.01		1.3									0.22				0.14
	3BLA	0.49	0.46	0.55		1.4	3.1	0.33	9.5	6.6	2.7	6	5.4		3.3	1.7	8.6	
	4BLA								<0.01	0.24		<0.01	0.04			<0.01		
3BLA	2BLA				0.19									0.65				0.03
	4BLA	0.44	5.8	0.51	0.14	0.36	0.06	0.49	5.8	15	1.1	2	11	<0.01	0.19	3.3	0.03	
	5BLA								<0.01	0.04								
4BLA	3BLA						<0.01										0.02	0.68
	5BLA								7.1	6.6								
5BLA	3BLA																	<0.01
	4BLA	3.5	1.2	3.1	3.1	1.5	2.2	0.44			11	0.97	0.26	2.6	0.17	0.22	2.1	7
	2BMA						0.09	0.67	0.61	0.54	0.04	0.02	0.01		3.5	1.1	0.7	
2BMA	4BLA				0.01									<0.01				0.05
	5BLA	0.1	0.05	0.07	2.9	0.38					<0.01	<0.01		2				2.3
Time slice 3500AD																		
1BRT	2BLA	3.5		3.6		3.9	6.5	4.4	14	9.8	4.3	3.5	<0.01		8	1.3	6.1	
	3BLA								<0.01									
2BLA	1BRT		0.44		3.4								0.03	1.3				2.3
	3BLA						0.12		1.5	1.5					0.27		1.1	
	4BLA									<0.01								
3BLA	2BLA	0.91	3.3	0.86	2.6	1		0.97			0.32	1.5	1.5	3.4		1.3		5.2
	4BLA	<0.01	0.97	<0.01		<0.01	<0.01	<0.01	0.27	5.5	<0.01		2.1		<0.01	0.37		
4BLA	2BLA																	<0.01
	3BLA	0.98		0.91	<0.01	0.57	0.98	0.7			1.7	2.2		0.19	0.66		2.6	4.9
	5BLA									0.27								
5BLA	3BLA	<0.01									<0.01	<0.01					<0.01	0.04
	4BLA	8	3.4	7.6	4.5	4.8	5.7	3.4	0.12	<0.01	20	7.5	3.8	3.8	3.1	1.3	7.1	9.9
	2BMA								0.04	0.08					0.64	0.1	<0.01	
2BMA	4BLA	<0.01		<0.01	0.05	<0.01		<0.01			0.07			0.03				0.36
	5BLA	2.3	0.95	2.1	5	1.4	0.42	0.13			2.3	0.11		3.7			0.04	4.3

From	To	Bedrock case, *n*																
		1	**2**	**3**	**4**	**5**	**6**	**7**	**8**	**9**	**10**	**11**	**12**	**13**	**14**	**15**	**16**	**17**
Time slice 5000AD																		
1BRT	2BLA	2.9		3		3.7	5.6	3.9	14	10	4	3.6	0.04		7.3	1.1	5.5	
	3BLA								<0.01	<0.01								
2BLA	1BRT		0.4		3.4								<0.01	1.5				2.5
	3BLA						0.09		1.9	1.6					0.14		0.67	
	4BLA									<0.01								
3BLA	1BRT																	<0.01
	2BLA	1.1	3.6	1	2.4	0.98		1.2			0.4	1.1	1.6	3.9		2.1		5.7
	4BLA	<0.01	0.83					<0.01	0.37	5.6			2		<0.01	0.15		
4BLA	2BLA																	<0.01
	3BLA	1.2		1.1	<0.01	0.6	1.1	0.86			1.9	1.5		0.22	1.1		3.3	5.4
	5BLA								<0.01	0.45								
5BLA	2BLA																	<0.01
	3BLA										<0.01	<0.01					0.01	0.05
	4BLA	7.6	3.3	7.1	4.4	4	5.3	3	0.02	<0.01	19	6.3	3.1	4	3.3	1.5	7.5	10
	2BMA								0.11	0.12					0.58	0.08		
2BMA	3BLA																	<0.01
	4BLA	<0.01		<0.01	0.05	<0.01					0.04			0.03				0.43
	5BLA	1.9	0.92	1.8	4.7	1.1	0.35	0.08			1.9	0.06		3.8			0.08	4.5
Time slice 9000AD																		
1BRT	2BLA	2.9		3		3.5	5.8	4	14	11	4.1	3.7	0.04		7.5	1.2	5.5	
2BLA	1BRT		0.36		3.3								<0.01	1.5				2.5
	3BLA						0.09		2	1.7					0.19		0.76	
	4BLA									<0.01								
3BLA	2BLA	1.1	3.6	0.97	2.3	1		1.2			0.38	1.1	1.5	3.6		1.9		5.4
	4BLA	<0.01	0.76	<0.01		<0.01	<0.01	<0.01	0.41	5.7	<0.01		2.2		<0.01	0.19		
4BLA	2BLA																	<0.01
	3BLA	1.3		1	<0.01	0.59	1.1	0.82			1.8	1.5		0.23	0.92		3.1	5.3
	5BLA								0.01	0.56								
5BLA	3BLA										<0.01	<0.01					0.01	0.05
	4BLA	7.6	3.4	7.1	4.3	4.1	5.4	3.1	0.01		19	6.2	2.9	4.1	3.1	1.4	7.5	11
	2BMA								0.12	0.15					0.71	0.09		
2BMA	4BLA	<0.01		<0.01	0.05	<0.01					0.03			0.03				0.45
	5BLA	2	0.88	1.9	4.7	1.1	0.34	0.08			2	0.05		3.8			0.05	4.6

[1)] Fraction of particles released in SFR 3 disposal rooms that cross adjacent rooms in SFR 3, expressed in percentage. Coloured by value; high = red, <0.01% = white, none = blank.

7 Summary and conclusions

As a part of the license application for the expansion of SFR, a project has been initiated to assess the radiological safety for the entire repository after closure (SR-PSU). Two different climate conditions are studied in SR-PSU, temperate and periglacial conditions (Odén et al. 2014). Hydrogeological modelling tasks within the SR-PSU project have been defined in terms of so-called Task Descriptions (TDs). This present report summarises the methodology, setup, and results of the groundwater flow modelling task TD11, which represents the final modelling stage under temperate conditions.

The groundwater flow model, developed in SDM-PSU (SKB 2013), is used to assess performance measures for the existing repository (SFR 1) and its planned extension (SFR 3). The combined effects of bedrock heterogeneity, parameterisation uncertainty, and the transient flow regime on performance measures are assessed in a sensitivity analysis. The sensitivity analysis consists of 17 so-called Bedrock cases (model parameterisations), which are studied as steady state solutions under six selected time slices (i.e. stages of shoreline retreat).

The sensitivity analysis has a threefold outcome: 1) demonstration of the hydrogeological setting under temperate climate conditions, as a dynamic system, 2) performance measures are delivered to users within SR-PSU, and 3) new principles are introduced to the DarcyTools environment.

Performance measures

The key performance measures (output) from the groundwater flow modelling are:

- Disposal-room cross flow, Q (m^3/s).
- Particle exit location at the bedrock/regolith interface.
- Flow-related transport resistance along bedrock flow paths, F_r (y/m).
- Advective travel times along bedrock flow paths, $t_{w,r}$ (y).

A performance measure of supporting character is:

- Length of bedrock flow paths, L_r (m).

The particle-tracking results for each bedrock case and time slice have been exported to different users with SR-PSU.

Characteristics of the hydrogeological setting

The results demonstrate the understanding of the present day hydrogeological characteristics of the site, as well as, how these conditions are predicted to change during future stages of shoreline retreat. The altering flow regime is addressed by comparing steady-state flow solutions at selected stages of shoreline retreat, referred to as “time slices”. The current flow regime is characterised as modest and upward-directed. As the hydrostatic pressure underneath the Baltic Sea retreats further away from SFR, the flow regime becomes successively governed by local topography, and grows with an increasingly horizontal component. After c. 5000 AD the flow regime close to SFR is approximately stationary (i.e. largely unaffected by further shoreline withdrawal).

This transient character of the hydrogeological setting is reflected in all studied performance measures. For example, the cross flow through disposal rooms, Q, increases during the early stages of shoreline displacement, to reach approximately stationary conditions at 5000 AD (Figure 6-21). Another example is the evolution of the repository discharge areas, i.e. where groundwater flow from the repository meets the ground surface. Up to c. 3500 AD, the discharge areas essentially move with the retreating Baltic Sea shoreline (Figure 6-19), but appear more or less identical in the 5000 AD and 9000 AD time slices (Figure 6-20). This pattern in successively relocating discharge areas is also observed in terms of increasing particle-trajectory lengths, L_r, up to c. 5000 AD (Figure 6-22). As the horizontal component in the flow field grows stronger, the advective travel time, $t_{w,r}$, and flow-related transport resistance, F_r, decrease (Figure 6-23 and Figure 6-24), which signifies that, in the determination of these performance measures, the significance of increasing flows outweighs the increasing path lengths. Similarly, the change in $t_{w,r}$ and F_r between the 5000 AD and 9000 AD time slices is indistinguishable.

Performance of SFR 1

The existing SFR 1 exhibits somewhat higher range of variability in simulated disposal-room cross flow, which is related to its sensitivity to the parameterisation of ZFMNNW1209 (i.e. the observed variability is high for 1BLA and 1BMA, although this is specific to the HCD realisations studied; instead the variability should be interpreted as generic, applying to all four rock caverns). In essence, all particles from SFR 1 discharge to biosphere object 157_2. With the exception of the particular flow regime under current, submerged conditions (see Appendix C), the existing disposal facility SFR 1 have consistently somewhat poorer performance measures, as compared to the planned extension SFR 3.

Performance of SFR 3

During the early stages, SFR 3 has exit locations both north and south of the SFR pier, but as the horizontal component in flow successively grows, the exit locations are driven north. Most particles from SFR 3 discharge into biosphere object 157_2, although owing to its deeper location, a smaller number of particles discharge to biosphere objects related to biosphere object 116. The deeper location of SFR 3 renders systematically longer path lengths, longer advective travel times, and higher flow-related transport resistance, as compared to SFR 1.

Representative Bedrock cases

The local parameterisation of deformation zones that intersect disposal rooms has been identified as a key uncertainty for the evaluation of cross flows through the disposal rooms. Two crucial deformation zones are identified: ZFMNNW1209 (formerly referred to as Zone 6; which intersects all four rock vaults of SFR 1) and ZFMWNW0835 (intersecting rock vaults 4BLA, 5BLA, and 2BMA in SFR 3; Figure 4-9). Based on a statistical ranking analysis of simulation results, three Bedrock cases are selected as representative for covering the range in observed cross flow through disposal rooms (Section 6.2.3). The results of these three Bedrock cases are presented in additional detail in this report, and the flow solutions have been exported to the near-field modelling team (Abarca et al. 2013). Previous hydrogeological modelling in SR-PSU has identified that the assumed depth trend in deformation-zone parameterisation may amplify parameterisation uncertainty. It is therefore noteworthy that the Bedrock case representing low tunnel flows is *not* based on the assumed depth trend (see discussion in 4.2.2).

Introduced principles to the DarcyTools environment

The execution of the SR-PSU modelling tasks has necessitated introducing approaches, along with corresponding code-development, which are "more or less" new in the DarcyTools environment. Besides the necessity to meet the SR-PSU objectives, the introduction of these concepts is of more general value to the DarcyTools modelling community. The most important are:

- **Automatization**: Altogether 102 model setups are addressed in the sensitivity analysis (17 Bedrock cases × 6 time slices). The file management is highly complex, even for a single model setup (Section 2.3), and therefore the analysis was fully automatized. The benefits of automatization include: 1) optimising computational efficiency, 2) minimising the risk of manual errors, and 3) allowing full traceability in file management. In summary, the approach came out very well.
- **Mixed top-boundary conditions**: The concept is to: 1) simulate groundwater level in unsaturated areas, e.g. the highly conductive pier above SFR, but 2) prescribe head in over-saturated areas, e.g. topographical basins with low-conductive sediments. Visual inspection of results (Section 6.1) and the evaluation of recharge and discharge in biosphere objects (Section 6.3) indicate that the simulation results are realistic and that the principles have been properly implemented.
- **Post-process particle tracking**: The performance measures of over 300,000,000 particle trajectories have been exported to different users within SR-PSU. To accommodate this challenging task within the given time frame, a post-process particle tracking algorithm had to be developed (i.e. executed outside the flow solver).

References

SKB's (Svensk Kärnbränslehantering AB) publications can be found at www.skb.se/publications. References to SKB's unpublished documents are listed separately at the end of the reference list. Unpublished documents will be submitted upon request to document@skb.se.

Abarca E, Idiart A, de Vries L M, Silva O, Molinero J, von Schenk H, 2013. Flow modelling on the repository scale for the safety assessment SR-PSU. SKB TR-13-08, Svensk Kärnbränslehantering AB.

Bosson E, Sassner M, Sabel U, Gustafsson L-G, 2010. Modelling of present and future hydrology and solute transport at Forsmark. SR-Site Biosphere. SKB R-10-02, Svensk Kärnbränslehantering AB.

Brydsten L, Strömgren M, 2013. Landscape development in the Forsmark area from the past into the future (8500 BC – 40,000 AD). SKB R-13-27, Svensk Kärnbränslehantering AB.

Curtis P, Markström I, Petersson J, Triumf C-A, Isaksson H, Mattsson H, 2011. Site investigation SFR. Bedrock geology. SKB R-10-49, Svensk Kärnbränslehantering AB.

Dershowitz W, Winberg A, Hermanson J, Byegård J, Tullborg E-L, Andersson P, Mazurek M, 2003. Äspö Hard Rock Laboratory. Äspö Task Force on modelling of groundwater flow and transport of solutes. Task 6c. A semi-synthetic model of block scale conductive structures at the Äspö HRL. SKB IPR-03-13, Svensk Kärnbränslehantering AB.

Follin S, 2008. Bedrock hydrogeology Forsmark. Site descriptive modelling, SDM-Site Forsmark. SKB R-08-95, Svensk Kärnbränslehantering AB.

Holmén J G, Stigsson M, 2001. Modelling of future hydrogeological conditions at SFR. SKB R-01-02, Svensk Kärnbränslehantering AB.

Joyce S, Simpson T, Hartley L, Applegate D, Hoek J, Jackson P, Swan D, Marsic N, Follin S, 2010. Groundwater flow modelling of periods with temperate climate conditions – Forsmark. SKB R-09-20, Svensk Kärnbränslehantering AB.

Odén M, Follin S, Öhman J, Vidstrand P, 2014. SR-PSU Bedrock hydrogeology. Groundwater flow modelling methodology, setup and results. SKB R-13-25, Svensk Kärnbränslehantering AB.

SKB, 2008. Geovetenskapligt undersökningsprogram för utbyggnad av SFR. SKB R-08-67, Svensk Kärnbränslehantering AB. (In Swedish.)

SKB, 2013. Site description of the SFR area at Forsmark at completion of the site investigation phase, SDM-PSU Forsmark. SKB TR-11-04, Svensk Kärnbränslehantering AB.

SKB, 2014a. Climate and climate related issues for the safety assessment SR-PSU. SKB TR-13-05, Svensk Kärnbränslehantering AB.

SKB, 2014b. Initial state report for the safety assessment SR-PSU. SKB TR-14-02, Svensk Kärnbränslehantering AB.

SKB, 2014c. Input data report for the safety assessment SR-PSU. SKB TR-14-12, Svensk Kärnbränslehantering AB.

Svensson U, Ferry M, Kuylenstierna H-O, 2010. DarcyTools version 3.4. Concepts, methods and equations. SKB R-07-38, Svensk Kärnbränslehantering AB.

Öhman J, Bockgård N, Follin S, 2012. Site investigation SFR. Bedrock hydrogeology. SKB R-11-03, Svensk Kärnbränslehantering AB.

Öhman J, Follin S, Odén M, 2013. Site investigation SFR. Bedrock hydrogeology – Groundwater flow modelling. SKB R-11-10, Svensk Kärnbränslehantering AB.

Unpublished documents

SKBdoc id, version	Title	Issuer, year
1395200 ver 1.0	TD05-Effects in ECPM translation	SKB, 2013
1395214 ver 2.0	TD08-SFR3 effect on the performance of the existing SFR1	SKB, 2013
1395215 ver 1.0	TD10-SFR3 adaptation to hydrogeological conditions	SKB, 2013
1396127 ver 1.0	Detailed study of nbgrad	SKB, 2013
1396258 ver 1.0	Jordbergsonderingar och installation av grundvattenrör på Piren SFR, Forsmark. (In Swedish.)	Sweco, 2012

Appendix A

Modelling sequence and traceability in data management

The different steps in the TD11 modelling approach are presented in general terms in Chapters 3, 4, and 5 in the main report. This appendix provides the details on the execution of simulations, with focus on the traceability in handling of all input and output; not only at each given execution step, but also in the transfer between different steps in the modelling sequence. An overview of the modelling sequence, which is broken down into four separate file-management routines, is presented in Appendix A1.

As the conceptual framework and principles of the TD11 modelling approach is presented main report provides, this appendix focuses on the numerical execution of the modelling sequence. That is: specification to file names of all input and output data and codes used to manage traceability in the handling of all files during the different steps in the simulation sequence. This is broken down into three subsections:

- Preparation of input data, file conversion, and parameterization (Appendix A2).
- Model setup and execution of the flow simulations (Appendix A3).
- Post-processing to extract results (Appendix A4).

The reader is referred to the main report for a more comprehensive exposé on the rationale and context of the different execution steps.

A1 Overview of modelling sequence

As explained in Section 2.3, TD11 addresses a total of 102 model setups (i.e. all combinations of 17 bedrock cases, and 6 stages of shoreline retreat). Each model setup is defined by a combination of the variables <**Bedrock case**> and <**time slice**> (i.e. Table 2-1 and Table 2-2 in the main report). Here the brackets, < >, and colour marking are used to denote the variables in the sensitivity analysis, and have a key role for the traceability in data management. Even a single model setup is complex, involving multiple input files that are being processed in several steps (Figure A-1). There are (at least) three reasons to apply automatized data-file management in the modelling sequence:

- **Minimisation of data-handling related errors**: automatizing ensures that: 1) all model setups are handled consistently (i.e. all model setups are treated the *same* way), and 2) application of input files is consistent with the specified <**Bedrock case**>/ <**time slice**>case (i.e. follows specifications in Table 2-1 and Table 2-2).
- **Traceability:** automatizing provides traceable data management via the source codes, and also maintains a strict traceability between sequences by means of case-specific filenames for intermediate input and output (i.e. all I/O filenames are tagged by relevant specification to <**Bedrock case**> and/or <**time slice**>). No output can be propagated until all required input data are available.
- **Time efficiency**: automatizing allows: 1) parallel processing in different working directories and 2) continuous processing over weeks, day and night.

Consequently, data file management is automatized as far as possible. The modelling sequence is divided into four main sequences (Figure A-1), which are handled by file-managing routines to maintain traceability between input and output:

a) **Data and grid preparation:** managed by a range of customized tools (see footnotes to Figure A-1).

b) **ECPM upscaling:** managed by [TD11_Manage_ECPM_setups.f90], see Section 5.2.

c) **Final model setup and flow simulation:** managed by [TD11_Manage_DT_runs_NEW_Pier_All_RLDM.f90], see Section 5.3.

d) **Post processing:** flow-field analysis, managed by [Get_flows_TD11.f] (Section 5.4.1), and particle tracking, managed by [P_track_random_TD11_deplete_loops.f] (Section 5.4.2).

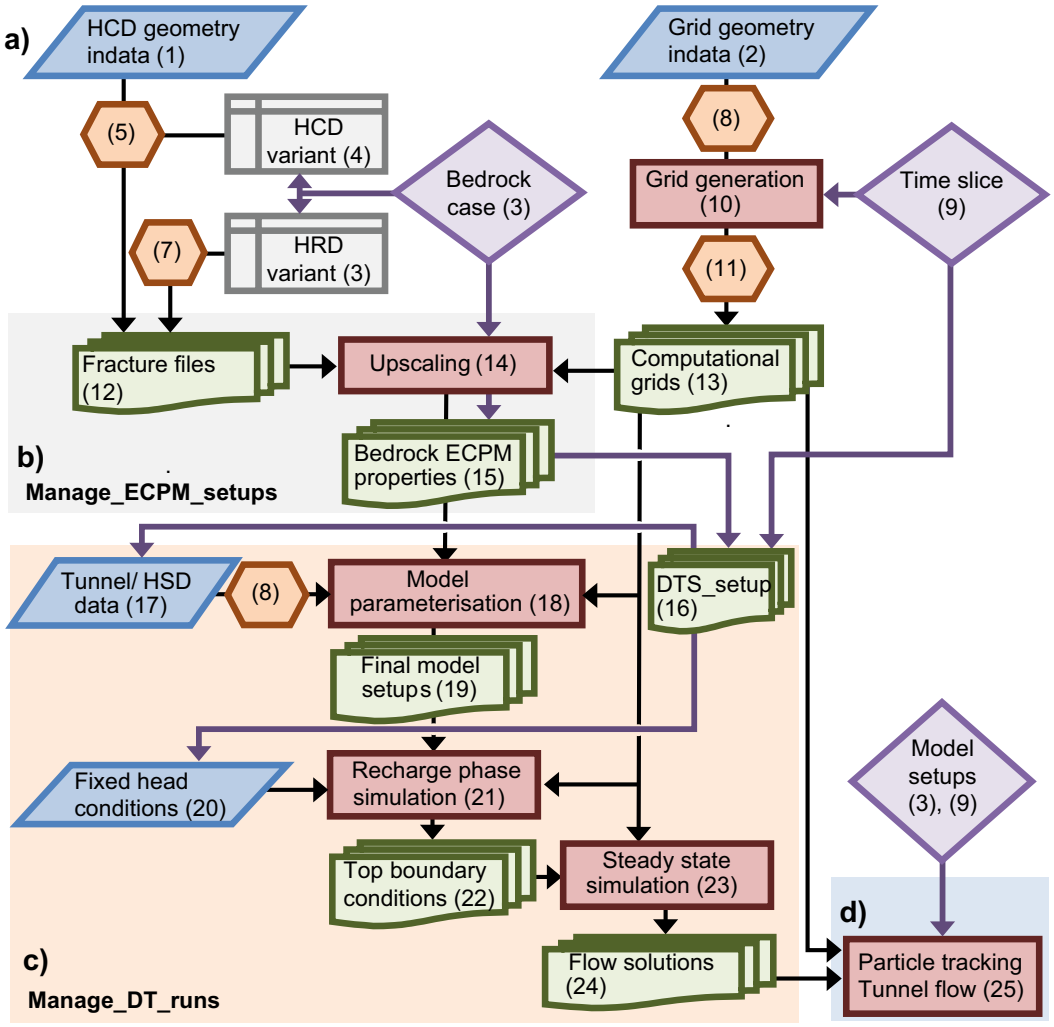

Figure A-1. *Model execution structure consisting of four sequences; a) data and grid preparation, b) upscaling ECPM properties, c) model-setup finalisation and flow simulation, and d) post processing.*

The file-managing routines are controlled by manually constructed input files, in which the list of bedrock cases (Table 2-2) and time slices (Table 2-1) are specified. Their purpose is to monitor and manage the parallel processing in different working directories, while maintaining strict traceability between input and output. The file managing codes typically operate in the following sequence:

1) Read the manually listed <**Bedrock case**> and/or <**time slice**> from the input text file.
2) Write and execute a DOS-command batch file (*.bat) that copies all required input files into the current working folder.
3) Check that all necessary input files exist in the local working directory.
4) Write the necessary DarcyTools input (i.e. construct the "cif.xml" file), but also specify information on the data set in either of two types of control files: [ECPM_setup.txt] and [DTS_setup.txt] (footnotes 15) and 16) in Figure A-1).
5) Execute relevant DarcyTools module (FracGen, PropGen, or DTS). Within the DTS module, the file [DTS_setup.txt] is used to tag <**Bedrock case**> and <**time slice**> to all output data filenames. It is also used, for example to prescribe the sea level for the specified <**time slice**>.
6) Write and execute a DOS-command batch file (*.bat) that creates a local folder into which all relevant output and input data are copied.
7) Steps 3-6 may be repeated, but at the end mark the current <**Bedrock case**> / <**time slice**> as "DONE" and proceed to the next in sequence (return to Step 1).

1) **HCD geometry in the SFR Regional domain**; based on geological deformation-zone model (Curtis et al. 2011), SFR_DZ_MASTER_v1.0, but includes extension of six lineaments (SFR DZ MASTER v1.0-hydro_extensions.xml). Used file: [SFR DZ MASTER v1.0.DT].

2) **Geometric data for grid discretisation**; Geometry of model domains, regolith layers, lakes, rivers, tunnels, and tunnel plugs are described in Chapter 3.

3) **Defined bedrock cases**; The TD11 sensitivity analysis involves 17 bedrock cases (Table 2-2; i.e. parameterisation variants). A <**Bedrock case**> consists of: a) a HCD parameterisation variant (<**HCD variant**>; Section 4.2.2) and b) a HRD variant (or realization, R**XX**; Section 4.2.1). Traceability and consistent management of the specified bedrock cases (i.e. file transfer between modelling sequences) is provided by two control files: [ECPM_setup.txt] (footnote 15) and [DTS_setup.txt] (footnote 16).

4) **HCD variant**; the internal heterogeneity and conceptual uncertainty in HCD parameterisation inside the SFR Regional domain is addressed by HCD parameterisation variants (Section 4.2.2). Ten <**HCD variant**> are selected for analysis (Table 4-4).

5) **HCD parameterisation:** A selection of 10 HCD-parameterisation variants is applied to deterministically modelled deformation zones inside SFR Regional domain using Fortran code [Assign_SFR_HCDs heterogeneity_TD11.f]. Sequence described in Table A-5. Output is in DarcyTools "known-fracture" format: [R_Param_SFR_<**HCD variant**>], where <**HCD variant**> is specified in (3).

6) **HRD variants**; the heterogeneity in the rock mass outside deformation zones is addressed by HRD variants. Three stochastic coupled realisations of DFN and Unresolved PDZs inside SFR Regional domain (R03, R18, and R85) are studied in the sensitivity analysis (Table 4-2).

7) **File preparation**; Parameterisation, generation, and removal of isolated fractures follows the procedure described in Öhman et al. (2013) (summarized in Section 4.2.1). All files are converted into DarcyTools "known-fracture" format and rotated into the model coordinate system, as described in Öhman et al. (2013). Used files: [R_SFR_DFN_connected_R**XX**_L1BC_knwn] and [R_Unresolved_PDZ_R**XX**_knwn], for HRD variants **XX** = 03, 18 and 85.

8) **File preparation**; All delivered geometry data, e.g. tunnel data (stl), topography and bedrock surface DEMs (xyz), lakes and rivers (GIS shape) are converted into DT "object"-format and rotated into the model coordinate system (details in Chapter 3).

9) **Time slices**; Model performance is evaluated at 6 stages of shoreline retreat, defined as <**time slice**> in Table 2-1. In the modelling sequence, <**time slice**> controls: a) *cell marking* of inactive cells, topography, lakes, and rivers in grid generation (10), b) RLDM regolith layering in *HSD parameterisation* (18), and c) *fixed-head criteria* during recharge phase simulations (20). <**time slice**> is tagged in the control file [DTS_setup.txt] (16) to ensure consistent file management.

10) **Grid generation**; One grid per time slice is generated [xyz_<**time slice**>_L1BC] by means of the DarcyTools module GridGen (Section 5.1). Notably, the discretisation is *static*, to facilitate time-independent compatibility in upscaled ECPM properties, while cell marking is *time dependent* to reflect the modelled dynamics in RLDM (shore line, DEM, lakes, and rivers; Brydsten and Strömgren 2013). Grid generation commands are traceable via the standardised Compact Input File [TD11_cif_<**time slice**>.xml] and [TD11_GGN_<**time slice**>.log], where <**time slice**> is specified in (9).

11) **Grid modification**: Identified inconsistencies in the computational grid are edited via the DarcyTools module PropGen, compiled from: [prpgen_GRID_RE-write.f] (Section 5.1).

12) **Fracture files**; The bedrock parameterisation in the flow model (HRD and HCD) is defined based on an underlying set of fracture files. These fracture files are prepared in the standard DarcyTools "known-fracture" format for the subsequent step of upscaling into ECPM properties (14). The principle in TD11 for analysing the sensitivity to bedrock parameterisation is: 1) the uncertainty and heterogeneity *inside* the SFR Regional domain is addressed in terms of variants (Section 4.2), while 2) the bedrock parameterisation *outside* the SFR Regional domain is static (Section 4.3).

13) **Computational grids**; Six DarcyTools grids are generated, with *time-dependent* cell marking to reflect the landscape dynamics modelled in RLDM (Brydsten and Strömgren 2013), but with *static* discretisation for time-independent compatibility with upscaled ECPM properties. Used files: [xyz_<**time slice**>_L1BC], where <**time slice**> is specified in (9).

14) **Upscaling bedrock ECPM properties**; The ECPM properties for a given <**Bedrock case**>, (3), are upscaled from fracture files by means of the DarcyTools module FracGen (GEHYCO algorithm). Traceability between input (12) and output (15) is provided via automatized file-management, using the Fortran code [TD11_Manage_ECPM_setups.f90] (details in Section 5.2).

15) **Bedrock ECPM properties;** In DarcyTools, hydraulic fracture properties are approximated by those of a porous medium and referred to as Equivalent Continuous Porous Medium (ECPM) properties. Upscaled bedrock ECPM properties (conductivity, free fracture volume, and flow-wetted surface area), define the hydraulic domains HCD and HRD in the final model setup (18). File management and applied filename conventions for ECPM-upscaling input/output are described in Table A-8. A control file is generated and stored along with data output files [ECPM_setup.txt].

16) **DTS_setup.txt;** control file defining model setup, combined from [ECPM_setup.txt] (15) and specified <**time slice**> in (9). Used to ensure traceability and consistency in file-management, between parameterisation (14) and final model output (25), and also to maintain name conventions for output files.

17) **HSD and tunnel data**; The final model setup (18) requires geometric and hydraulic data for the HSD and tunnels are described in Sections 3.2 and 3.3. control file [DTS_setup.txt] in (16) defines the grid and RLDM regolith layers for the specific <**time slice**>;

18) **Model parameterisation;** The final model setup for subsequent flow simulations, (21) and (23), is merged from three sub-domains: 1) the bedrock (HCD and HRD) is assigned ECPM properties (15), 2) HSD is parameterised based on RLDM regolith layering for <**time slice**> (Table 4-5), and 3) tunnel backfill parameterisation (i.e. assuming intact tunnel plugs; Table 4-1). Minimum values are also applied for conductivity and porosity. Performed by means of the DarcyTools module PropGen, compiled from: [prpgen_TD11_Model_parameterisation.f]. <**time slice**> is specified in [DTS_setup.txt], (16).

19) **Final model parameterisation**; The final model parameterisation for a given <**Bedrock case**>, (3), defines all three hydraulic domains HCD, HRD, and HSD (also includes tunnel backfill parameterisation). The grid parameterisation consists of the properties: permeability, porosity, and flow-wetted surface area, which are employed in flow simulations, (21) and (23), and post processing, (25). File management and applied filename conventions for input/output are described in Table A-9.

20) **Fixed head conditions**; Rivers, lakes, and the seafloor are assigned fixed head based on RLDM data for the <**time slice**>, specified in control file [DTS_setup.txt], (16). A so-called basin-filled DEM for the specific <**time slice**> is used as a criterion for maximum head in top-layer grid cells; described in Section 5.3.2.

21) **Recharge phase simulation**; The top-boundary condition for the subsequent steady-state phase, (23), is determined in this preceding simulation. Head in the ground-surface layer is simulated by a principle of combining locally variable recharge and fixed-head conditions, (20). Key outputs are: 1) the solved top-boundary condition, and 2) visualisation for verifications (Table A-10). Simulation premises traceable via [fif RECHARGE_TD11_NEW_Pier.f].

22) **Top boundary condition**; Input/output of the recharge-phase simulation are documented in Table A-10. [<**HCD variant**>_DFN_R**XX**_L1BC_<**time slice**>_rstslv] is used as a fixed-head boundary condition for the top layer of grid cells in the subsequent steady state simulation, (23).

23) **Steady state simulation**; Based on the fixed-head condition in the model top boundary, the flow solution is progressed to better convergence. Simulation premises traceable via [fif_TD11_Steady_state_NEW_Pier.f] and the DarcyTools Compact Input File: [<**HCD variant**>_DFN_R**XX**_L1BC_<**time slice**>_cif.xml].

24) **Flow solutions**; Input/output of the steady-state simulation are documented in Table A-11. The two key outputs are: [<**HCD variant**>_DFN_R**XX**_L1BC_<**time slice**>_Flow_solution.dat], used in post processing, (25) , and [<**HCD variant**>_DFN_R**XX**_L1BC_<**time slice**>_rstslv], delivered to Comsol near-field simulations.

25) **Post processing**; Performance measures are extracted from the flow solutions (24): tunnel cross flows are extracted with [Get_flows_TD11.f], and particle tracking is executed by [P_track_random_TD11_deplete_loops.f]. Input/output of particle tracking is documented in Table A-13, following the [DTS_setup.txt] convention, (16), (described in more detail in [TD11_Exit_locations_2013-01-15__READ_ME_____.txt]).

A2 Preparation of input model files

This section provides details on the preparation of geometric data for the top boundary of the model (regolith layers, lakes, and rivers), but also bedrock parameterisation. The inventory of tunnel geometry data is rather extensive, and therefore presented separately in Appendix B.

Regolith-layer geometry (results of RLDM modelling)

The top boundary in the flow model is defined by the regolith, which consists of three components: 1) Quaternary deposits, 2) filling material, and 3) peat. The regolith-layer geometry is delivered from the Regolith-Lake Development Model (RLDM; Brydsten and Strömgren 2013). Modelled regolith-layer data are defined in terms of upper-surface elevations (Table A-1) and are delivered for the 6 selected <**time slice**> (Table 2-1). The processing of RLDM data for input to the DarcyTools modelling is summarised below and presented in Table A-2.

Table A-1. Regolith data files delivered from RLDM.

Filenames[1)]	Description	Usage
pdem<time slice>.asc pdem<time slice>.xyz	Upper peat surface elevation (m). Peat starts to form –500 AD. This layer is therefore missing in earlier time steps.	HSD parameterisation Point data used for basin filling, defining lake/river objects, grid generation
lpgd<time slice>.asc	The upper surface of lacustrine accumulation of postglacial deposits, elevation (m). Lacustrine accumulation begins 1500 AD. This layer is therefore missing in earlier time steps.	HSD parameterisation
mpgd<time slice>.asc	The upper surface of marine accumulation of post glacial deposits, elevation (m). The same layer is used from 7000 AD to 55000 AD	HSD parameterisation
gkl<time slice>.asc	The upper surface of glacial clay, elevation (m). The same layer is used from 7000 AD to 55000 AD	HSD parameterisation
fill<time slice>.asc	The upper surface of filling, elevation (m). This layer is used for all time steps.	HSD parameterisation
glfl<time slice>.asc	The upper glaciofluvial-material surface elevation (m). Thickness is constant during all time steps.	HSD parameterisation
till<time slice>.asc	The upper till surface elevation (m). Thickness is constant during all time steps.	HSD parameterisation
bedr<time slice>.asc bedr<time slice>.xyz	The upper bedrock surface, level in the height system RH 70 (m). The level has been corrected for all layers from –8000 AD to 55000 AD using the Sea shoreline curve for the reference scenario.	HSD parameterisation Point data not used[2)]

[1)] Selected <time slice> are: 2000AD, 2500AD, 3000AD, 3500AD, 5000AD, and 9000AD. Extensions *.asc are in GIS raster format, while *.xyz is in point-data ASCII format.

[2)] Owing to the “fixed-bedrock” convention used, the bedrock surface is modelled as static. The bedrock surface is therefore defined by the original definition in the static regolith model [bedrock_up_v2_2000AD.xyz], GIS #12_08.

Table A-2. RLDM data processing in 3 steps.

Purpose [input]	Execution code [output]
1. Conform to DarcyTools elevation reference system	
Convert regolith layer elevations (Table A-1) into fixed-bedrock format. [*.asc], [*.xyz]	Future_HSD_data_to_fixed_Bedrock_format.f90 (adds suffix *"**_Fixed_bedrock**") [*_Fixed_bedrock.asc], [*_Fixed_bedrock.xyz]
2. Basin fill uppermost regolith layer (i.e. "DEM")	
Fill local topographical basins above sea level [pdem*_Fixed_bedrock.xyz]	Basin_fill_DEMs.f90 (adds prefix "**Filled_**"*) [Filled_pdem*_Fixed_bedrock.xyz] [Filled_pdem*_Fixed_bedrock.plt]
Fill local topographical basins below sea level. [Filled_pdem*_Fixed_bedrock.xyz]	Manual_Basin_fill_DEMs_adjustments.f90 (replaces files "**Filled_**"*) [Filled_pdem*_Fixed_bedrock.xyz]
File-format conversion to GIS raster format. [Filled_pdem*_Fixed_bedrock.xyz]	Create_Upper_DEM_ASC.f90 (extension *".**asc**") [Filled_pdem*_Fixed_bedrock.asc]
3. DarcyTools objects in grid generation	
Construct DarcyTools object defining topography and bedrock surface [Filled_pdem*_Fixed_bedrock.xyz] [bedrock_up_v2_2000AD.xyz]	DEM_to_DT_object.f (extensions *".**dat**", *".**plt**") [Filled_pdem*_Fixed_bedrock.dat], [Filled_pdem*_Fixed_bedrock.plt] [bedrock_up_v2_2000AD.dat], [bedrock_up_v2_2000AD.plt]
Construct a universal DarcyTools object, defining maximum RLDM topography 2000 AD to 9000 AD [Filled_pdem*_Fixed_bedrock.xyz]	DEM_Maximum_Z.f (extensions *".**dat**", *".**plt**") [MAX_Filled_DEM_2000AD_to_9000AD(onlyRLDM).dat] [MAX_DEM.plt]
Rotate DarcyTools objects into local model coordinate system [Filled_pdem*_Fixed_bedrock.dat], [bedrock_up_v2_2000AD.dat], [MAX_Filled_DEM_2000AD_ to_9000AD(onlyRLDM).dat]	Rotate_DT_objects.f90 (adds prefix "**R_**"*) [R_Filled_pdem*_Fixed_bedrock.dat], [R_bedrock_ up_v2_2000AD.dat], [R_MAX_Filled_DEM_2000AD_ to_9000AD(onlyRLDM).dat]

Conversion to fixed-bedrock format

One of the main objectives of TD11 is to study effects of shoreline retreat resulting from the on-going shoreline retreat. The DarcyTools simulations employ the bedrock surface as a fix reference system for elevation (i.e. at land uplift per 1970, m RHB 70). In this fixed-bedrock reference system, shoreline retreat is modelled by means of relative sea level displacement (SKB 2014c; Section 3.3.5).

However, all delivered regolith data (Table A-1) account for the land uplift (i.e. the bedrock surface elevation is not constant over time). The first step in processing RLDM data is therefore to encompass the delivered RLDM elevation data to the fixed-bedrock reference system, such that the bedrock elevation is constant over time. The elevation data are back-calculated by means of land-lift data (SKB 2014c transferred into an ASCII input file [FILES_TO_CONVERT.in]) and Fortran code [Future_HSD_data_to_fixed_Bedrock_format.f90]. For traceability, the adjusted filenames, *.asc and *.xyz, are given the suffixes "*_Fixed_bedrock.asc" and "*_Fixed_bedrock.xyz" (Table A-2).

Basin filling the uppermost RLDM layer (i.e. "DEM") to control surface head

Surface runoff is not modelled explicitly in DarcyTools. Consequently, excess ground-surface head may occur locally where net precipitation exceeds recharge (i.e. head locally exceeding topography). This model artefact is circumvented by iteratively controlling that the simulated head in the uppermost cell layer in the model does not exceed ground surface; the principles of this modelling approach is explained in detail in Sections 5.3.2 and 6.1. As such, the uppermost RLDM layer, also referred to as "DEM", has a central role in defining the local upper bound for simulated head at ground surface. Note that areas modelled as submerged in RLDM (lakes, rivers, or below sea level) are treated separately (Sections 3.3.3, 3.3.4, and 3.3.5).

However, the landscape dynamics modelling (RLDM) only resolves surface water above a certain scale, and consequently, the DEM contains local depressions below the scale for deterministic RLDM modelling. Such depressions may be peat-filled or hold surface water, e.g. minor lakes, wetlands, or pools. Irrespectively of which, it can be argued that the simulated head in local depressions should not be bounded by the elevation of the actual basin floor, but instead by the topographical threshold of the basin (i.e. the maximum water level, if entirely water filled). In other words, a necessary preparatory step for implementation as a head criterion in simulations is to process the topography data such that all local basins are eliminated and replaced by basin-threshold levels. This procedure is referred to as "basin-filling", and is explained below.

One filled DEM is prepared for each time slice [Filled_pdem<**time slice**>_Fixed_bedrock.asc], by filling local topographical depressions until reaching the surrounding geometric threshold. During this process, elevations in areas deterministically modelled as submerged are kept fixed (i.e. lakes, rivers, or below sea level). Thus, the final basin-filled DEMs slope towards: 1) the sea, 2) a lake with specified threshold (RLDM), or 3) a modelled river. The basin-fill is conducted in three steps (Table A-2):

1) Automatized filling [Basin_fill_DEMs.f90], millimetre by millimetre, of topographical basins above sea level for a given <**time slice**> (Figure 3-5). To avoid unmotivated filling along the seafloor, basins below sea level are not included. Basins extending *partly* below sea level are handled manually, in a second step, as it is difficult to determine if their geometric thresholds are above sea level based on algorithms.
2) Manual filling [Manual_Basin_fill_DEMs_adjustments.f90] of remaining basins that are identified by visual inspection as *isolated* from the sea for a given <**time slice**>. Isolated basins are *partly* below sea level, but have a geometric threshold above sea level (Figure 3-6). The purpose is to avoid erroneous identification of local inland sea-cells in simulations, which otherwise may render inaccurate particle exit locations. The SFR tunnel entry is an example of a basin *partly* below sea level. For example, known lake levels are used as thresholds for the 2000 AD <**time slice**>.
3) The basin-filled DEMs are exported into GIS raster format, by means of the Fortran code [Create_Upper_DEM_ASC.f90].

The basin filled DEM is used as a criterion for maximum local groundwater level (i.e. the maximum head in a local depression is determined by the *geometric* threshold of the surrounding DEM elevations). Although the basin-fill is a substantial improvement for constraining surface head in flow simulations, it does *not guarantee* absence of local depressions, due to inexact matching between RLDM and the DarcyTools grid. The inexact matching is due to: 1) discretisation differences (e.g. the DarcyTools grid has variable refinement) and 2) coordinate-system differences (e.g. the DarcyTools grid has a rotated coordinate system).

Constructing DarcyTools objects to implement HSD in grid generation

In the standard DarcyTools procedure, the model top boundary is defined by removal of grid cells above topography (i.e. as defined by a DEM DarcyTools object). TD11 addresses several stages of shoreline retreat (time slices), during which the topography alters due to landscape dynamics. The altering topography is honoured by using time-specific computational grids [xyz_<**time slice**>_L1BC], where the model top boundary is defined by [R_Filled_pdem<**time slice**>_Fixed_bedrock.dat]. For time efficiency, a *cell inactivation* method is used, where:

3) cells are *permanently* deleted, if located above the maximum DEM elevation, determined over the time period 2000 to 9000AD, [R_MAX_Filled_DEM_2000AD_to_9000AD(onlyRLDM).dat].
4) cells are *inactivated* in the time-specific grid, if located above the DEM for the particular <**time slice**>, determined by [R_Filled_pdem<**time slice**>_Fixed_bedrock.dat].

The benefit of this method is that the discretisation of all time-specific grids is identical, which allows re-using the same upscaled ECPM properties for all time slices (i.e. ECPM upscaling is a time-consuming step that is only valid for a specific grid discretisation). The top boundary is defined as the uppermost layer of active cells in the grid (i.e. immediately below a permanently deleted cell or a temporarily inactivated cell). The regolith is defined as above computational cells above the bedrock surface [R_bedrock_up_v2_2000AD.dat]. This particular file is the original data source for bedrock surface (GIS #12_08; [bedrock_up_v2_2000AD.xyz]), defined in the static regolith model. Due to the "fixed-bedrock" reference convention, all bedrock surface data are identical (apart from negligible round-off errors).

Transferring RLDM lake geometry into "DarcyTools object"-format

Implementation of geometric data in the DarcyTools grid generation requires that data are converted into the so-called "DarcyTools object" file format. Therefore, time-specific DarcyTools objects representing lakes at a given time slice are constructed, in the following 4 steps:

1. RLDM lake vector shapes (lakes_<**time slice**>.shp) and RLDM topography point data (pdem<**time slice**>_Fixed_bedrock.xyz) are joined in ArcGIS. Topographical points (x,y,z) falling inside, and on the border of, a lake vector object are exported as a text file, under the name [Lake_<Lake ID>_<**time slice**>.txt] . All lakes for a given <**time slice**> is stored in a separate working directory, which also includes a directory list [List_of_LAKES.txt], containing the filenames and threshold data for all lakes.
2. Lake data [Lake_<Lake ID>_<**time slice**>.txt] are transformed into watertight 3D CAD volumes [Lake_<Lake ID>_<**time slice**>.**stl**], enclosing each lake water volume. The conversion is made by the code [Make_Lakes.F90], which extrudes the volume between the bottom and the surface of a lake. The extrusion is facilitated by duplicating a unit CAD cuboid [Box_Template.txt], which locally is vertically bounded by the bottom (i.e. local RLDM topography) and the surface (i.e. the specified threshold) of a lake. The CAD objects are also translated from their original RT90 coordinate system by [–1626000., –6692000.].
3. By means of the DarcyTools module OGN, CAD volumes [Lake_<Lake ID>_<**time slice**>.stl] are then converted into so-called "DarcyTools objects" [Lake_<Lake ID>_<**time slice**>.**dat**] and Tecplot output [Lake<Lake ID>.plt]. The conversion is a standard DarcyTools procedure. The TecPlot output facilitates 3D visualisation and verification against topographical depressions in the RLDM DEMs.
4. Finally, lake objects [Lake_<Lake ID>_<**time slice**>.dat] are rotated into the local DarcyTools coordinate system [**R**_Lake_<Lake ID>_<**time slice**>.dat] by means of the Fortran code [Rotate_DT_objects.f90]. Pivot point in local coordinate system: [6400. 9200.], rotation angle: 32.58816946°.

These time-specific, individual lake objects [R_Lake_<Lake ID>_<**time slice**>.dat] are only used to define lake cells in the computational grid. Grid refinement of lake is controlled by a joined, time-independent DarcyTools object [R_MAX_EXTENSION_ALL_LAKES.dat], which confines the maximal extension of all lakes (horizontally and vertically) for all time slices. This object is constructed parallel to the preparation of time-specific, individual lake objects, described above. The purpose of time-independent grid refinement (i.e. refining) is time efficiency, as ECPM conversion becomes compatible with all grids (motivated in Section 3.3.2).

Table A-3. Prescribed head for lake cells, identified by DarcyTools cell markers.

Lake ID	Lake threshold	DarcyTools marker, for <time slice>					
	(m, elevation)	2000AD	2500AD	3000AD	3500AD	5000AD	9000AD
107	–6.24				158	189	214
108	–15.23					188	
110	–6.05				157		
114	–33.49						215
116	–14.24					187	216
117	–5.72				156	186	
118	–5.13			136	155	185	
120	–2.6		123	135	154	184	
121	–10.42					183	
123	–10.91					182	
124	0.48	103	122	134	153		
125	0.4	104					
126	–12.24					181	
129	5.82	105	121	133	152		
132	3.66	106	120	132	151		
134	–1.35		119	131	150	180	217
136	0.42	107	118	130	149	179	
142	1.82	108	117	129	148		
144	0.41	109	116	128	147		
146	–13.87					178	218
148	0.56	110	115	127	146	177	
149	5.32	111	114	126	145	176	
150	–8.22				144	175	219
151	–16.83						220
152	–15.41					174	221
153	–8.29				143	173	
154	–15.36					172	222
155	–6.6				142	171	
156	–6.06				141	170	223
157	–13.99					169	
159	–11.84					168	
160	–7.09				140	167	
163	–16.19					166	224
164	–20.19						225
165	–18.62						226
166	–16.2					165	227
167	–16.99						228
170	–10.14					164	229
173	–10.53					163	230
175	–10.06					162	
176	–4.95			125	139	161	
177	–8.73					160	
178	–7.59				138		
179*)	–1.67*)	112	113	124	137	159	
180	–20.34						231
184	–24.24						232

*) Lake 179 is the Biotest lake. It is prescribed sea-level head at 2000 AD.

Transferring RLDM river data to DarcyTools

Rivers (streams and brooks rather) are treated as prescribed head-boundary conditions in the flow model (Section 3.3.4). Similarly to how lakes are represented, "river cells" are implemented in the computational grid by means of so-called "DarcyTools objects" (Table A-4). In the flow simulations, any cell identified as a river (i.e. all river cells are assigned the same marker = 102) is prescribed a head value that is linearly interpolated between the nearest two points in an input text file [River_head.in] (Table A-4). Riverbed head is not provided in RLDM data, but is estimated according to principles described below.

DarcyTools objects representing rivers at different time slices are constructed, in 4 steps:

1. RLDM river data are prepared for DarcyTools modelling by combining river data (GIS vector format) with topography data (GIS raster format). To facilitate this joint analysis, the river nodes are exported into a text file (vattendrag_SDEADM.UMEU_FM_GEO_10171.txt. This river-node list is organised in such a way that the corresponding element list of river-segments is straight-forward to construct manually [Connectivity_list.dat]. The modelled river geometry in RLDM is "stationary" (rivers do not meander or vanish over time). Therefore, the nodal data, exported at "maximal river extension" (i.e. a late stage of shoreline retreat, t > 9000 AD), represent the river geometry at any given <**time slice**>, provided the nodes below sea level are inactivated in the subsequent flow simulations.
2. Two corrections are made to [Connectivity_list.dat]: 1) junctions between river branches are forced to occur at the nearest common river node, and 2) river starting locations (i.e. origin point of tributaries) are harmonized with topography data (i.e. a few river nodes that are inconsistent with raster topography data are removed).
3. The local riverbed head is interpolated for each <**time slice**> and stored in a condensed input file for flow simulations [River_head.in] (see Table A-4). In this interpolation, three types of river nodes are treated as deterministic, fixed values:
   a. The starting point of river tributaries (taken as local topography elevation),
   b. River nodes inside lakes (i.e. any node falling inside [Lake_<Lake ID>_<**time slice**>.txt] is assigned head equal to lake threshold, Table A-3),
   c. River segments below sea level are temporarily set equal to sea level, but are later inactivated in the subsequent flow simulations.

Remaining river nodes are treated as flexible points and are interpolated by iterations [Interpolate_River_Head.f90], until:

   a. Head variability along the riverbed is smoothened out, such that the river gradient is directed towards the sea, and
   b. Difference between river head and local RLDM topography is minimized (node topography elevation extracted from [pdem<**time slice**>_Fixed_bedrock.xyz]).

4. For the grid generation, watertight 3D CAD volumes [Filled_Streams_<**time slice**>_z25.**stl**] are constructed based on the node list and the element list. This conversion is made by the code [Make_Rivers.F90], which extrudes a 5 m wide channel, extending from below the local estimated riverbed head (H(x,y) –1 m) to a fixed elevation of 25 m (note that any part extending above ground surface is eliminated in the grid generation). The CAD objects are also translated from their original RT90 coordinate system by [–1626000., –6692000.].
5. Next, the DarcyTools module OGN, is used to convert the CAD volumes [Filled_Streams_<**time slice**>_z25.stl] into so-called "DarcyTools objects" [Filled_Streams_<**time slice**>_z25.**dat**] and Tecplot output [Filled_Streams_<**time slice**>_z25.**plt**]. This conversion is a standard DarcyTools procedure. The TecPlot output facilitates 3D visualisation and verification against RLDM topography.
6. Finally, the river objects [Filled_Streams_<**time slice**>_z25.dat] are rotated into the local DarcyTools coordinate system [**R**_Filled_Streams_<**time slice**>_z25.dat] by means of the Fortran code [Rotate_DT_objects.f90]. Pivot point in local coordinate system: [6400. 9200.], rotation angle: 32.58816946°.

Table A-4. Input data files used to prescribe head in rivers.

Input file	Description
R_Filled_Streams_<time slice>_z25.dat	Geometric DarcyTools object used in grid generation to define river cells above sea level at <time slice>. All river cells are given the cell marker 102.
River_head.in	Input text file used to prescribe fixed head along riverbeds in flow simulations. Local riverbed head is estimated for 4,821 points (x,y,H) along river trajectories. (x,y) are in local rotated model coordinates. H is available in 6 columns, one for each <time slice>. The prescribed head for a riverbed cell is linearly interpolated between the two nearest points.

Parameterisation of HCD-variant input files

The selected HCD variants (Table 4-4) are prepared for simulations in the so-called "known-fracture format", which is a file format that is accepted by DarcyTools. This is facilitated by means of the Fortran code [Assign_SFR_HCDs heterogeneity_TD11.f], which for traceability has the file-naming convention [**Param_SFR_HCD_**<**HCD variant**>] for output files (Table A-5).

All HCD variants have identical deterministic geometry (i.e. structural uncertainty is not addressed in the sensitivity analysis). The HCD geometry is defined in [SFR DZ MASTER v1.0.DT], which is combined from two data sources:

1) The geological model v.1.0 (Curtis et al. 2011) [SKBdoc 1244246 SFR_DZ_MASTER_v1.0], and
2) Complementary geometry of six HCDs that, based on lineament data, extend outside the SFR Regional domain [SFR DZ MASTER v1.0-hydro_extensions] (see recommendations in Öhman et al. 2013; Section 3.2).

The reason for extending 6 HCDs is to eliminate the risk of particle-tracking artefacts that are related to model-boundary termination of zones. Note that these HCDs (NNW3113, NNW0999, NS3154, NNE3266, NNE3265, and NNE3264) are not defined in the deformation-zone model outside the SFR Regional domain (Section 4.3). The parameterisation data are: [Conditional_DZ_data.dat], conditional values at borehole intercepts (Öhman et al. 2013, Table A-2), and two variants of effective HCD transmissivity [DZ_data.dat] (SKB 2013, Appendix 6), or [DZ_data_NO_Depth-trend.dat] (Table 4-3).

Table A-5. Implementation of selected HCD variants.

Purpose [input]	Execution [output]
1. Define structural geometry data	
Triangulate surfaces of 6 extended HCDs [SFR DZ MASTER v1.0-hydro_extensions.xml]	RVS_info.bat [LINEAMENT_EXTENSIONS.DT]
Combine extended HCDs with geological model v.1.0 (Curtis et al. 2011) [SKBdoc 1244246 SFR_DZ_MASTER_v1.0.xml] [LINEAMENT_EXTENSIONS.DT]	RVS_info.bat Manual merging in text editor [SFR DZ MASTER v1.0.DT]
2. Parameterise HCD variants	
Generate HCD variants in DarcyTools "known-fracture" format, by combining: 1. Structural geometry [SFR DZ MASTER v1.0.DT] 2. Hydraulic data [DZ_data.dat]/ [DZ_data_NO_Depth-trend.dat] 3. Conditional data [Conditional_DZ_data.dat] 4. Tabulated inverse cumulative normal distribution [Norm_dist.dat]	[Assign_SFR_HCDs heterogeneity_TD11.f] (Export fracture file with prefix "**Param_SFR_**"*) [Param_SFR_<HCD variant>] [Param_SFR_<HCD variant>.plt]
3. Rotation	
Rotate DarcyTools known-fracture files into local model coordinate system [Param_SFR_<HCD variant>]	Rotate_DT_objects.f90 (adds prefix "**R_**"*) [R_Param_SFR_<HCD variant>]

A different approach was taken to construct the model input files for BASE_CASE2. It can be summarised in the following steps:

1) Most ECPM properties (condx.dat, condz.dat, fws.dat, poro.dat) are taken from BASE_CASE1 (hence the name BASE_CASE2),
2) A separate HCD geometry was created with identical parameterisation to BASE_CASE1 [R_Param_SFR_HCD_CD#DEP_HOM], but where the four zones: ZFMWNW0001, ZFMNW0002, ZFMWNW3259, and ZFMWNW0813 are excluded, and
3) The ECPM conductivity orthogonal to the Southern boundary belt in the rotated model coordinate system (condy.dat), was upscaled from the file [R_Param_SFR_HCD_CD#DEP_HOM].

Bedrock parameterisation outside the SFR Regional domain

Earlier analyses have demonstrated that the performance measures of SFR are primarily controlled by the bedrock parameterisation in the near-field (i.e. local structures and local fracture network). The sensitivity analysis of the bedrock parameterisation is therefore confined to the SFR Regional domain (Figure 3-1). The bedrock description outside the SFR Regional domain is taken from SR-Site/SDM-Site Forsmark and kept constant in all model setups (i.e. defined by data in Table A-6). Note that the filename tags "WITH_HOLE" and "med_hål_i_mitten" denote removal of fractures/HCD geometry inside the SFR Regional domain (explained in Öhman et al. 2013); this is necessary to avoid artificial overlaps at the SFR Regional domain. Similarly, truncations of the SDM-Site sheet joints inside the SFR Regional domain are described in Öhman et al. (2013).

Table A-6. Fracture files used outside SFR Regional domain.

Filename[1)]	Description	Source
PFM_zoner_med_hål_i_mitten	Parameterized HCD, outside SFR Regional domain Exclusion of HCD geometry inside SFR Regional domain (+ entire ZFM871) described in Öhman (2010, Section 3.3.2). Converted from "dt" into "known-fracture format".	861006_DZ_PFM_REG_v22_SJ.dt
UPDATED_SERCO_DFN_WITH_HOLE	Stochastic DFN outside SFR Regional domain in "known-fracture format" (Figure 4-10). Original file from SDM-Site Forsmark, expanded to cover flow domain, as described in TD10.	SRS-FFM01-06_v4_alterFinal_nocpm_r1_sets1-65_all_96.asc EXTENDED_SERCO_DFN_WITH_HOLE
PLU_sheet_joints_truncated	Hydraulic deterministic structures (HCD), converted from ifz into "known-fracture format", and locally reduced transmissivity near SFR ramp, as described in Öhman et al. (2012, Section 3.4.1).	081006_sheet_joints_v5.ifz
Parameterized_SFR_BRIDGES	Used to fill in geometric discontinuities when merging SFR HCDs with those in SDM-Site Forsmark. Parameterised and converted from xml into "known-fracture format" via RVSinfo.	SKBdoc 1282650 – SFR DZ MASTER v1.0-bridges.xml

[1)] All fracture files are rotated into the local model coordinate system. The prefix "R_" is added to all rotated files, denoting the rotated coordinate system.

In essence, the parameterisation outside the SFR Regional domain is identical to the one in TD10. However, the HRD outside the SFR Regional domain is parameterised based on a single DFN realisation, and a consequence of the updated model flow domain (Figure 3-1) is that the coverage of the DFN realisation must be expanded (this was done during TD10). This DFN realisation was originally delivered from SR-Site [SRS-FFM01-06_v4_alterFinal_nocpm_r1_sets1-65_all_96.asc] (Table A-6) but has been expanded in two steps within the SR_PSU project:

1) The original DFN realisation was first expanded to conform to the SDM-PSU flow domain. The file [EXTENDED_SERCO_DFN_WITH_HOLE] was constructed by a duplication procedure described in Öhman et al. (2013).
2) The flow domain update for TD10 (Section 3.1.1), requires additional expansion resulting in [UPDATED_SERCO_DFN_WITH_HOLE] (Figure 4-10), where the SDM-PSU file was used as a starting point. The adjustments are traceable via the Fortran code [Update_Sercos_DFN.f90].

It should be noted that the DFN realisation outside SFR Regional domain lack DFN coverage above z = 0 m elevation (in terms of fracture centres). This is compensated by applying a minimum bedrock conductivity of 3×10^{-8} m/s above z = –10 m elevation (see Table 4-5).

The fracture files representing the bedrock outside the SFR Regional domain are specified in Table A-6. It should be noted that all fracture files used in the model are rotated into the DarcyTools coordinate system, which tags the prefix "R_" to all filenames with rotated data.

A3 Management of model files in simulation

Computational grids are generated by means of the DarcyTools module GridGen (Section 5.1). The grids are unstructured, which allows the flexibility of local refinement (e.g. near ground surface and tunnel geometry). The discretization is carried out via a sequence of commands specified in the standardised Compact Input File on xml-format, [cif.xml] (Svensson et al. 2010). A discretisation command consists of a geometric reference (i.e. DarcyTools objects in Chapter 3) and either: 1) a specification on local maximum cell side length (Table A-7), and/or 2) classification of grid subdomains by means of a cell marker ID (Table A-7). Cell-marker IDs have a key role in subsequent modelling; for example they are used in property assignment, boundary conditions, and particle release points.

Two types of inconsistencies are noted in the generated grids:

1) HSD cells on top of: a) an inactivated cell, b) a lake cell, or c) a river cell, are inactivated,
2) Particle-release locations inside the silo (Mk = 15) are constrained to a maximum elevation of z = –80 m elevation (any Mk = 15 above z = –80 are set to Mk = 21; Figure 4-2).

In a secondary step, these inconsistencies are edited by means of the DarcyTools module PropGen, as compiled from: [prpgen_GRID_RE-write.f].

Table A-7. Grid generation.

Input files	Description
[TD11_cif_<time slice>.xml]	Compact Input File in xml-format, specifying the sequence of discretization commands (i.e. commands specify local grid refinement via geometry of DarcyTools objects)
Geometry data	Prepared in so-called DarcyTools-object format (Section 3). Complete list of input geometry used is traceable via the Compact Input File.

Output files	Description
[xyz_<time slice>_L1BC]	Computational grid used in flow simulations. Six grids are generated with identical discretisation, but different cell classification to reflect the landscape dynamics modelled in RLDM. The identical discretisation implies time-independency in compatibility with upscaled ECPM properties.
[ggnSFR_<time slice>.plt]	Tecplot output, visualising discretisation and cell marking in tunnels (e.g. Figure 3-3) and flow-domain cross sections
[TD11_GGN_<time slice>.log]	Log file per default generated by GridGen

Grid discretisation, in summary[1)] Domain, defined by [geometric object]	Max. cell side length[2)] (m) Delimitation	ΔL_H	ΔL_Z
Flow domain [R_Updated_WD_model_domain.dat] –1,100 m ≤ z ≤ [R_MAX_Filled_DEM_2000AD_to_9000AD(onlyRLDM).dat]	Outside SFR Regional domain	128	
SFR Regional domain	z ≥ –180 m	8	
Inside [R_SFR_modellområde_v01.dat]	–400 ≤ z < –180 m	16	
	–1,100 ≤ z < –400 m	64	
HSD	Outside SFR Regional domain	32	1
Above [R_bedrock_up_v2_2000AD.dat]	Inside SFR Regional domain	8	0.5
Tunnels (including disposal rooms and tunnel plugs)[3)] [R_Entire_L1BC.dat] and [R_Entire_SFR1_(silo_mod).dat]		2	
Silo walls: border [R_SFR-1_Silo_Outer_bnd.dat][3)]		1	
Volume enclosing particle-exit locations[4)]	z ≥ –60 m	16	
	–200 ≤ z < –60 m	32	
Volume enclosing Sheet-joints[4)]		16	

Domain		Delimitation	Cell marker ID
Bedrock	HCD and HRD	Outside SFR Regional domain	1
		Inside SFR Regional domain	10
RLDM objects	Cell inactivation	Above [R_Filled_pdem<time slice>_Fixed_bedrock.dat]	999
	HSD	Above [R_bedrock_up_v2_2000AD.dat]	100
	Ground surface	[R_Filled_pdem<time slice>_Fixed_bedrock.dat]	101
	Rivers	[R_Filled_Streams_<time slice>_z25.dat]	102
	Lakes	[R_Lake_<Lake ID>_<time slice>.dat]	Table A-3
Tunnels	SFR 1	Backfilled tunnel sections (Table B-1)	16
	L1BC	Backfilled tunnel sections (Table B-1)	28

Domain		Delimitation	Cell marker ID
Disposal rooms	1BTF	[R_1BTF_del1_yellow.dat]	11
	2BTF	[R_2BTF_del1_yellow.dat]	12
	1BLA	[R_1BLA_del1_yellow.dat]	13
	1BMA	[R_1BMA_del1_yellow.dat]	14
	Silo, interior	[R_Silo_del4_mitt_yellow.dat]	15[5)]
	2BLA	[R_2BLA_del1_yellow.dat]	22
	3BLA	[R_3BLA_del1_yellow.dat]	23
	4BLA	[R_4BLA_del1_yellow.dat]	24
	5BLA	[R_5BLA_del1_yellow.dat]	25
	2BMA	[R_2BMA_del1_yellow.dat]	26
	1BRT	[R_1BRT_del1_yellow.dat]	27
Plugs	Blue plugs	Mechanical concrete plugs (Table B-1)	30
	Brown	Bentonite plugs (Table B-1)	31
	Green	Filter-material plugs (Table B-1)	32
	Pink	Bentonite plugs in ramp (Table B-1)	33
	Silo, exterior	[R_SFR-1_Silo_Outer_bnd.dat][3)]	21[5)]

[1)] This summary only presents an overview of grid discretisation. Full details are traceable via [TD11_cif_<**time slice**>.xml] and [TD11_GGN_<**time slice**>.log].

[2)] Refinement expressed in terms of maximum side lengths of cells, in the horizontal and/or vertical direction, ΔL_H and ΔL_z, respectively.

[3)] Discretisation of tunnel geometry based on CAD definitions for TD10.

[4)] Approximate refinement volumes for particle-exit locations and sheet joints specified directly in Compact Input File (i.e. not based on formal CAD geometry). Details provided in [TD11_cif_<**time slice**>.xml].

[5)] The differentiation between Silo interior and Silo exterior is demonstrated in Figure 4-2.

File management in ECPM translation

As explained in Section 5.2, DarcyTools employs a geometric upscaling concept to transfer fracture-network characteristics onto its computational grid, in terms of Equivalent Continuous Porous Medium (ECPM) properties. These ECPM properties are the result of: 1) a given set of input fracture files and 2) a given grid discretisation, and therefore the results are only valid for a specific grid discretisation. The six stages of landscape dynamics, as modelled in RLDM, are represented by six grids with "time-dependent" cell marking (Section 5.1). However, the *discretisation* is identical in all grids and therefore ECPM properties are generic for all grids.

ECPM upscaling is featured by the DarcyTools module FracGen (GEHYCO algorithm) (Svensson et al. 2010), for which all input data are specified in a standardised Compact Input File, on xml-format [cif.xml]. As described in Section 2.3, the file management is automatized (Figure A-1). The ECPM upscaling is managed by means of [TD11_Manage_ECPM_setups.f90] in 6 steps:

1) Identify a <**Bedrock case**> from the manual input file [List_of_model_setups_for_ECPM.txt].
2) Ensure existence of all required input files (Table A-8),
3) write the Compact Input File for FracGen, i.e. a temporary cif.xml specifying input files for the given <**Bedrock case**>,
4) execute FracGen with the temporary cif.xml,
5) write control file [ECPM_setup.txt],
6) write and execute [Store_data.bat], which creates the folder [<**Bedrock case**>_L1BC] in which ECPM-property files are stored (Table A-8).

Table A-8. ECPM conversion [DarcyTools module FracGen].

Input files	Description
List_of_model_setups_for_ECPM.txt	List of bedrock cases (Table 2-2).
Cif.xml	Compact Input File in xml-format, which is the default input file for the DarcyTools module FracGen, specifying involved indata for ECPM upscaling (fracture files and computational grid). The input file is automatically generated by [TD11_Manage_ECPM_setups.f90] and is not stored.
[xyz_L1BC]	Computational grid (i.e. time-independent, as discretisation is static in all grids)
One HRD variant in Table 4-2	Stochastic realisation of bedrock outside deterministic deformation zones, inside the SFR Regional domain
One HCD variant in Table 4-4	Parameterisation variant of deterministic deformation zones inside the SFR Regional domain
R_Parameterized_SFR_SBA1_to_SBA8	Deterministic representation of SBA structures, inside the SFR Regional domain
All fracture files in Table A-6	Static bedrock parameterisation outside the SFR Regional domain
Output files[1)]	
[ECPM_setup.txt]	Control file specifying <**Bedrock case**>
[<**Bedrock case**>_L1BC_condx.dat]	Cell-wall ECPM conductivity in x-direction (rotated coordinate system)
[<**Bedrock case**>_L1BC_condy.dat]	Cell-wall ECPM conductivity in y-direction (rotated coordinate system)
[<**Bedrock case**>_L1BC_condz.dat]	Cell-wall ECPM conductivity in z-direction
[<**Bedrock case**>_L1BC_frevol.dat]	Cell ECPM free volume (i.e. intersectional volume sum of fracture aperture, Equation (5-1), used to calculate bedrock porposity)
[<**Bedrock case**>_L1BC_fws.dat]	Cell ECPM flow-wetted surface area (i.e. intersectional sum of fracture area)

[1)] <Bedrock case> = <HCD variant>"_DFN_RXX" (see Table 2-2).

Managing flow simulations

The execution of flow simulations (Section 5.3) is managed by the fortran code [TD11_Manage_DT_runs_NEW_Pier_All_RLDM.f90] in 6 steps:

1) Identify a <**Bedrock case**> from the manual input file [List_of_model_setups_for_DTS.txt].
2) Retrieve and ensure the existence of required input files (Table A-9).
3) Loop steps 4 to 6 for all six <**time slice**>.
4) Write the control file [DTS_setup.txt], which is used in subsequent model parameterisation, flow simulations, and particle tracking.
5) Write Compact Input Files for the subsequent flow simulations (cif.xml for the recharge and steady state simulations, respectively).
6) Write and execute [Run_DarcyTools.bat], which:
   a. Creates a local folder [RUN_<**time slice**>] in the working folder [<**Bedrock case**>_L1BC],
   b. Finalises the model setup, by launching [prpgen_TD11_Model_parameterisation.f] (Table A-9),
   c. Solves head for the model top boundary in a recharge phase, under premises specified in [fif-RECHARGE_TD11_NEW_Pier.f] (Table A-10).
   d. Applies the top-boundary condition to solve the full flow field, under premises specified in [fif_TD11_Steady_state_NEW_Pier.f] (Table A-11).
   e. Renames output/input to tag <**Bedrock case**> and <**time slice**> in file names.
   f. Moves simulation input/output files into the local run folder [RUN_<**time slice**>].

Following the standard procedure in DarcyTools modelling, the upscaled bedrock properties (Table A-8) and the HSD parameterisations are combined (Table A-9) to form the final model setup, i.e. Step 6b above. However, the approach to implement HSD layering in detail is a novelty in DarcyTools modelling, and therefore the concept is presented below.

Numerical implementation of HSD conductivity

Soil cells are identified by two DarcyTools cell markers: 1) mk = 100, representing general soil, defined as cells above bedrock surface, and 2) mk = 101, representing the uppermost, contiguous cell-layer intersected by the DEM of the current time slice. The HSD parameterisation is facilitated by a separate subroutine "HSD" of [prpgen_TD11_Model_parameterisation.f], which can be summarized in 6 steps:

1) Use DarcyTools cell markers to identify grid cells classified as HSD.
2) Match the DarcyTools grid cell, by coordinate, to relevant raster point(s) in RLDM (Table A-1).
   a) DarcyTools cells below the RLDM resolution are matched to the *nearest* RLDM point.
   b) DarcyTools cells exceeding RLDM resolution are matched to *an array* of RLDM points .
   c) Matching cells by coordinate requires back-rotation and translation into the RT90 coordinate system.
3) Calculate an effective HSD conductivity for the cell, based on the fractional intersection thicknesses, b_i, between the cell-wall control volume and the layer i, which has hydraulic conductivities K_{hi} and K_{vi} (Table 4-5).
   a) Effective horizontal conductivity is calculated as *arithmetic* mean of all $b_i \times K_{hi}$.
   b) Effective vertical conductivity is calculated as *harmonic* mean of all $b_i \times K_{vi}$.
4) Defaults are applied at inconsistencies between the DarcyTools grid and the RLDM data (i.e. for cells where $\Sigma b_i = 0$ m).
   a) Outcrops are set to K = 10^{-7} m/s, for cell markers = 101 where RLDM thickness = 0 m.
   b) Till is assumed, for cells located outside the horizontal coverage of RLDM.
   c) The *uppermost* or *lowest* RLDM layer with non-zero thickness is assumed, respectively, if the grid and RLDM layer elevations should mismatch vertically.
5) To avoid model artefacts (Figure 4-12), the conductivity of filling in the Pier, and its surroundings, are propagated 2 grid cells horizontally (i.e. 2×8 = 16 m horizontally; performed outside subroutine).
6) Based on data interpretation (Figure 4-13), the Pier, and its surroundings, is parameterized as *till* below an elevation of –3 m (performed outside subroutine; Figure 4-14).

Table A-9. Final model setup [prpgen_TD11_Model_parameterisation.f][1].

Input files	Description
[DTS_setup.txt]	Defines <Bedrock case> and <time slice>
[xyz_<time slice>_L1BC]	Computational grid (Table A-7)
[<Bedrock case>_L1BC_<time slice>_L1BC_condx.dat]	Cell-wall ECPM bedrock conductivity in x, y, and z-directions (Table A-8)
[<Bedrock case>_L1BC_<time slice>_L1BC_condy.dat]	
[<Bedrock case>_L1BC_<time slice>_L1BC_condz.dat]	
[<Bedrock case>_L1BC_<time slice>_L1BC_frevol.dat]	Cell ECPM free volume (Table A-8; i.e. intersectional volume sum of fracture aperture, Equation (5-1))
[Filled_pdem<time slice>_Fixed_bedrock.asc]	Upper surface of basin-filled DEM, z (m, elevation; fixed-bedrock format)
[lpgd<time slice>_Fixed_bedrock.asc]	Upper surface of lacustrine accumulation of postglacial deposits, z (m, elevation; fixed-bedrock reference)
[mpgd<time slice>_Fixed_bedrock.asc]	Upper surface of marine accumulation of post glacial deposits, z (m, elevation; fixed-bedrock reference)
[gkl<time slice>_Fixed_bedrock.asc]	Upper surface of glacial clay, z (m, elevation; fixed-bedrock reference)
[fill<time slice>_Fixed_bedrock.asc]	Upper surface of filling, z (m, elevation; fixed-bedrock reference)
[glfl<time slice>_Fixed_bedrock.asc]	Upper surface of glaciofluvial-material, z (m, elevation; fixed-bedrock reference)
[till<time slice>_Fixed_bedrock.asc]	Upper surface of till, z (m, elevation; fixed-bedrock reference)
[bedr<time slice>_Fixed_bedrock.asc]	Static bedrock surface, z (m, elevation; fixed-bedrock reference)
Table 4-5	HSD conductivity parameterisation (hard coded in separate subroutine)
Table 4-1	Tunnel backfill parameterisation (hard coded in separate subroutine). Identification via cell markers.
Output files	
[<Bedrock case>_L1BC_<time slice>_PERMX]	Cell-wall ECPM permeability in x, y, and z-directions
[<Bedrock case>_L1BC_<time slice>_PERMY]	
[<Bedrock case>_L1BC_<time slice>_PERMZ]	
[<Bedrock case>_L1BC_<time slice>_PORO]	Cell ECPM porosity
[<Bedrock case>_L1BC_<time slice>_ECPM_K.plt]	Tecplot output for visualisation. Contains conductivity of tunnel-walls (e.g. Figure 4-3) and flow-domain cross sections.

[1] <Bedrock case> = <HCD variant>"_DFN_RXX" (see Table 2-2). <time slice> defined in Table 2-1.

Input/output of the "Recharge-phase" simulation

Table A-10. "Recharge-phase" simulation [fif RECHARGE_TD11_NEW_Pier.f][1].

Input files	Description
[DTS_setup.txt]	Defines <Bedrock case> and <time slice>
[cif.xml]	Automatically generated standard Compact Input File. Not stored. Replaced by final CIF (Table A-11).
[xyz_<time slice>_L1BC]	Computational grid (Table A-7)
[<Bedrock case>_L1BC_<time slice>_PERMX]	Cell-wall ECPM permeability in x,y, and z-direction (Table A-9)
[<Bedrock case>_L1BC_<time slice>_PERMY]	
[<Bedrock case>_L1BC_<time slice>_PERMZ]	
[Filled_pdem<time slice>_Fixed_bedrock.asc]	Upper surface of basin-filled DEM, z (m, elevation; fixed-bedrock format). Defines maximum-head criterion for ground-surface cells.
Output files	
[<Bedrock case>_L1BC_<time slice>_hist<1-8>]	History files logging convergence statistics (e.g. Figure 6-5 and Figure 6-6)
[<Bedrock case>_L1BC_<time slice>_rstslv]	Flow solution (standardised DarcyTools restart file). The head solution in ground-surface cells is propagated as a top-boundary condition for the "Steady-state phase".
[<Bedrock case>_L1BC_<time slice>_GWT_recharge.plt	Tecplot ground-surface output for visualisation (e.g. Figure 6-1 to Figure 6-4)

[1] <Bedrock case> = <HCD variant>"_DFN_RXX" (see Table 2-2). <time slice> defined in Table 2-1.

Input/output of the “Steady-state” phase

Table A-11. “Steady-state” phase simulation [fif_TD11_Steady_state_NEW_Pier.f][1].

Input files	Description
[DTS_setup.txt]	Defines <Bedrock case> and <time slice>
[xyz_<time slice>_L1BC]	Computational grid (Table A-7)
[<Bedrock case>_L1BC_<time slice>_cif.xml]	Automatically generated standard Compact Input File
[<Bedrock case>_L1BC_<time slice>_PERMX]	Cell-wall ECPM permeability in x,y, and z-directions (Table A-9)
[<Bedrock case>_L1BC_<time slice>_PERMY]	
[<Bedrock case>_L1BC_<time slice>_PERMZ]	
[<Bedrock case>_L1BC_<time slice>_rstslv]	Flow solution from the “Recharge phase” (Table A-10), defining a fixed-head condition for the top boundary (standardised DarcyTools restart file).
Output files	
[<Bedrock case>_L1BC_<time slice>_hist<1-8>]	History files, logging convergence statistics, appended from the Recharge phase (Table A-10).
[<Bedrock case>_L1BC_<time slice>_rstslv]	Final steady-state solution (DarcyTools restart file). Not used.
[<Bedrock case>_L1BC_<time slice>_Flow_solution.dat]	Final steady-state solution, accessable for Post processing (Section 5.4; Table A-12; Table A-13). Contains cell-wall Darcy velocity and cell-centre pressure.
[<Bedrock case>_L1BC_<time slice>_Tunnel_flows.dat]	Disposal-room cross-flows, ASCII text
[<Bedrock case>_L1BC_<time slice>_Tunnel_walls.plt]	Tecplot output for visualisation (containing conductivity, head, and cross-flow for all tunnel walls)
[<Bedrock case>_L1BC_<time slice>_DTS_output.plt]	Tecplot output for visualisation (containing conductivity, head, cell markers, and Darcy flux for vertical and horizontal flow-domain cross sections)

[1] <Bedrock case> = <HCD variant>”_DFN_RXX” (see Table 2-2). <time slice> defined in Table 2-1.

A4 Post-processing model output

The performance measures are extracted from the flow solutions by means of post processing the obtained flow solutions (details in Section 5.4.1 and 5.4.2). Disposal-facility cross flow is extracted by means of the FORTRAN code [Get_flows_TD11.f], and particle tracking is executed by means of the FORTRAN code [P_track_random_TD11_deplete_loops.f]. The input/output of the flow analysis is documented in Table A-12, while the input/output for particle tracking is documented in Table A-13.

Table A-12. Flow-field analysis [Get_flows_TD11.f][1].

Input files	Description
[Directory_Get_flow.txt]	Defines <Bedrock case>
[xyz_<time slice>_L1BC]	Computational grid (from Table A-7)
[<Bedrock case>_L1BC_<time slice>_Flow_solution.dat]	Final steady-state solution, containing cell-wall Darcy velocities and cell-centre pressures (result from Table A-11).
[objects_sfr_20121130.asc][2]	Raster data identifying biosphere objects
Output files	
[Cell-net_flows.dat]	Calculated cell-net flow over tunnel walls, maximum local disposal-room gradient and overall disposal-room gradient
[Biosphere_Cell-net_flows.dat]	Net recharge/discharge across bedrock surface inside biosphere objects (mm/yr)
[<Bedrock case>_L1BC_<time slice>Bio_Q.plt]	Tecplot output for verification and visualisation purposes.

[1] <Bedrock case> = <HCD variant>”_DFN_RXX” (see Table 2-2). <time slice> defined in Table 2-1.

[2] Delivered by Emma Bosson, 2013-03-18. Raster data linked to biosphere object ID via [objects_sfr_20121130.dbf].

The input and output data files are summarized in Table A-13. In addition to the standardised output [<**Bedrock case**>_L1BC_<**time slice**>_<**Release location**>_<**File type**>.dat], so-called disposal-room *interactions* are exported in a separate output file [Assembled_Cross-List.dat] (ASCII format). Disposal-room interactions are statistics on the fraction of released particles from one disposal room that crosses one or more adjacent disposal rooms.

Table A-13. Particle tracking [P_track_random_TD11_deplete_loops.f][1)].

Input files	**Description**
[Directory_for_P-tracking.txt]	Defines <**Bedrock case**> and <**time slice**>
[xyz_<**time slice**>_L1BC]	Computational grid (from Table A-7)
[<**Bedrock case**>_L1BC_fws.dat]	ECPM flow-wetted surface area (cell property from Table A-8)
[<**Bedrock case**>_L1BC_<**time slice**>_PORO]	ECPM porosity (cell property from Table A-9)
[<**Bedrock case**>_L1BC_<**time slice**>_Flow_solution.dat]	Final steady-state solution, containing cell-wall Darcy velocities and cell-centre pressures (result from Table A-11).

Output files: <Bedrock case>_L1BC_<time slice>_<Release location>_<File type>.dat

<Release location>	**Markers**		**Tunnels**	**No. particles**
All_SFR1_D_	11–15	SFR-1	All 5 disposal rooms	1,000,000
SFR-1_1BTF_(11)	11	SFR-1	1BTF	100,000
SFR-1_2BTF_(12)	12	SFR-1	2BTF	100,000
SFR-1_1BLA_(13)	13	SFR-1	1BLA	100,000
SFR-1_1BMA_(14)	14	SFR-1	1BMA	100,000
SFR-1_Silo_(15)	15	SFR-1	Silo1	100,000
All_SFR2_D_	22–27	L1BC	All 6 disposal rooms	1,000,000
SFR-2_2BLA_(22)	22	L1BC	2BLA	100,000
SFR-2_3BLA_(23)	23	L1BC	3BLA	100,000
SFR-2_4BLA_(24)	24	L1BC	4BLA	100,000
SFR-2_5BLA_(25)	25	L1BC	5BLA	100,000
SFR-2_2BMA_(26)	26	L1BC	2BMA	100,000
SFR-2_1BRT_(27)	27	L1BC	1BRT_del1	100,000
<**File type**>.dat				
Exit_loc	Exit locations, or recharge locations, at the bedrock surface depending on direction of particle tracking. 15 data colums defined in TD11_Exit_locations_2013-01-30__READ_ME_____.txt			
Discharge	2-D histogram of exit locations used for visualisation in TecPlot format, resolving number of particles per m^2 and mean travel time.			
Recharge	2-D histogram of recharge locations used for visualisation in TecPlot format, resolving number of particles per m^2 and mean travel time.			
FORWARD_Paths	3-D trajectories from forward particle tracking (max 3000 exported). Used to visualise user-specified performance measures in TecPlot.			
BACKWD_Paths	3-D trajectories from backward particle tracking (max 3000 exported). Used to visualise user-specified performance measures in TecPlot.			

[1)] <Bedrock case> = <HCD variant>"_DFN_RXX" (see Table 2-2). <**time slice**> defined in Table 2-1. "deplete_loops" refer to a version of the algorithm where artificial bedrock retention properties, accumulated in "looping trajectory segments" (see separate PM on <nbgrad>), are removed.

Appendix B

Tunnel geometry data

All tunnel geometry data, i.e. SFR 1, SFR 3 and tunnel plugs (Section 3.2), are available in the CAD format (SKB 2014c). The implementation of tunnel geometry into the DarcyTools computational grid (Figure 3-3) requires processing of delivered data (Table B-1). The original CAD files are converted into the so-called DarcyTools-object format (changing file extension to *.dat; Table B-1). These geometric objects (*.dat) are translated and rotated into the local model coordinate system (adding the prefix "R_"*.dat). Filename of DarcyTools objects are shortened, as DarcyTools has an upper limit of 32 characters in object names. Typically, the substrings "SFR 1", "L1BC", and "plugg" can be omitted. Filename traceability from original CAD files to the applied DarcyTools object files is provided by means of Table B-1.

Table B-1. Used tunnel/tunnel plug geometry.

Source data (CAD STereoLithography format)	Rotated DarcyTools object
Disposal rooms of the existing SFR 1	
SFR1_1BTF_del1_yellow.stl	R_1BTF_del1_yellow.dat
SFR1_2BTF_del1_yellow.stl	R_2BTF_del1_yellow.dat
SFR1_1BLA_del1_yellow.stl	R_1BLA_del1_yellow.dat
SFR1_1BMA_del1_yellow.stl	R_1BMA_del1_yellow.dat
SFR1_Silo_del1_topp_yellow.stl	R_Silo_del1_topp_yellow.dat
SFR1_Silo_del2_under_topp_yellow.stl	R_Silo_del2_under_topp_yellow.dat
SFR1_Silo_del3_yttre_yellow.stl	R_Silo_del3_yttre_yellow.dat
SFR1_Silo_del4_mitt_yellow.stl	R_Silo_del4_mitt_yellow.dat
SFR1_Silo_del5_undre_yellow.stl	R_Silo_del5_undre_yellow.dat
Disposal rooms of SFR 3	
L1BC_1BRT_del1_yellow.stl	R_1BRT_del1_yellow.dat
L1BC_2BLA_del1_yellow.stl	R_2BLA_del1_yellow.dat
L1BC_3BLA_del1_yellow.stl	R_3BLA_del1_yellow.dat
L1BC_4BLA_del1_yellow.stl	R_4BLA_del1_yellow.dat
L1BC_5BLA_del1_yellow.stl	R_5BLA_del1_yellow.dat
L1BC_2BMA_del1_yellow.stl	R_2BMA_del1_yellow.dat
Backfilled tunnels of SFR 1	
SFR1_1BT_del1_white.stl	R_1BT_del1_white.dat
SFR1_1BT_del2_white.stl	R_1BT_del2_white.dat
SFR1_1BT_del3_white.stl	R_1BT_del3_white.dat
SFR1_1BT_del4_genomstick_white.stl	R_1BT_del4_genomstick_white.dat
SFR1_1BT_del5_white.stl	R_1BT_del5_white.dat
SFR1_1BT_del7_white.stl	R_1BT_del7_white.dat
SFR1_1BT_del9_white.stl	R_1BT_del9_white.dat
SFR1_1BT_del10_genomstick_white.stl	R_1BT_del10_genomstick_white.dat
SFR1_1BT_del11_white.stl	R_1BT_del11_white.dat
SFR1_1BT_del12_white.stl	R_1BT_del12_white.dat
SFR1_1BT_del13_nedre_stick_white.stl	R_1BT_del13_nedre_stick_white.dat
SFR1_1BT_del14_nedre_stick_white.stl	R_1BT_del14_nedre_stick_white.dat
SFR1_1BT_del15_white.stl	R_1BT_del15_white.dat
SFR1_1BT_del16_white.stl	R_1BT_del16_white.dat
SFR1_1BT_del17_white.stl	R_1BT_del17_white.dat
SFR1_1BT_del18_white.stl	R_1BT_del18_white.dat
SFR1_1BT_del19_white.stl	R_1BT_del19_white.dat

Source data (CAD STereoLithography format)	Rotated DarcyTools object
Disposal rooms of the existing SFR 1	
SFR1_1BT_del20_white.stl	R_1BT_del20_white.dat
SFR1_1BT_del26_white.stl	R_1BT_del26_white.dat
SFR1_1BT_del27_white.stl	R_1BT_del27_white.dat
SFR1_1BT_del28_white.stl	R_1BT_del28_white.dat
SFR1_1BT_del34_white.stl	R_1BT_del34_white.dat
SFR1_1BT_del35_anslutning_schakt_white.stl	R_1BT_del35_ansl_schakt_white.dat
SFR1_1BT_del36_undre_del_white.stl	R_1BT_del36_undre_del_white.dat
SFR1_1BT_del37_undre_del_white.stl	R_1BT_del37_undre_del_white.dat
SFR1_1BT_del38_undre_del_white.stl	R_1BT_del38_undre_del_white.dat
SFR1_1BT_del39_undre_del_white.stl	R_1BT_del39_undre_del_white.dat
SFR1_1BT_del40_undre_del_white.stl	R_1BT_del40_undre_del_white.dat
SFR1_1BT_del53_undre_del_white.stl	R_1BT_del53_undre_del_white.dat
SFR1_1BT_del54_undre_del_schakt_white.stl	R_1BT_del54_undre_del_sch_white.dat
SFR1_1DT_del1_white.stl	R_1DT_del1_white.dat
SFR1_1DT_del2_white.stl	R_1DT_del2_white.dat
SFR1_1DT_del3_white.stl	R_1DT_del3_white.dat
SFR1_1DT_del4_white.stl	R_1DT_del4_white.dat
SFR1_1DT_del5_white.stl	R_1DT_del5_white.dat
SFR1_1DT_del6_white.stl	R_1DT_del6_white.dat
SFR1_1DT_del7_white.stl	R_1DT_del7_white.dat
SFR1_1DT_del8_white.stl	R_1DT_del8_white.dat
SFR1_1DT_del11_white.stl	R_1DT_del11_white.dat
SFR1_1DT_del12_white.stl	R_1DT_del12_white.dat
SFR1_1DT_del15_white.stl	R_1DT_del15_white.dat
SFR1_1DT_del16_white.stl	R_1DT_del16_white.dat
SFR1_1DT_del17_white.stl	R_1DT_del17_white.dat
SFR1_1DT_del18_white.stl	R_1DT_del18_white.dat
SFR1_1DT_del19_white.stl	R_1DT_del19_white.dat
SFR1_1DT_del20_white.stl	R_1DT_del20_white.dat
SFR1_1DT_del21_white.stl	R_1DT_del21_white.dat
SFR1_1DT_del22_white.stl	R_1DT_del22_white.dat
SFR1_1DT_del23_white.stl	R_1DT_del23_white.dat
SFR1_1DT_del24_white.stl	R_1DT_del24_white.dat
SFR1_1DT_del25_white.stl	R_1DT_del25_white.dat
SFR1_1DT_del26_white.stl	R_1DT_del26_white.dat
SFR1_1DT_del27_white.stl	R_1DT_del27_white.dat
SFR1_1DT_del28_white.stl	R_1DT_del28_white.dat
SFR1_1DT_del29_white.stl	R_1DT_del29_white.dat
Backfilled tunnels of SFR 3	
L1BC_1BST_del1_white.stl	R_1BST_del1_white.dat
L1BC_1RTT_del1_white.stl	R_1RTT_del1_white.dat
L1BC_1RTT_del2_white.stl	R_1RTT_del2_white.dat
L1BC_1RTT_del3_white.stl	R_1RTT_del3_white.dat
L1BC_1RTT_del4_white.stl	R_1RTT_del4_white.dat
L1BC_1RTT_del6_white.stl	R_1RTT_del6_white.dat
L1BC_1RTT_del8_white.stl	R_1RTT_del8_white.dat
L1BC_1RTT_del9_white.stl	R_1RTT_del9_white.dat
L1BC_1RTT_del10_white.stl	R_1RTT_del10_white.dat
L1BC_1RTT_del11_white.stl	R_1RTT_del11_white.dat
L1BC_1RTT_del12_white.stl	R_1RTT_del12_white.dat
L1BC_1RTT_del13_white.stl	R_1RTT_del13_white.dat
L1BC_1RTT_del14_white.stl	R_1RTT_del14_white.dat
L1BC_1TIT_del1_white.stl	R_1TIT_del1_white.dat
L1BC_1TIT_del2_white.stl	R_1TIT_del2_white.dat

Source data (CAD STereoLithography format)	Rotated DarcyTools object
Disposal rooms of the existing SFR 1	
L1BC_1TIT_del3_white.stl	R_1TIT_del3_white.dat
L1BC_1TIT_del4_white.stl	R_1TIT_del4_white.dat
L1BC_2DT_del1_white.stl	R_2DT_del1_white.dat
L1BC_2DT_del2_white.stl	R_2DT_del2_white.dat
L1BC_2DT_del3_white.stl	R_2DT_del3_white.dat
L1BC_2DT_del4_white.stl	R_2DT_del4_white.dat
L1BC_2DT_del5_white.stl	R_2DT_del5_white.dat
L1BC_2TT_del4_white.stl	R_2TT_del4_white.dat
Mechanical concrete plugs in SFR 1 (Blue plug)	
SFR1_1BT_del21_silotunnel_blue_plugg.stl	R_1BT_del21_silotunnel_blue.dat
SFR1_1BT_del29_blue_plugg.stl	R_1BT_del29_blue_plugg.dat
SFR1_1BT_del33_blue_plugg.stl	R_1BT_del33_blue_plugg.dat
SFR1_1BT_del41_undre_del_blue_plugg.stl	R_1BT_del41_undre_del_blue.dat
SFR1_1BT_del52_undre_del_blue_plugg.stl	R_1BT_del52_undre_del_blue.dat
SFR1_1BTF_ut_del2_blue_plugg.stl	R_1BTF_ut_del2_blue.dat
SFR1_1BTF_ut_del4_blue_plugg.stl	R_1BTF_ut_del4_blue.dat
SFR1_1TT_del1_blue_plugg.stl	R_1TT_del1_blue.dat
SFR1_1TT_del10_blue_plugg.stl	R_1TT_del10_blue.dat
SFR1_1TT_del4_blue_plugg.stl	R_1TT_del4_blue.dat
SFR1_1TT_del7_blue_plugg.stl	R_1TT_del7_blue.dat
Mechanical concrete plugs in SFR 3 (Blue plug)	
L1BC_1BST_del2_blue_plugg.stl	R_1BST_del2_blue.dat
L1BC_1IN_del2_blue_plugg.stl	R_1IN_del2_blue.dat
L1BC_1RTT_del15_blue_plugg.stl	R_1RTT_del15_blue.dat
L1BC_1UT_del2_blue_plugg.stl	R_1UT_del2_blue.dat
L1BC_2IN_del2_blue_plugg.stl	R_2IN_del2_blue.dat
L1BC_2TT_del3_blue_plugg.stl	R_2TT_del3_blue.dat
L1BC_2UT_del2_blue_plugg.stl	R_2UT_del2_blue.dat
L1BC_3IN_del2_blue_plugg.stl	R_3IN_del2_blue.dat
L1BC_3UT_del2_blue_plugg.stl	R_3UT_del2_blue.dat
L1BC_4IN_del2_blue_plugg.stl	R_4IN_del2_blue.dat
L1BC_4UT_del2_blue_plugg.stl	R_4UT_del2_blue.dat
L1BC_5IN_del2_blue_plugg.stl	R_5IN_del2_blue.dat
L1BC_5UT_del2_blue_plugg.stl	R_5UT_del2_blue.dat
L1BC_6IN_del2_blue_plugg.stl	R_6IN_del2_blue.dat
L1BC_6UT_del2_blue_plugg.stl	R_6UT_del2_blue.dat
Bentonite plugs in SFR 1 (Brown plug)	
SFR1_1BST_del4_brown_plugg.stl	R_1BST_del4_SFR1_brown.dat[1)]
SFR1_1BST_del6_brown_plugg.stl	R_1BST_del6_brown.dat
SFR1_1BST_del7_brown_plugg.stl	R_1BST_del7_brown.dat
SFR1_1BST_del8_brown_plugg.stl	R_1BST_del8_brown.dat
SFR1_1BST_del10_brown_plugg.stl	R_1BST_del10_brown.dat
SFR1_1BST_del11_brown_plugg.stl	R_1BST_del11_brown.dat
SFR1_1BST_del12_brown_plugg.stl	R_1BST_del12_brown.dat
SFR1_1BST_del14_brown_plugg.stl	R_1BST_del14_brown.dat
SFR1_1BST_del15_brown_plugg.stl	R_1BST_del15_brown.dat
SFR1_1BST_del16_brown_plugg.stl	R_1BST_del16_brown.dat
SFR1_1BST_del18_brown_plugg.stl	R_1BST_del18_brown.dat
SFR1_1BST_del19_brown_plugg.stl	R_1BST_del19_brown.dat
SFR1_1BT_del22_silotunnel_brown_plugg.stl	R_1BT_del22_silotunnel_brown.dat
SFR1_1BT_del23_silotunnel_brown_plugg.stl	R_1BT_del23_silotunnel_brown.dat
SFR1_1BT_del24_silotunnel_brown_plugg.stl	R_1BT_del24_silotunnel_brown.dat
SFR1_1BT_del25_silotunnel_brown_plugg.stl	R_1BT_del25_silotunnel_brown.dat
SFR1_1BT_del30_brown_plugg.stl	R_1BT_del30_brown_plugg.dat

Source data (CAD STereoLithography format) Disposal rooms of the existing SFR 1	Rotated DarcyTools object
SFR1_1BT_del31_brown_plugg.stl	R_1BT_del31_brown_plugg.dat
SFR1_1BT_del32_brown_plugg.stl	R_1BT_del32_brown_plugg.dat
SFR1_1BT_del42_undre_del_brown_plugg.stl	R_1BT_del42_undre_del_brown.dat
SFR1_1BT_del43_undre_del_brown_plugg.stl	R_1BT_del43_undre_del_brown.dat
SFR1_1BT_del44_undre_del_brown_plugg.stl	R_1BT_del44_undre_del_brown.dat
SFR1_1BT_del45_undre_del_brown_plugg.stl	R_1BT_del45_undre_del_brown.dat
SFR1_1BT_del46_undre_del_brown_plugg.stl	R_1BT_del46_undre_del_brown.dat
SFR1_1BT_del47_undre_del_brown_plugg.stl	R_1BT_del47_undre_del_brown.dat
SFR1_1BT_del48_undre_del_brown_plugg.stl	R_1BT_del48_undre_del_brown.dat
SFR1_1BT_del49_undre_del_brown_plugg.stl	R_1BT_del49_undre_del_brown.dat
SFR1_1BT_del50_undre_del_brown_plugg.stl	R_1BT_del50_undre_del_brown.dat
SFR1_1BT_del51_undre_del_brown_plugg.stl	R_1BT_del51_undre_del_brown.dat
SFR1_1BTF_ut_del3_brown_plugg.stl	R_1BTF_ut_del3_brown.dat
SFR1_1TT_del2_brown_plugg.stl	R_1TT_del2_brown.dat
SFR1_1TT_del3_brown_plugg.stl	R_1TT_del3_brown.dat
SFR1_1TT_del5_brown_plugg.stl	R_1TT_del5_brown.dat
SFR1_1TT_del6_brown_plugg.stl	R_1TT_del6_brown.dat
SFR1_1TT_del8_brown_plugg.stl	R_1TT_del8_brown.dat
SFR1_1TT_del9_brown_plugg.stl	R_1TT_del9_brown.dat
SFR1_1TT_del11_brown_plugg.stl	R_1TT_del11_brown.dat
SFR1_1TT_del12_brown_plugg.stl	R_1TT_del12_brown.dat
Bentonite plugs in SFR 3 (Brown plug)	
L1BC_1BST_del3_brown_plugg.stl	R_1BST_del3_brown.dat
L1BC_1BST_del4_brown_plugg.stl	R_1BST_del4_L1BC_brown.dat[1)]
L1BC_1IN_del1_brown_plugg.stl	R_1IN_del1_brown.dat
L1BC_1UT_del1_brown_plugg.stl	R_1UT_del1_brown.dat
L1BC_2IN_del1_brown_plugg.stl	R_2IN_del1_brown.dat
L1BC_2NDB_del1_brown_plugg.stl	R_2NDB_del1_brown.dat
L1BC_2TT_del1_brown_plugg.stl	R_2TT_del1_brown.dat
L1BC_2TT_del2_brown_plugg.stl	R_2TT_del2_brown.dat
L1BC_2UT_del1_brown_plugg.stl	R_2UT_del1_brown.dat
L1BC_3IN_del1_brown_plugg.stl	R_3IN_del1_brown.dat
L1BC_3NDB_del1_brown_plugg.stl	R_3NDB_del1_brown.dat
L1BC_3UT_del1_brown_plugg.stl	R_3UT_del1_brown.dat
L1BC_4IN_del1_brown_plugg.stl	R_4IN_del1_brown.dat
L1BC_4UT_del1_brown_plugg.stl	R_4UT_del1_brown.dat
L1BC_5IN_del1_brown_plugg.stl	R_5IN_del1_brown.dat
L1BC_5UT_del1_brown_plugg.stl	R_5UT_del1_brown.dat
L1BC_6IN_del1_brown_plugg.stl	R_6IN_del1_brown.dat
L1BC_6UT_del1_brown_plugg.stl	R_6UT_del1_brown.dat
Filtermaterial plugs in SFR 1 (Green plug)	
SFR1_1BST_del1_green_plugg.stl	R_1BST_del1_green.dat
SFR1_1BST_del2_green_plugg.stl	R_1BST_del2_green.dat
SFR1_1BST_del3_green_plugg.stl	R_1BST_del3_green.dat
SFR1_1BST_del5_green_plugg.stl	R_1BST_del5_green.dat
SFR1_1BST_del9_green_plugg.stl	R_1BST_del9_green.dat
SFR1_1BST_del13_green_plugg.stl	R_1BST_del13_green.dat
SFR1_1BST_del17_green_plugg.stl	R_1BST_del17_green.dat

Source data (CAD STereoLithography format) Disposal rooms of the existing SFR 1	Rotated DarcyTools object
Bentonite plugs in ramp of SFR 1 (Pink plug)	
SFR1_1BT_del6_pink_plugg.stl	R_1BT_del6_pink_plugg.dat
SFR1_1BT_del8_pink_plugg.stl	R_1BT_del8_pink_plugg.dat
SFR1_1DT_del9_pink_plugg.stl	R_1DT_del9_pink.dat
SFR1_1DT_del10_pink_plugg.stl	R_1DT_del10_pink.dat
SFR1_1DT_del13_pink_plugg.stl	R_1DT_del13_pink.dat
SFR1_1DT_del14_pink_plugg.stl	R_1DT_del14_pink.dat
Bentonite plugs in ramp of SFR 3 (Pink plug)	
L1BC_1RTT_del5_pink_plugg.stl	R_1RTT_del5_pink.dat
L1BC_1RTT_del7_pink_plugg.stl	R_1RTT_del7_pink.dat

[1)] Owing to an inconsistency in delivered file names, the objects must be differentiated by means of specification to "SFR 1" or "L1BC".

One part of the SFR 3 ramp is not watertight (L1BC_2DT_del3_white.stl). Gaps in the CAD object imply ambiguity in classification of cells by cell markers (e.g. in this case, a cluster of adjacent bedrock cells become erroneously classed as part of the SFR 3 ramp in the grid generation). This leakage was mended by inserting 4 triangles (Table B-2), after which the CAD data was converted into the DarcyTools object [R_2DT_del3_white.dat]. Even so, *a single cell bedrock cell* (centre coordinates 6706, 9950, –78, in the rotated model coordinate system) is still erroneously classed in the grid generation. This particular cell was therefore separately re-classed as bedrock, by introducing a "single point object" [R_BEDROCK_Fix_L1BC_2DT_del3_white.dat].

Table B-2. Additional triangles in SFR 3 ramp (L1BC_2DT_del3_white).

Triangle	Node	X (m)	Y (m)	z (m)
1	1	7059.81	9663.58	–93.74
	2	7061.24	9663.28	–93.76
	3	7097.52	9640.16	–96.85
2	1	7097.30	9639.82	–96.45
	2	7059.81	9663.58	–93.74
	3	7061.24	9663.28	–93.76
3	1	7059.81	9663.58	–93.74
	2	7062.40	9668.35	–93.64
	3	7066.85	9665.51	–94.02
4	1	7061.24	9663.28	–94
	2	7059.81	9663.58	–93.74
	3	7066.85	9665.51	–94.02

Appendix C

Bedrock parameterisation and early performance measures

A main conclusion of the particle-tracking analysis (Section 6.4) is that, owing to the deeper location of the planned extension, SFR 3, its performance measures will exceed those of the existing facility, SFR 1 (i.e. SFR 3 is expected to have higher F_r and $t_{w,r}$). However, in the more detailed analysis of output for the three bedrock cases 1, 11, and 15 (Sections 6.4.4 and 6.4.5), it is noted that the reverse may apply under early flow regime (Figure 6-27a, Figure 6-28a, and Figure 6-30a). In other words, SFR 1 *may* have better performance measures in some, but not in all cases, and only so for the 2000 AD time slice.

This result may seem counterintuitive, and therefore this matter is scrutinised in further detail. The performance measures primarily reflect two aspects: 1) the pathways taken through the bedrock, and 2) the magnitude of flow along paths. The study is therefore broken down into two parts: an analysis of particle trajectories (Section C1) and an analysis of the relationship between disposal-room cross flow and the changing flow regime (Section C2).

C1 Analysis of particle trajectories

Firstly, it can be noted that the direction of pathways clearly changes over time (e.g. 2000AD: upward flow paths through ZFMNNW1209 and silo ceiling, 3000 AD sideways/downward flow paths through ZFMNNW1209 and silo invert; Figure C-1). As the physical route of pathways change notably during the early changes in flow regime, and the changing route differs among the two facilities, it can be concluded that the relationship between SFR 1/SFR 3 performance measures may vary over time (i.e. particularly at the earliest stages of shoreline retreat). Furthermore, it can be noted how the magnitude in flow along the trajectories directly scales travel time (c.f. colour-scaling of particle trajectories over time in Figure C-1).

Secondly, the particle trajectories from the two facilities have negligible physical overlap at early time slices (Figure C-2). It can also be noted that the vertical trajectories at 2000 AD are short and thus their performance measures reflect comparatively little averaging over rock mass. The maximum fracture size (side length of 300 m for highly transmissive fractures) is large compared to the short vertical trajectories occurring at 2000 AD (i.e. path lengths on the order 100 to 200 m; Figure 6-31a to Figure 6-33a). Consequently, the performance measures are particularly sensitive to the bedrock parameterisation at the 2000 AD time slice (that is, sensitive to deformation-zone parameterisation in combination with the potential existence of large, transmissive stochastic fractures). Owing to its absence of deformation-zone intersections, the silo is particularly "sensitive" to presence of stochastic transmissive fractures (Figure C-2). For example the silo pathways in DFN realisation R18 follow a highly transmissive fracture, which is located just above the silo ceiling (Figure C-3; i.e. this fracture does not intersect the silo, and hence it is not shown).

In conclusion: the vertical flow regime during 2000 AD provides a substantially deviating setting for the performance measures, and hence *it is not surprising that unexpected relationships between SFR 1/SFR 3 are observed for this particular time slice*.

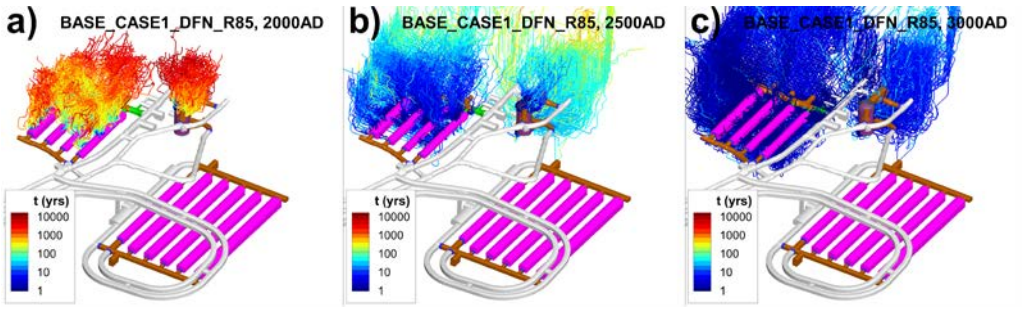

Figure C-1. *Trajectories from SFR 1, base-case bedrock parameterisation for different time slices.*

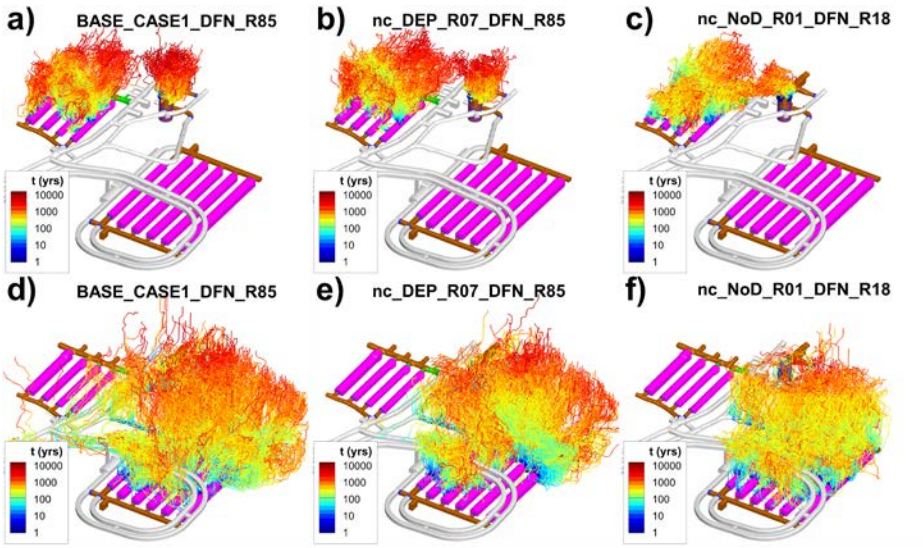

Figure C-2. *Trajectories from SFR 1 and SFR 3, three bedrock parameterisations, 2000 AD (longest travel times occurring from silo in DFN R85).*

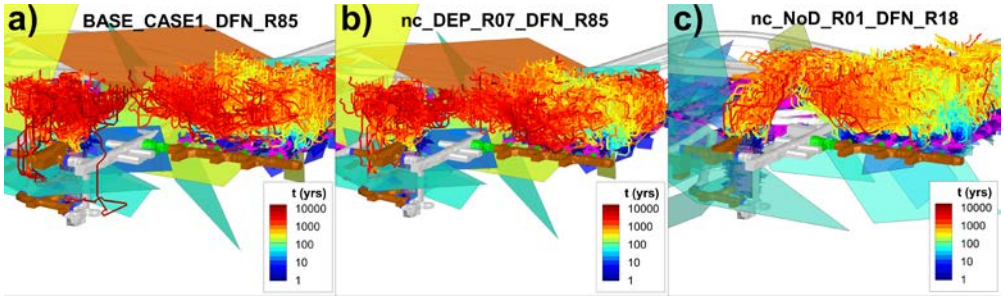

Figure C-3. *Close-up of trajectories from SFR 1 and intersecting fractures, three bedrock parameterisations, 2000 AD.*

Moreover, the performance measures in Sections 6.4.4 and 6.4.5 reflect the lumped characteristics of the disposal rooms that comprise the two facilities SFR 1 and SFR 3 (i.e. average characteristics of several disposal rooms). Among the different disposal rooms, the performance measures of the silo stand out for two reasons: 1) being the only disposal room without deformation-zone intersection, and 2) its low-conductive technical barriers (Figure C-2). Particle release in SFR 1 is volume-proportional, where 25.4% of the particles are released in the silo. Thus, in a direct comparison between the lumped performance measures of SFR 1/SFR 3, it must be kept in mind that SFR 3 has no equivalence of the silo, and therefore 25.4% of the particles from SFR 1 reflect a subset with longer travel times (although, as discussed above, particularly "sensitive" to stochastic DFN realisation; Figure C-2).

In conclusion: in a comparison between the SFR 1/SFR 3 performance measures, it must be taken into account that these reflect lumped characteristics of disposal rooms with varying conditions, and, in particular*, the longest travel times for SFR 1 are associated to the silo*.

Comparatively short travel times are noted for the bedrock case [nc_NoD_R01_DFN_R18], both from the silo and from the rock vaults, via ZFMNNW1209 (Figure C-3c). Inspection of the simulated head fields demonstrate that this discrepancy is related to the trajectory gradient, or driving potential over the trajectory. The following is noted (Figure C-4; Table C-1):

- By 2000AD, all four rock caverns of SFR 1 have substantially *lower* trajectory gradients as compared to those in SFR 3.
- Taken as an average for the four rock caverns of SFR 1, the trajectory gradients by 2000 AD are about four times lower in [BASE_CASE1_R85] and [nc_DEP_R07_R85], as compared to [nc_NoD_R01_DFN_R18].
- At later stages of shoreline retreat, e.g. 3000AD, the four rock caverns of SFR 1 have systematically *higher* trajectory gradients (in comparison to the silo and SFR 3).

The deformation zone ZFMNNW1209 has been identified as a controlling structure for the flow through SFR 1 rock caverns, and therefore it would seem plausible that the simulated gradients are intimately related to parameterisation variants of the structure (Figure C-5). What is typical for [nc_NoD_R01_DFN_R18] is that its parameterisation is based on the assumption that *no general depth trend exists in HCD transmissivity* (i.e. "NoD" stands for "No Depth trend"), as opposed to the other two HCD variants with depth trend (Figure C-5).

In conclusion, out of the two aspects of performance measures studied: 1) physical pathways through the bedrock, and 2) driving potential along paths, it seems likely that the latter provides the explanation to the observed "reverse characteristics" at the early flow regime. It is also suspected that this issue is somehow connected to the assumption concerning HCD depth trend. Therefore, the relationship between disposal-room cross flow of both facilities, the changing flow regime, and the assumption concerning HCD depth trend is pursued in Section C2.

Table C-1. Hydraulic gradient over median trajectory for selected time slices[1].

Case[2]	1BMA	1BLA	2BTF	1BTF	Silo	1BRT	2BLA	3BLA	4BLA	5BLA	2BMA
2000AD											
1	6.2E-6	7.5E-6	7.6E-6	1.1E-5	1.4E-5	2.4E-5	2.0E-5	2.0E-5	2.0E-5	2.2E-5	2.3E-5
11	6.0E-6	7.5E-6	7.4E-6	9.8E-6	1.6E-5	2.2E-5	1.9E-5	1.8E-5	1.7E-5	1.7E-5	1.8E-5
15	1.6E-5	1.6E-5	1.8E-5	2.1E-5	2.3E-5	3.3E-5	3.1E-5	3.0E-5	2.9E-5	2.8E-5	2.7E-5
3000AD											
1	3.1E-3	3.8E-3	4.0E-3	3.8E-3	2.3E-3	2.9E-3	2.9E-3	2.8E-3	2.8E-3	2.9E-3	2.9E-3
11	2.8E-3	3.7E-3	3.8E-3	4.1E-3	2.6E-3	2.7E-3	2.6E-3	2.6E-3	2.6E-3	2.6E-3	2.6E-3
15	3.1E-3	3.5E-3	3.8E-3	3.8E-3	2.3E-3	2.7E-3	2.7E-3	2.7E-3	2.6E-3	2.6E-3	2.6E-3

[1] Colour shading by magnitude [–], as compared separately over time slices; high = red, low = blue. "Median trajectory" refers to the particle trajectory with median travel time.

[2] Bedrock cases: 1 = BASE_CASE1_R85, 11 = nc_DEP_R07_R85, and 15 = nc_NoD_R01_R18.

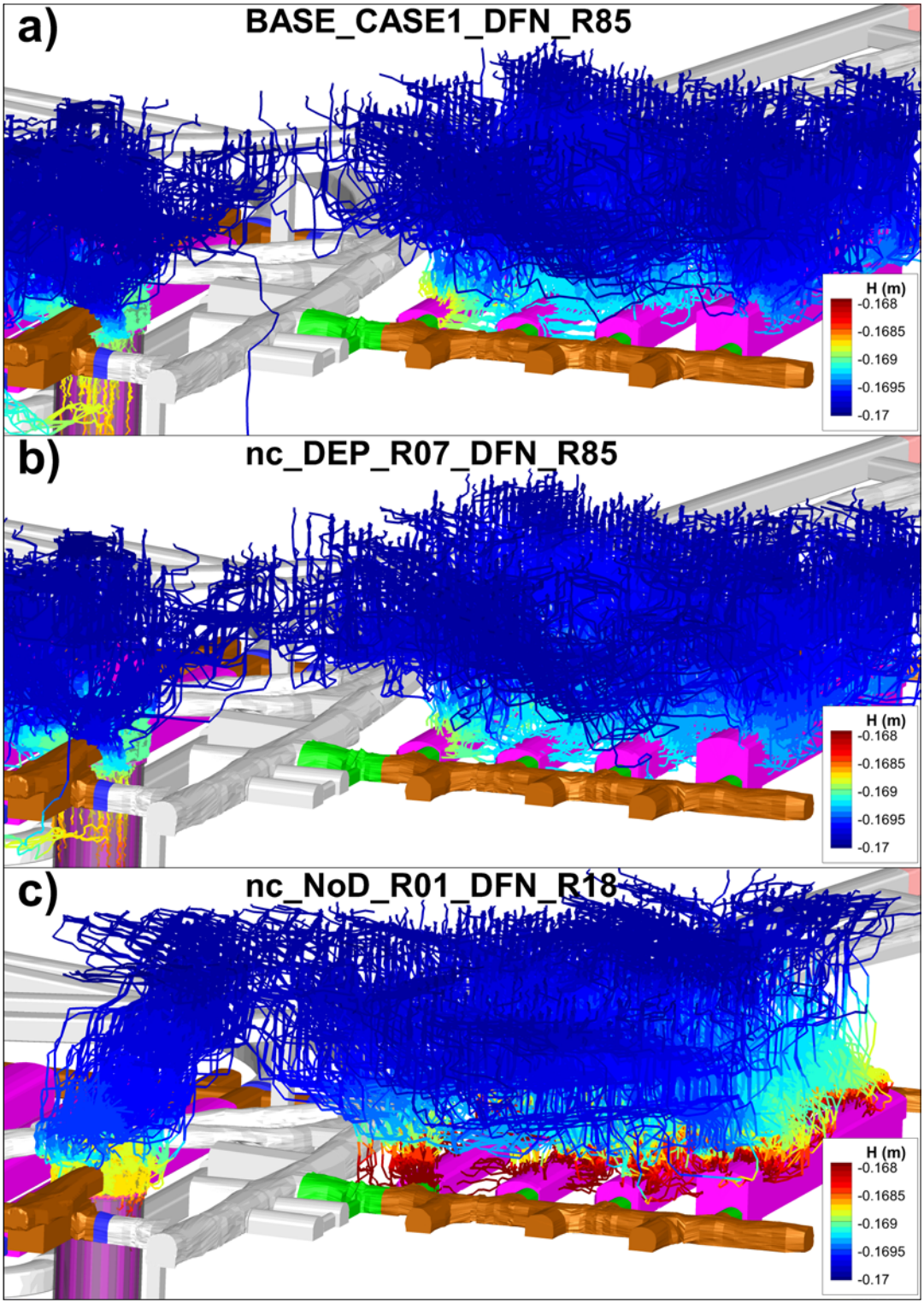

Figure C-4. *Gradient over trajectories from SFR 1, three bedrock parameterisations, 2000 AD. The hydraulic gradient is notably higher in the HCD parameterisation variant without depth trend.*

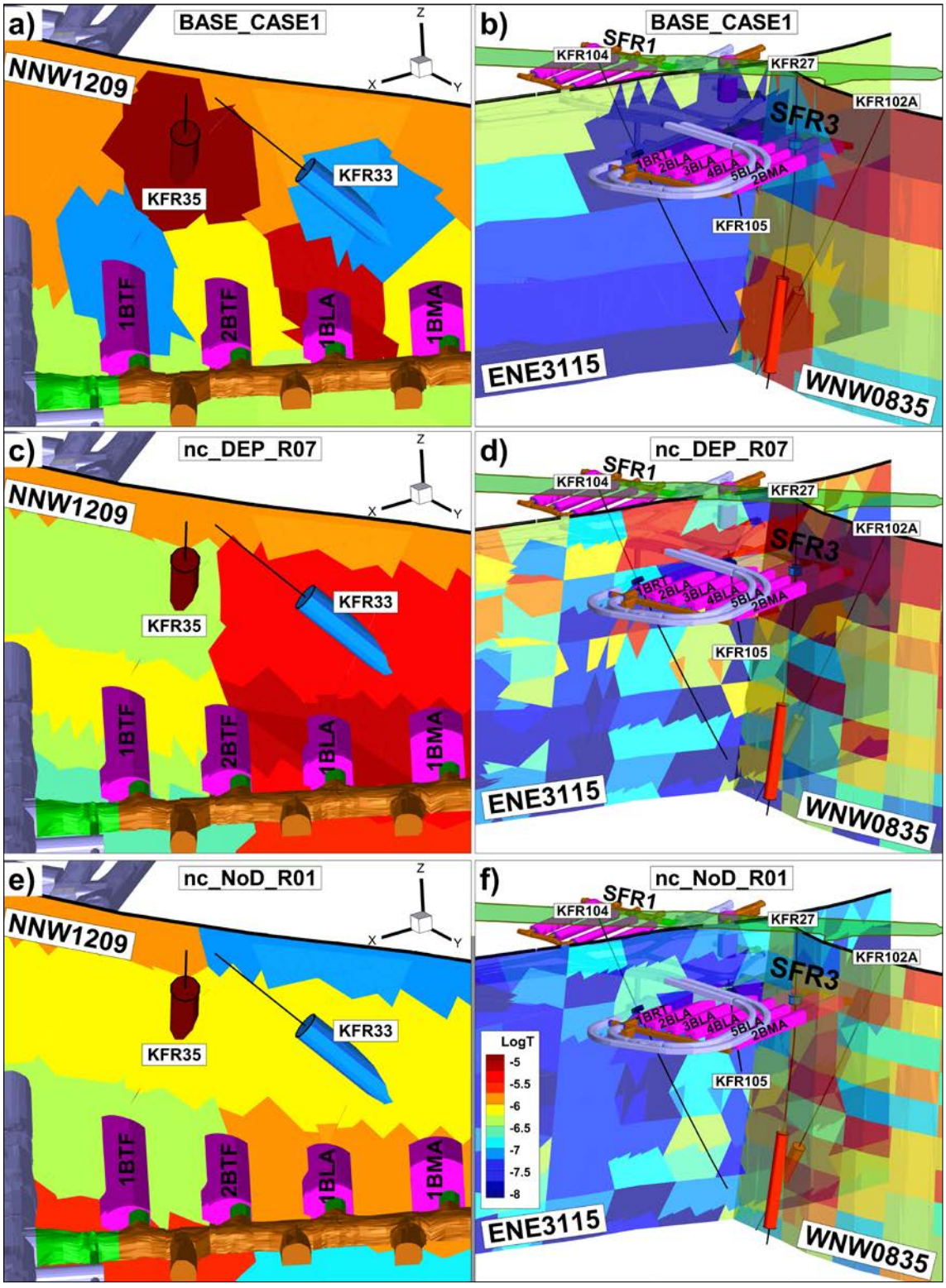

Figure C-5. *HCD parameterisation at rock-cavern intersections. Note that NoD = "No depth trend".*

C2 Analysis of tunnel flow (2000 AD and 2500AD)

Under certain conditions, the performance measures of SFR 1 may outdo those of SFR 3, in spite of its shallower location. It is suspected that this may relate to the assumption concerning HCD depth trend. This notion is studied further in this section, by comparing the early changes in disposal-room cross flow for the different bedrock cases. Notably, the cross flow in the four rock caverns of SFR 1, is about twice as high in [nc_NoD_R01_DFN_R18], *without* HCD depth trend, as it is in the two HCD variants with depth trend. Again, this may at first seem counterintuitive, particularly as this bedrock case was identified as the "low tunnel-flow bedrock case". However, it must be remembered that the three representative bedrock cases were selected to represent future stages of shoreline retreat, and based on observed deviances in disposal room-flow patterns for time slice 2000 AD (Section 6.2.3), it was decided not to include those simulation results in Equation (6-2) and Table 6-3.

Quantifying the change in disposal-room cross flow as a ratio between the magnitudes at 2500 AD and those at 2000AD, Q_{2500AD}/Q_{2000AD} (–), reveals a distinct pattern related to HCD parameterisation. What is common for all depth-trend HCD parameterisations (i.e. BASE_CASE and "DEP"; Table C-2) is that the flow in all four rock caverns of SFR 1 exhibit a drastic increase between the two time slices 2000 AD and 2500 AD. The SFR 1 caverns have an average ratio of 80, as compared to a ratio of 30 for the rock caverns of SFR 3 (Table C-2). Notably, among the HCD parameterisations *without* depth trend (i.e. "NoD"), ratios are smaller in general, c. 20, and the difference between SFR 1 and SFR 3 is insignificant. After the 2500 AD time slice, the rate of change in flow decreases considerably, as well as any differences related to HCD parameterisation.

In conclusion: during the 2000 AD time slice, the cross flows in the four rock caverns of SFR 1 are exceptionally low for HCD parameterisation variants that incorporate the assumed depth trend. Both F_r and $t_{w,r}$ scale inversely with Q, and hence the unexpectedly high performance measures for SFR 1 (i.e. exceeding SFR 3, which is exclusive for the 2000 AD time slice and HCD parameterisation without depth dependence), is highly consistent with the early evolution in tunnel flow (Table C-2).

Table C-2. Increasing flow across disposal rooms during early changes in flow regime, expressed as ratio Q_{2500AD}/Q_{2000AD} [–].

Bedrock case	1BTF	2BTF	1BLA	1BMA	Silo	1BRT	2BLA	3BLA	4BLA	5BLA	2BMA
BASE_CASE1_R85	66.3	64.5	81.9	90.1	36.0	12.6	20.2	32.3	31.7	16.9	16.8
BASE_CASE2_R85	80.8	75.8	97.0	107.0	46.3	20.0	28.7	42.3	43.5	25.6	26.8
BASE_CASE1_R18	66.0	36.3	23.7	94.3	31.7	18.1	21.5	22.8	33.1	33.0	44.4
CD_DEP_R01_R85	56.2	59.6	111.0	114.0	40.8	14.8	24.0	40.4	34.8	19.1	21.3
CD_DEP_R07_R85	73.2	72.6	121.5	102.2	42.0	11.6	18.8	30.7	37.6	15.3	19.6
nc_DEP_HOM_R03	43.3	39.8	46.3	111.1	22.9	22.5	33.7	30.2	31.5	39.7	24.9
nc_DEP_HOM_R85	64.6	66.1	108.7	84.6	28.3	13.2	22.5	31.4	33.2	22.7	18.9
nc_DEP_R01_R18	57.3	43.3	64.0	109.5	36.5	41.2	47.9	57.8	65.1	68.7	41.5
nc_DEP_R01_R85	65.6	67.0	121.5	118.1	41.7	33.6	53.4	74.1	60.6	39.6	26.8
nc_DEP_R07_R18	67.6	56.1	73.6	82.9	27.3	18.8	20.7	32.5	50.7	53.1	53.9
nc_DEP_R07_R85	75.7	93.3	125.5	105.4	23.5	15.6	24.5	37.5	49.5	31.4	31.2
nc_NoD_R01_R18	17.1	10.1	12.9	19.0	15.2	14.3	16.7	18.4	21.0	24.3	26.2
nc_NoD_HOM_R85	19.8	21.1	33.5	20.8	11.2	6.2	10.8	18.1	15.1	10.6	11.0
nc_NoD_R01_R03	15.8	13.5	17.7	29.1	13.8	17.4	23.8	24.2	16.7	34.2	22.2
nc_NoD_R01_R85	22.0	23.5	41.3	28.5	17.0	10.2	16.8	29.1	22.8	15.7	16.2
nc_NoD_R07_R03	18.3	12.4	12.7	16.9	9.9	9.6	12.1	16.5	14.0	26.1	17.7
nc_NoD_R07_R85	26.1	24.0	28.6	17.8	9.1	6.2	11.4	17.9	16.7	13.6	13.0

[1)] Colour shading by magnitude [–]; high = red, low = blue.

[2)] Bedrock cases: 1 = BASE_CASE1_R85, 11 = nc_DEP_R07_R85, and 15 = nc_NoD_R01_R18 marked in yellow.

What is specific for the 2000 AD flow regime is that, no local groundwater table is expected in the surroundings of the existing facility (i.e. at least not significantly above sea level), and hence the flow field consists of long (and probably deep) flow paths recharging from "elevated land in the Forsmark inland" (e.g. Figure 6-15a). It would then seem plausible that an assumed HCD depth trend tends to constrain such long-range flow paths, i.e. low-transmissive HCD at depth forming hydraulic bottlenecks, which hamper upward-directed flow in rock caverns during submerged conditions. In particular for SFR 1, the assumption regarding depth trend is central for the upstream hydraulic connection to Singö, via the gently dipping ZFM871, which extends below the SFR 1 facility (Figure C-6). The particular constellation of the underlying ZFM871 and surrounding zones could explain why SFR 1 is more strongly affected by the HCD depth trend, than SFR 3 is.

Already by 2500AD, the flow regime has shifted towards local recharge from the pier, and hence recharging flow paths from the Forsmark inland are of comparatively lesser significance (Figure 6-15b). This would imply that in turn the HCD parameterisation at depth is also of lesser significance, although, to the contrary, elevated transmissivity in upper parts of deformation zones, as imposed by the depth-trend parameterisation, tends to facilitate horizontal flow in the shallow bedrock (e.g. SFR 1 rock caverns intersected by ZFMNNW1209; Figure C-1). Consequently, local recharge from the pier is expected to make rock-cavern cross flow less dependent on recharge via ZFM871.

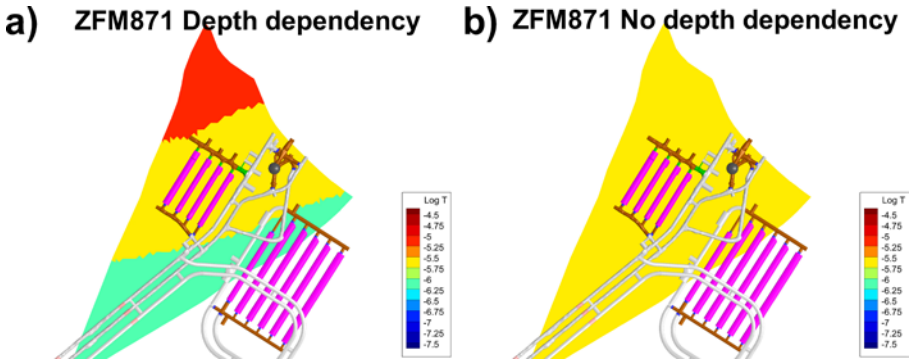

Figure C-6. *HCD depth-trend parameterisation variants of ZFM871; a) assumed transmissivity depth trend hampers the upstream hydraulic connection to Singö and b) expected value in variants "NoD", where depth trend is not assumed.*

Appendix D

Model domains and size of stochastic fractures

Fracture size is the most uncertain parameter in the DFN model. The hydro-DFN model SFR v. 1.0 was calibrated by means of a Connectivity analysis (Öhman et al. 2012), in which the fracture size distribution is inferred from the ratio between the total population of fractures mapped as open and its subset of hydraulically connected fractures. The two most important assumptions in this method are that: 1) measured fracture transmissivity is proportional to fracture size (i.e. side length of square fracture), and 2) the lower fracture-size cut off in the borehole data, r_0, corresponds to borehole radius, r_{bh} = 0.038 m.

Truncation of small fractures in large-scale application

Due to the nature of power-law scaling fractures, the computational demand increases drastically with inclusion of smaller fractures. Apart from the practical limitations in computational capacity, introducing a minimum-size cut off, to exclude fractures below a certain size, is motivated by the fact that small fractures are of minor significance for regional-scale flow: 1) they are less connected (even for vast amounts of generated small fractures, their contribution to the overall hydraulic connectivity is minor), 2) small fractures are assumed to have lower transmissivity, and 3) fracture sizes below grid resolution (cell size) provide no additional correlation of the ECPM conductivity field.

As the rule of thumb in DarcyTools modelling, it is recommended that the minimum fracture size should correspond to the grid resolution (cell size). In the uppermost 180 m, the cell size varies from 2 to 8 m (Table A-7). Consequently, the minimum fracture side length varies from 2 to 4 m in this depth interval (more precisely, a minimum side length of 2 m is applied to the horizontal set – which is interpreted as the most conductive, while 4 m is applied to the other sets). At depth, where the cell size varies between 16 to 64 m (Table A-7), the minimum fracture side length is set to 16 m for all fracture sets.

DarcyTools is based on the continuum porous-medium approach, which relies on the assumption that the hydraulic properties of a flowing fracture network can be approximated by those of a porous medium (Section 2.1). Thus, truncation of small fractures introduces the distinction between bedrock properties regarded as *immobile* (i.e. assumed not accessible to flow and therefore neglected in modelling) versus *kinematic*, which are the underlying properties in the determination of performance measures (i.e. bedrock properties along flow paths; Section 5.2). To summarize, truncation of small fractures is necessary out of practical limitations, but more importantly necessary to ensure a conservatory approach in context of model simplifications (i.e. as flow in small fractures is negligible, they must not be allowed to contribute to porosity, and flow-wetted surface area in the determination of performance measures along flow paths; Section 5.4.2). A more detailed analysis of the relative significance of small fractures is presented in SKBdoc 1395200.

Upper size-cut off in the DFN model

A corner stone in the hydrogeological model lies in the distinction between deterministic and stochastic modelling. The crossover between the two modelling concepts is determined by the resolution level in the geological model of deformation zones (Curtis et al. 2011). That is, the size of the smallest structure that is handled deterministically sets the upper bound, or upper cut off, for size of features to be handled in the stochastic modelling. Two modelling scales were defined for the site-descriptive modelling for SFR (SKB 2008): an SFR Local model domain (red line in Figure D-1) and an SFR Regional domain (orange line in Figure D-1). The applied resolution level for deterministic structures in the SFR Local domain was 300 m, and for the SFR Regional domain it was 1,000 m. The established modelling approach is to develop separate DFN models for the two domains, with different underlying data and with different upper cut offs for fracture size. In this aspect, it was decided to depart from the standard praxis, due to site-specific circumstances for SFR that are described below.

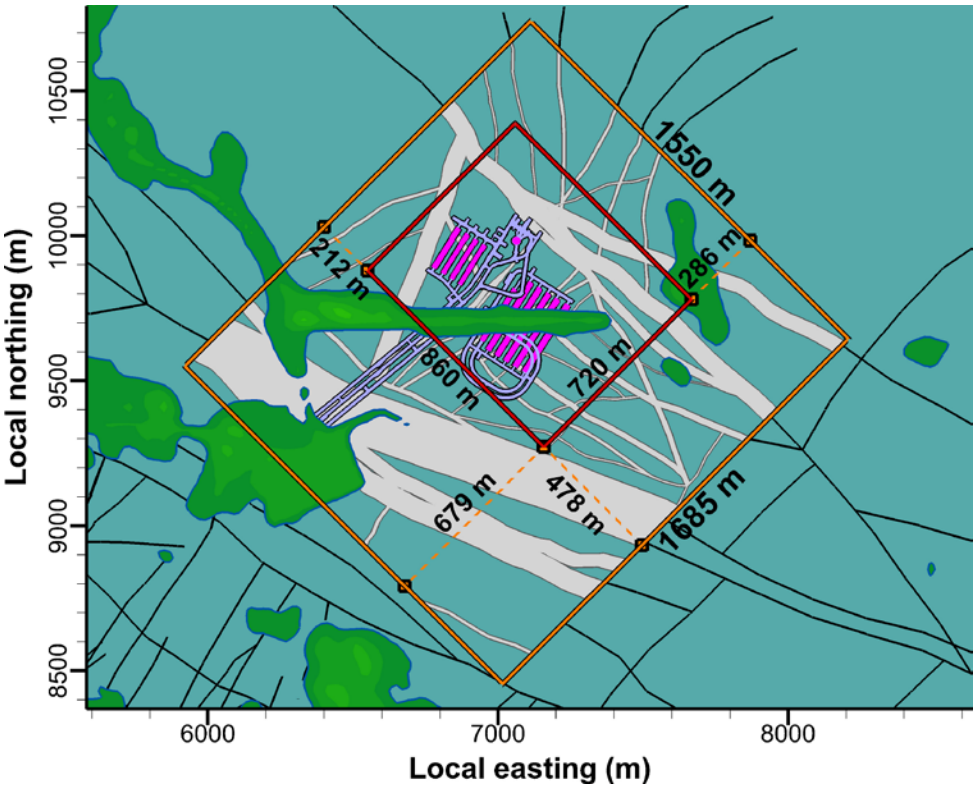

Figure D-1. *Dimensions of domains for SFR modelling, as defined in SKB (2008); SFR Regional domain (orange) and SFR Local domain (red).*

In essence, all the underlying data of the DFN model calibration are contained within the SFR Local domain (Öhman et al. 2012). Basically, there are no data at hand to provide better information for the surrounding bedrock just outside the SFR Local domain, and therefore the DFN model is assumed to be applicable over the entire SFR Regional domain (i.e. in lack of contrary evidence). Furthermore, the upper cut off in fracture size was set to 300 m, in common to both domains, although, *strictly speaking*, the deterministic modelling for the SFR Regional domain employed a resolution level of 1,000 m. The rationale for this is presented below.

It can be noted that the area south to southwest of the SFR Local domain is largely covered by the Singö deformation zone, and its splays, and that therefore the DFN model has a subordinate role in this area (i.e. any uncertainty concerning the DFN model is subordinate to the uncertainty regarding parameterisation of the Singö deformation zone in this area; Figure D-1).

Owing to the dominant flow direction, the parameterisation in area to the north of SFR is far more important in flow simulations; it is found to be the primary area for determining performance measures by means of particle tracking (Section 6.4). In this region, the gap between the Local and Regional domains narrows down to a "corridor" of less than 300 m width (Figure D-1). It is not realistic to apply the higher cut off in size particularly inside this narrow slab (although, by strict definitions according to the resolution level in the geological modelling, otherwise should be 1,000 m).

The reason for this is that the area is very close to the SFR disposal rooms (c. 150 m; Figure D-1), an area that has been analysed in great level of detail (Curtis et al. 2011). Hence, the generation of stochastic 1,000 m-scale features in this area would require careful handling of any large features intersecting the SFR Local domain, in context of its 300 m resolution level applied in the geological modelling. Numerically, any unrealistic occurrence of large fractures in the SFR Local domain can

be avoided by, for example implementing a "guard-zone" to prevent stochastic features larger than 300 m in side length from intersecting the domain boundary. However, it should also be noted that the area outside the SFR Regional domain includes large fractures, some of which intersect the Regional domain boundary (i.e. with a maximum side length of 1,000 m; Figure D-2). In context of these circumstances, it is judged that the additional level of complexity in employing nested DFN generation, to handle variable size cut offs, outweighs its benefits.

In summary, the decision to apply the DFN model for the entire SFR Regional domain – with a constant size-cut off of 300 m, was taken with consideration to: 1) the spatial dimensions of model domains in relation to the proximity to SFR disposal rooms (Figure D-1), 2) resolution level of the geological modelling (Curtis et al. 2011), and 3) the embedding DFN realisation, taken from SR-Site/SDM-Site Forsmark (Figure D-2).

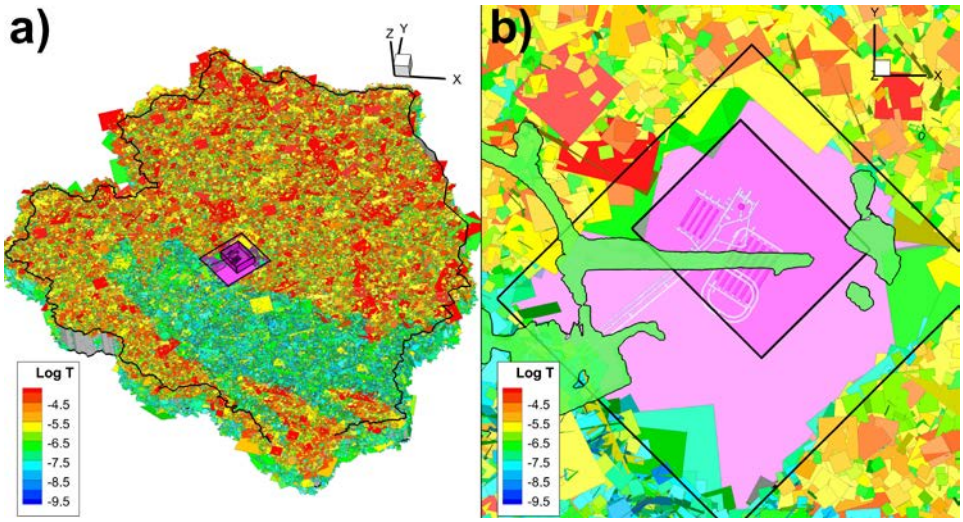

Figure D-2. *SFR modelling domains embedded in surrounding DFN realisation for SR-Site/SDM-Site Forsmark (Section 4.3).*